Development and Application of Reaction Route Graph Representation and Analysis of Catalytic Reaction Networks

A Dissertation Submitted to the Faculty of the
WORCESTER POLYTECHNIC INSTITUTE

In partial fulfillment of the requirements for the
Degree of Doctor of Philosophy in Chemical Engineering

By

_____

Patrick D. O'Malley
October 17th, 2016

Approved:

_____   _____

Prof. Ravindra Datta, Advisor   Prof. N. Aaron Deskins
WPI Department of Chemical Engineering   WPI Department of Chemical Engineering

_____   _____

Prof. George T. Heineman   Prof. Michael T. Timko
WPI Department of Computer Science   WPI Department of Chemical Engineering

_____

Prof. Susan Roberts, Dept. Head
WPI Chemical Engineering Department

Abstract

Chemical reactions can have a staggering amount of molecular complexity. Reaction mechanisms have been proposed with over one hundred elementary reaction steps that occur in the same system simultaneously. While several methods exist to simplify and make sense of the pathways and kinetics via which these reactions proceed, e.g., reaction graphs, sensitivity or flux analysis, microkinetic analysis, and comparison of energy landscapes, etc., these methods all have limitations and are often not able to capture a comprehensive picture of the kinetics of system.

It has been found useful to view these mechanisms as a network, i.e., a reaction graph. These graphs enable the visualization of the pathways of the reaction and can provide an analytical tool for pathway and kinetic analysis. However, many of the specific graph-theoretic approaches in the literature are not the most suitable for kinetic analysis of complex mechanisms; as they are simply not based on rules that are rigorous enough to fully enumerate all the pathways or provide quantitative analysis of the reaction rates. Our Reaction Route (RR) Graph approach is different in that it depicts the mechanism by a graph that is consistent with all physical and chemical laws associated with reaction networks, particularly being consistent with mass and energy conservation, i.e., Kirchoff's Flux Law (KFL) and Kirchoff's Potential Law (KPL). Because of their adherence to these laws, RR Graphs are able to provide an accurate graph-theoretical tool not only for depicting all reactions routes as walks (hence the name RR Graph) but also for pruning mechanisms and allowing a simplified but accurate quantitative description of reaction rates.

This adherence to KFL and KPL does mean that the construction and implementation of these graphs can be prohibitively difficult for large mechanisms. For large reaction systems,

especially nonlinear mechanisms, it is not realistic to generate these graphs by hand. And although there exists an analytical solution to find a determinant matrix for the RR Graph of a mechanism, the process involves an exhaustive search for a solution which experiences a combinatorial explosion as the number of steps gets very large. This leads to the idea of developing an algorithm for a computer program that can determine how to generate these graphs automatically. Unfortunately, the same combinatorial explosion is present such that for a moderately sized twenty step mechanism, it could take an average computational processor over a decade to find a solution. We have determined, however, that this brute force combinatorial approach can be avoided if heuristics could be developed to bridge gaps in our knowledge of how these graphs are constructed. Thus, developing a better analytical approach and/or a tighter set of heuristics for a computer algorithm are the overarching goals of this work.

To make progress toward developing such heuristics, a set of microkinetic mechanisms were analyzed with the notion that the realization of the RR Graphs would highlight a better approach to their construction and usage. In particular, a very large linear reaction system, a smaller linear system and two non-linear reaction systems were analyzed to develop insights into how each graph is manually constructed and analyzed. Furthermore, kinetic analysis was done for these mechanisms and compared to experimental data and other analytical tools to prove not only the validity of the RR Graphs, but also how they are a significant improvement over more commonly used approaches for mechanistic and kinetic analysis.

Based on the lessons learned through a consideration of these examples, a set of heuristics are established and enumerated with the ultimate goal of developing an intuitive algorithm that can help automate drawing and kinetic analysis via RR Graphs of complex mechanisms.

Acknowledgements

I would like to thank my advisor, Professor Ravindra Datta, for the opportunity to work with him on such a challenging project. He has shown great patience in instructing me on the topic of catalytic reactions and fuel cells. I was often impressed with his ability to provide feedback on the spot and his vast knowledge of chemistry and engineering. I admire his perseverance in furthering the understanding of reaction chemistry through a methodology that, at least to me, is incredibly fascinating, despite the difficulties I have had wrapping my head around it.

I would also like to thank others who have helped me with this research. The late Professor Ilie Fishtik was of great help in showing how to properly draw the RR graphs and I wish I had taken the opportunity to learn more from him. Thanks to Dr. Saurabh Vilekar for providing feedback for some of my analysis and Professor George Heineman for his work on the graph automation project and for helping me understand it. Also, thanks to my other committee members, Professor Aaron Deskins and Professor Mike Timko for their time and interest.

I am very appreciative of the culture created by the WPI Chemical Engineering staff and faculty who have always been courteous and welcoming. Thank you for the funding made available to me via Teaching Assistanceship, which allowed me to continue my research. Thanks to Felicia and Tiffany for keeping this place running. Thanks to my fellow fuel cell lab mates: Drew, Jason, Nick and Susan. A big thank you to my good friend Stanley who definitely helped by keeping me company and encouraging me.

I would like to credit much of my success to my parents, Karen and Kevin. They have given me every opportunity to achieve whatever dream I desired. I truly owe them everything and

Table of Contents

List of Figures

List of Tables

xi

Nomenclature

Symbols

a_i	Activity of terminal species i
A_ρ	Affinity of elementary reaction ρ
$\mathscr{A}_\rho$	A Dimensionless reaction affinity of elementary reaction ρ
$\mathscr{A}_{OR}$	A Dimensionless affinity of the overall reaction
$\mathscr{A}_{OR}$	A Dimensionless affinity of intermediate reaction
BE_{Ik}	Binding energy of intermediate species, I_k
$\vec{E}_\rho$	Activation energy of the forward reaction
$\bar{E}_\rho$	Activation energy of the reverse reaction
F	Faraday's constant, 96,487 C eq^{-1}
ΔG_ρ	Gibbs free energy change of the elementary reaction ρ
$\Delta G_\rho^{\pm,\circ}$	Gibbs-free energy of activation
ΔG_{ad}°	Standard enthalpy of formation in the gas phase
$H_{I_k(g)}^\circ$	Standard enthalpy of formation in the adsorbed phase
$\Delta H_\rho^{\pm,\circ}$	Enthalpy of activation
h	Planck's constant
I_k	Intermediate species k
$I_\rho^\bullet$	Maximum branch current
i	Fuel cell current density
i^*	Current density (per metal catalyst surface)
i_0^*	Exchange current density (per metal catalyst surface)
K_ρ	Equilibrium constant of the elementary reaction ρ
K_{OR}	Equilibrium constant of the overall reaction

$\vec{k}_\rho$	Forward rate constant of the elementary reaction ρ
$\overleftarrow{k}_\rho$	Backward rate constant of the elementary reaction ρ
k_B	Boltzman's constant
m	Number of independent ORs
M	distinct direct ORs
$m_{\rho j}$	Incidence coefficient
n	Number of terminal species
N_{Av}	Avogadro's number
$N_{i,Z}$	Flux of species i in the membrane along the z direction
p	Number of elementary reactions
p_i	Partial pressure of species i
q	Number of linearly independent intermediate species
Q_k	intermediate QSS condition
r	Rank of formula matrix
R	Gas Constant
R_ρ	Resistance of elementary reaction ρ
$R_\rho^\bullet$	Resistance of elementary reaction s_ρ , when s_ρ is the RDS
R_{OR}	Total resistance of the overall reaction network
r_ρ	Net rate of the elementary reaction ρ
r_{OR}	Net rate of the overall reaction
$\vec{r}_\rho$	Forward rate of elementary reaction ρ
$\overleftarrow{r}_\rho$	Reverse rate of elementary reaction ρ
$\vec{r}_\rho^\bullet$	Maximum rate of the elementary reaction ρ
$\overleftarrow{r}_\rho^\bullet$	Maximum forward rate of the elementary reaction ρ
S	Unoccupied surface site
ΔS_ρ	Entropy change the elementary reaction ρ
$\Delta S_\rho^{\pm,\circ}$	Entropy of activation

$S^{\circ}_{I_k(g)}$	Standard entropy of formation of the species I_k in gas phase
$S_{trans,I_k(g)}$	Translational entropy of the species I_k in the gas phase
s_{ρ}	Elementary reaction ρ
T	Temperature
T_{ref}	Reference temperature (K)
T_i	Terminal species i
V	Voltage (V)
$X_{DRC,\rho}$	Degree of Rate Control of step s_{ρ}
z_{ρ}	Reversibility of reaction s_{ρ}
z_{OR}	Reversibility of overall reaction
z_{IR}	Reversibility of an intermediate reaction
$\Delta(\mathrm{ZPE}_{I_k})$	zero point energy correction to binding energy of the intermediate species, I_k

Greek Symbols

$\vec{\alpha}_{\rho k}$	Stoichiometric coefficient of intermediate species k I in reaction step $s\rho$ asa reactant
$\bar{\alpha}_{\rho k}$	Stoichiometric coefficient of intermediate species k I in reaction step $s\rho$ as a product $\boldsymbol{\alpha}$ intermediate sub-matrix
$\vec{\beta}_{\rho i}$	Stoichiometric coefficient of the terminal species i in reaction step $s\rho$ as a reactant
$\bar{\beta}_{\rho i}$	Stoichiometric coefficient of the terminal species i in reaction step $s\rho$ as a product
β_{ρ}	Symmetry factor
ρ	Elementary reaction
σ_{ρ}	Stoichiometric number for the elementary reaction ρ
Λ_{ρ}	Pre-exponential factor
θ_k	Surface coverage of intermediate species k
$\theta^{\bullet}_{k,\rho}$	Surface coverage of intermediate species k when ρ s is the RDS
μ	Number of linearly independent reaction routes

ω_ρ	Step weight for reaction ρ s
$\vec{\omega}_\rho$	Forward step weight for reaction ρ s
$\overleftarrow{\omega}_\rho$	Reverse step weight for reaction ρ s
v_i	Stoichiometric coefficient of terminal species i in an overall reaction
$v_{\rho i}$	Stoichiometric coefficient of species i in reaction ρ
$v_{\rho e^-}$	Stoichiometric coefficient of electrons in reaction ρ
γ	reduced stoichiometric sub-matrix
γ_k	Stoichiometric coefficient of intermediate species Ik in an intermediate reaction
γ_{ki}	Stoichiometric coefficient of terminal species i in an intermediate reaction
η_ρ	Overpotential of electrode reaction ρ ρ ,0 = Φ −Φ (V)
ψ	Dimensionless electrode overpotential, $0.5F\eta/RT$

Abbreviations

BE	Binding energy
DFT	Density Functional Theory
DRC	Degree of Rate Control
ER	Empty route
FER	Full Enumeration of ERs
FR	Full route
HER	Hydrogen evolution reaction
HOR	Hydrogen oxidation reaction
HT	Heyrovsky-Tafel
IN	Intermediate node
IR	Intermediate reaction
IRR	Intermediate reaction route
KFL	Kirchhoff's Flux law
KPL	Kirchhoff's Potential law
LHHW	Langmuir-Hinshelwood-Hougen-Watson
MARI	Most abundant reactive intermediate
MEA	Membrane electrode assembly

OR	Overall reaction
ORR	Oxygen reduction reaction
PEM	Polymer electrolyte membrane
QSS	Quasi-steady state
QE	Quasi-equilibrium
RH	Relative humidity
RR	Reaction Route
RDS	Rate determining step
RLS	Rate limiting step
TN	Terminal node
UBI-QEP	Unity Bond Index – Quadratic Exponential Potential
VH	Volmer-Heyrovsky
VT	Volmer-Tafel

Chapter 1. Introduction

The difference between having a feasible, profitable process technology and having one that fails, can be as small as finding the right catalyst. Unfortunately, predicting the performance of a particular catalyst and finding the right catalyst is not yet a hard science and can take a large amount of resources. It takes considerable time and other resources to set up and perform experiments or simulations. Developing an understanding of what pathways a reaction can take can also take years of research. An example is the Haber-Bosch process for ammonia synthesis from elemental N_2 and H_2 developed in early 20th century that resulted in synthesis of artificial fertilizers and a key technological advance in overcoming hunger worldwide. The iron catalysts for the industrial process were developed by Fritz Haber and Carl Bosch after a dozen years of painstaking research (today's formulation differs little from original) involving 2,500 different formulations based on practically all elements of the periodic table [1]. Haber and Bosch were subsequently awarded the Nobel Prize for this work. It took another 60 years before the mechanism (Table 1.1) and energetics (Figure 1.1) were established by Gerhard Ertl [2], who also received the Nobel Prize.

S_ρ	Reaction Step
S_1 :	$H_2 + S \rightleftarrows 2H{\bullet}S$
S_2 :	$N_2 \rightleftarrows N_2{\bullet}S$
S_3 :	$N_2{\bullet}S \rightleftarrows 2N{\bullet}S$
S_4 :	$N{\bullet}S + H{\bullet}S \rightleftarrows NH{\bullet}S$
S_5 :	$NH{\bullet}S + H{\bullet}S \rightleftarrows NH_2{\bullet}S$
S_6 :	$NH_2{\bullet}S + H{\bullet}S \rightleftarrows NH_3{\bullet}S$
S_7 :	$NH_3{\bullet}S \rightleftarrows NH_3$

Table 1.1: Catalytic synthesis of ammonia mechanism [1].
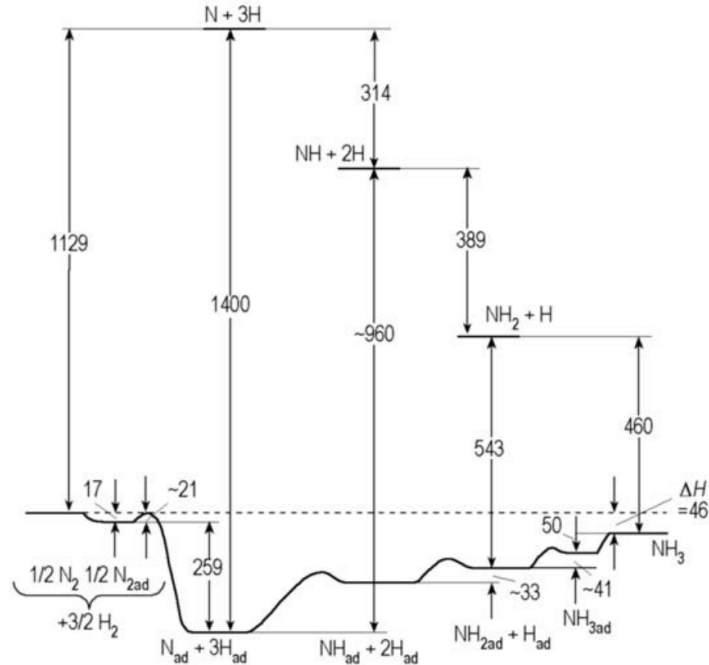
Figure 1.1: Energy landscape for ammonia production [2].

Furthermore, operating conditions such as temperature, reactant concentration, or electrical overpotential for electrochemical processes, can impact the reaction rate just as much, so that understanding mechanism as well as kinetics is important. Years of research have been devoted to some reactions without coming to a hard conclusion about the kinetics of the reaction. For example, the oxygen reduction reaction (ORR) on the cathode of a proton exchange membrane (PEM) fuel cell is one of the major sources for energy lost in the operation of a fuel cell [3]. Thus, many studies have been conducted to better understand the mechanism and kinetics of this reaction [3-11]. Platinum catalysts are an effective but high cost catalyst for this reaction and there is a high interest in developing a cheaper alternative, so that research on ORR catalysts and mechanism continues. Although the mechanism for the ORR has been well researched, it has not yet been unequivocally established. Thus, for each new potential catalyst, a large set of elementary reaction

steps must be considered including their step kinetics, as bottleneck steps can vary with the catalyst.

This is an issue with many reaction systems; there are so many different directions the reaction path can take, that it can be practically overwhelming. Recently, development of quantum mechanical calculation software has provided us a powerful tool for understanding the mechanism and kinetics of complex chemical catalytic reactions. Often we are concerned with optimizing the conditions to improve the overall rate on a given catalyst, but we also might be attempting to push the reaction in a certain direction to avoid a particular side product, which might require a different catalyst formulation. In either case, very thorough research is required to grasp the scope of all the theoretical steps in a mechanism on a given catalyst. Then, to start to understand the impact of each step, a calculation of the elementary reaction step energetics may be done using, e.g., density functional theory (DFT) or other methods. This provides the energy change and the energy barriers for each step, but does not provide us with enough insight to exclude any of the proposed steps. Conventionally, for kinetic analysis, 1) the Langmuir-Hinshelwood-Hougen-Watson (LHHW) approach, 2) the quasi-steady state (QSS) assumption and, 3) the microkinetic approach are used with a goal to determine a single rate-determining step (RDS). One could also use a simple flux analysis, or Campbell's Degree of Rate Control (DRC) [13] to find the RDS. These approaches to reduce and better understand these systems usually oversimplify the mechanism and make unwarranted assumptions that could lead to ignoring important steps in the reaction network.

There is, thus, a need for developing a rigorous approach that does not make arbitrary assumptions, e.g., excluding all but one elementary step, or assuming there exists a single most abundant reactive intermediate (MARI). These efforts could lead to the misidentification the rate-limiting steps (RLS), because there might be more than one step that control the rate of reaction,

and more than one pathway that contributes materially, especially as conditions change. The Reaction Route Graph approach gives us this tool. Through a graph-theoretical analysis of all the elementary steps, each step and each pathway simultaneously is present on the graph produced by this method and contributes to the flux. If further provided with the activation energies that can be obtained through DFT, the Unity Bond Index – Quadratic Exponential Potential (UBI-QEP) method [14-17] or other methods, a rigorous kinetic analysis and pruning can be undertaken. In the RR Graph approach, each step is considered as a resistance to the overall reaction. In other words, we can look at the graphs in the same way as an electrical circuit diagram, since conformity with KCL and KPL makes RR Graph completely analogous to electrical circuits. We thus liken reaction rate to current and chemical affinity, or Gibbs free energy, change to voltage for both individual steps and overall reaction (OR). RR Graphs are further able to evaluate the resistance of each step and by combining those resistances appropriately, as if it were an electrical circuit, the (OR) resistance can be obtained, and hence the OR rate. Analysis of step resistance and those for parallel pathways also allow rigorous and transparent pruning. To demonstrate the superiority of this method, a direct comparison of the results of the RR Graph approach and those of Campbell's DRC is made in this thesis.

When we start to look at more complicated catalytic reactions, we find that the size of these networks can reach dozens and sometimes over a hundred elementary reactions [29]. With so many reactions taking place, it is difficult to visualize the staggering number of pathways for the overall reaction. One approach to this problem is to depict the network as a mathematical graph similar to the commonly used chemical mechanism schematics, as it is easier to analyze the reaction steps and reaction paths based on graph theory. This idea of using graphs to represent chemical reactions is not unique – in fact there exist many alternate approaches [18-23]. What is common among

these approaches, however, is that they do not rigorously follow all the rules of graph theory and chemical kinetics. Most egregious is the fact that energy and mass are not strictly conserved as the pathways are followed. If the graph were to realistically represent a chemical network, one should be able to follow any path on the graph without gaining or losing extra energy or mass. This is simply not true for conventional graph tools such as p-graphs [18] or reaction graphs [19]. The RR Graph approach, on the other hand, is unique in this respect.

As an example, Figure 1.2 shows an RR Graph for a 12-step N_2O decomposition mechanism on Fe-ZSM-5 zeolite [29] summarized in Table 1.2 [30]. All the reaction pathways are represented on it as pathways between the terminal nodes, TN_1 and TN_2, and it is easy to see how the elementary steps are interconnected at intermediate nodes, n_1-n_8. Although it might not be intuitive, unlike conventional graphs or reaction schematics each node of the graph does not necessarily represent a single intermediate species, as it would then be impossible to guarantee consistence with mass balance laws. However, this allows the graph to be used for quantitative analysis of the reaction network, which will be discussed in great detail in the following chapters.

For comparison, Figure 1.3 is a depiction of the same mechanism as a conventional reaction schematic [31]. These schematics are built to visualize how the elementary reaction steps are interconnected. The key intermediate species are drawn, often with their chemical structure, which are connected by reactions steps represented by directed arrows. Other terminal and intermediate species are intermittently included with a "+" or "-" sign along the arrows to designate them as either a product or reactant. There is indeed a lot of useful chemistry insights to be gained from such a schematic, it is often difficult to visualize the alternate pathways of the reaction. In fact, we cannot confirm that all the pathways are even present. Most importantly, they cannot be used for quantitatively analyzing the network as they lack the rigorously guidelines of chemical or

graph theory laws, thus they are nothing more than a schematic representative of the mechanism, while the RR Graphs provide a quantitative representation. Of Course, what is lost in this RR Graph is the details of chemical structure, etc.
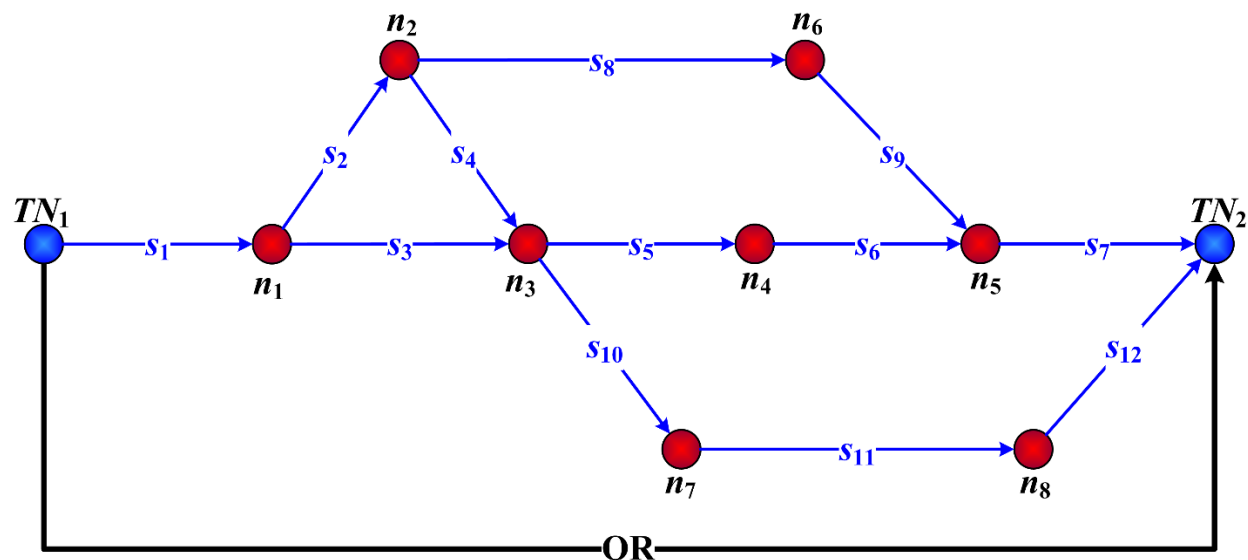
Figure 1.2: RR Graph representation of a 12-step reaction mechanism for N2O decomposition on Fe-ZSM-5. [29]
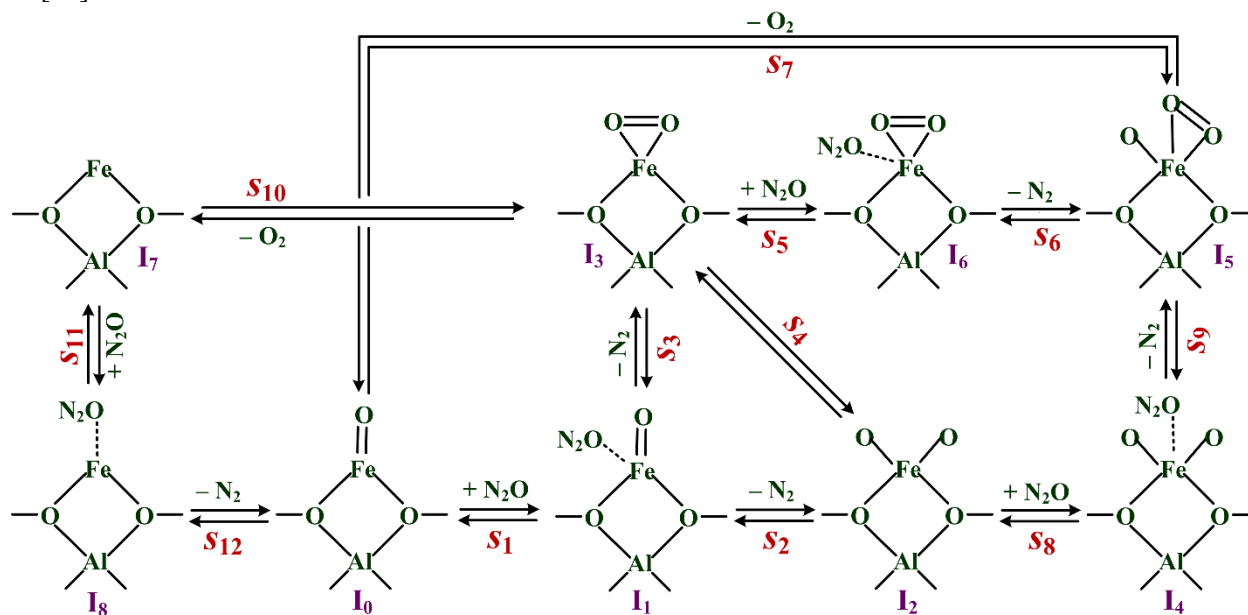
Figure 1.3: Schematic representation of a 12-step reaction mechanism for N_2O decomposition Fe-ZSM-5. [31]

6

S_ρ	Reaction Step
$S_1:$	$N_2O + I_0 \rightleftarrows I_1$
$S_2:$	$I_1 \rightleftarrows I_2 + N_2$
$S_3:$	$I_1 \rightleftarrows I_3 + N_2$
$S_4:$	$I_2 \rightleftarrows I_3$
$S_5:$	$N_2O + I_3 \rightleftarrows I_6$
$S_6:$	$I_6 \rightleftarrows I_5 + N_2$
$S_7:$	$I_5 + I_0 + O_2$
$S_8:$	$N_2O + I_2 \rightleftarrows I_4$
$S_9:$	$I_4 \rightleftarrows I_5 + N_2$
$S_{10}:$	$I_3 \rightleftarrows I_7 + O_2$
$S_{11}:$	$N_2O + I_7 \rightleftarrows I_8$
$S_{12}:$	$I_8 \rightleftarrows I_0 + N_2$

Table 1.2: 12-step reaction mechanism for N_2O decomposition on Fe-ZSM-5. $I_0 = Z^-[FeO]^+$; $I_1 = Z^-[FeO]^+(ON_2)$; $I_2 = Z^-[OFeO]^+$; $I_3 = Z^-[FeO_2]^+$; $I_4 = Z^-[OFeO]^+(ON_2)$; $I_5 = Z^-[O_2FeO]^+$; $I_6 = Z^-[FeO_2]^+(ON_2)$; $I_7 = Z^-[Fe]^+$; $I_8 = Z^-[Fe]^+(ON_2)$ [31].

Besides allowing reaction route and pathway analysis, the RR Graph approach, as previously mentioned, is a comprehensive tool for pruning mechanisms and providing a quantitative analysis of the kinetics. The reason for this is because it follows Kirchoff's Flux Law (KFL), or mass balance, and Kirchoff's Potential Law (KPL), or Hess's Law, both of which are central for electrical circuits [24-25]. KFL states that the flux entering a node should be equal to that exiting a node. KPL states that for any cycle in a graph (a cycle is any set of elementary steps, that, when added together, cancel out all the species, i.e., a closed walk on a graph), the net voltage

or thermodynamic potential is zero. For chemical reactions, we consider chemical potential as an analog to voltage, but this law holds true for any thermodynamic state property, which ultimately is a statement of Hess's Law. Thus, the RR Graph approach is completely analogous to electrical circuits and is hence a more rigorous and complete analytical tool than other graph-based reaction network approaches that are not consistent with KFL and/or KPL. Several mechanisms have been successfully analyzed through the RR Graph approach leading to the elucidation of dominant pathways and predictive equations for the overall reaction rate [26-29].

Currently, a limiting factor for the use of this approach is the difficulty in the construction of the graph for very large reaction systems, particularly non-linear ones, i.e., those with non-unit stoichiometric numbers [26]. As the number of elementary steps increases for a kinetic mechanism, the number of reaction routes increases factorially. A complete RR Graph has to include each one of these routes and combine them in such a way so that the graph is consistent with KFL and KPL, which proves to be quite restrictive, although usually resulting in a single unique solution. An analytical approach has been developed by us that produces an incidence matrix from which to draw the graph [24, 25]. However, it involves manual matrix row operations that is feasible for small systems, but for larger and especially non-linear systems, this process involves a lot of trial and error that is simply not practical. Non-linear systems, i.e., systems with higher than unit species stoichiometric coefficients in the mechanisms provide the most trouble, as they increase the complexity of the RR Graph by requiring each step to appear at least twice in the graph. These difficulties lead to the conclusion that in order to expand the utility of the RR Graph approach, a better, more efficient way to generate the RR Graph for a given mechanism is required.

Obviously, a computer program that could draw the graph automatically would be ideal. It would be best to have a publicly available program that could analyze a given reaction mechanism

and provide an RR graph that would be consistent with KFL and KPL. This would further enable any mechanism to be more easily analyzed via a graph that allows enumeration of the pathways of the reaction as walks. An evaluation of the kinetics would then allow the pruning of the graph, by eliminating pathways that provide impediments for the reaction to go through, or having a high resistance if one were to use an electrical analogy. Attempts were made to achieve this goal by implementing the heuristics and graph theory tools of the hand drawn method into such a complex program. However, the same combinatorial explosion still existed, e.g., an attempt to automate drawing the graph for water-gas shift (WGS) reaction mechanism in Chapter 3 was estimated to take decades of computational time to exhaust the search for a valid graph using the algorithm we have now.

To identify the shortcomings of our current understanding of this approach, an in depth examination of a larger system must be completed. A larger RR Graph can theoretically be hand drawn using the same methods as the smaller graphs we have so far investigated, but there are so many different orientations to consider for the placements of the steps that simple trial and error does not appear to be feasible. Brute force methods can be applied to the enumeration of the reaction routes, but a better approach to putting them together into a single graph has yet to be achieved.

The ultimate goal of this work is to identify heuristics on how these graphs may be constructed. Can we identify where certain elementary steps must be connected? Is there an order to how empty routes should be combined? Basically, there needs to be a set of instructions and theorems that can be implemented into a computer program that will significantly reduce the number of options that need to be search. Ideally, this would result in a deterministic matrix manipulation or other construction method that does not require any searching at all.

9

This thesis represents the efforts toward this goal. The approach taken here was to consider reaction systems with different characteristics and levels of complexity so that the manual system of RR Graph construction could be delineated, leading to a set of heuristics. Of course, it must be mentioned that for microkinetic analysis the RR Graph is not essential, just as a circuit diagram is not essential for an electric circuit. What is required is a set of KFL and KPL relations. However, no one can argue the utility of an electric circuit diagram. The RR Graphs are similarly invaluable especially for RR enumeration, flux analysis and for pruning.

Chapter 2 of this thesis gives a thorough description of the theory of Reaction Route Graphs along with the electrical analogy approach that is used to prune the graphs and derive the rate expression. This provides the groundwork for the algorithm and the process for the analysis of the mechanisms in the subsequent chapters. Two of our previous implementations of RR Graph analysis are given as illustrations, one that shows of the WGS reaction on Pt (111) catalyst and another that considers the hydrogen evolution reaction (HER). Other graph theory approaches for analyzing reaction networks available in the literature are examined for comparison and the advantages of the RR Graphs are made clear.

Chapter 3 provides the WGS reaction on Pt-Re as an example of mechanism analysis and pruning. In addition, a comparison was made between the RR Graph approach and Campbell's Degree of Rate Control (DRC), one of the more commonly used and powerful techniques to identify rate determining or rate limiting steps and intermediates. This comparison demonstrates the shortcomings of the DRC method in identifying the rate limiting steps, and how the RR Graph approach is able to quantitatively analyze the system without these pitfalls.

A further example of a non-linear system of interest to us is given in Chapter 4, where the oxygen reduction reaction (ORR) is considered over several catalysts. This example also

demonstrates the value of the RR Graph for analyzing the same system under a wide range of conditions and dozens of alternate catalyst formulations.

Chapter 5 provides an analysis of the methane dry reforming (MDR) reaction on Ni catalyst, a reaction system of current interest for CO_2 mitigation. Of particular note is the presence of multiple overall reactions (OR) in this mechanism. This chapter demonstrates the difficulty of determining which of the may ORs should be considered and how to properly draw the RR Graph for multiple ORs.

Chapter 6 summarizes the current methodology for improving the heuristics for generating RR Graphs. The RR Graph approach developed by us has already demonstrated its versatility and proven via a number of examples considered so far. If the technique could be automated it would represent development of a new tool for reaction network analysis with broad utility. The current attempts to design a program for automating the graph drawing process is discussed along with a detailed list of what is believed to be the rules or guidelines for drawing the graphs. It also exhibits our current limitations by providing an example of the largest mechanism that could be graphed using the program, a 13-step mechanism of methanol steam reformation on Pt(111). Further discussion is given on how analyzing larger and non-linear systems will lead to identifying patterns in the constructed graphs, eventually leading to the development of tighter heuristics to follow for the construction process, e.g., for a currently prohibitively large NO_X decomposition mechanism as an example.

Chapter 7 proposes future work into the nitrous oxide decomposition system, as well as other possible mechanisms worth studying via the RR Graph approach.

1.1 References

1   G. Ertl, Primary steps in catalytic synthesis of ammonia. *J. Vac. Sci. Technol. A.* 1, 1247-1253 (1983)

2   M. Appl, Ammonia, 2 Production Processes. *Ullmann's Encyclopedia of Industrial Chemistry* (2012). Wiley

3   A.J. Herron, J. Jiao, K. Hahn, G. Peng, R.R. Adzic, M. Mavrikakis, Oxygen Reduction Reaction on Platinum-Terminated ;Onion-structured' Alloy Catalysts. *Electrocatalysis* DOI 10.1007/s12678-012-0087-0 (2012)

4   J.L. Zhang, M.B. Vukmirovic, Y. Xu, M. Mavrikakis, R.R. Adzic, Controlling the catalytic activity of platinum-monolayer electrocatalysts for oxygen reduction with different substrates. *Chem. Int. Ed.* 44(14), 2132–2135 (2005)

5   M.B. Vukmirovic, J. Zhang, K. Sasaki, A.U. Nilekar, F. Uribe, M. Mavrikakis, R.R. Adzic, Platinum monolayer electrocatalysts for oxygen reduction. *Electrochim. Acta* 52(6), 2257–2263 (2007)

6   R.R. Adzic, J.X. Wang, Configuration and site of O2 adsorption on the Pt(111) electrode surface. *J. Phys. Chem.* B 102(45), 8988–8993 (1998)

7   J.K. Nørskov, J. Rossmeisl, A. Logadottir, L. Lindqvist, J.R. Kitchin, T. Bligaard, H. Jonsson, Origin of the overpotential for oxygen reduction at a fuel-cell cathode. *J. Phys. Chem.* B 108(46), 17886–17892 (2004)

8   Rodrigo Ferreira de Moraisa, Philippe Sautetb, David Loffredab, Alejandro A. Francoa, "A multiscale theoretical methodology for the calculation of electrochemical observables from ab

initio data: Application to the oxygen reduction reaction in a Pt(1 1 1)-based polymer electrolyte membrane fuel cell" *Electrochimica Acta* 56 (2011) 10842– 10856

9   Guang-Feng Wei, Ya-Hui Fang, and Zhi-Pan Liu, "First Principles Tafel Kinetics for Resolving Key Parameters in Optimizing Oxygen Electrocatalytic Reduction Catalyst", *J. Phys. Chem*, 116, 12696−12705 (2012)

10   Matthew P. Hyman and J. Will Medlin "Mechanistic Study of the Electrochemical Oxygen Reduction Reaction on Pt(111) Using Density Functional Theory", *J. Phys. Chem. B*, *110,* 15338-15344 (2006)

11   Wang, J. X., Zhang, J., and Adzic, R. R., "Double-Trap Kinetic Equation for the Oxygen Reduction Reaction on Pt(111) in Acidic Media," *J. Phys. Chem. A*., 111, 12702-12710 (2007a)

12   Fishtik, I., Callaghan, C. A., and Datta, R., "Reaction Route Graphs. I. Theory and Algorithm," *J. Phys. Chem. B*, 108, 5671-5682 (2004a).

13   Campbell, C. T. (2001), "Finding the rate-determining step in a mechanism: comparing DeDonder relations with the "Degree of Rate Control"," *Journal of Catalysis*, *204*(2), 520-524.

14   A. GroB, *Surf. Sci.* 500 (2002) 347-367.

15   M. Neurock, *J Catal*. 216 (2003) 73-88.

16   F. Ruette, M. Sanchez, A. Sierraalta, C. Mendoza, R. Anez, L. Rodriguez, O.Lisboa, J. Daza, P. Manrique, Z. Perdomo, M. Rosa-Brussin, *J. Mol. Catal. A: Chemical.* 228 (2005) 211-225.

17   Desai, M. Neurock, Electrochimica Acta. 48 (2003) 3759-3773.

18   O.N. Temkin, A.V. Zeigarnik, D.G. Bonchev, Chemical Reaction Networks: A Graph-Theoretical Approach, CRC Press, New York, 1996.

19 L. T. Fan, Y.-C. Lin, S. Shafie, B. Bertok, F. Friedler, "Exhaustive Identification of Feasible Pathways of the Reaction Catalyzed by a Catalyst with Multiactive Sites via a Highly Effective Graph-Theoretic Algorithm: Application to Ethylene Hydrogenation," Ind. Eng.Chem. Res, 2012, dx.doi.org/10.1021/ie200718w

20 J.A. Papin, J. Stelling, N.D. Price, S. Klamt, S. Schuster, B.O. Palsson, "Comparison of network-based pathway analysis methods," Trends in Biotechnology 22 (2004) 400-405.

21 Schuster, S., Dandekar, T., Fell. D.A. "Detection of Elementary Flux Modes in Biochemical Networks: A Promising Tool for Pathway Analysis and Metabolic Engineering." Trends Biotechnol .,17, 53–60 (1999).

22 B.O. Palsson, Systems Biology: Simulation of Dynamic Network States, Cambridge University Press, Cambridge, UK, 2011.

23 D. A. Beard, H. Qian, Chemical Biophysics: Quantitative Analysis of Cellular Systems, Cambridge University Press, Cambridge, 2008.

24 Fishtik, I., Callaghan, C. A., and Datta, R. (2004a), "Reaction route graphs. I. Theory and algorithm," *The Journal of Physical Chemistry B*, *108*(18), 5671-5682.

25 Fishtik, I., Callaghan, C. A., & Datta, R. (2004b), "Reaction route graphs. II. Examples of enzyme-and surface-catalyzed single overall reactions," *The Journal of Physical Chemistry B*, *108*(18), 5683-5697.

26 Callaghan, C. A., Vilekar, S. A., Fishtik, I., & Datta, R. (2008), "Topological analysis of catalytic reaction networks: Water gas shift reaction on Cu (111)," *Applied Catalysis A: General*, *345*(2), 213-232.

27 Vilekar, Saurabh A, Fishtik, Ilie, Datta, Ravindra, "Kinetics of the Hydrogen Electrode Reaction" *Journal of The Electrochemical Society*, 157 7 B1040-B1050 (2010)

28 S.A. Vilekar, I. Fishtik, R. Datta, in: I. Halasz (Ed.), A comprehensive graph-theoretic approach for mechanistic and kinetic analysis of zeolite catalysis: N_2O decomposition on Fe-ZSM-5, *Transworld Research Network*, Kerala, India, 2010, pp. 49-79.

29 S.A. Vilekar, I. Fishtik, R. Datta, *Chem. Eng. Sci*. 64 (2009) 1968-1979.

30 Heyden, A.; Bell, A. T.; Keil, F. J., (2005), "Kinetic modeling of nitrous oxide decomposition on Fe-ZSM-5 based on parameters obtained from first-principles calculations. *J. Catal.* 109, (5), 1857-1873.

31 Heyden, A. (2005), "Theoretical investigation of the nitrous oxide decomposition over iron zeolite catalysis. Ph.D. Thesis, Hamburg University of Technology, Germany.

Chapter 2. Reaction Route and Graph Theory

The RR Graph approach has been developed to provide a comprehensive tool for chemical reaction networks that goes beyond the current methods to elucidate the different reaction pathways, provide their fluxes, and identify the important pathways as well as kinetic steps. One can visualize a chemical network as a roadmap that covers the space through which the reaction proceeds and can take many pathways to get from the products to the reactants. The RR Graph approach creates this roadmap and is able to assign each pathway a quantitative estimate of traffic flux and how difficult it is to traverse that pathway and the key steps that impede a pathway can be identified. This chapter discusses the theory behind RR Graphs as well as the graph-theory to which it relates. Several examples of chemical reaction networks are provided and the advantages of using RR Graphs are discussed. Finally, other graph-theoretical approaches are discussed for comparison.

2.1 Reaction Route Theory

This section presents in detail the theory behind the RR Graph approach. The underlying linear algebra and graph theory are important parts of the approach that need to be explained. The basic approach for construction a minimal linear RR Graph can be implemented into a program to automate the process, but for more complicated systems, this approach does not apply. Hopefully, this approach will eventually be extended to provide a fully analytical approach to constructing the graphs without needing a brute force or a trial-and-error method for finding the incidence matrix of the graph. First, an understanding of the definitions used in this study is provided.

To avoid confusion, the terms used in the approach related to graph theory are defined, since alternate terminology and representation for reaction networks in graph theory exists in the

literature. We define a Reaction Route Graph G_R as an ordered, connected, directed (i.e., a digraph), planar or nonplanar, cycle graph comprising B directed branches or edges, each representing an elementary or an overall reaction $\{OR, s_1, s_2, \ldots, s_\rho, \ldots s_p\}$, and N nodes $\{n_1, n_2, \ldots, n_N\}$, that illustrate how the reaction steps are interconnected to allow for all of the direct reaction routes to be traced [1, 2]. Edges are depicted on the graph as directed arrows and nodes are circles, typically blue for terminal nodes (nodes that have the OR incident) and red for intermediate nodes, which are connected to elementary reactions. If all given reactions are represented only once in the graph, it is termed a minimal reaction route graph, $G_{R,min}$. It has been determined empirically that for mechanisms with stoichiometric coefficients other than unity, that the graph will need to represent each elementary reaction step twice. As per the convention in graph theory, when an edge originates at a node n_j, it is said to be incident from the node n_j. When an edge terminates at a node n_j, it is said to be incident to the node n_j. Two or more edges are parallel if they have in common the same pair of starting and ending nodes. The orientation of the edge is simply assumed, and the reaction may actually proceed in either direction. There can, of course, be more than one overall reaction in a graph, which leads to more complexity, but can typically treated in the construction of the graph as another elementary step reaction. It may be remarked that the nodes in the reaction route graphs defined above do not denote single intermediates or terminal species as is almost universally the case in the so-called "reaction graphs" [3], but simply the interconnection of reactions involved in reaction routes, hence the reason for labeling these "reaction route graphs." As a result, a node n_j here represents properties associated with the sum of products of the reactions incident to the node plus the sum of reactants of the reactions incident from the node with an appropriate sign (negative for reactions incident to, and

positive for reactions incident from a node, as discussed later in the context of the incidence matrix).

Following the detailed RR Graph theory first presented by Fishtik et al. [1], we consider a set of p elementary reaction steps s_ρ ($\rho = 1,2, \ldots, p$): $\sum_{i=1}^{l} \nu_{\rho i} B_i = 0$, involving species B_i ($i = 1, 2, \ldots, l$). The stoichiometric coefficient $\nu_{\rho i}$ of species i in the reaction s_ρ is, positive for a product, negative for a reactant and zero for an inert. All reactions are considered to be reversible. The reversibility and direction of the reaction flux for a reaction can be determined by the sign and magnitude of its affinity [1]. The affinity is a state function characteristic of the reaction and its distance from equilibrium, which is defined as the negative of the step's Gibbs free energy change, or as the difference of the forward affinity $\vec{A}_\rho$ minus the revers affinity $\bar{A}_\rho$ [4]:

$$A_\rho = \sum_{i=1}^{l} (-\vec{\nu}_{\rho i})\mu_i - \sum_{i=1}^{l} \bar{\nu}_{\rho i}\mu_i = \vec{A}_\rho - \bar{A}_\rho \tag{2.1}$$

where μ_i is the chemical potential of species B_i. This provides the condition for the reaction equilibrium, as well as the direction of spontaneous reaction rate r_ρ (i.e., forward for $A_\rho > 0$, or for $\vec{A}_\rho > \bar{A}_\rho$, and reverse for $A_\rho < 0$, or for $\vec{A}_\rho < \bar{A}_\rho$), as expressed succinctly by the De Donder inequality, $P_\rho \equiv A_\rho r_\rho \geq 0$ [4].

The rate of an elementary reaction step is given by [5]

$$r_\rho = \vec{r}_\rho - \bar{r}_\rho = \vec{k}_\rho \prod_{i=1}^{l} a_i^{-\vec{\nu}_{\rho i}} - \bar{k}_\rho \prod_{i=1}^{l} a_i^{\bar{\nu}_{\rho i}} \tag{2.2}$$

where a_i is the activity of the species B_i. With the use of $\mu_i = \mu_i^0 + RT \ln a_i$, Eq. (2.1) may be written in the form

$$\mathcal{A}_\rho = \ln\left(\frac{\vec{r}_\rho}{\overleftarrow{r}_\rho}\right) = \ln\left(\frac{1}{z_\rho}\right) \tag{2.3}$$

which is the so-called De Donder relation, where $\mathcal{A}_\rho = A_\rho/(RT)$ is the dimensionless affinity.

It is more useful to write an elementary reaction step s_ρ for a catalytic reaction in a more explicit form in terms of the reaction intermediates I_i and the terminal species T_i:

$$s_\rho : \alpha_{\rho 0}I_0 + \sum_{k=1}^{q} \alpha_{\rho k}I_k + \sum_{i=1}^{n} \beta_{\rho i}T_k = 0 \quad (\text{for } \rho = 1,2, \ldots, p) \tag{2.4}$$

For simplicity, a single type of active site I_0 (denotes by S for a heterogeneous catalyst) is assumed here, not included in I_k by virtue of site balance. The stoichiometric coefficients of the intermediates I_k are $\alpha_{\rho k}$ ($k = 1, 2, \ldots, q$) and for the terminal species T_i are $\beta_{\rho i}$ ($i = 1,2, \ldots, n$). The De Donder affinity, thus, becomes

$$\mathcal{A}_\rho : \ln K_\rho - \alpha_{\rho 0}\ln a_0 - \sum_{k=1}^{q} \alpha_{\rho k}\ln a_k - \sum_{i=1}^{n} \beta_{\rho i}\ln a_i \tag{2.5}$$

where $K_\rho = \vec{k}_\rho/\overleftarrow{k}_\rho$ is the equilibrium constant for the elementary reaction. The species activities a_i may be replaced by a suitable composition measure, e.g., the site fraction θ_i for the intermediates in heterogeneous catalysis and partial pressure or concentration for terminal species. Thus, the affinity may be computed, e.g., from elementary reaction energetics and numerical results of a microkinetic analysis for a given set of conditions and a specified reactor configuration [6].

The overall stoichiometric matrix $\hat{\iota}$ is written with the rows corresponding to reactions (including the overall reaction (OR), $\sum_{i=1}^{n} v_{OR,i}T_i$, as the first row) and the columns to the species with the intermediates followed by the terminal species:

19

$$\mathbf{v} = \begin{bmatrix} 0 & 0 & \cdots & 0 & v_{OR,1} & v_{OR,2} & \cdots & v_{OR,n} \\ \alpha_{11} & \alpha_{12} & \cdots & \alpha_{1q} & \beta_{11} & \beta_{12} & \cdots & \beta_{1n} \\ \alpha_{21} & \alpha_{22} & \cdots & \alpha_{2q} & \beta_{12} & \beta_{22} & \cdots & \beta_{2n} \\ \vdots & \vdots & \vdots & \vdots & \vdots & \vdots & \vdots & \vdots \\ \alpha_{p1} & \alpha_{p2} & \cdots & \alpha_{pq} & \beta_{p1} & \beta_{p2} & \cdots & \beta_{pn} \end{bmatrix} \qquad (2.6)$$

in which the active sites are excluded because of the site mass balance and, of course, the stoichiometric coefficients of the intermediates in the OR are zero. In general, we find that rank v = $m \leq p$, where p is the number of elementary steps. We further define the stoichiometric submatrix of v, involving only reaction intermediates,

$$\boldsymbol{\alpha} = \begin{bmatrix} \alpha_{11} & \alpha_{12} & \cdots & \alpha_{1q} \\ \alpha_{21} & \alpha_{22} & \cdots & \alpha_{2q} \\ \vdots & \vdots & \vdots & \vdots \\ \alpha_{p1} & \alpha_{p2} & \cdots & \alpha_{pq} \end{bmatrix} \qquad (2.7)$$

referred to as the intermediates stoichiometric matrix [6]. It is assumed here that the surface intermediates are linearly independent, i.e., rank $\boldsymbol{\alpha} = q$, which would generally be smaller than p. If this is not the case, then the linearly dependent columns may be arbitrarily omitted.

A reaction route (RR) is defined as an appropriate linear combination of the sequential elementary reaction steps $s_1, s_2, ..., s_p$ that eliminates all of the reaction intermediates, thus resulting in the OR [6]. As mentioned previously, an infinite variety of RRs is possible if no additional restrictions are imposed. Thus, following Milner [7], we require the RRs to be direct: that is, the elementary reaction steps involved in a direct RR (henceforth denoted simply as RR) are minimal. This means that if an elementary reaction is omitted from the given RR, then it becomes impossible to eliminate all of the reaction intermediates by linearly combining the remaining elementary reactions. Milner [7] showed that a RR involves several elementary reaction steps less than or

20

equal to the rank $\alpha +1 = q + 1$, because the number of elementary reaction steps in a RR are independent. Thus, if the selected $q + 1$ steps from among the given set of p elementary reactions are $s_{i1}, s_{i2}, ..., s_{iq}, s_{iq+1}$ where $i_1, i_2, ..., i_q, i_{q+1}$, is a set of integers satisfying the conditions, $1 \leq i_1 < i_2 < ... < i_q < i_{q+1} \leq p$, then the kth reaction route yields(RR-35) $OR = \sum_{h=1}^{q+1} \sigma_{kh} s_{ih}$ or

$$RR_k : -OR + \sum_{h=1}^{q+1} \sigma_{kh} s_{i_h} = 0 \qquad (2.8)$$

(for $k =1, 2, \ldots, Q$)

The total number of possible direct RRs (Q) is less than or equal to the total number of ways of selecting $q + 1$ independent elementary reactions from among a total of p [6].

$$Q \leq \frac{p!}{(q+1)!(p-(q+1))!} \qquad (2.9)$$

Typically, the number of distinct RRs is significantly fewer than this number, as many of the resulting routes end up being redundant due to some reactions having steps that must be included in all RRs.

Fishtik and Datta [8] have shown that the stoichiometric numbers σ_{kh} may be obtained from the intermediates stoichiometric matrix of the chosen $q + 1$ elementary reaction steps from among p for the kth RR, i.e.,

$$
\sigma_{kh} = \begin{bmatrix}
\alpha_{i_1,1} & \alpha_{i_1,2} & \cdots & \alpha_{i_1,q} & 0 \\
\alpha_{i_2,1} & \alpha_{i_2,2} & \cdots & \alpha_{i_2,q} & 0 \\
\vdots & \vdots & \vdots & \vdots & \vdots \\
\alpha_{i_{h-1},1} & \alpha_{i_{h-1},2} & \cdots & \alpha_{i_{h-1},q} & 0 \\
\alpha_{i_h,1} & \alpha_{i_h,2} & \cdots & \alpha_{i_h,q} & 1 \\
\alpha_{i_{h+1},1} & \alpha_{i_{h+1},2} & \cdots & \alpha_{i_{h+1},q} & 0 \\
\vdots & \vdots & \vdots & \vdots & \vdots \\
\alpha_{i_q,1} & \alpha_{i_q,2} & \cdots & \alpha_{i_q,q} & 0 \\
\alpha_{i_{q+1},1} & \alpha_{i_{q+1},2} & \cdots & \alpha_{i_{q+1},q} & 0
\end{bmatrix}
\tag{2.10}
$$

For each RR, the $q + 1$ selected elementary reactions fall into one of three possible scenarios:

1) They are linearly independent and the RR is a *full route* (FR) that produces an OR.

2) They are linearly dependent and the RR is an empty route (ER) or a cycle that results in no terminal species.

3) They are linearly dependent and there are two or more full RRs or ERs that involve a subset of the same $q + 1$ elementary reactions. The resulting RR then is a zero RR, i.e., a RR in which all of the stoichiometric numbers are equal to zero.

Eq. (2.8) may alternatively be written in matrix form, i.e., $\boldsymbol{\sigma s} = 0$, or

$$
\begin{bmatrix}
\sigma_{OR,1} & \sigma_{11} & \sigma_{12} & \cdots & \sigma_{1p} \\
\sigma_{OR,2} & \sigma_{21} & \sigma_{22} & \cdots & \sigma_{2p} \\
\vdots & \vdots & \vdots & \vdots & \vdots \\
\sigma_{OR,Q} & \sigma_{Q1} & \sigma_{Q2} & \cdots & \sigma_{Qp}
\end{bmatrix}
\begin{pmatrix}
s_{OR} \\
s_1 \\
s_2 \\
\vdots \\
s_p
\end{pmatrix}
=
\begin{pmatrix}
0 \\
0 \\
\vdots \\
0
\end{pmatrix}
\tag{2.11}
$$

where $\boldsymbol{\sigma}$ is the reaction route matrix and $\boldsymbol{s} = (s_{OR}, s_1, s_2, \ldots, s_p)^{\mathrm{T}}$ is the reaction vector. The following mathematical theories are known to be applicable for RRs in which the stoichiometric numbers

are +1, -1, or 0. The latter sections will discussion why stoichiometric numbers other than these lead to issues in the matrix manipulations.

The thermodynamic affinities of the OR and the elementary reactions follow the same linear combination, i.e., [6]

$$A_{OR} = \sum_{\rho=1}^{p} \sigma_{k\rho} A_{\rho} = 0 \qquad (2.12)$$

or $\boldsymbol{\sigma s} = 0$, where $\boldsymbol{A}$ is the affinity vector, i.e., $\boldsymbol{A} = (A_{OR}, A_1, A_2, \ldots, A_p)^{\mathrm{T}}$ and A_{OR} represents the affinity of the OR. Alternatively, this may be written in terms of the dimensionless affinity, $\mathscr{A}_{OR} = -\Delta G_{OR} / RT$.

2.1.1 Realization of Reaction Route Graph

The realization of the RR Graph can be achieved through the determination of an incidence matrix, which is essentially a matrix that charts how each node is connect. There are two alternate ways of obtaining the incidence matrix for a RR Graph: either from the RRs matrix or from the overall stoichiometric matrix. In principle, it is possible to construct the RR Graph directly from the RR matrix $\boldsymbol{\sigma}$ by trial and error, because it contains all the graph connectivity information. Thus, the following algorithm may be followed [1]:

Step 1: Derive and select a fundamental RR matrix $\boldsymbol{\sigma}_f$. Rearrange the matrix to the form $\boldsymbol{\sigma}_f = [\boldsymbol{\sigma}_t : \mathbf{I}_l]$ by column interchange. This procedure, thus, simultaneously identifies the links (corresponding to the columns of the identity matrix), with the remaining branches being twigs of the resulting tree selected by the choice of the full and empty RRs. Clearly, there are other possible trees and, thus, $\boldsymbol{\sigma}_f$ is not unique.

Step 2: Obtain the corresponding fundamental cut-set matrix from the relation $\mathbf{X}_f = [\mathbf{I}_{N-1}:-\boldsymbol{\sigma}_t^T]$ for this tree.

Step 3: In view of the fact that $\mathbf{M}_f$ and $\mathbf{X}_f$ are row equivalent, $\mathbf{M}_f$ is obtained from $\mathbf{X}_f$ via elementary row operations such that, at most, each column of the resulting matrix consists of one +1 value and one -1 value, where the remaining values are zeros.

Step 4: Obtain the complete incidence matrix $\mathbf{M}$ from $\mathbf{M}_f$ by adding the missing row, so that the sum of elements is zero in each column.

The same steps can be used to find the incidence matrix based on the stoichiometric matrix, where the transpose of the stoichiometric matrix $\mathbf{v}^T$ is used in place of the cut-set matrix $\mathbf{X}_f$ and the elementary row operations are then performed. This method requires much more trial and error and elementary row operations, so the former method is likely more suitable to computer automation as it directs the algorithm to a closer matrix to the incidence matrix, require less computation time and searching.

This approach does not apply to mechanisms with stoichiometric coefficients other than unity and is not practical for larger, non-linear systems. Thus, a less deterministic method has been developed that relies more on manually piecing the graph together. The first step in this process is the same as the above, in that a fundamental RR Graph matrix is selected from the possible Reaction Routes of the mechanism. It is useful to enumerate all the pathways, (FRs and ERs) as well as the QSS mass balances of the mechanism to be able to check the resulting RR Graph to see if it does, in fact, contain the complete set of RRs. From this enumeration, we select a linearly independent set of routes, typically 1 FR for each overall reaction in the mechanism and the remainder are cycles (ERs). This allows the construction of a subgraph that includes all the cycles,

24

known as a cycle graph, which then easily becomes the completed RR Graph by adding the FRs to the cycle graph by including the ORs.

Obtaining the cycle graph can be difficult, as the steps in each cycle need to be in a particular order, so that certain edges are incident to the same node in the correct direction. The most effective method is to take two cycles and fuse them along an edge that is common in both. For example, in Figure (2.1), the hypothetical ER_1 and ER_2 both share an s_3 edge, so we could then fuse them together along the nodes incident to s_3. This forms a fused graph that has three cycles ER_1 $(+s_1 - s_2 + s_3)$, ER_2 $(+s_3 - s_4 + s_5)$ and a new cycle: $+s_1 - s_2 + s_4 - s_5$. Care must be taken to ensure that any new cycles created are valid. If the sum of the species of the new cycle of $(+s_1 - s_2 + s_4 - s_5)$ do not add to zero, it is not a cycle and the fused graph is not valid and must be discarded, as it does not follow energy balance laws, (i.e. Kirchoff's Potential Law, KPL). It is useful to look for cycles that share multiple steps that proceed in the same direction, as it is more likely that those steps are required to be next to each other in series on the graph. Eventually, through educated guesses and trial and error, one can achieve a valid cycle graph and each of nodes of the graph must be checked to see if they follow mass conservation laws (i.e. Kirchoff's Flux Law, KFL) by being equivalent to a QSS mass balance for a species, or a combination of multiple species QSS mass balance equation. Typically, for systems with mechanisms with stoichiometric coefficients other than unity, a cycle graph will not have balanced nodes unless a mirror image of the cycle graph is fused along the unbalanced nodes. This satisfies the presumption that each step must appear twice in the graph that is symmetric and allows the balancing of most nodes. The remaining FRs can then be added, which is generally trivial as all routes will generally have the steps remaining to be place on the graph and it is not critically to put these steps on the graph in any

particular order, or before or after the cycle graph, although reaction paths may dictate a preference. Chapter 4 provides a detailed of this process for the Oxygen Reduction Reaction.
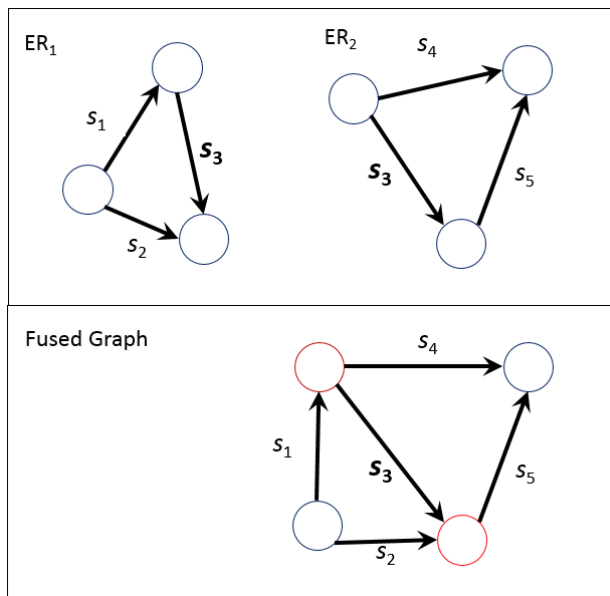
Figure 2.1: Example of a fused cycle graph

2.1.2 Electrical Analogy

Perhaps the most important characteristic of the RR Graphs is that they are analogous to electrical circuits. The laws that govern the behavior of electrical circuits are very well developed and accepted [9], so applying them to chemical reaction networks can be quite beneficial. The two laws of most interest are Kirchoff's Current/Flux Law (KCL/KFL) and Kirchoff's Potential/Voltage Law (KPL/KVL).

KFL states: the step rate r_ρ (likened to edge current I_ρ) of all edges incident at a node j sum up to zero (from mass conservation, along with the fact that $V_{node} = 0$). In other words, $\Delta r_j \equiv \sum_{\rho=1}^{p} v_{\rho i} r_\rho = 0$, where the incidence coefficient $m_{\rho j} = 1$ if an edge leaves the node j, and $m_{\rho j}$

26

$=-1$, if an edge is coming into the node j. In fact, $m_{\rho j}$ are elements of the incidence matrix of the RR Graph [1].

KPL states: the step affinity, i.e., negative Gibbs free energy change for a reaction step, $\mathcal{A}_\rho = -\Delta G_\rho / RT$ (likened to step voltage V_ρ) of all edges in a closed walk (starting and ending at the same node), or a cycle, sum up to zero, i.e., $\sum_{\rho=1}^{P} \sigma_{kj} \mathcal{A}_\rho = 0$, where the stoichiometric number $\sigma_{g\rho} = +1$, if an edge is directed in the direction of the walk around a cycle, and $\sigma_{g\rho} = -1$, if an edge is directed in the opposite direction [1].

Because of the rigorous limitation we apply to RR Graph construction, there is certainty in the consistence with mass and energy conservation laws such as these, which allows us to perform quantitative reaction analysis for the mechanism. Following this electrical analogy, although not essential, each elementary reaction step can also be considered as a resistor in circuit and the overall reaction can be considered as a voltage applied to the circuit, or as the dimensionless affinity $\mathcal{A}_{OR}$.

The resistance of each step (R_ρ) now needs to be established and is defined as the inverse of the net step rate, between its limiting values [1],

$$R_\rho \equiv \frac{1}{\vec{r}_\rho - \overleftarrow{r}_\rho} \int_{\overleftarrow{r}_\rho}^{\vec{r}_\rho} \frac{1}{r_\rho} dr_\rho = \frac{\ln(\vec{r}_\rho / \overleftarrow{r}_\rho)}{\vec{r}_\rho - \overleftarrow{r}_\rho} \tag{2.13}$$

These relations lead the relationship that we refer to as Ohm's Law of Kinetics [1],

$$r_\rho \equiv \frac{\mathcal{A}_\rho}{R_\rho} \tag{2.14}$$

27

This relation is based on the definition of a reaction resistance, which unlike the resistance in electrical circuits, is not a constant, but rather changes with reaction conditions, especially temperature, as the rate (r_p) would almost certainly change with composition and especially with temperature.

Since the RR Graphs are drawn so that they are consistent with KFL and KPL and Ohm's law kinetics representation, there is a quantitative correspondence between RR Graphs and their electrical circuit analogs. As a result, the overall resistance of the network might be calculated in terms of step resistances, with the result that the overall rate may be written as

$$ r_{OR} = \frac{\mathscr{A}_{OR}}{R_{OR}} \tag{2.15} $$

Where R_{OR} is the resistance of all the elementary steps added together as if they were resistors comprising an electrical circuit. This allows the calculation of the overall rate based on known kinetic data. Further, a predicted rate can be approximated *a priori* through Rdot kinetics described next.

2.1.3 Rdot Kinetics

Unfortunately, determining the resistances of chemical reactions through QSS analysis or other methods, analytical or numerical, may not always be practical. However, approximate Rdot resistances of these steps, $R_p^{\bullet}$, can be approximated *a priori* by following the LHHW approach by taking the rate of the forward reaction when that step is considered to be the rate determining step (RDS). For each step we calculate $R_p^{\bullet}$, by considering s_p to be the RDS while others are at quasi-equilibrium (QE), which allows the q linearly independent unknown intermediate site fractions to

28

be determined by identifying the appropriate intermediate reactions (IRs) or pathways for the formation of intermediates. These IRs are found by a linear combination of steps s_j that eliminates all the intermediate species except that of interest, I_k, formed from terminal species along with some reference intermediate, e.g., the vacant site S in case of catalytic reactions [9], i.e.,

$$\sum_{IR_k} \sigma_{kj} s_j = IR_k \tag{2.16}$$

In analogy with KPL, the affinity of this IR_k

$$\sum_{IR_k} \sigma_{kj} \mathscr{A}_\rho = \mathscr{A}_{IR_k} \tag{2.17}$$

Using the definition of step reversibility

$$z_p = \bar{r}_\rho / \vec{r}_\rho = \exp(-\mathscr{A}_\rho) \tag{2.18}$$

we have

$$z_{IR_k} = \prod_{IR_k} (z_j)^{\sigma_{kj}} = \prod_{IR_k} \left(\frac{\bar{r}_j}{\vec{r}_j} \right)^{\sigma_{kj}} \tag{2.19}$$

Applying the step kinetics in terms of step weights, ω_ρ, which is the combined known constants the rate equation for step ρ, usually the rate constants and activity of terminal species, then noting that, all intermediates but I_k and the reference intermediate, i.e., vacant sites S (in case of a catalytic reaction), are eliminated by the stoichiometric numbers chosen to produce the IR

$$z_{IR_k} = \left(\frac{\theta_{k,\rho}^\bullet}{\theta_{0,\rho}^\bullet} \right)^{\gamma_k} \prod_{IR_k} \left(\frac{\bar{\omega}_\rho}{\vec{\omega}_\rho} \right)^{\sigma_{kj}} \tag{2.20}$$

29

Further, if we select all the steps s_j in Eq. (2.31), such that it does not include the step s_ρ under consideration as the RDS, or in other words, all the selected steps are among the QE steps, $z_{IR_k} = 1$, we have

$$\frac{\theta_{k,\rho}^\bullet}{\theta_{0,\rho}^\bullet} = \left\{ \prod_{IR_k} \left(\frac{\vec{\omega}_\rho}{\bar{\omega}_\rho} \right)^{\sigma_{kj}} \right\}^{1/\gamma_k} \qquad (2.21)$$

Note that we use the notation $\theta_{k,\rho}^\bullet$ to represent site fraction of I_k when s_ρ is the RDS. Finally, the site fractions thus calculated are used in the site balance, $1 = \sum_{k=0}^{q} \theta_{k,\rho}^\bullet$, written in the form

$$\frac{1}{\theta_{0,\rho}^\bullet} = \sum_{k=0}^{q} \frac{\theta_{k,\rho}^\bullet}{\theta_{0,\rho}^\bullet} \qquad (2.22)$$

Thus, the reference site fraction $\theta_{0,\rho}^\bullet$ can be determined and, from it, all the remaining site fractions $\theta_{k,\rho}^\bullet$. As a result, the forward rate of the RDS, and hence the step resistance, $R_\rho^\bullet$ as per Eq. (2.13), can be evaluated *a priori*. The next section includes a detailed example of this process.

2.2 Example of RR Graph Analysis for Nonlinear Systems: Hydrogen Oxidation Reaction and Hydrogen Evolution Reaction

An example of RR Graph construction via determination of the incidence matrix for a linear mechanism in solved by Fishtik et al [1]. Here, we illustrate the procedure for a nonlinear mechanism. The mechanism of the hydrogen oxidation reaction (HOR) and its reverse, the hydrogen evolution reaction (HER), is an example of a mechanism that is important to the understanding of fuel cell performance and has been extensively researched to determine the pathways and kinetics [10-24]. Vilekar et al. [25] was able to apply the RR Graph approach to this

reaction network to both validate and explained the understood dual-pathway kinetics as well as develop an accurate rate expression, which is an excellent demonstration of the process of the RR Graph approach

The mechanism used for this research is the well accepted mechanism based on the Tafel, Volmer, Heyrovsky steps [26-28]. Table (2.1) and Table (2.2) for basic and acidic electrolytes respectively, show the Volmer (s_V), Tafel (s_T) and Heyrovsky (s_H) steps along with the coefficient of that step the corresponds to one of the three pathways (VT, VH and HT) for both alkaline and acidic medium.

	Elementary Reactions	$\sigma_{VT,\rho}$	$\sigma_{VH,\rho}$	$\sigma_{HT,\rho}$
s_V:	$H{\cdot}S + OH^- \rightleftarrows H_2O + S + e^-$	+2	+1	
s_T:	$H_2 + 2S \rightleftarrows 2H{\cdot}S$	+1		-1
s_H:	$H_2 + S + OH^- \rightleftarrows H_2O + H{\cdot}S + e^-$		+1	+2
s_{OR}:	$H_2 + 2OH^- \rightleftarrows 2H_2O^+ + 2e^-$			

Table 2.1: HOR mechanism in alkaline electrolyte [26-28]

	Elementary Reactions	$\sigma_{VT,\rho}$	$\sigma_{VH,\rho}$	$\sigma_{HT,\rho}$
s_V:	$H{\cdot}S + H_2O \rightleftarrows H_3O^+ + S + e^-$	+2	+1	
s_T:	$H_2 + 2S \rightleftarrows 2H{\cdot}S$	+1		-1
s_H:	$H_2 + S + H_3O^+ \rightleftarrows H_3O^+ + H{\cdot}S + e^-$		+1	+2
s_{OR}:	$H_2 + 2H_2O \rightleftarrows 2H_3O^+ + 2e^-$			

Table 2.2: HOR mechanism in acidic electrolyte [26-28]

These pathways shown can be considered as full routes (FRs) and along with an empty route (ER) that must exist, these routes must exist within the RR Graph. Those route are enumerated as such [25]:

$$FR_{VH}: (+1)s_V + (+1)s_H - s_{OR} = 0 \qquad (2.23)$$

$$FR_{VT}: (+2)s_V + (+1)s_T - s_{OR} = 0 \qquad (2.24)$$

$$FR_{HT}: (+1)s_H + (-1)s_T - s_{OR} = 0 \qquad (2.25)$$

$$ER_1: (+1)s_V + (-1)s_H + (+1)s_T = 0 \qquad (2.26)$$

However, for this 3 elementary step mechanism with 1 independent intermediate, only $\mu = q - p = 3 - 1 = 2$ routes are linearly independent and a set of only 2 of these reaction routes is needed to construct the RR Graph. Since the graph must follow KFL we must also consider any quasi-steady state (QSS) conditions. In this example with only one intermediate, there is only one QSS condition: $Q_{HS}: (-2)r_T + (+1) r_V + (-1) r_H = 0$. We can now start constructing the RR Graph by selecting FR_{VH} and ER_1 as our set of independent routes. We find the best method is to create a graph containing all the cycles (ERs) and, in this case for which there is a stoichiometric coefficient of 2 in the mechanism, the cycle graph must contain 2 of each elementary reaction step. Typically, this is achieved by mirroring the cycle graph and fusing nodes in such a way that the QSS conditions are satisfied for those fused nodes. We note that by fusing ER_1 with its mirror along the edge of s_T that it creates two nodes that satisfy the QSS condition of $(2)s_T$ and $(1)s_H$ edges entering a node and $(1)s_V$ leaving the same node (as well as the reverse of that condition). Thus, the cycle graph is found and FR_{VH} is then added to complete the RR Graph (Figure 2.2).

All three pathways and the single ER can be traced on this graph as walks and the QSS conditions are satisfied, thus we find that this graph satisfies all the conditions of a completed and valid RR Graph. [25]
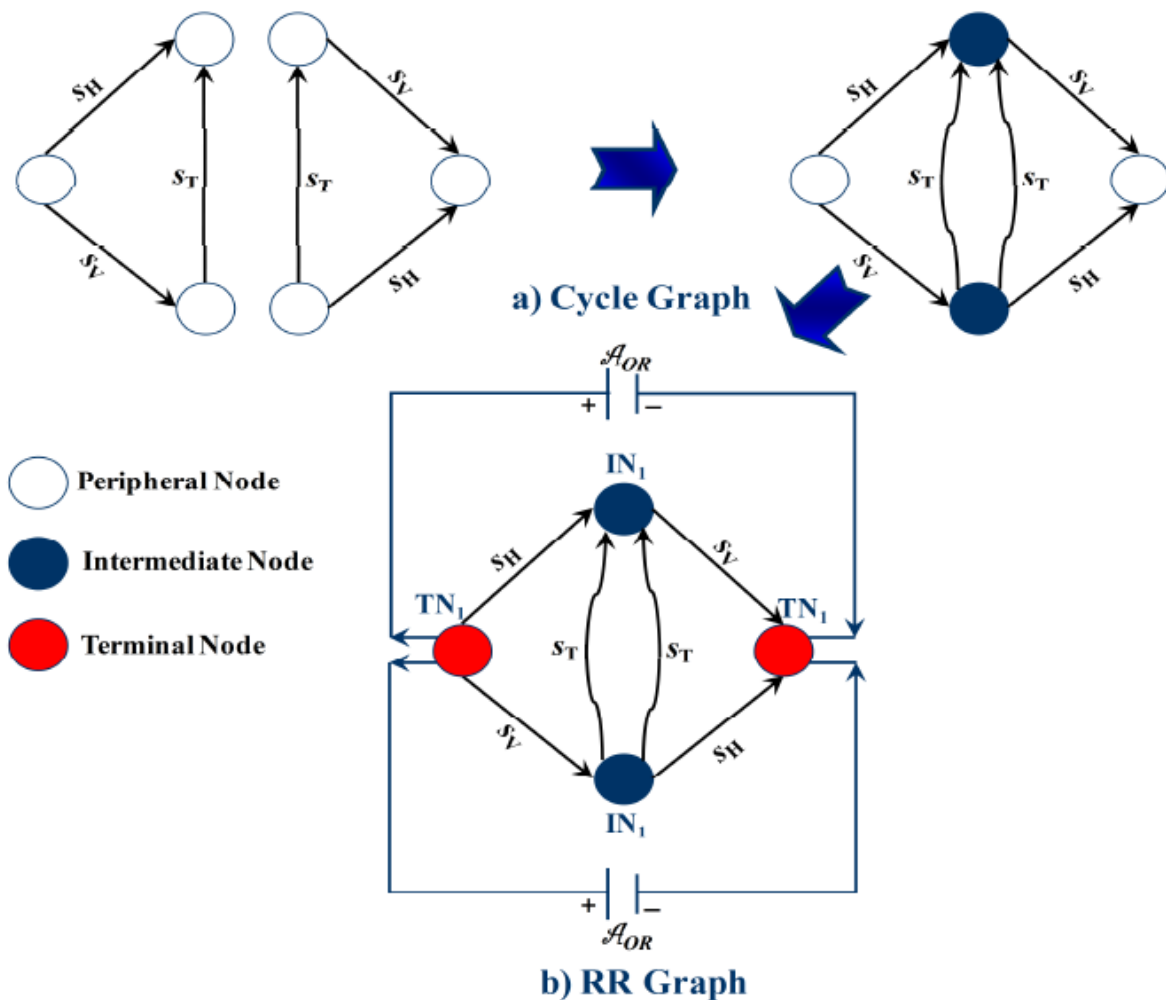
Figure 2.2: RR Graph construction for the 3-step HOR/HER mechanism.

We can now analyze the reaction network using the electrical analogy and Rdot kinetics explained in Chapter 2.1.3 and 2.1.4. Following the electrical analogy, we treat each reaction step as a resistor in an electrical circuit and the overall rate of the reaction (r_{OR}) can be expressed as:

$$2r_{OR} = \frac{\mathcal{A}_{OR}}{R_{OR}} \tag{2.27}$$

33

The rate on the left-hand side of has been doubled since the network involves the OR twice. The overall resistance R_{OR}, can be obtained by adding the resistances of each step together in the same manner as if it were an electrical circuit. Utilizing a Δ-Y conversion [29, 30], the overall resistance for the network in Figure (2.2) is equal to [25]:

$$R_{OR} = \frac{R_T R_V + R_H (R_T + 4R_V)}{(R_T + R_V + R_H)} \tag{2.28}$$

which are found from numerical analysis.

The step resistances can alternately be found *a priori* by utilizing the Rdot kinetics detailed in section 2.1.4, based on the step weights of the elementary steps. The step kinetics for this elementary reaction rates are [25]

$$r_T = \vec{\omega}_T (1 - \theta_{H \cdot S})^2 - \bar{\omega}_T \theta_{H \cdot S} \tag{2.29}$$

$$r_V = \vec{\omega}_V \theta_{H \cdot S} - \bar{\omega}_V (1 - \theta_{H \cdot S}) \tag{2.30}$$

$$r_H = \vec{\omega}_H (1 - \theta_{H \cdot S}) - \bar{\omega}_H \theta_{H \cdot S} \tag{2.31}$$

where the site balance, $\theta_0 + \theta_{HS} = 1$, has been substituted to eliminate θ_0 from the equations. The step weights in the above equation set may be written as [25]

$$\vec{\omega}_T = \vec{k}_T a_{H_2} \qquad \bar{\omega}_T = \overleftarrow{k}_T \tag{2.32}$$

$$\vec{\omega}_T = \vec{\omega}_{V,0} e^{\psi} \qquad \bar{\omega}_V = \bar{\omega}_{V,0} e^{-\psi} \tag{2.33}$$

$$\vec{\omega}_H = \vec{\omega}_{H,0} e^{\psi} \qquad \bar{\omega}_H = \bar{\omega}_{H,0} e^{-\psi} \tag{2.34}$$

34

where we introduce the dimensionless electrode overpotential, $\psi = \dfrac{1}{2}\dfrac{F\eta}{RT}$. Further, for the case of alkaline electrolytes, the parameters above, in terms of the rate constants at equilibrium electrode potential and the activities of the terminal species, are [25]

$$\vec{\omega}_{V,0} = \vec{k}_{V,\Phi_0} a_{OH^-} \qquad\qquad \bar{\omega}_{V,0} = \bar{k}_{V,\Phi_0} a_{H_2O} \tag{2.35}$$

$$\vec{\omega}_{H,0} = \vec{k}_{H,\Phi_0} a_{OH^-} a_{H_2} \qquad\qquad \bar{\omega}_{H,0} = \bar{k}_{H,\Phi_0} a_{H_2O} \tag{2.36}$$

Furthermore, in these expressions, the activity of water is usually assumed to be unity, i.e., $a_{H_2O} = 1$, for saturated conditions, while the activity of hydrogen is written as its partial pressure, i.e., $a_{H_2} = p_{H_2}$, in atm.

Following the Rdot method, the resistance of each step are now calculate $R_\rho^\bullet$ as the resistance of the step s_ρ when it is the rate-determining step (RDS), with all other steps are at quasi-equilibrium. $R_{OR}^\bullet$ can next be calculated *a priori* following the LHHW approach explained in Chapter 2.1.4. Thus, for s_T, we find [25]

$$R_T^\bullet = \frac{1}{\vec{r}_T^\bullet} = \frac{1}{\bar{\omega}_T (\theta_{0,T}^\bullet)^2} \tag{2.37}$$

The intermediate route to isolate H·S is IR$_{H \cdot S}$= (+1)sv. Using Eq. (2.29), we thus have $\theta_{H \cdot S,T}^\bullet / \theta_{0,T}^\bullet = \bar{\omega}_V / \vec{\omega}_V$. Then, Eq. (2.30) gives us $1/\theta_{0,T}^\bullet = 1 + \bar{\omega}_V / \vec{\omega}_V$ and substituting into Eq. (2.37) we obtain [25]

$$R_T^\bullet = \frac{1}{\bar{\omega}_T}\left(1 + \frac{\bar{\omega}_V}{\vec{\omega}_V}\right)^2 = \frac{1}{\bar{\omega}_T}\left(1 + \frac{\bar{\omega}_{V,0}}{\vec{\omega}_{V,0}} e^{-2\psi}\right)^2 \tag{2.38}$$

Following the same process for s_H and s_V, we obtain [25]

$$R_H^\bullet = \frac{1}{\vec{\omega}_{H,0}e^\psi}\left(1 + \frac{\tilde{\omega}_{V,0}}{\vec{\omega}_{V,0}}e^{-2\psi}\right) \tag{2.39}$$

$$R_V^\bullet = \frac{1}{\vec{\omega}_{V,0}e^\psi}\left(1 + \frac{\tilde{\omega}_{H,0}}{\vec{\omega}_{H,0}}e^{-2\psi}\right) \tag{2.40}$$

This allows us to obtain an expression for $R_{OR}^\bullet$ and r_{OR}, where $r_{OR} = E_{OR}/R_{OR}^\bullet$, which can then yield an expression for current density $i = v_{OR,e^-}Fr_{OR}$ where r_{OR} is in units of mol cm^{-2} s^{-1} and v_{OR,e^-} is the stoichiometric coefficient of electrons in the overall electrode reaction. Thus we have [25]

$$i = \frac{v_{OR,e^-}F(e^{2\psi} - e^{-2\psi})}{e^{2\psi}(2R_{OR}^\bullet)} \tag{2.41}$$

Then substituting for the expression for $R_{OR}^\bullet$ in Eq. (2.41)

$$i = \frac{v_{OR,e^-}F}{e^{2\psi}}\frac{(R_T + R_V + R_H)}{R_T R_V + R_H(R_T + 4R_V)}(e^{2\psi} - e^{-2\psi}) \tag{2.42}$$

Using the step resistances and simplification results in an explicit equation for the current density

$$i = \frac{(v_{OR,e^-}F)\vec{\omega}_T\vec{\omega}_{V,0}^2\left\{1 + \frac{\tilde{\omega}_{H,0}}{\vec{\omega}_T\vec{\omega}_{V,0}}(\vec{\omega}_{V,0}e^\psi + \tilde{\omega}_{V,0}e^{-\psi}) + \frac{\tilde{\omega}_{H,0}e^\psi + \tilde{\omega}_{H,0}e^{-\psi}}{\vec{\omega}_{V,0}e^\psi + \tilde{\omega}_{V,0}e^{-\psi}}\right\}(e^{2\psi} - e^{-2\psi})}{(\vec{\omega}_{V,0}e^\psi + \tilde{\omega}_{V,0}e^{-\psi})^2 + (\vec{\omega}_{H,0}e^\psi + \tilde{\omega}_{H,0}e^{-\psi})\left\{\frac{4\vec{\omega}_T\vec{\omega}_{V,0}}{\vec{\omega}_{H,0}} + (\vec{\omega}_{V,0}e^\psi + \tilde{\omega}_{V,0}e^{-\psi})\right\}} \tag{2.43}$$

This was the first explicit rate expression in the literature to ever include the kinetics of all three accepted reaction pathways [25].

It is of great interest, however, to discern whether or not each pathway is significant to the overall reaction. For the case of the HER in alkaline medium, kinetic data based on fitted experimental rate data from literature is available for Pt catalyst in 0.5M NaOH solution at 296K (Tables 2.3 & 2.4) [31, 32]. From this data we can plot $1/R_\rho^\bullet$ versus overpotential η (Figure 2.4). This plot shows the Volmer step to be the fastest over the calculated range, but the other steps may be rate-limiting over a subset of the range.

	Elementary Reactions	$\vec{k}_{\rho,\Phi_0}$	$\overleftarrow{k}_{\rho,\Phi_0}$
s_T:	$H_2 + 2S \rightleftarrows 2H \cdot S$	$\vec{k}_T = 8.8 \times 10^{-10}$	$\overleftarrow{k}_T = 8.8 \times 10^{-10}$
s_V:	$H \cdot S + OH^- \rightleftarrows H_2O + S + e^-$	$\vec{k}_{V,\Phi_0} = 4.4 \times 10^{-7}$	$\overleftarrow{k}_{V,\Phi_0} = 4.4 \times 10^{-8}$
s_H:	$H_2 + S + OH^- + e^- \rightleftarrows H_2O + H \cdot S + e^-$	$\vec{k}_{H,\Phi_0} = 2.4 \times 10^{-10}$	$\overleftarrow{k}_{H,\Phi_0} = 2.4 \times 10^{-9}$

Table 2.3: Reaction rate constants for HER on Pt in 0.5M NaOH at 296 K [31].

Finally, Figure 2.3 provides QSS rates for the HOR/HER mechanism in alkaline medium obtained numerically by solving the KFL relations for each of the three two-step mechanisms as well for the case of the 3-step mechanism. It is evident that the HT mechanism is not a significant contributor over any part of the range of overpotentials considered here for the alkaline system. Furthermore, the VH and VT mechanisms have a limited range of potentials where either is the sole dominant mechanism.

Figure 2.3 also plots the rate obtained from the explicit rate expression for the complete 3-step mechanism based on QSS relations. Although the results of these expressions are approximations, they are highly accurate as shown in comparison with the QSS numerical results over the entire range of potentials of interest for both HOR and HER. Clearly, the expression is

adequate in the overpotential range of $-0.3\,\text{V} < \eta < -0.24\,\text{V}$ for HER and $0.13\,\text{V} < \eta < 0.3\,\text{V}$ for HOR in the alkaline system.

Further, there is a great asymmetry in the Volmer-Tafel mechanism, described by the form of the denominator in the expression (Eq. 2.43). This mechanism is important for HER in an alkaline system in the overpotential range of $-0.1\,\text{V} < \eta < 0\,\text{V}$. $-0.1\,\text{V} < \eta < 0\,\text{V}$. For HOR in an alkaline system, the VT mechanism is only applicable in a narrow overpotential range of $0 < \eta < 20\,\text{mV}$.

Finally, for the kinetic data provided in Figure 2.4, this relation provides an exchange current density of $i_0 = 1.7 \times 10^{-4}\,\text{A cm}^{-2}$ for HER on Pt in 0.5M NaOH at $T = 296$ K. This value compares well with that predicted using the correlation provided by Chiavlo et al. [31] based on an extension of the Temkin development for a single reaction route. Others have also suggested i_0 to be $\sim 10^{-4}\,\text{A cm}^{-2}$ on Pt for alkaline electrolytes [24].

The RR Graph approach thus allows the visualization of the pathways for the HER/HOR and it enables the determination of an explicit rate equation that incorporates all three of these pathways, which is not possible with conventional chemical analysis techniques. Through the Rdot method, the rate and current density can be determined *a priori* with the appropriate kinetic data and given the conditions of the reaction.
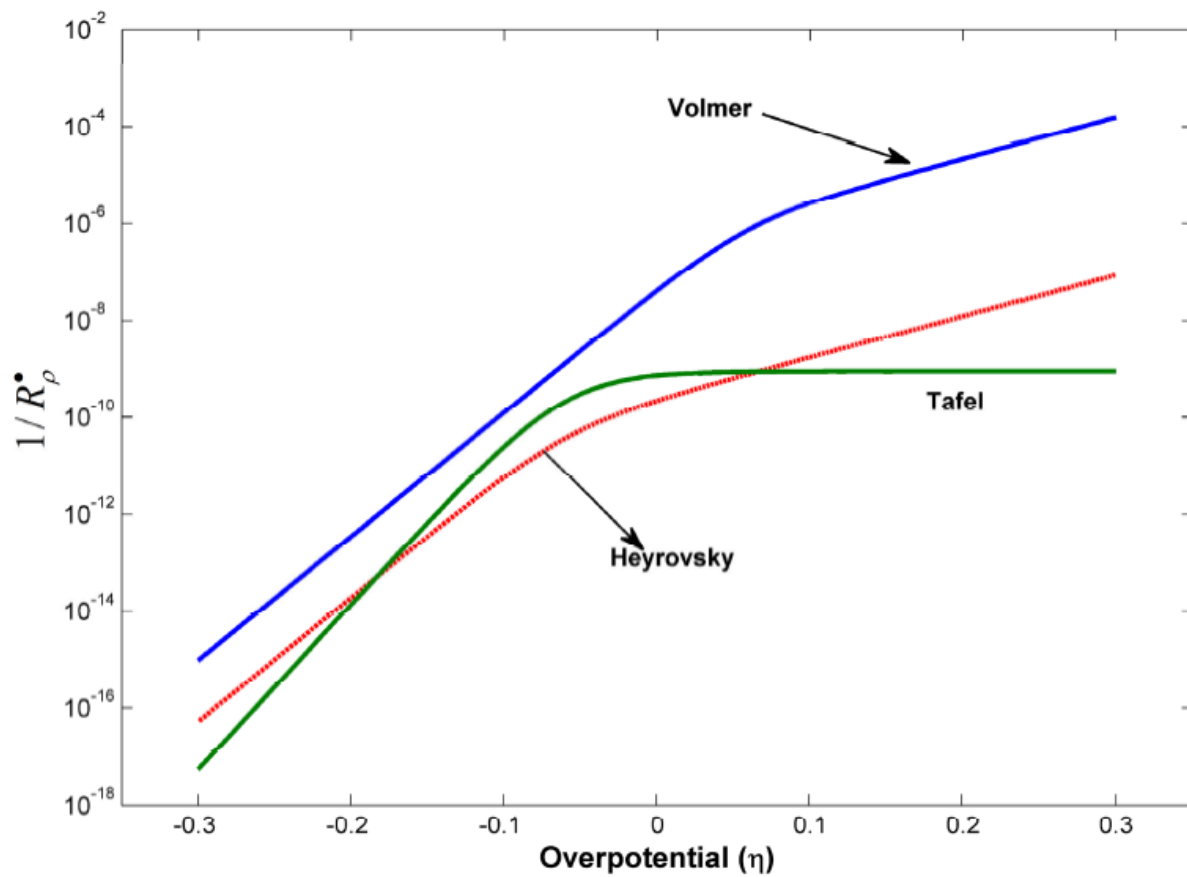
Figure 2.3: Semilog plot of vs. $R_\rho^\bullet$ overpotential, η (V) for hydrogen electrode reaction on Pt in alkaline medium. [25]
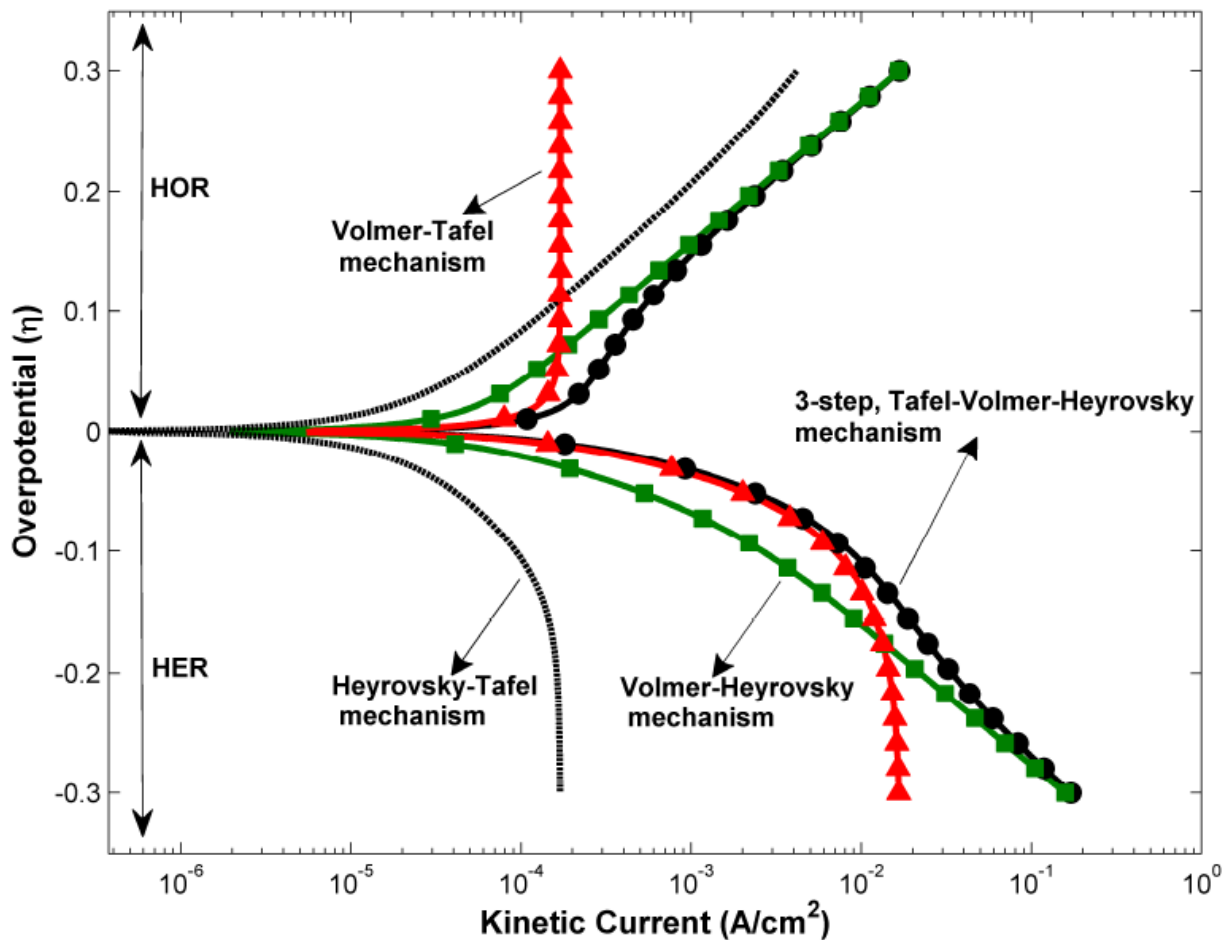
Figure 2.4: Semilog plot of overpotential (V), η vs. absolute value of kinetic current, i for hydrogen electrode reaction on Pt in alkaline medium. Solid lines represent data obtained from solving QSS equation for the 3-step Tafel-Volmer-Heyrovsky (black) mechanism and each of the 2-step mechanism, namely, Volmer-Heyrovsky (green), Volmer-Tafel (red) and Heyrovsky-Tafel (dotted, black) mechanism, while symbols represent calculations from Ohm's law. ● 3-step mechanism, ■ 2-step Volmer-Heyrovsky mechanism Eq. (8.49), ▲ 2-step Volmer-Tafel mechanism. [25]

2.4 Additional Reaction Systems

Next are described two further examples of reaction systems of a complicated nature for which the RR Graph approach can provide insights into the kinetics and mechanism. The first example is the oxygen reduction reaction (ORR) that has relatively few steps, but is of current interest as there is a need to search several catalysts to optimize costs and activity for the reaction. The latter considers a nitrous oxide decomposition mechanism that consists of over one hundred elementary steps that is difficult to analyze due to its sheer size and is considered in more detail in Chapter 6. Analyzing these cases will further demonstrate the breadth of the capabilities of the RR Graph approach and highlight the points of the graph construction we require a further understanding to automate the process of generating these graphs.

2.4.1 Oxygen Reduction Reaction

The ORR is an important reaction to understand the operation and optimization of a fuel cell. This reaction occurs at the cathode side of the fuel cell and is a large factor in the performance of the cell due to the significant overpotential for this reaction. Even for an expensive catalyst where the kinetics are very favorable such as platinum, there is still a large energy loss at this step of the fuel cell process. Therefore, there is significant value is finding a cheaper and/or better catalyst for this reaction. A deeper understanding of the mechanism and its kinetics would greatly assist the process of selecting this catalyst. Unfortunately, the ORR reaction mechanism is difficult to analyze due to the complexity of the associated multielectron transfer and its dependence on the electrode material and electrolyte. Rotating-ring disk electrode has been widely employed to probe the ORR mechanism and kinetics.

Many studies have been done to develop a comprehensive mechanism for the pathways of the ORR reaction [49-58]. The pathways proposed by these work that are considered feasible are listed as such [58]:

1) The *dissociative* mechanism, which involves the dissociation of O_2 followed by the hydrogenation of adsorbed O and OH to water.

2) The *peroxyl* mechanism, which involves the formation of OOH, followed by O-O bond scission to yield adsorbed OH and O.

3) The *peroxide* mechanism, which involves the hydrogenation of OOH to HOOH, which either desorbs or undergoes O-O bond scission.

4) The *aquoxyl* mechanism, which involves adding an additional H atom to OOH, which then undergoes O-O bond scission.

Each of these mechanisms may or may not be significant for a particular catalyst, thus for the evaluation of a new catalyst each of them must be considered to be feasible.

Vilekar [60] has studied this reaction based on a simple 4-step reaction mechanism on Pt catalyst proposed by Wang et al. [57] (Table 2.6) and considers only the dissociative mechanism, either through a 2 step pathway FR_1 ($s_1 + s_4$) or a 3 step pathway: FR_2 ($s_1 + s_2 + s_3$). Other pathways are excluded because of the intermediate species considered for this catalyst and conditions are not stable enough [51, 53, 59]. Vilekar [60] was able to apply the RR Graph theory and construct an RR Graph (Figure 2.5) from which a predictive rate equation and an equation for the electrode current density (i) using the Rdot method was obtained (Eqs. 2.40 & 2.41) that shows good agreement with experimental results (Figure 2.6).

$$r_{OR} \approx \frac{E_{OR}}{R_{OR}^\bullet} = \frac{E_{OR}}{R_4^\bullet + \cfrac{1}{\cfrac{1}{R_2^\bullet} + \cfrac{1}{R_1^\bullet + R_3^\bullet}}} \tag{2.40}$$

$$i = v_{OR,e^-} F r_{OR} = \frac{v_{OR,e^-} F(1 - z_{OR})}{R_4^\bullet + \cfrac{1}{\cfrac{1}{R_2^\bullet} + \cfrac{1}{R_1^\bullet + R_3^\bullet}}} \tag{2.41}$$

In Chapter 4, a new RR Graph analysis is presented using the more detailed mechanism proposed by Herron et al. [49] seen in Table 2.5. Several different catalysts are considered and their activities are evaluated over a range of temperatures and electrical overpotential with the goal of providing a tool to easily quantify the activity of a catalyst for which the kinetic data is available. Future analysis may be performed based on more extensive mechanisms as proposed by Ford et al. [58] that included all of the previously mentioned pathways.

	Elementary Reactions
s_1:	½ O_2 + S $\rightleftarrows$ O·S
s_2:	½ O_2 + H^+ + e^- + S $\rightleftarrows$ OH·S
s_3:	O·S + H^+ + e^- $\rightleftarrows$ OH·S
s_4:	OH·S + H^+ + e^- $\rightleftarrows$ H_2O

Table 2.4: 4-step ORR reaction mechanism on Pt(111) in acidic medium [57]

Elementary Reactions	
s_1:	$O_2 + 2S \rightleftarrows 2O{\cdot}S$
s_2:	$O{\cdot}S + H^+ + e^- \rightleftarrows OH{\cdot}S$
s_3:	$OH{\cdot}S + H^+ + e^- \rightleftarrows H_2O + S$
s_4:	$O_2 + H^+ + e^- \rightleftarrows OOH{\cdot}S$
s_5:	$OOH{\cdot}S + S \rightleftarrows O{\cdot}S + OH{\cdot}S$
s_6:	$OOH{\cdot}S + H^+ + e^- \rightleftarrows HOOH{\cdot}S$
s_7:	$HOOH{\cdot}S + S \rightleftarrows 2OH{\cdot}S$

Table 2.5: 7-step ORR reaction mechanism [49]
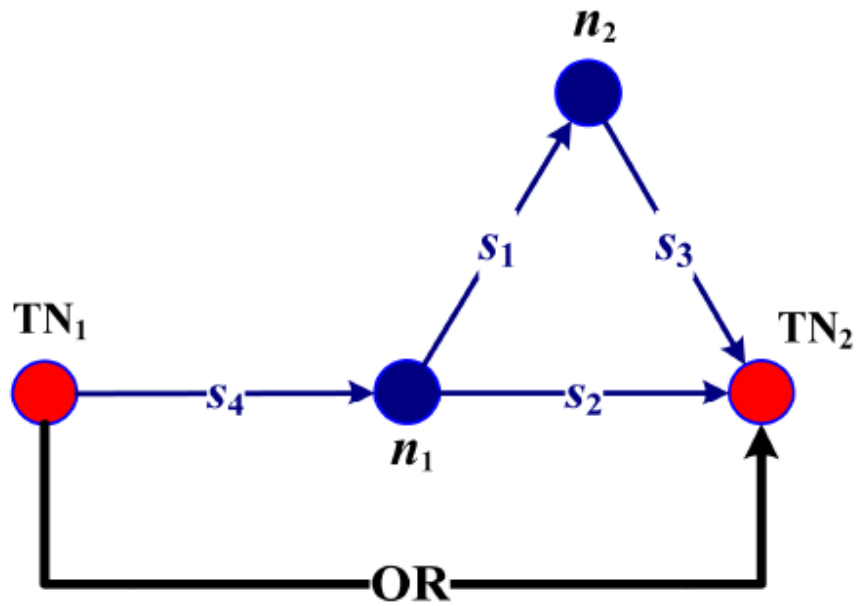
Figure 2.5: RR Graph for the 4-step ORR mechanism [25]
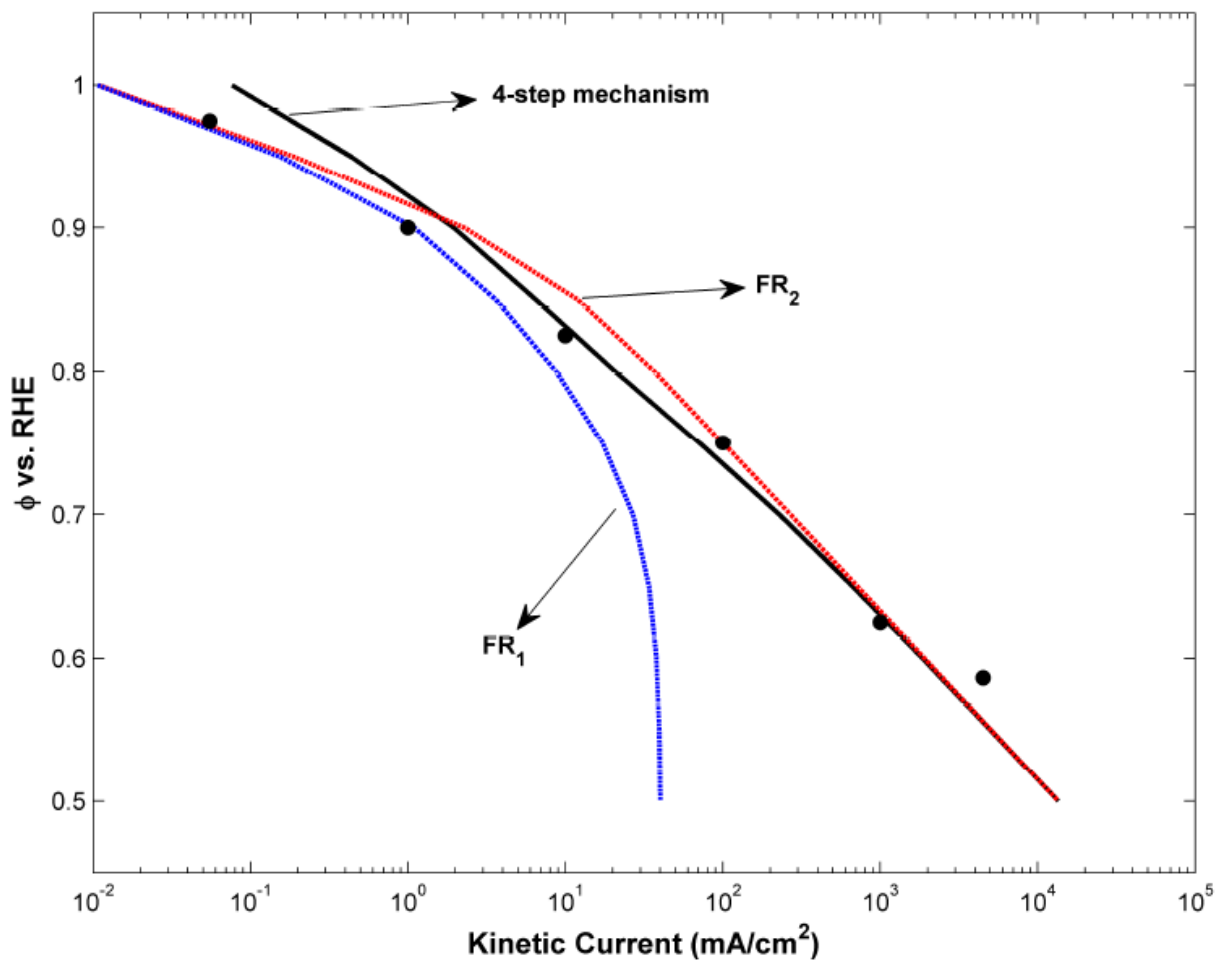
Figure 2.6: Potential (V) vs. kinetic current for ORR on Pt electrode in 0.1 M HClO₄ solution. Symbols (●) represent the experimental data [25]. Solid line represents kinetic current for the 4-step mechanism from Ohm's law (Eq. (8.77)). Dotted lines represent the kinetic current for the limiting case via FR_1 (blue) and FR_2 (red) [25]

2.4.1 N$_2$O Decomposition on Fe-ZSM-5 catalyst

Nitrous oxide (N$_2$O) decomposition briefly discussed in Chapter 1, is an increasingly important reaction as emission standards are steadily getting tighter and for good reason as nitrous oxide is considered one the most harmful greenhouse gases. Nitric acid plants are the largest contributor to atmospheric nitrous oxide and introducing a catalytic decomposition stage in the process can greatly reduce the nitrous oxide emission from the plant [61]. Understanding the kinetics of this reaction will facilitate the selection of the most effective catalyst and make progress towards the complete remove of nitrous oxide emission.

Heyden et al. have proposed a 104 step mechanism for the decomposition of nitrous oxide on an iron zeolite catalyst (Fe-ZSM-5) [62]. This research provides a rigorous analysis of the energy and transition states of the intermediates for this mechanism. An impressive amount of work was done to produce a comprehensive list of the kinetic data for each reaction step through DFT. The full mechanism is included and discussed further in Chapter 6 (Table 6.2), although a full RR Graph could not be drawn.

Several individual pathways of this mechanism are analyzed in detail, but could still benefit from the RR Graph approach. The most important goal would be to visualize the pathways of the reaction or an RR Graph and enable the quantitative analysis of all the pathways simultaneously through the Rdot approach. If the mechanism could further be reduced significantly, it would provide great insight to the steps which determine the direction and magnitude of the reaction network.

2.4 Other Reaction Graphs and Their Limitations

The idea of representing a network of chemical reactions as a graph is not a novel idea, other efforts to visualize reaction pathways have been attempted. However, they invariably adopt

the approach that each node represents a specific species, in direct analogy with reaction schematics drawn conventionally. Representing the nodes in this way is fine for monomolecular mechanisms or for some network visualization, but they do not allow the same rigorous analysis that RR Graphs provide. They simply do not follow both KFL and KPL which means that they violate basic mass and energy conservation laws.

One example that is used for biological networks (such as Figure 2.7) is the concept of elementary modes and extreme pathways as proposed by Schuster *et al.* [36, 37] and Palsson *et al.* [36-38]. These methods use nodes to represent individual species and directed arrows to represent reactions steps. Further, they make use of an algebraic stoichiometric algorithm, developed by Happel and Sellers [40], to enumerate their pathways, with some special constraints, in addition to flux analysis. The pathways enumerated by Schuster *et al.* [36, 37] are known as "elementary modes," that is, they contain a minimal number of steps, and are, in fact, simply the "direct" pathways of Milner [41]. Palsson *et al.* [36, 38] additionally consider reaction steps that are irreversible, so that pathways in which the step may be traversed in the opposing direction are discounted, the resulting pathways being labeled "extreme pathways." In addition to a substantial preoccupation with pathway enumeration by these groups, other investigators have been concerned with thermodynamic consistency [39] and flux analysis [42]. A schematic diagram of the chemical pathways (Figure 2.9) is another such method that does not have a comprehensive depiction of all the pathways, but is useful for visualizing some of the major pathways [43] along with some understanding of the chemistry of the mechanism.
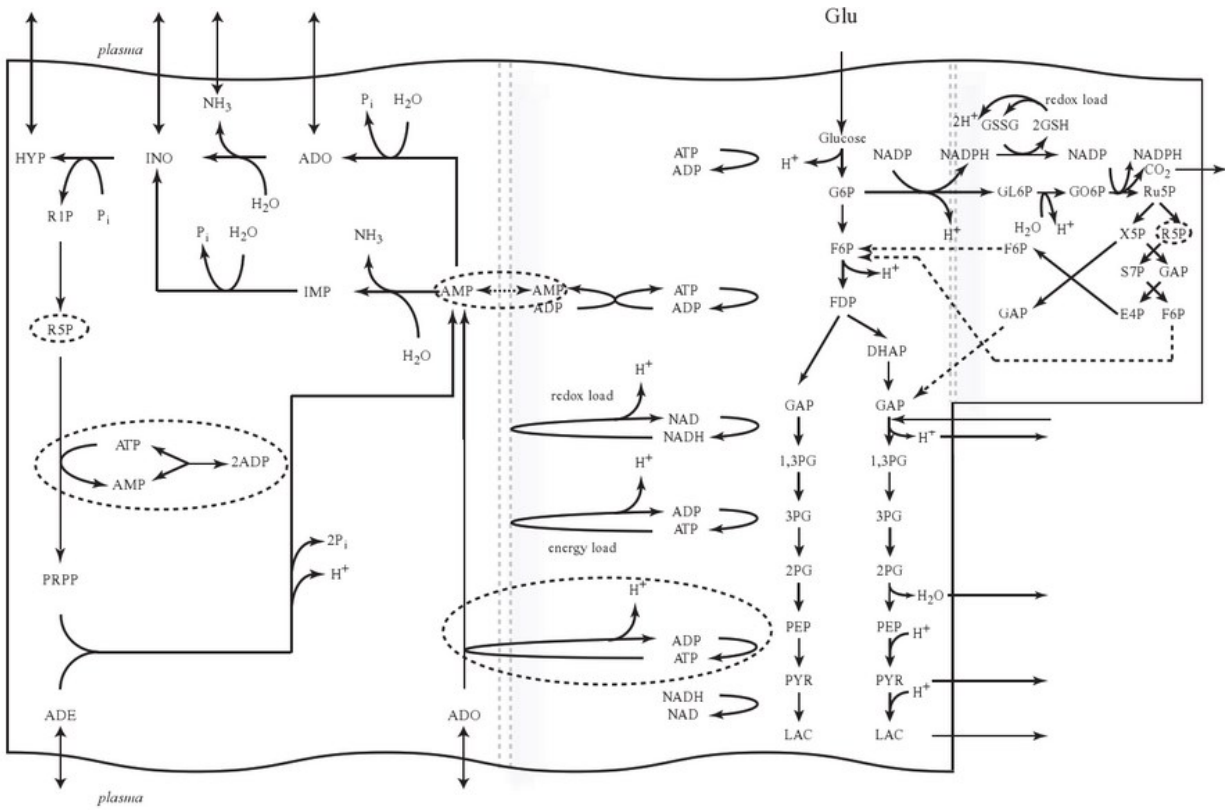
Figure 2.7: An example of a network proposed by of the core metabolic network in the human red blood cell comprised of glycolysis, the pentose pathway, and adenine nucleotide metabolism. [42]
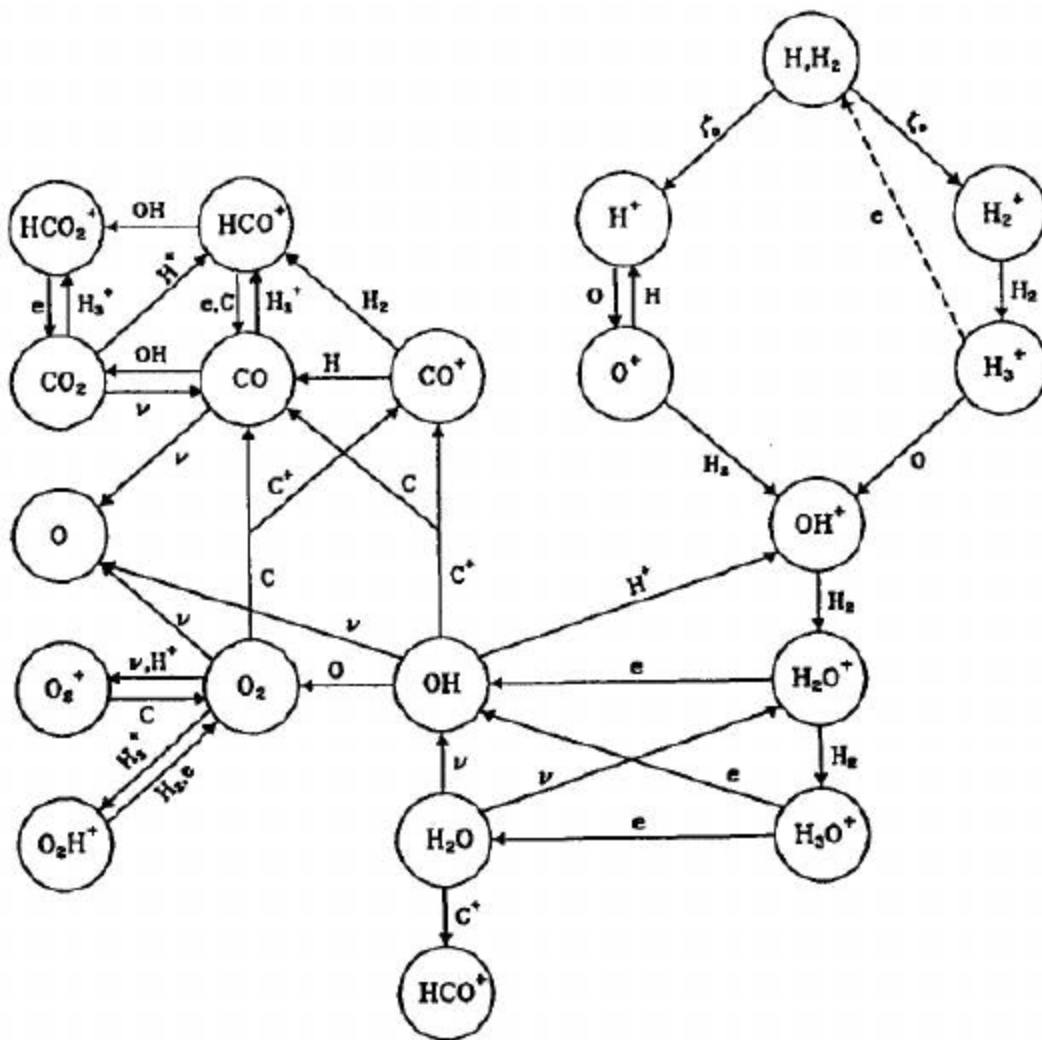
Figure 2.8: Example of a Chemical Pathway graph [43]

One of the more prominent of these alternate graph techniques being developed is the idea of a P-graph (or process graphs) proposed by Fan et al [34]. These graphs are focused mainly on pathway enumeration, and are directed bipartite graphs which use circles for representing an active species, node and horizontal bars for representing elementary-reaction step nodes with direct arcs linking them [34]. An example of a P-graph is shown in (Figure 2.9). Creating a P-graph involves following an algorithm to find a set of reaction steps that are connected through graph theory calculations [44, 45]. Similar to RR Graph construction, the idea of finding smaller subgraphs to

combine into larger graphs. However, P-graphs do not include the idea of maintaining thermodynamically consistent cycles, so instead of focusing on fusing cycle graphs, the approach more closely resembles a tree branching out.
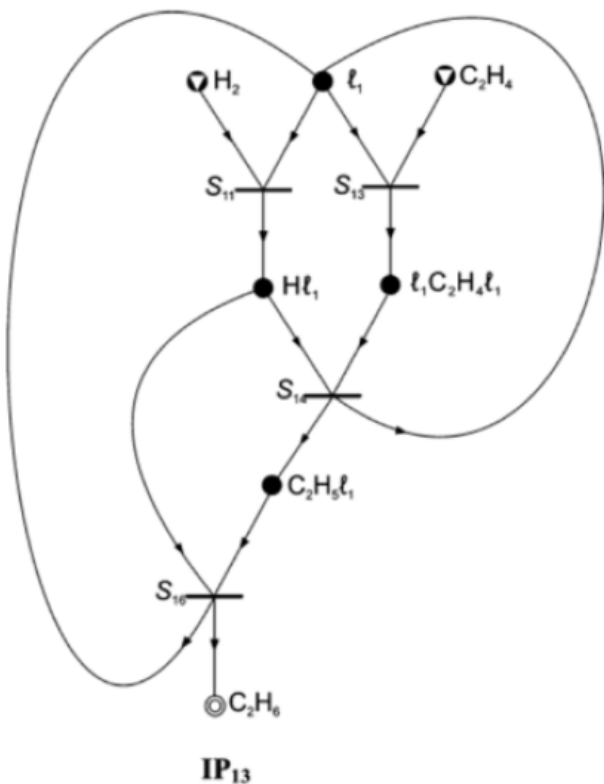
Figure 2.9: Example of a P-graph of the reaction $H_2 + C_2H_4 \rightarrow C_2H_6$ by Fan et al. [44]

In detail, the graph is determined through a deterministic approach included here [44]: Let O be the set of elementary-reaction steps and M be the set of chemical or active species under consideration; then, $O \subseteq \mathcal{P}(M) \times \mathcal{P}(M)$, where $O \cap M = \emptyset$. If (α, β) is a reaction step, i.e. $(\alpha, \beta)\epsilon O$, then α is called the input set, and β, the output set of the step. Pair (M, O) is termed a P-graph with the set of vertices $M \cup U$ and the set of arcs $\{(x, y): y=(\alpha, \beta)\epsilon O$ and $x\epsilon \alpha\} \cup \{(y, x): y=(\alpha, \beta)\epsilon O$ and $x\epsilon\beta\}$. P-graph (M, O) is identified to be a subgraph of (M', O'), i.e. $(M, O)\subseteq(M', O')$, if $M \subseteq M'$ and $O \subseteq O'$. The union of P-graphs (M_1, O_1) and (M_2, O_2) results in the P-graph $(M_1 \cup M_2, O_1 \cup O_2)$. The resulting P-graph represents a reaction network which starts from

50

reactants (precursors) to final products (targets). The graph is considered to be a *feasible reaction pathway* if it follows the six axioms proposed by Fan et al. [44, 47]:

(R1) Every final product (target) is totally produced by the reaction steps represented in the pathway.

(R2) Every starting reactant (precursor) is totally consumed by the reaction steps represented in the pathway.

(R3) Every active intermediate produced by any reaction step represented in the pathway is totally consumed by one or more reaction steps in the pathway, and every active intermediate consumed by any reaction step represented in the pathway is totally produced by one or more reaction steps in the pathway.

(R4) All reaction steps represented in the pathway are defined a priori.

(R5) The network representing the pathway is acyclic.

(R6) At least one elementary-reaction step represented in the pathway activates a starting reactant (precursor).

These axioms represent a consistence to mass balance laws, similar to KFL. Additionally, the graph is considered to be *combinatorially feasible* if it follows the included seven other axioms proposed by Fan et al [44, 47]:

(T1) Every final product (target) is represented in the network.

(T2) Every starting reactant (precursor) is represented in the network.

(T3) Each reaction step represented in the network is defined a priori.

(T4) Every active species represented in the network has at least one path leading to a final product (target) of the overall reaction.

(T5) Every chemical or active species represented in the network must be a reactant for or a product from at least one reaction step represented in the network.

(T6) A reactant of any elementary reaction represented in the reaction network is a starting reactant (precursor), if it is not produced by any reaction step represented in the network.

(T7) The network includes at most either the forward or reverse step of each elementary reaction represented in the network.

Essentially, what these axioms propose is that the P-graph must include all the species and reactions steps in the mechanism and that the graph starts at the reactants and proceeds towards the products. These axioms, while dealing with stoichiometry, do not include any notion of thermodynamics, thus there is no consistence with KPL, so there is no possibility for quantitative reaction analysis, as proceeding through a walk in a given P-graph may break the law of conservation of energy, as it is possible to have a disparity between the summation of the chemical potential changes of steps you proceed through and what it actually should be on the graph, i.e. there are no guarantee that there are thermodynamically consistent cycles.

These graphs all use nodes to represent individual species [33], which is likely due to the conventional representation of reaction mechanisms taught in college chemistry and biochemistry courses, wherein chemical species are drawn, often with structural detail, and are connected by arrows representing chemical reactions. Unfortunately, this practice limits the utility of the resulting graphs, rendering them inconsistent, for example, with KPL [39]. In fact, thermodynamic inconsistence of a graph goes hand-in-hand with its unsuitability for graph-theoretic enumeration

of reaction pathways. Finally, these graphs are non-unique, because each individual could draw them differently, and there is no easy way to tell if two given graphs are the same. In summary, none of these existing graph-theoretic methodologies provide a comprehensive graphical depiction of a given reaction network, including pathway, thermodynamic, and kinetic analyses, as offered by the RR Graph methodology.

2.5 Conclusions

This chapter details the past efforts to develop the RR Graph methodology as well as the motivations to pursue this research, mostly based on how it improves on other, more conventional methods. It is important to recognize that this methodology is imperative to the full understanding of complex reaction networks. For catalytic and electrocatalytic applications, this understanding is critical to successfully selecting the correct catalyst and parameters for operation. The following mechanistic analyses will further demonstrate the capabilities of this methodology and Chapter 6 explains how to further improve upon it.

2.6 References

1. Fishtik, I., Callaghan, C. A., and Datta, R. (2004a), "Reaction route graphs. I. Theory and algorithm," *The Journal of Physical Chemistry B*, *108*(18), 5671-5682.

2. Fishtik, I., Callaghan, C. A., & Datta, R. (2004b), "Reaction route graphs. II. Examples of enzyme-and surface-catalyzed single overall reactions," *The Journal of Physical Chemistry B*, *108*(18), 5683-5697.

3. Temkin, O. N.; Zeigarnik, A. V.; Bonchev, D. Chemical Reaction Networks: A Graph-Theoretical Approach; *CRC Press*: New York, 1996.

4. De Donder, T.; Rysselberghe, P. Thermodynamic Theory of Affinity; *Stanford University Press*: Palo Alto, CA, 1936.

5. Laidler, K. J. *Chemical Kinetics*, 3rd ed.; Addison-Wesley: Reading, MA, 1987.

6. Fishtik, I.; Datta, R. *Surf. Sci*. 2002, 512, 229.

7. Milner, P. C. J. *Electrochem. Soc*. 1964, 111, 228.

8. I. Fishtik, R. Datta, Studies in Surf. Sci. Catal. 133 (2001) 123-130.

9. L.O. Chua, C.A. Desoer, E.S. Kuh, Linear and Nonlinear Circuits, Mc-Graw Hill, New York, 1987.

10. J.X. Wang, T.E. Springer, R.R. Adzic, J. Electrochem. Soc. 153 (2006) A1732-A1740.

11. Y. Ishikawa, J.J. Mateo, D.A. Tryk, C.R. Cabrera, J. Electroanal. Chem. 607 (2007) 37-46.

12. A.B. Anderson, N.M. Neshev, R.A. Sidik, P. Shiller, Electrochim. Acta. 47 (2002) 2999-3008.

13. Y. Cai , A.B. Anderson, J. Phys. Chem. B. 108 (2004) 9829 -9833.

14. M.R. Gennero de Chialvo, A.C. Chialvo, Phys. Chem. Chem. Phys. 3 (2001) 3180-3184.

15. J.K. Norskov, T. Bligaard, A. Logadottir, J.R. Kitchin, J.G. Chen, S. Pandelov, U. Stimming, J. Electrochem. Soc. 152 (2005) J23-J26.

16. S. Wolfgang, T. Sergio, J. Electrochem. Soc. 153 (2006) L31-L32.

17. J. Meier, J. Schiøtz, P. Liu, J.K. Nørskov, U. Stimming, Chem. Phys. Lett. 390 (2004) 440-444.

18. J.X. Wang, T.E. Springer, P. Liu, M. Shao, R.R. Adzic, J. Phys. Chem. C. 111 (2007) 12425-12433.

19. P.M. Quaino, J.L. Fernandez, M.R. Gennero de Chialvo, A.C. Chialvo, J. Mol. Catal. A: Chemical. 252 (2006) 156-162.

20. B.E. Conway, L. Bai, J. Electroanal. Chem. 198 (1986) 149-175.

21. N. Krstajic, M. Popovic, B. Grgur, M. Vojnovic, D. Sepa, J. Electroanal. Chem. 512 (2001) 16-26.

22. N. Krstajic, M. Popovic, B. Grgur, M. Vojnovic, D. Sepa, J. Electroanal. Chem. 512 (2001) 27-35.

23. R.-B. Lin, S.-M. Shih, J. Chin. Inst. Chem. Eng. 39 (2008) 475-481.

24. N.M. Markovic, S.T. Sarraf, H.A. Gasteiger, P.N.J. Ross, J. Chem. SOC., Faraday Trans. 92 (1996) 3719-3725.

25. Vilekar, Saurabh A, Fishtik, Ilie, Datta, Ravindra, "Kinetics of the Hydrogen Electrode Reaction" *Journal of The Electrochemical Society*, 157 7 B1040-B1050 (2010)

26. J. Tafel, Z. *Phys. Chem*. 50 (1905) 641.

27. J. Heyrovsky, Recl. *Trav. Chim*. Pays-Bas. 46 (1927) 582.

28. T. Volmer, M. Erdey-Gruz, Z. *Phys. Chem*. Abt. A. 150 (1930) 203.

29. I. Fishtik, C.A. Callaghan, J.D. Fehribach, R. Datta, *J. Electroanal. Chem*. 576 (2005) 57-63.

30. N. Balabanian, T. Bickart, Electrical Network Theory, John Wiley, New York, 1969.

31. M.R. Gennero de Chialvo, A.C. Chialvo*, J. Electrochem. Soc.* 147 (2000) 1619-1622.

32. L. Bai, *J. Electroanal. Chem*. 355 (1993) 37.

33. O.N. Temkin, A.V. Zeigarnik, D.G. Bonchev, Chemical Reaction Networks: A Graph-Theoretical Approach, CRC Press, New York, 1996.

34. L. T. Fan, Y.-C. Lin, S. Shafie, B. Bertok, F. Friedler, "Exhaustive Identification of Feasible Pathways of the Reaction Catalyzed by a Catalyst with Multiactive Sites via a Highly Effective Graph-Theoretic

35. Algorithm: Application to Ethylene Hydrogenation," Ind. Eng.Chem. Res, 2012, dx.doi.org/10.1021/ie200718w

36. J.A. Papin, J. Stelling, N.D. Price, S. Klamt, S. Schuster, B.O. Palsson, "Comparison of network-based pathway analysis methods," Trends in Biotechnology 22 (2004) 400-405.

37. Schuster, S., Dandekar, T., Fell. D.A. "Detection of Elementary Flux Modes in Biochemical Networks: A Promising Tool for Pathway Analysis and Metabolic Engineering." Trends Biotechnol .,17, 53–60 (1999).

38. B.O. Palsson, Systems Biology: Simulation of Dynamic Network States, Cambridge University Press, Cambridge, UK, 2011.

39. D. A. Beard, H. Qian, Chemical Biophysics: Quantitative Analysis of Cellular Systems, Cambridge University Press, Cambridge, 2008.

40. Happel, J., Sellers, P. H. Analysis of the Possible Reaction Mechanisms for a Chemical Reaction System. Adv. Catal. 32, 273−323 (1983).

41. Milner, P. C., "The Possible Mechanisms of Complex Reactions involving Consecutive Steps," J. Electrochem. Soc., 111, 228-232 (1964).

42. G.A. Stephanopoulos, A.A. Aristidou, J. Nielsen, Metabolic Engineering Principles and Methodologies, Academic Press, San Diego (1998).

43. Yung, Yuk L. DeMore, William B., Photochemistry of Planetary Atmospheres, Oxford University Press, 1998, p. 87

44. Fan, L.T., Bertok, B., Friedler, F., A graph-theoretic method to identify candidate mechanisms for deriving the rate law of a catalytic reaction, *Computer and Chemistry*, 26 (2002) 265-292

45. Fan, L.T. Shafie, S., Bertok, B., Friedler, F., Lee, D.-Y. Seo, H. Graph-theoretic approach for identifying catalytic or metabolic pathways, *Journal of the Chinese Institute of Engineers*, 28, 1021-1037

46. Fan, L. T., Zhang, T., Liu, J., Schlup, J. R., Seib, P. A., & Friedler, F. (2007). Assessment of sustainability-potential: Hierarchical approach. Industrial Engineering & Chemistry Research, 46(13), 4506–4516.

47. Friedler, F., Tarjan, K., Huang, Y. W., & Fan, L. T. (1992). Graph-theoretic approach to process synthesis: Axioms and theorems. Chemical Engineering Science, 47(8), 1973–1988.

48. Friedler, F., Tarjan, K., Huang, Y. W., & Fan, L. T. (1993). Graph-theoretic approach to process synthesis: Polynomial algorithm for maximal structure generation. Computers & Chemical Engineering, 17(9), 929–942.

49. Herron, A. J., Jiao, J., Hahn, K., Peng, G., Adzic, R. R, Mavrikakis, M., "Oxygen Reduction Reaction on Platinum-Terminated ;Onion-structured' Alloy Catalysts," *Electrocatalysis* DOI 10.1007/s12678-012-0087-0 (2012)

50. J.L. Zhang, M.B. Vukmirovic, Y. Xu, M. Mavrikakis, R.R. Adzic, Controlling the catalytic activity of platinum-monolayer electrocatalysts for oxygen reduction with different substrates. *Chem. Int. Ed.* 44(14), 2132–2135 (2005)

51. M.B. Vukmirovic, J. Zhang, K. Sasaki, A.U. Nilekar, F. Uribe, M. Mavrikakis, R.R. Adzic, Platinum monolayer electrocatalysts for oxygen reduction. *Electrochim. Acta* 52(6), 2257–2263 (2007)

52. R.R. Adzic, J.X. Wang, Configuration and site of O2 adsorption on the Pt(111) electrode surface. *J. Phys. Chem.* B 102(45), 8988–8993 (1998)

53. J.K. Nørskov, J. Rossmeisl, A. Logadottir, L. Lindqvist, J.R. Kitchin, T. Bligaard, H. Jonsson, Origin of the overpotential for oxygen reduction at a fuel-cell cathode. *J. Phys. Chem.* B 108(46), 17886–17892 (2004)

54. Rodrigo Ferreira de Moraisa, Philippe Sautetb, David Loffredab, Alejandro A. Francoa, "A multiscale theoretical methodology for the calculation of electrochemical observables from ab initio data: Application to the oxygen reduction reaction in a Pt(1 1 1)-based polymer electrolyte membrane fuel cell" *Electrochimica Acta* 56 (2011) 10842– 10856

55. Guang-Feng Wei, Ya-Hui Fang, and Zhi-Pan Liu, "First Principles Tafel Kinetics for Resolving Key Parameters in Optimizing Oxygen Electrocatalytic Reduction Catalyst", *J. Phys. Chem*, 116, 12696−12705 (2012)

56. Matthew P. Hyman and J. Will Medlin "Mechanistic Study of the Electrochemical Oxygen Reduction Reaction on Pt(111) Using Density Functional Theory", *J. Phys. Chem. B*, *110,* 15338-15344 (2006)

57. Wang, J. X., Zhang, J., and Adzic, R. R., "Double-Trap Kinetic Equation for the Oxygen Reduction Reaction on Pt(111) in Acidic Media," *J. Phys. Chem. A.*, 111, 12702-12710 (2007a)

58. Ford, Denise C., Nilekar, A. U., Xub,Y., Mavrikakis, M. Partial and complete reduction of O2 by hydrogen on transition metal surfaces, *Surface Science* 604 (2010) 1565-1575

59. N. M. Markovic, T.J. Schmidt, V.Stamenkovic, P.N. Ross, Fuel Cells-From Fundamentals to Systems. 1 (2001) 105-116.

60. S. A. Vilekar (2010), Catalytic and Electrocatalytic Pathways in Fuel Cells (Doctoral dissertation). Retreved from Worcester Polytechnic Institute Electronic Theses & Dissertations. (etd-041910-094152)

61. Smit, A.W., Gent, M.M.C., van den Brink, R.W. (2001). *Market potential for reduction of N_2O emission at nitric acid plants*. Jacobs Engineering Nederland, Document 63578-0302.

62. Heyden, A., Hansen, N., Bell, A. T., Keil, F. J., Nitrous Oxide Decomposition over Fe-ZSM-5 in the Presence of Nitric Oxide: A Comprehensive DFT Study, *J. Phys. Chem. B* **2006,** *110,* 17096-17114

Chapter 3. Pruning Microkinetic Mechanisms through Reaction Route Graph Analysis Versus Campbell's Degree of Rate Control

Elucidation of the key molecular steps and pathways in an overall reaction is of central importance in developing a better understanding of catalysis. Campbell's degree of rate control (DRC) is the leading methodology currently available for identifying the germane steps and key intermediates in a catalytic mechanism. We contrast Campbell's DRC to our alternate new approach involving an analysis and comparison of the "resistance" and de Donder "affinity," i.e., the driving force, of the various steps and pathways in a mechanism, in a direct analogy to electrical networks. We show that our approach is as just rigorous and more insightful than Campbell's DRC. It clearly illuminates the bottleneck steps within a pathway and allows one to readily discriminate among competing pathways. The example used for a comparison of these two methodologies is a DFT study of the water-gas shift (WGS) reaction on Pt-Re catalyst published recently.

3.1 Introduction

A detailed understanding of the molecular mechanism of an overall reaction (OR) is of great importance in many fields including catalysis [1-4], combustion [5-7], environmental pollution [8-10], and metabolic modeling [11]. However, assembling a comprehensive molecular mechanism, complete with associated kinetic and thermochemical parameters, is a formidable task, given the often enormous number of possible steps and molecular intermediates. For instance, the GRI 3.0 mechanism for methane combustion [12] includes 325 reaction steps among 53 species.

Emulating such extensive gas-phase kinetic models, now in common usage in air pollution and combustion modeling, e.g., via CHEMKIN [7], catalytic reaction mechanisms are also becoming increasingly impressive in size, from dozens of steps [13-15] to over a hundred [16]. This, despite the fact that accurate prediction of kinetic and thermodynamic parameters on a given catalyst based on first-principles [17-19] and/or semi-empirical [20, 21] approaches is a significantly more daunting task than it is for gas-phase reactions. Typically, therefore, via the microkinetic approach [1,22-24], these step kinetics are incorporated in species mass balance differential equations for a given reactor, and solved numerically for the unknown concentrations of the surface intermediates, from which the individual rate of each step as well as that of the OR may be obtained. The numerical predictions may be finally compared to experimental data, e.g., in a parity plot under a variety of operating conditions [25], to determine if the proposed mechanistic steps and their computed kinetics are valid.

This modern computational "blackbox" approach is in stark contrast with the classical Langmuir-Hinshelwood-Hougen-Watson (LHHW) approach [26,27], in which, somewhat arbitrarily, a single rate-determining step (RDS) is assumed, the remaining steps being at quasi-equilibriums (QE). If the resulting LHHW rate expression with fitted rate and equilibrium parameters agrees with experiments, the RDS is deemed [28].

There is needed a middle ground between these two extremes that retains the rigor of modern predictive approach but endows it with insight to make the analysis and subsequent mechanism reduction more transparent. We describe such an approach here.

Whether the postulated molecular and kinetic complexity of a microkinetic network is justified in reality is, thus, an open and important question. In other words, it is much easier to propose a mechanistic step than to dispose-off one. On the other hand, the parsimonious Ockham's

razor [30] would recommend the simplest mechanism that can explain observations. For instance, Lu and Law [31] were able to reduce the complex GRI 3.0 [12] from 325 down to a 15-step mechanism that was found to be accurate in its predictions over a broad range of conditions. Such reduction, if done insightfully, is, of course, very desirable, as kinetic systems are often computationally challenging [32], especially when coupled with transport equations, as in microkinetics [1,25], or in computational fluid dynamics (CFD). If key steps could be identified, the researchers could devote more of their energies to accurately characterizing their kinetic/thermodynamic parameters, and focus on these in the design of more active and/or selective catalysts [33].

Some of the tools that are currently in use for simplifying complex catalytic chemistry models include: 1) a pictorial comparison of the energy landscape of different pathways for pathway discrimination [25], 2) a comparison of step reversibility, as proposed by Dumesic [34], and 3) evaluation of Campbell's degree of rate control (DRC) [35-38] for identifying important steps and dominant surface intermediates.

The first of these, although intuitively appealing, is a qualitative graphical tool, while the second involves only a thermodynamic criterion, not kinetic [36,39]. The most rigorous tool available so far is Campbell's DRC, which involves evaluating a normalized differential change in the rate of the overall reaction (OR), r_{OR}, for a normalized differential change in the forward rate constant of a given step s_ρ, holding invariable *all* step *equilibrium* constants and all *other* step *rate* constants, i.e., $(X_{DRC,\rho} = \partial \ln r_{OR} / \partial \ln \vec{k}_\rho)_{K_\rho, \vec{k}_{r \neq \rho}}$. Campbell's DRC is powerful and derives from the broader concept of parametric sensitivity used widely in the analysis of kinetic and reactor systems [3,7,40,41]. However, it is a "black box" numerical approach.

Here, we discuss an alternate approach based on electrical network analogy of a reaction mechanism within the reaction route (RR) graph analysis approach [42-45] developed by us, which involves an evaluation of the reaction step "affinity," or driving force, and "resistance" under a variety of conditions. It is just as rigorous and substantially more revealing than Campbell's DRC, allowing transparent pruning of complex catalytic reaction networks. The example that we use for this study involves the DFT study of the water-gas shift (WGS) reaction on Pt-Re [4]. It is shown that while Campbell's DRC leads to erroneous conclusions for this example, our approach allows rigorous mechanism analysis and reduction, eventually leading to a simplified but accurate rate law.

An expansive starting mechanism is, of course, not necessarily exhaustive, and could well miss one or more critical steps. One does not know *a priori* which elementary steps really occur, and which are the real intermediates. The intermediates are generally too fleeting to be detected via spectroscopic techniques, so that one has to depend on quantum mechanical methods for insights. However, these are extremely time consuming for an exhaustive search. Therefore, one is limited by pointers in the literature and one's own chemical intuition to assemble a good mechanism, followed by use of DFT to find their energetics. Clearly, however, there is a risk that an important reaction is overlooked. The approach presented here, of course, cannot overcome any such deficiency of a given mechanism. It is, thus, only an ex post method to check the consistency of the network found by experimental and DFT procedures, and as a useful tool for reducing/pruning the network.

3.2 Theory

Since Campbell's DRC is a form of parametric sensitivity analysis, we start below with a discussion of the latter first.

3.2.1 Parametric Sensitivity Analysis

Consider a system (e.g., a catalyst, or a catalytic reactor), as shown schematically in Figure 3.1, characterized by its steady-state "response" variable $y_j = y_j(\mathbf{a})$ (e.g., conversion, selectivity, composition of a reactant or a product, the rate of the OR, or the rate of generation/consumption of a species, etc.), which may be an explicit expression, a numerical solution, or simply tabular data, where ϕ is a vector of p independent system parameters, (e.g., step rate constants , pre-exponential factors, or activation barriers, etc.), and $\mathbf{a}$ is a vector of n input, or "imposed," variables (e.g., species activities, temperature, pressure, flow rate, etc.).
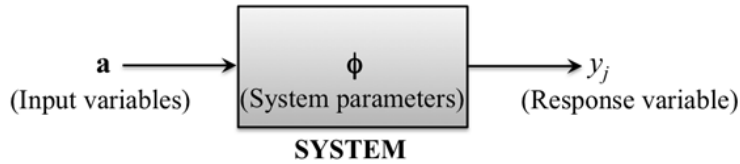
Figure 3.1: A chemical system (e.g., a catalyst) as a (black) box, with response (r), e.g., conversion or OR rate, determined by input variables (e.g., species composition vector, $\mathbf{a}$) and system parameters (e.g., step activation energy vector, ϕ).

The *total* differential change in the response variable y_j due to incremental changes in *all* system parameters ϕ_ρ $(\rho = 1, 2, \ldots, p)$

$$dy_j(\mathbf{a}) = \frac{\partial y_j}{\partial \phi_1}d\phi_1 + \frac{\partial y_j}{\partial \phi_2}d\phi_2 + \cdots + \frac{\partial y_j}{\partial \phi_\rho}d\phi_\rho + \cdots + \frac{\partial y_j}{\partial \phi_p}d\phi_p = \sum_{\rho=1}^{p}S_{y_j,\phi_\rho}d\phi_\rho \qquad (3.1)$$

where the *absolute* local sensitivity coefficient is defined as

$$S_{y_j,\phi_\rho}(\mathbf{a},\phi_\rho) \equiv \frac{\partial y_j(\mathbf{a},\phi_\rho)}{\partial \phi_\rho} = \lim_{\Delta\phi_\rho \to 0}\frac{y_j(\mathbf{a},\phi_\rho + \Delta\phi_\rho) - y_j(\mathbf{a},\phi_\rho)}{\Delta\phi_\rho} \qquad (3.2)$$

64

which may be an analytical expression if y_j is an explicit expression [3], or a numerical, or even an experimental value, and depends on the input variables vector **a** and the balance system parameters in **φ** that remain unchanged.

As an aside, the local sensitivity coefficients may also be used, along with an estimate of the uncertainty in each parameter, σ_ρ, e.g., those of the rate constants in their DFT estimation,[47] to obtain the overall uncertainty in the response variable, via an estimate of its variance,[9] via

$$\sigma_{y_j}^2(\mathbf{a}) = \sum_{\rho=1}^{p}\left(\frac{\partial y_j}{\partial \phi_\rho}\right)^2 \sigma_\rho^2 = \sum_{\rho=1}^{p} S_{y_j,\phi_\rho}^2 \sigma_\rho^2$$ where each term in the summation is an estimate of the

contribution of the uncertainty in each parameter ϕ_ρ to the overall uncertainty in the response variable y_j.

It is, however, often preferable to define an alternate *normalized* (or a *relative*) local sensitivity coefficient

$$X_{y_j,\phi_\rho}(\mathbf{a},\phi_\rho) \equiv \frac{\phi_\rho}{y_j}\cdot\frac{\partial y_j(\mathbf{a},\phi_\rho)}{\partial \phi_\rho} = \frac{\partial \ln y_j(\mathbf{a},\phi_\rho)}{\partial \ln \phi_\rho} = \frac{\phi_\rho}{y_j}\cdot S_{y_j,\phi_\rho}(\mathbf{a},\phi_\rho) \qquad (3.3)$$

in which the parameter ϕ_ρ as well as the response function y are normalized, so that it has the additional virtue of being dimensionless.

Once computed, these p sensitivity indices may be written as a row normalized sensitivity coefficient vector,

$$\mathbf{X}_j^T(\mathbf{a},\phi_\rho) = (X_{y_j,\phi_1} \quad X_{y_j,\phi_2} \quad \cdots \quad X_{y_j,\phi_p}) = \left(\frac{\partial \ln y_j}{\partial \ln \phi_1} \quad \frac{\partial \ln y_j}{\partial \ln \phi_2} \quad \cdots \quad \frac{\partial \ln y_j}{\partial \ln \phi_p}\right) \qquad (3.4)$$

Further, as above, from the definition of the total derivative for y_j

$$d \ln y_j = \sum_{\rho=1}^{p} \left(\frac{\partial \ln y_j}{\partial \ln \phi_1} \right) d \ln \phi_\rho = \sum_{\rho=1}^{p} X_{y_j, \phi_\rho} d \ln \phi_\rho \qquad (3.5)$$

3.2.2 Campbell's Degree of Rate Control

The generic parametric sensitivity coefficient defined above is of broad utility in a variety of fields [6-11]. On the other hand, Campbell's degree of rate control (DRC) [35-37] is a specialized version developed for use in pruning microkinetic models in catalysis, with the following stipulations: 1) It is defined as the normalized sensitivity coefficient of the *rate of the OR* (i.e., the response variable, $y_j = r_{OR}$) with respect to 2) the *forward* rate constant of step s_ρ, (i.e., the system parameter, $\phi_\rho = \vec{k}_\rho$), while 3) holding constant *all other* step *rate* constants, as well as 4) *all* step *equilibrium* constants (including that of the step s_ρ), i.e.,

$$X_{DRC,\rho}(\mathbf{a}, \vec{k}_\rho) \equiv \frac{\vec{k}_\rho}{r_{OR}} \cdot \left(\frac{\partial r_{OR}}{\partial \vec{k}_\rho} \right)_{\mathbf{a}, K_\rho, \vec{k}_{r \neq \rho}} = \left(\frac{\partial \ln r_{OR}}{\partial \ln \vec{k}_\rho} \right)_{\mathbf{a}, K_\rho, \vec{k}_{r \neq \rho}} = \left\{ \frac{\partial \ln r_{OR}}{\partial (-\Delta \vec{G}_\rho^{\ddagger, o} / RT)} \right\}_{\mathbf{a}, K_\rho, \vec{k}_{r \neq \rho}} \qquad (3.6)$$

Here, the last equality stems from the thermodynamic transition-state theory (TTST) relation for the rate constant, i.e., $\vec{k}_\rho = \kappa (k_B T / h) \exp(-\Delta \vec{G}_\rho^{\ddagger, o} / RT)$, where $\Delta \vec{G}_\rho^{\ddagger, o}$ is the Gibbs free energy (GFE) of activation for the forward step. Further, since $\Delta \vec{G}_\rho^{\ddagger, o} = \Delta \vec{H}_\rho^{\ddagger, o} - T \Delta \vec{S}_\rho^{\ddagger, o} \cong \vec{E}_\rho - T \Delta \vec{S}_\rho^{\ddagger, o}$, the differential change in $\ln \vec{k}_\rho$ may be brought about by incrementally changing the activation energy $\vec{E}_\rho$ of the step s_ρ, holding the entropy of activation $\Delta \vec{S}_\rho^{\ddagger, o}$ constant [37].

The key aspect, thus, that distinguishes Campbell's DRC from simply being the normalized sensitivity coefficient with respect to the forward rate constant [8], is that the thermodynamics of the step s_ρ, are not altered in Campbell's DRC as $\vec{k}_\rho$ is varied incrementally, so that $\bar{k}_\rho$ changes concomitantly such that $\Delta \vec{k}_\rho / \vec{k}_\rho = \Delta \bar{k}_\rho / \bar{k}_\rho$. This is so because the equilibrium constant that is

held constant for the elementary step and its forward and reverse rate constants are interrelated via the TTST relation

$$K_\rho = \exp\left(-\frac{\Delta G_\rho^{\rm o}}{RT}\right) = \exp\left(-\frac{\Delta \vec{G}_\rho^{\ddagger,{\rm o}} - \Delta \bar{G}_\rho^{\ddagger,{\rm o}}}{RT}\right) = \frac{\vec{k}_\rho}{\bar{k}_\rho} \qquad (3.7)$$

Further, the Gibbs free energy (GFE) of activation for the forward step in Eq. (3.6) is

$$\Delta \vec{G}_\rho^{\ddagger,{\rm o}} \equiv G_{f,\rho}^{\ddagger,{\rm o}} + \sum_{i=1}^{n} v_{\rho i} G_{f,i}^{\rm o} \qquad (3.8)$$

where $G_{f,\rho}^{\ddagger,{\rm o}}$ is the standard (for unit activity) GFE of formation of the transition-state complex (TSC) of step s_ρ, $G_{f,i}^{\rm o}$ is that of the reactant species i in step s_ρ, and $v_{\rho i}$ is the stoichiometric coefficient of species i in step s_ρ (by convention, $v_{\rho i} < 0$ for reactants and $v_{\rho i} > 0$ for products).

It is assumed next that the incremental change in $\Delta \vec{G}_\rho^{\ddagger,{\rm o}}$ in Eq. (3.6) is brought about by incrementally perturbing the standard GFE of formation of the TSC of step s_ρ, i.e., $G_{f,\rho}^{\ddagger,{\rm o}}$, rather than that of any of the reactant species $G_{f,i}^{\rm o}$ in the step s_ρ. Then Campbell's DRC, Eq. (3.6), may alternately be written in the form [37]

$$X_{DRC,\rho} = \left\{ \frac{\partial \ln r_{OR}}{\partial(-G_{f,\rho}^{\ddagger,{\rm o}} / RT)} \right\}_{\mathbf{a}, G_{f,i}^{\rm o}, G_{f,r\neq\rho}^{\ddagger,{\rm o}}} \qquad (3.9)$$

where all other standard GFE of formation of species are held constant, as well as that for the TSCs of all other steps. The incremental change in the standard GFE of formation of the TSC may further be brought about by incrementally changing the standard enthalpy of formation of the TSC of the step, $H_{f,\rho}^{\ddagger,{\rm o}}$, holding the entropy of formation of the TSC $S_{f,\rho}^{\ddagger,{\rm o}}$ constant [37].

An alternate way to view Eq. (3.9) is as a reaction forming the particular TSC from the reactants of the *overall reaction* (OR), or from terminal species, rather than from those in the step s_ρ, so that the Campbell's DRC may then be construed as a derivative with respect to the equilibrium constant of reaction of formation of the TSC of step ρ from the OR terminal reactants.[37] This may be accomplished by appropriately combining the elementary steps into the so-called intermediate reactions (IR) [42-44].

There are different ways in which the Campbell's DRC, once hence numerically computed for all the steps in a microkinetic model, may be utilized for identification of key steps and model reduction [48]. One such method is the so-called principal component analysis (PCA) [41,49,50] in which the eigenvalues and eigenvectors of the matrix $\mathbf{X}^T\mathbf{X}$ are computed. The dominant eigenvalues then indicate the principal eigenvectors, and the biggest elements of these eigenvectors provide the most significant steps in the mechanism.

A second approach is to simply compare Campbell's DRC of a given step as a fraction of its sum for all steps, where the latter may be obtained from Eqs. (3.5) and (3.6), which for equal relative variation of the rate constants (i.e., for $d\vec{k}_1/\vec{k}_1 = d\vec{k}_2/\vec{k}_2 = \cdots d\vec{k}_\rho/\vec{k}_\rho \equiv d\vec{k}/\vec{k}$)

$$\frac{d\ln r_{OR}}{d\ln \vec{k}} = \sum_{\rho=1}^{p} X_{DRC,\rho} \tag{3.10}$$

and describes the total normalized change in the OR rate as a result of an equal normalized differential change in the rate constants of all steps in a microkinetic mechanism.

In fact, it has been often conjectured [3,36,51] (based on some numerical examples, although not proven mathematically) that $\sum_{\rho=1}^{p} X_{DRC,\rho} = 1$. Therefore, Campbell [35,36] suggests

simply comparing the absolute numerical value of the DRC for each step for model reduction and for identification of the rate-determining step (RDS), if any. However, in more recent work, it has been found that the common assertion that $\sum_{\rho=1}^{p} X_{DRC,\rho} = 1$ is incorrect [25].

At any rate, the larger the calculated value of $X_{DRC,\rho}$, the greater the degree of control that the step s_ρ exerts on the overall rate. A positive value for $X_{DRC,\rho}$ suggests that increasing the rate constant $\vec{k}_\rho$ would increase r_{OR}, so that the corresponding step s_ρ may be considered as a rate-limiting step (RLS). On the other hand, a negative value for $X_{DRC,\rho}$ suggests an inhibiting step. A $X_{DRC,\rho} \to 0$ indicates a quasi-equilibrated (QE) step. On the other hand, a $X_{DRC,\rho} \to 1$ indicates a RDS. Once the key steps in a mechanism are hence identified, one can, in principle, design a better catalyst based on these insights [33,38].

It is possible to generalize Campbell's sensitivity analysis approach to determine the so-called degree of *thermodynamic* control (DTC) of a step [37], defined, in analogy to Eq. (3.9), as

$$X_{DTC,k} \equiv \left\{ \frac{\partial \ln r_{OR}}{\partial (-G_{f,k}^{\circ} / RT)} \right\}_{\mathbf{a}, G_{f,i \neq k}^{\circ}, G_{f,\rho}^{\ddagger,\circ}} \tag{3.11}$$

where the relative change in the rate of the OR is evaluated in response to a small relative change in the standard-state GFE change of the step s_ρ, made by changing the GFE of formation of the intermediate k in that step, holding constant all other GFE extrema (minima as well as saddle points in the energy landscape). Further, as above, the GFE of formation in Eq. (3.11) may be written in terms of the equilibrium constant of an IR forming the desired intermediate from terminal species, by appropriately linearly combining the elementary steps.

69

In view of Eqs. (3.9) and (3.11), both the degree of *rate* control (DRC) and the degree of *thermodynamic* control (DTC) may be viewed from a common standpoint [37], with the standard GFE of formation of the *TSC* being varied in one, while the standard GFE of formation of the *intermediate* of interest being varied in the other.

Stegelmann et al. [37] further conjectured (although also not proven mathematically), based on numerical examples, that the degree of thermodynamic control is proportional to the surface coverage of the intermediate k,

$$X_{DTC,k} = -\sigma \cdot \theta_k \qquad (3.12)$$

with the proportionality constant σ varying typically between 1 and 2, being the number of sites involved in the RDS. Further, they found that the degree of thermodynamic control is always zero or negative, i.e., rate remains unchanged or reduces when an intermediate is stabilized depending on whether or not it is a dominant species on the surface. Increasing the coverage of an already abundant surface intermediate can reduce OR rate by suppressing those of others further.

In summary, $X_{DRC,\rho}$ may be used to determine the kinetically significant TSCs in a microkinetic mechanism, while $X_{DTC,k}$ may be used for identifying the key reactive intermediates, i.e., those that exert a dominant control on the rate of the OR. This then offers the potential of increasing the OR rate by changing the appropriate step energies through catalyst design.

As a practical matter in catalyst design, of course, it is not possible to simply change GFE of one transition state or of one intermediate and nothing else.[38] The GFE of activation and that of a step are, in fact, related via the commonly observed linear-free energy relation [52],

$$\frac{d(\Delta \vec{G}_\rho^{\ddagger,\mathrm{o}})}{d(\Delta G_\rho^\mathrm{o})} = \beta_\rho \qquad (3.13)$$

Other such relations that describe the commonly observed interrelation between kinetics and thermodynamics are the Brønsted-Evans-Polanyi-Semenov relation,[3,53] $d(\vec{E}_\rho) = \beta_\rho d(\Delta H_\rho^\mathrm{o})$.

3.2.3 Electrical Analogy and Reaction Networks

A virtue of Campbell's DRC is that it is general tool of microkinetic model reduction, i.e., without regard to the degree of complexity of a molecular mechanism, which may involve multiple parallel pathways. However, a limitation is that it is simply a numerical sensitivity analysis tool for a chemical system treated as a proverbial "black box" (Figure 3.1).

On the other hand, Horiuti provided an alternate criterion for identifying the RDS in a sequence [34, 54], i.e., the RDS is the only exergic step ($A_\rho = -\Delta G_\rho > 0$, where A_ρ is the de Donder affinity) in a sequence, the remaining steps being at quasi-equilibrium (QE) ($A_\rho \to 0$). However, the step affinity is simply its thermodynamic driving force, akin to voltage across an electrical element in an electrical circuit, the rate (current) of a step (electrical element) being also determined by its kinetics (resistance) as well. Further, of course, there can be, and often is, more than one step with $A_\rho > 0$ [54].

Thus, identification of significant steps simply based on perturbation of the rate constant or activation barriers, as via Campbell's DRC [36], or alternately based on simply the thermodynamic driving force, the de Donder affinity [34,54], both provide only a partial perspective, as the net rate of a step involves *both* kinetics and thermodynamics, i.e.,

$$r_\rho = \vec{r}_\rho - \overleftarrow{r}_\rho = \vec{r}_\rho(1 - z_\rho) = \vec{r}_\rho(1 - e^{-\mathscr{A}_\rho}) \qquad (3.14)$$

71

where $z_\rho \equiv \vec{r}_\rho / \overleftarrow{r}_\rho$ is the step reversibility [34], and $\mathscr{A}_\rho = A_\rho / RT$ is dimensionless de Donder affinity, while $A_\rho = -\Delta G_\rho$ is the de Donder affinity for reaction step s_ρ[55].

In other words, one needs *both* thermodynamic (affinity, or reversibility) and kinetic (resistance) characteristics of a reaction step to judge its significance in the overall scheme of things. The electrical network analogy based on the reaction route (RR) Graph approach [42-44] incorporates both of these aspects. It, thus, comprehensively incorporates and illuminates the network structural constraints embodied by the two Kirchhoff's laws (mass balance, and Hess's law) described below, which further ascribe to reaction networks complete and quantitative correspondence to electrical networks. Further, the pictorial representation of the reaction network not only provides the corresponding electrical circuit but makes abundantly clear which pathways and steps are dominant and which may be neglected. It is, thus, a comprehensive and a transparent approach. For its application, however, one first needs the complete, or at least its simplified version, RR Graph, obtained for a given mechanism as described below.

3.2.3.1 The Reaction Route (RR) Graph and the Electrical Analogy

The Reaction Route (RR) Graph of a mechanism for an OR comprising of *p* reaction steps s_ρ among $q + 1$ intermediate species and *n* terminal species (OR reactants and products), is a quantitative graph theoretical depiction of the reaction network, in which the steps as well as the OR, are represented individually as directed (arrows pointed in the assumed direction) branches, or edges, interconnected at nodes, or vertices, n_j, so that *all* reaction routes (RRs) may be traced on it as closed walks, or cycles, and the nodal connectivity to branches is consistent with quasi steady-state (QSS) mass balance of one or a linear combination of species.

An example of a RR Graph is shown in Figure 3.2, which, as described below, is the RR Graph for the WGS mechanism on Pt-Re provided in Table 3.1. Once the RR Graph of a mechanism is obtained, the equivalent electrical network is obtained simply by replacing the individual branches by their step resistances, and the OR by an electromotive force (EMF) providing the OR driving force of OR affinity, as shown in Figure 3.3 for the WGS example.

While, graphically, an RR is a closed walk starting and ending at the same node, mathematically, it is a linear combination of reaction steps, $RR_g : \sum_\rho \sigma_{g\rho} s_\rho = 0$. Here $\sigma_{g\rho}$ is stoichiometric number (usually, 0, ±1 or ±2) of step s_ρ in the gth RR, which provides the number and direction of a step in a walk. Mathematically, $\sigma_{g\rho}$ is determined from the requirement to eliminate *all* species, intermediate as well as terminal, in a RR. When the reaction steps involved in a RR do not include the OR, then the RR is called an empty route (ER). When the OR is included, then the RR is a full route (FR). In fact, subtracting one FR from another results in an ER, because the OR gets cancelled in the process. Further, note that for this the sequence of steps is arbitrary.

There are, however, some walks that are not closed, i.e., they start and end at different nodes. These are called intermediate reaction routes (IRRs). In these, not all species are eliminated. Thus, the resulting intermediate reaction (IR), typically includes both terminal species and specified intermediate species.

As per the Horiuti-Temkin theorem, furthermore, an independent *RR* set is any set of $\mu = p - q$ *RR*s, which may include any *FR*s and *ER*s, so long as they include among them all of the steps in the mechanism. Moreover, the number of linearly independent ERs is given by $\mu - 1 = p - (q + 1)$. In other words, any set of *RR*s (*ER*s and *FR*s) that includes all the steps including the OR is an appropriate independent set, e.g., an appropriate set is $\mu - 1$ *ER*s and one *FR*.

s_ρ	$\vec{E}_\rho$	$\vec{\Lambda}_\rho$	Elementary Reactions	$\overleftarrow{E}_\rho$	$\overleftarrow{\Lambda}_\rho$	$\vec{\omega}_\rho$	$\overleftarrow{\omega}_\rho$
s_2:	0	1.00×10^{13}	$H_2O + S \rightleftarrows H_2O{\cdot}S$	0	1.00×10^{13}	$\vec{k}_2 p_{H_2O}$	$\overleftarrow{k}_2$
s_3:	0	1.00×10^{13}	$CO + S \rightleftarrows CO{\cdot}S$	0	3.30×10^{12}	$\vec{k}_3 p_{CO}$	$\overleftarrow{k}_3$
s_4:	44.16	1.00×10^{13}	$H_2O{\cdot}S + S \rightleftarrows OH{\cdot}S + H{\cdot}S$	44.16	7.89×10^{12}	$\vec{k}_4$	$\overleftarrow{k}_4$
s_5:	44.24	1.00×10^{13}	$OH{\cdot}S + S \rightleftarrows O{\cdot}S + H{\cdot}S$	42.24	9.88×10^{12}	$\vec{k}_5$	$\overleftarrow{k}_5$
s_6:	0	9.24×10^{12}	$2OH{\cdot}S \rightleftarrows H_2O{\cdot}S + O{\cdot}S$	0	7.53×10^{12}	$\vec{k}_6$	$\overleftarrow{k}_6$
s_7:	113.28	1.00×10^{13}	$CO{\cdot}S + O{\cdot}S \rightleftarrows CO_2{\cdot}S + S$	113.28	2.94×10^{13}	$\vec{k}_7$	$\overleftarrow{k}_7$
s_8:	0	1.00×10^{13}	$CO_2{\cdot}S \rightleftarrows CO_2 + S$	0	1.00×10^{13}	$\vec{k}_8$	$\overleftarrow{k}_8 p_{CO_2}$
s_9:	9.89	1.00×10^{13}	$2H{\cdot}S \rightleftarrows H_2 + 2{\cdot}S$	0	4.00×10^{10}	$\vec{k}_9$	$\overleftarrow{k}_9 p_{H_2}$
s_{10}:	2.88	1.00×10^{13}	$CO{\cdot}S + OH{\cdot}S \rightleftarrows COOH{\cdot}S + S$	2.88	3.23×10^{12}	$\vec{k}_{10}$	$\overleftarrow{k}_{10}$
s_{11}:	118.08	1.99×10^{12}	$COOH{\cdot}S + S \rightleftarrows CO_2{\cdot}S + H{\cdot}S$	66.24	9.89×10^{13}	$\vec{k}_{11}$	$\overleftarrow{k}_{11}$
s_{12}:	95.04	3.74×10^{12}	$COOH{\cdot}S + O{\cdot}S \rightleftarrows CO_2{\cdot}S + OH{\cdot}S$	95.04	4.97×10^{10}	$\vec{k}_{12}$	$\overleftarrow{k}_{12}$
s_{13}:	31.68	1.00×10^{13}	$COOH{\cdot}S + OH{\cdot}S \rightleftarrows CO_2{\cdot}S + H_2O{\cdot}S$	31.68	1.08×10^{12}	$\vec{k}_{13}$	$\overleftarrow{k}_{13}$
s_{14}:	90.24	1.00×10^{13}	$CO_2{\cdot}S + H{\cdot}S \rightleftarrows HCOO{\cdot}S{\cdot}S$	90.24	1.00×10^{13}	$\vec{k}_{14}$	$\overleftarrow{k}_{14}$
s_{15}:	175.68	1.00×10^{13}	$HCOO{\cdot}S{\cdot}S + O{\cdot}S \rightleftarrows CO_2{\cdot}S + OH{\cdot}S + S$	175.68	1.00×10^{13}	$\vec{k}_{15}$	$\overleftarrow{k}_{15}$
s_{16}:	128.64	1.65×10^{11}	$HCOO{\cdot}S{\cdot}S + OH{\cdot}S \rightleftarrows CO_2{\cdot}S + H_2O{\cdot}S + S$	128.64	1.00×10^{13}	$\vec{k}_{16}$	$\overleftarrow{k}_{16}$

Table 3.1: The Microkinetic Model for WGS on Pt–Re. The Letter 'S' is a Surface Site. Activation Energies in kJ/mol; the Units of the Pre–exponential Factors are $atm^{-1}\ s^{-1}$ for Adsorption and Desorption Reactions and s^{-1} for Surface Reactions. ω_ρ is the Reaction Step Weight in Terms of Rate Constant, k and Partial Pressure of Terminal Species. The Forward and Reverse Rate Constants ($\vec{k}_\rho$ and $\overleftarrow{k}_\rho$, Respectively) are Calculated by: $\vec{k}_\rho = \vec{\Lambda}_\rho \exp\left(-\dfrac{\vec{E}_\rho}{RT}\right)$ and $\overleftarrow{k}_\rho = \overleftarrow{\Lambda}_\rho \exp\left(-\dfrac{\overleftarrow{E}_\rho}{RT}\right)$.
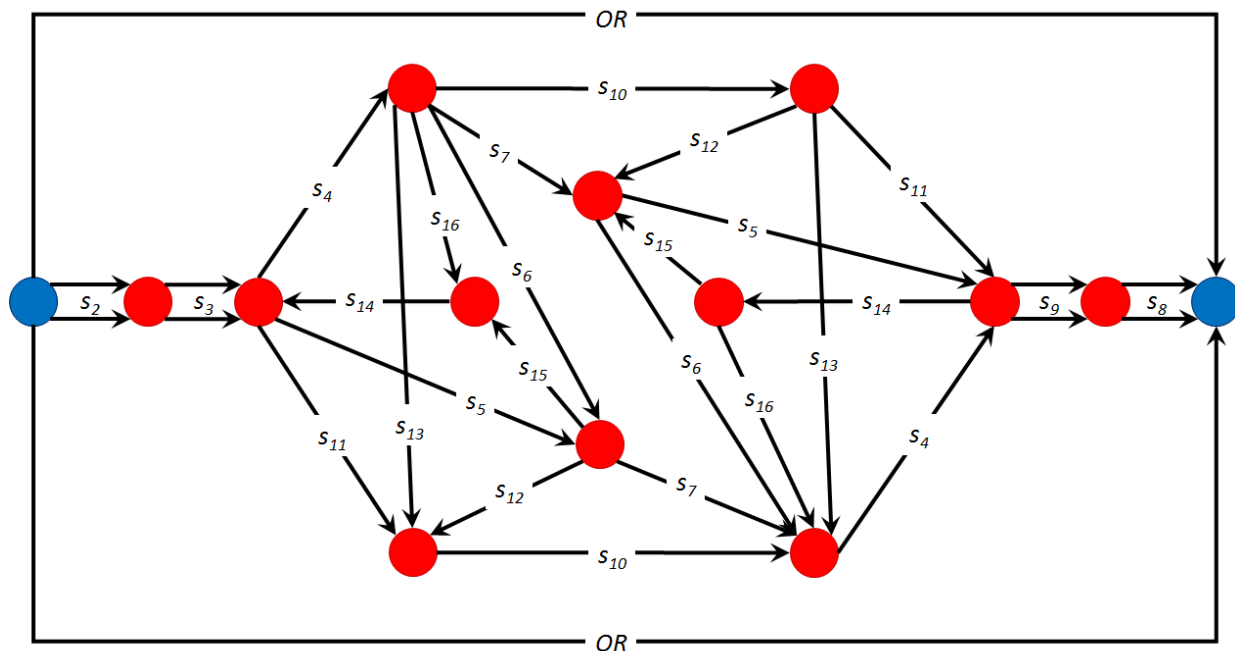
Figure 3.2: Complete RR Graph for the WGS reaction on Pt-Re.
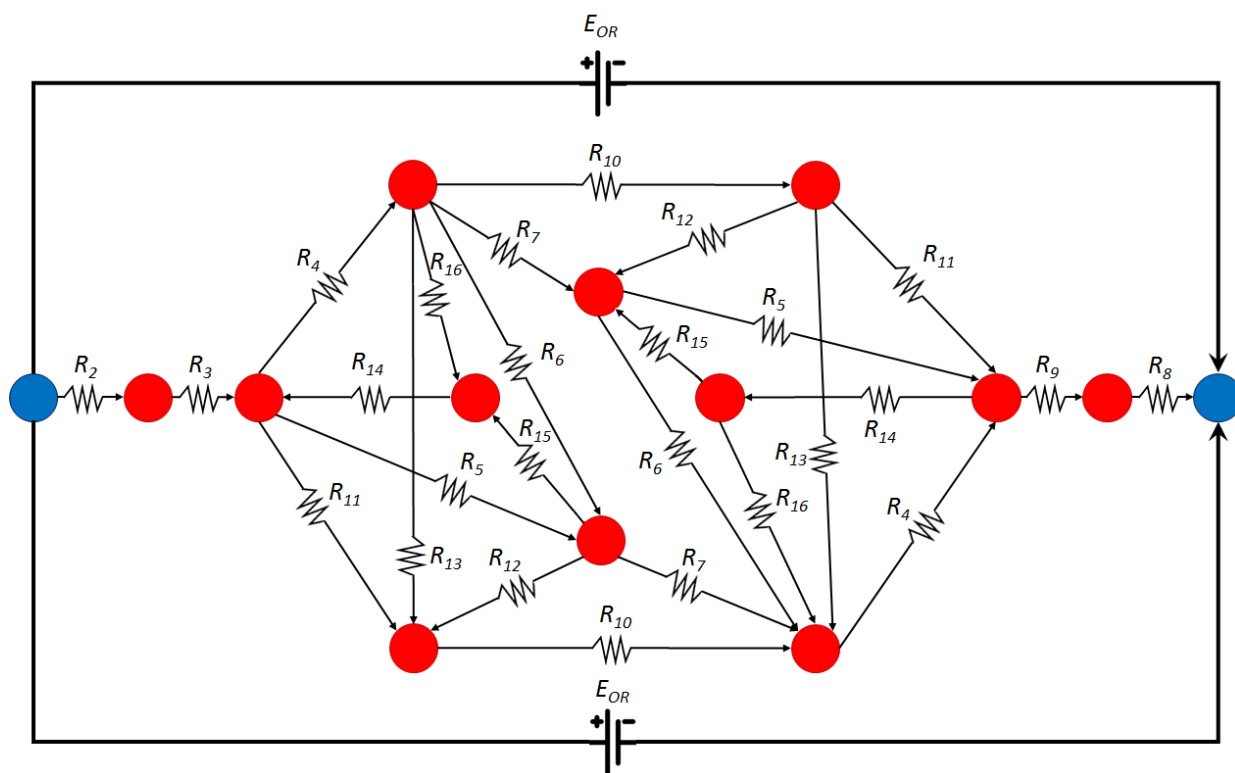
Figure 3.3: An Electrical Analogy for the WGS reaction.

As indicated above, the RR Graph is a useful, quantitative, graph-theoretical representation of the molecular mechanism that provides: 1) consistence of nodes with *species mass balance*, i.e.,

Kirchhoff's Flux Law (KFL), alternately, Kirchhoff's First Law, i.e., the quasi-steady state (QSS) assumption of kinetics, or the Bodenstein approximation; 2) consistence of RRs with the state-property of thermodynamic functions (e.g., Gibbs free energy, G, enthalpy H, and entropy S), i.e., Kirchhoff's potential law, or KPL, also called Kirchhoff's second law, alternately known as *Hess's law*, according to which change in a thermodynamic state property along a cycle is zero; 3) *graphical* enumeration of all possible reaction routes as closed walks, normally done from *stoichiometric* analysis [55]; and 4) *minimality*, or directness [57], of both RRs as well as nodal degree, namely, the number of branches incident on a node.

It, actually, turns out that the second and third property above, i.e., consistence with KPL and enumeration of RRs, are mathematically equivalent. In other words, a RR Graph that is consistent with KPL is automatically amenable to a graph-theoretic enumeration of all RRs, and *vice versa*. As a result, we are concerned only with the two requirements of consistence with the two Kirchhoff's laws, along with their directness, i.e., the number of steps involved in the KPL and KFL relations are minimal.

3.2.3.2 Drawing the RR Graph or Electrical Network

The first step in the use of the RR Graph approach is, of course, to construct the RR Graph or electrical network from a given mechanism. It turns out that this is often not a trivial matter, because of the fact that the three basic requirements, namely, KFL, KPL, and minimality impose strict limitations on the topology of the resulting RR Graph, so that often only a unique solution of is admissible. We have so far found no more than two RR Graphs for any reaction system. The preferred method to draw the RR Graph for a given mechanism is to start with a set of independent cycles (KPL relations) that are drawn and combined in a way to ensure compatibility with KFL relations.

Thus, the recipe for drawing the RR Graph is as follows [42]: 1) Start with a set of independent RR matrix σ in which there is a single OR (or an independent number of ORs), and the remaining are ERs (ERs may be obtained by subtracting one FR from another other); 2) Obtain a set of KFL relations by starting with the QSS relations for the individual species and linearly combining them to obtain a set with minimality ($\leq p - q + 1$); 3) Draw the ERs as cycles, as well as the FR, with steps drawn as branches, interconnected at nodes; 4) Combine ERs, one at a time, by merging common branches as far as one can go. The resulting sub-graph containing the ERs is called the cycle graph; 5) If a step is repeated in a RR, i.e., if $\sigma_{g\rho} = +2$, then duplicate the cycle graph, flipping it on an axis; 6) Fuse minimal number of nodes to merge the cycle graphs, ensuring that the fused nodes are also direct or minimal; 7) Merge with the FR that includes the OR, to obtain the complete RR Graph; and finally, 8) Check to make sure that connectivity at all the nodes is consistent with appropriate KFL relations.

Finally, it should be remarked that the QSS analysis is used in our approach to obtain the KFL relations that provide the nodal connectivity of the RR Graph. However, once determined, the RR Graph can be used for the analysis of non-steady-state cases as well.

3.2.3.3 Kirchhoff's Laws and The Electrical Network Analogy

Since consistence with the two Kirchhoff's laws is central to the RR Graph architecture, these are defined next, and impose important constraints on the kinetics and thermodynamics of reaction networks.

Thus, *Kirchhoff's Flux Law (KFL)* implies that the branch rate, r_ρ (likened to branch current) of all branches incident at a node j sum up to zero, i.e., $\Phi_j : \sum_\rho m_{\rho j} r_\rho = 0$, where the

incidence coefficient $m_{\rho j} = +1$, if a branch leaves a node, and $m_{\rho j} = -1$, if a branch is coming into it.

Kirchhoff's Potential Law (KPL) implies that a thermodynamic potential change across a branch ΔY_ρ, (e.g., ΔH_ρ, ΔG_ρ, or ΔS_ρ, likened to branch voltage drop) of all branches in a cycle or RR, sum up to zero, i.e., $\sum_\rho \sigma_{g\rho} \Delta Y_\rho = 0$, where the stoichiometric number $\sigma_{g\rho} = +1$, if a branch is directed in the direction of the walk, and $\sigma_{g\rho} = -1$, if a branch is directed in the opposite direction.

The requirement of consistence with the two Kirchhoff's laws confers on the RR Graphs a one-to-one correspondence with electrical circuits, which is a useful analogy because of the vast and well-grounded literature on circuit analysis [58]. Thus, the electrical analog of the RR Graph is obtained by simply replacing the branches by resistors and the OR by an EMF, as shown in Figure 3.3.

Even though, the electrical analogy is complete without the following, for convenience, we may write the rate of a reaction step in the form of Ohm's law [42]

$$r_\rho \equiv \frac{\mathcal{A}_\rho}{R_\rho} \qquad (3.15)$$

where $\mathcal{A}_\rho$ is the dimensionless step affinity akin to voltage in an electrical circuit. It is in turn related to the ratio of the rate in the forward direction $\vec{r}_\rho$ to that in the reverse direction, $\overleftarrow{r}_\rho$, via the de Donder relation [34,54]

$$\mathcal{A}_\rho = \ln\left(\frac{\vec{r}_\rho}{\overleftarrow{r}_\rho}\right) = \ln\left(\frac{1}{z_\rho}\right) \tag{3.16}$$

which stems from the thermodynamic consistence of elementary step kinetics, so that the step resistance, by combining the last two equations, is

$$R_\rho = \frac{\ln(\vec{r}_\rho/\overleftarrow{r}_\rho)}{\vec{r}_\rho - \overleftarrow{r}_\rho} \tag{3.17}$$

Clearly, unlike electrical resistance which is substantially constant, this definition of kinetic resistance of a step, strongly depends on reaction conditions, especially, temperature.

Now that the RR Graph follows KFL, KPL, as well as Ohm's law, it is *completely* consistent with a resistive network [58]. Consequently, we can write the overall rate as the ratio of the affinity of the OR and the overall resistance of the reaction network

$$r_{OR} \equiv \frac{\mathcal{A}_{OR}}{R_{OR}} \tag{3.18}$$

where the OR resistance of the network is obtained in terms of the individual step resistances, in a manner similar to the electrical circuit [58].

3.2.3.4 Use of the Electrical Analogy for Microkinetic Analysis and Pruning

To obtain the rates for the elementary steps as well as for the *OR,* one needs to first solve for the unknown intermediates concentrations θ_k ($k = 0, 1, 2, \ldots, q$), for which the number of relations needed are ($q + 1$). One of these is always the mass balance of intermediates, e.g., site balance, i.e., site fractions add up to unity, $1 = \sum_{k=0}^{q} \theta_k$. The remaining are the q independent KFL relations applied to the nodes in the RR Graph, which are essentially linear combinations of the q

quasi-steady state (QSS) relations, i.e., the Bodenstein approximation that assumes that the concentrations of the intermediate species are invariant with time. In these are substituted step kinetics. We club together in the mass-action kinetics, the product of the *known* rate parameters and activities of terminal species into *reaction weights*, ω_ρ, leaving behind the rates explicitly in terms of the *unknown* intermediates concentrations and *known* ω_ρ. In fact, for non-linear kinetic systems, numerical solution of this set of differential equations can be computationally easier than root finding for a set of nonlinear algebraic relations resulting from the corresponding QSS equations.

The q KFL equations incorporating step kinetics and combined with site balance are solved for the unknown intermediate activities, or site fractions, θ_k. For linear systems this would result in explicit expressions in terms of ω_ρ, while for nonlinear systems, in general, only numerical results for a given set of conditions (activities of terminal species and temperature) are possible. Once the unknown intermediates surface converges θ_k are hence evaluated, all the step rates as well as the *OR* rate can be determined. Additionally, it becomes apparent that all the step rates are simply linear combinations of only μ independent step rates or RR fluxes. It may be noted that this procedure is different from conventional microkinetic analysis, in which θ_k are obtained from a solution of mass balance (partial or ordinary differential) equations of all species in a given reaction system and for a given set of reaction conditions.

These hence calculated step rates when written on the RR Graph electrical network can quickly reveal which pathways provide the bulk of the flux. Thus, one way to prune the mechanism is to use the RR Graph and dropping branches that contribute negligibly to the OR rate, i.e.

$r_\rho/r_{OR} \to 0$, which can often result in clear and drastic pruning. Of course, this needs to be done over a range of conditions of interest to ensure the robustness of the pruned network.

Additionally, once the step rates in the forward direction $\vec{r}_\rho$ and in the reverse direction, $\tilde{r}_\rho$ are determined as above for a given set of conditions, one can readily compute step affinities (Eq. 3.16) as well as step resistance (Eq. 3.17), which may also be provided on the RR Graph. Steps whose resistance R_ρ is a significant fraction of R_{OR} are kinetically significant, and are termed as the rate-*limiting* steps (RLS), the others are not. In fact, step resistances can be plotted over a broad range of conditions, especially temperature to determine whether the significant steps change. In case there is a step with $R_\rho \to R_{OR}$, it may be denoted as the rate *determining* step (RDS).

Finally, a comparison of step affinities $\mathcal{A}_\rho$ (or step reversibity, z_ρ, Eq. 3.16) to those for the OR $\mathcal{A}_{OR}$ (or OR reversibility, z_{OR}), i.e., $\mathcal{A}_\rho/\mathcal{A}_{OR}$, also sheds light on which steps are at QE and which are not. Steps with $\mathcal{A}_\rho \to 0$, or with reversibility $z_\rho \to 1$ (Eq. 3.17), are at QE, while those steps whose $\mathcal{A}_\rho$ is a significant fraction of that of the OR $\mathcal{A}_{OR}$ are the RLSs. Further, it is noteworthy that if there are parallel pathways that contribute significantly to the OR flux, then as per KPL, the affinity drop over all parallel pathways is the same, i.e., there are RLSs in all parallel pathways!

An additional possibility is to compare ratio of the power dissipation in each step [42], namely, $r_\rho\mathcal{A}_\rho$, to that in the OR, $r_{OR}\mathcal{A}_{OR}$

$$\sum_{\rho=1}^{P}\left(\frac{r_\rho\mathcal{A}_\rho}{r_{OR}\mathcal{A}_{OR}}\right)=1 \qquad (3.19)$$

81

which stems from the conservation of energy [42], i.e., $\displaystyle\sum_{\rho=1}^{p} r_\rho \mathscr{A}_\rho = r_{OR}\mathscr{A}_{OR}$.

In summary, a comparison of the dissipation as above, along with three different RR Graphs labeled with step rates, step affinities, and step resistances can completely illuminate the reaction network, laying bare the important pathways, RLSs, as well as the QE steps. Additionally, plots of step resistances in comparison with that of the OR resistance over a range of temperatures can provide unequivocal evidence of the identity of the crucial steps and pathways in a microkinetic mechanism.

3.2.3.5 Deriving an Explicit Rate Expression for a Pruned Microkinetic Mechanism

Once the mechanism has been suitably pruned as described above, and the corresponding reduced RR Graph obtained, we have shown [59,60] that an accurate, *albeit* approximate, explicit rate law may be obtained in the spirit of the LHHW methodology, but following the so-called Rdot approach, even for nonlinear systems, and those with more than one RLSs, for which it is not ordinarily possible to obtain explicit rate expressions. Such explicit rate expressions are, of course, of immense value in the design and analysis of industrial reactors.

The expression for the OR rate takes the form

$$r_{OR} = \frac{(1-z_{OR})}{R_{OR}^\bullet} = \frac{1}{R_{OR}^\bullet}\left(1 - \frac{1}{K_{OR}}\prod_{i=1}^{n} a_i^{\nu_i}\right) \tag{3.20}$$

where the overall resistance of the reduced network is computed from its equivalent electrical network in terms of the step Rdots. These in turn are computed from

$$R_\rho^\bullet = \frac{1}{\vec{r}_\rho^\bullet} \tag{3.21}$$

82

where the resistance $R_\rho^\bullet$ (Rdot) is equal to the inverse of the rate of the forward step ($1/\vec{r}_\rho^{\,\bullet}$) (Eq. 3.21), under conditions that it is the RDS, i.e., when the entire driving force (affinity) for the OR occurs across it, the other steps being at QE. In other words, step $\vec{r}_\rho^{\,\bullet}$ is obtained following the LHHW approach, with which there is broad familiarity and ease.

In short, the step resistances $R_\rho^\bullet$ can be obtained *a priori* via the LHHW methodology, by treating each of the steps as RDS, in turn, and using the QE approximation for the remaining to determine any unknown activities of the intermediate species in $\vec{r}_\rho^{\,\bullet}$. The basic idea is that for a given RDS, the q linearly independent unknown intermediate site fractions are determined by identifying the appropriate intermediate reactions, or IRs, or pathways for the formation of intermediates that may be considered to be at QE, i.e., all involved steps have $\mathscr{A}_j \to 0$. An IR results from an appropriate linear combination of steps s_j that eliminates all of the intermediate species except that of interest, I_k, formed from terminal species along with the vacant site S. It is important to pick QE steps s_j that don't violate a KPL relation. For instance, if the RDS s_ρ ($\mathscr{A}_\rho \approx \mathscr{A}_{OR}$) under consideration is a part of an ER, clearly all the steps in the parallel branch of the ER cannot be at QE ($\mathscr{A}_j \to 0$), since that would violate the KPL for the cycle. This is, of course, not true when the cycle contains the OR, for which the affinity drop is equal to $\mathscr{A}_{OR}$.

Finally, the resulting rate law can be further simplified if the surface coverages of some of the intermediates are negligible, as is often the case. In fact, sometimes only a single intermediate is the most abundant reactive intermediate (MARI) on the surface [27].

3.3 Results and Discussion

We will follow the example of the WGS reaction, which we have analyzed before via the RR Graph approach [45], but using a recent DFT microkinetic model for the Pt-Re(111) catalyst [46]. This system with a single OR is not only of great practical significance in a variety of processes, but also is one in which the microkinetic models developed are of significant, although not overwhelming, complexity, so that our RR Graph based paring approach can be illustrated meaning and without excessive complexity. We will then compare the RR approach to Campbell's DRC for the same mechanism to directly compare the deductions and insights provided by the two alternate approaches.

It should be noted that the mechanism presented cannot be guaranteed to be exhaustive in listing the possible steps and intermediates that occur within this system. The approach presented does not widen the scope of a mechanism that is theorized through experimentation and DFT calculations, and thus will not be able to suggest what further steps or intermediates should be included in the mechanism. The major benefits are confirming the consistency of the DFT calculations and the connectivity of the steps, as well as pruning the mechanism down to the steps and kinetics that are most important to driving the reaction in the desired direction.

3.3.1 Constructing the RR Graph

The mechanism for the WGS on Pt-Re is shown in Table 3.1 with $p = 15$ elementary reaction steps s_ρ, and 1 overall reaction, OR. There are a total of 13 unique species which can be divided into $n = 4$ terminal species i.e., the reactants (H_2O and CO) and products (CO_2 and H_2) and, $l = 9$ surface intermediates ($H_2O \cdot S$, $CO \cdot S$, $H \cdot S$, $CO_2 \cdot S$, $OH \cdot S$, $O \cdot S$, $COOH \cdot S$, $HCOO \cdot S$ and S) where S stands for a free active site on the catalyst surface. Due to the site conservation, however, only $q = 8$ out of $l = 9$ intermediates are independent. The RR Graph can be constructed

84

based on a complete list of stoichiometrically enumerated RRs and nodes [59,60]. However, this rigorous mathematical enumeration of the complete list of pathways is tedious and unnecessary, since only a handful of RRs are independent.

According to Horiuti-Temkin theorem, only $\mu = p - q = 15 - 8 = 7$ RRs are linearly independent from the complete set of enumerated FRs and ERs for this system. Any appropriate set may be chosen. Additionally, only $\mu - 1 = 7 - 1 = 6$ of the ERs are linearly independent. Thus, a set of 7 linearly independent RRs may be readily determined by finding 6 independent ERs and one FR for the mechanism. These can, in fact, be determined simply from an inspection of the mechanism, thus avoiding the step of systematic stoichiometric algorithm as described in our earlier publications [42-45,59,60]. Such an independent set for this mechanism is provided in Table 3.2. In fact, the complete set of FRs and ERs can subsequently be determined topologically as walks, once the RR Graph is constructed. A direct FR for this system, as mentioned earlier, involves no more than $q + 1 = 8 + 1 = 9$ elementary steps, and contains no ERs. These FRs and ERs can be enumerated via manual counting or automated graph theoretical tools. This particular system contains 52 unique FRs and 33 unique ERs.

Cycle	s_2	s_3	s_4	s_5	s_6	s_7	s_8	s_9	s_{10}	s_{11}	s_{12}	s_{13}	s_{14}	s_{15}	s_{16}	OR_1
FR_1	+1	+1	+1	0	0	0	+1	+1	+1	+1	0	0	0	0	0	-1
ER_1	0	0	+1	0	0	0	0	0	0	0	0	0	+1	0	+1	0
ER_2	0	0	0	+1	0	0	0	0	0	0	0	0	+1	-1	0	0
ER_3	0	0	0	0	+1	0	0	0	0	0	0	0	0	-1	-1	0
ER_4	0	0	0	0	0	+1	0	0	-1	0	-1	0	0	0	0	0
ER_5	0	0	0	0	0	0	0	0	0	+1	-1	0	+1	-1	0	0
ER_6	0	0	0	0	0	0	0	0	0	0	-1	+1	0	-1	-1	0

Table 3.2: List of an Example of a Linearly Independent Set of Cycles for the WGS Mechanism in Table 3.1.

To construct the RR Graph, we begin by drawing the cycle graph by assembling the ERs together such that no reaction step is repeated in the graph by identifying common edges and nodes and fusing these "subgraphs" to produce a cycle graph that includes each ER. For example, in Figure (3.4a), ER_1 and ER_2 have in common a pair of nodes that have an s_{14} edge between them, so those cycle are fused along that edge.

We continue this process until we have a cycle graph that consists of the 6 linearly independent ERs. As suggested earlier for this example, each step, including the overall reaction step, should appear twice, and also the graph should be symmetric, which leads to the flipping and doubling of this fused graph (Figure 3.4b). We can clearly see that the two graphs have two edges (s_6 and s_7) in common that we can fuse to make it symmetrical. We then check each node to make sure that the KFL is satisfied, which are linear combinations of the species QSS relations provided in Table 3.3. We find the nodes highlighted in Figure (3.4c) to be considered as unbalanced, as they do not satisfy any KFL relation. These nodes can be balanced by adding two s_3 edges to one and two s_8 edges to the other. This creates two new unbalanced nodes to which we can add two s_2 edges and two s_9 edges. The steps s_2, s_3, s_8, and s_9 represent the adsorption and desorption steps that may be placed in any sequential order in the graph without affecting analysis or calculations, but the shown order makes the most sense in terms of how the mechanism proceeds. Finally, the OR is added twice to balance the terminal nodes, resulting in the complete RR Graph shown in Figure 3.2 and its electrical analogy in Figure 3.3.

Although in this example we are simply concerned with chemical steps, even surface or pore diffusion steps can be added within the RR Graph approach, as illustrated by Deveau et al. [61].

b)

c)
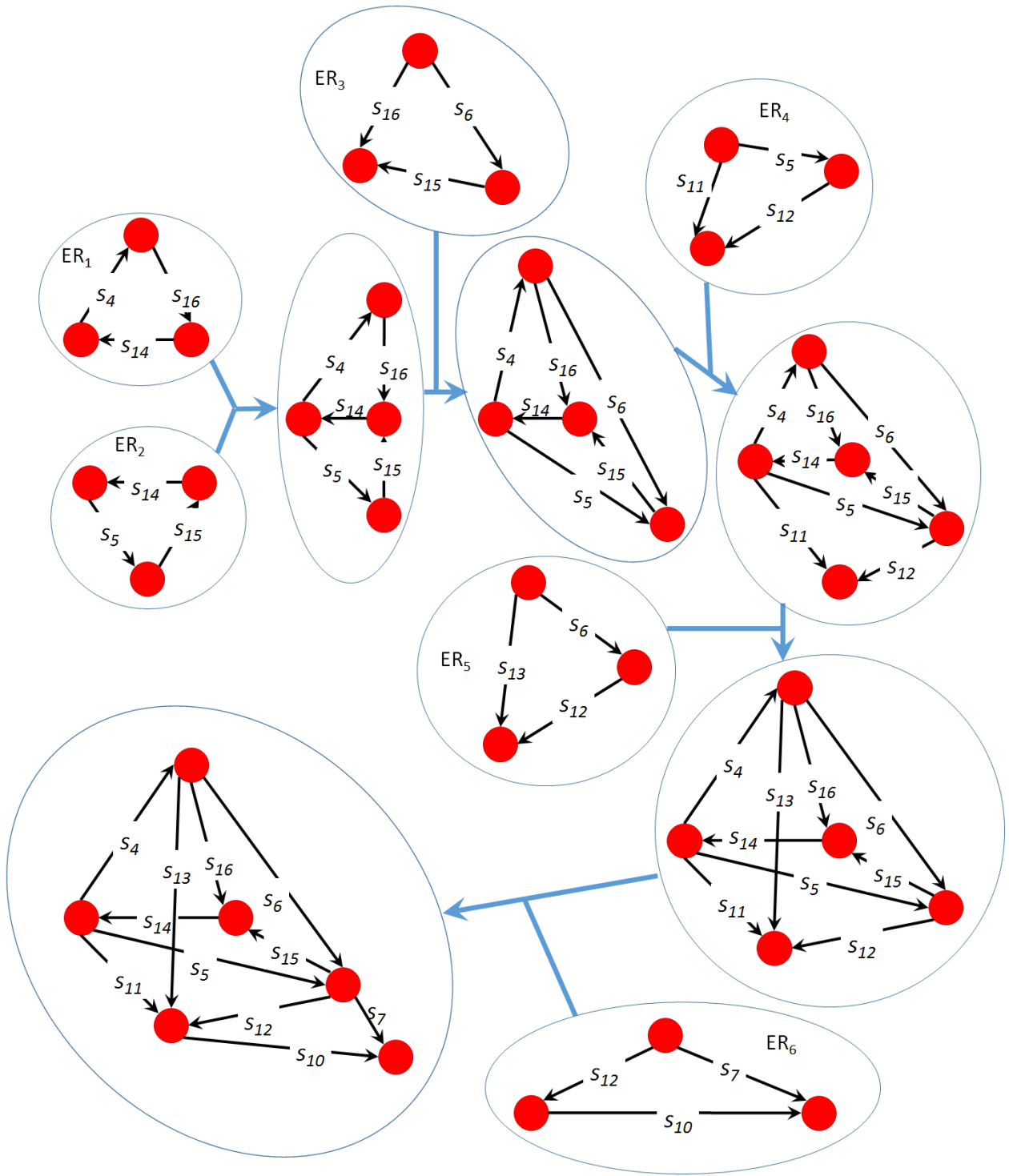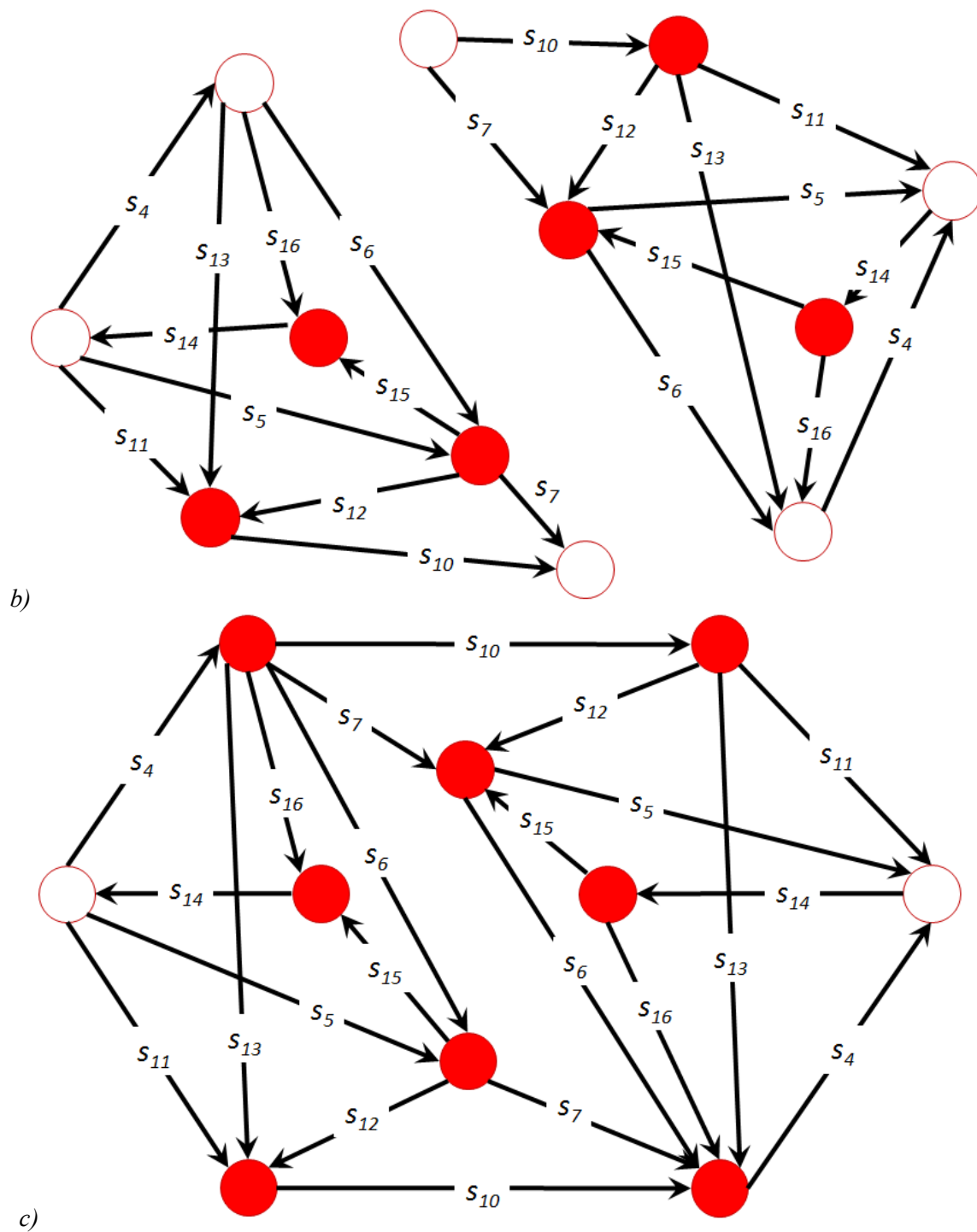
Figure 3.4a: Process of forming the RR Graph for the WGS reaction on Pt-Re. ERs are added in succession to form a cycle graph.

Figure 3.4b: Original and flipped cycle graphs with unfilled circles representing unbalanced nodes.

Figure 3.4c: The two cycle graphs having been merged along s_6 and s_7.

$Q_{H_2O \cdot S}:$ $\quad (+1)\, r_2 + (-1)\, r_4 + (+1)\, r_6 + (+1)\, r_{13} + (+1)\, r_{16} = 0$

$Q_{CO \cdot S}:$ $\quad (+1)\, r_3 + (-1)\, r_7 + (-1)\, r_{10} = 0$

$Q_{OH \cdot S}:$ $\quad (+1)\, r_4 + (-1)\, r_5 + (-2)\, r_6 + (-1)\, r_{10} + (+1)\, r_{12} + (-1)\, r_{13} + (+1)\, r_{15} = 0$

$Q_{H \cdot S}:$ $\quad (+1)\, r_4 + (+1)\, r_5 + (-2)\, r_9 + (+1)\, r_{11} + (-1)\, r_{14} = 0$

$Q_{O \cdot S}:$ $\quad (+1)\, r_5 + (+1)\, r_6 + (-1)\, r_7 + (-1)\, r_{12} + (-1)\, r_{15} = 0$

$Q_{CO_2 \cdot S}: (+1)\, r_7 + (-1)\, r_8 + (+1)\, r_{11} + (+1)\, r_{12} + (+1)\, r_{13} + (-1)\, r_{14} + (+1)\, r_{15} + (+1)\, r_{16} = 0$

$Q_{COOH \cdot S}: (+1)\, r_{10} + (-1)\, r_{11} + (-1)\, r_{12} + (-1)\, r_{13} = 0$

$Q_{HCOO \cdot S}: (+1)\, r_{14} + (-1)\, r_{15} + (-1)\, r_{16} = 0$

Table 3.3: QSS Relations for Each of the Intermediate Species.

3.3.2 Network Analysis and Pruning

The experimental WGS studies in Ref. (46) were performed on a Pt-Re catalyst primarily at a temperature $T = 548$ K, and pressure $p = 1$ atm, at various feed compositions. For our analysis, we chose parameters similar to those chosen by Carasquillo-Flores et al. [46], with a feed composition of H_2O (25%), CO (15%) and N_2 (balance), and a conversion, $X = 0.25$. A numerical solution of the KFL equations (QSS relations) for the intermediates concentrations under these conditions was then performed as described in section 3.2.3. A microkinetic approach based on differential equations was also used to estimate initial values for solving the KFL equations. The step weights ω_ρ for this were determined from terminal species partial pressures and the rate constants determined from the activation energies and pre-exponential factors for the Pt-Re catalyst as tabulated in Table 3.1 [46]. The determination of the intermediates concentrations hence allowed calculation of step rates along with reversibility, affinities and resistances for the

elementary reaction steps, which are summarized in Table 3.4. Finally, the rate of the OR can be obtained from the TNs (Figure 3.2), e.g. $r_{OR} = r_2 = r_9$.

It is immediately clear from Figure 3.2 that there is only one pathway where there is an appreciable flux, while for all other steps and pathways, the flux is negligible. This pathway consists of the adsorption/desorption steps (s_2, s_3, s_8, and s_9), dissociation of water (s_4), formation of carboxyl species (s_{10}), and the subsequent direct dehydrogenation of adsorbed carboxyl (s_{11}). This leads to a reduced RR Graph with a single FR (Figure 3.5), obtained by dropping those with negligible rates.

A look at the calculated resistance of each step for these conditions confirms this conclusion. It further indicates that s_4 and s_{10} have a much higher resistance than the other steps in the remaining FR. Thus, we can approximate the overall reaction rate in terms of the overall resistance being equal to the sum of the resistances of the two steps in sequence, and using Eq. (3.20):

$$r_{OR} = \frac{(1 - z_{OR})}{R_{OR}^{\bullet}} = \frac{1}{R_4^{\bullet} + R_{10}^{\bullet}} \left(1 - \frac{1}{K_{OR}} \prod_{i=1}^{n} a_i^{v_i} \right) \tag{3.22}$$

The electrical analogy for this is provided in Figure 3.6.

Reaction Step	Step Resistance	Rate (s^{-1})	Reversibility	Affinity
2	1.15E-10	0.0917	1.000	1.05E-11
3	1.26E-08	0.0917	1.000	1.15E-09
4	9.91	0.0917	0.403	9.09E-01
5	1.79E-07	1.0E-06	1.000	1.79E-13
6	2.38E-11	1.0E-07	1.000	2.38E-18
7	43.1	1E-20	1.000	4.31E-19
8	1.55E-13	0.0917	1.000	1.42E-14
9	7.92E-13	0.0917	1.000	7.26E-14
10	3.53E-01	0.0917	0.968	3.24E-02
11	1.56E-06	0.0917	1.000	1.43E-07
12	5.39E-03	1.0E-06	1.000	5.39E-09
13	4.89E-11	1E-15	1.000	4.89E-26
14	1.08E-10	1E-14	1.000	1.18E-24
15	3.58E-10	1E-16	1.000	3.58E-26
16	2.87E-12	1E-14	1.000	2.87E-26

Table 3.4: Step Resistances, Rates, Reversibilities and Affinities for each Step in the WGS Reaction.
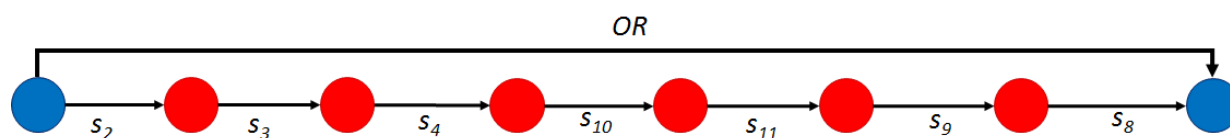
Figure 3.5: Reduced RR Graph for the WGS reaction on Pt-Re catalyst
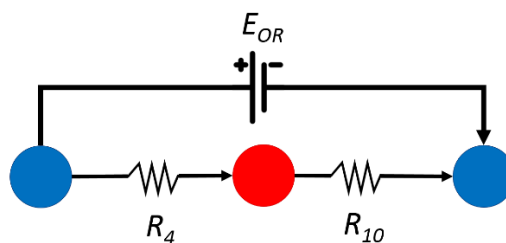
Figure 3.6: Simplified electrical analogy diagram for the WGS reaction on Pt-Re catalyst

In short, we can surmise based on this flux analysis and confirmed by the resistance comparisons of the steps, that the Full Route (FR) of ($s_2 + s_3 + s_4 + s_8 + s_9 + s_{10} + s_{11}$) is the only dominant pathway for the WGS on Pt-Re under these conditions and that steps s_4 and s_{10} can be considered as the two rate limiting steps (RLSs). This is confirmed for a range of temperatures as shown in Figure 3.7, which shows an evaluation of the resistances for the steps: s_4, s_{10} and s_{11}, all others being much smaller.
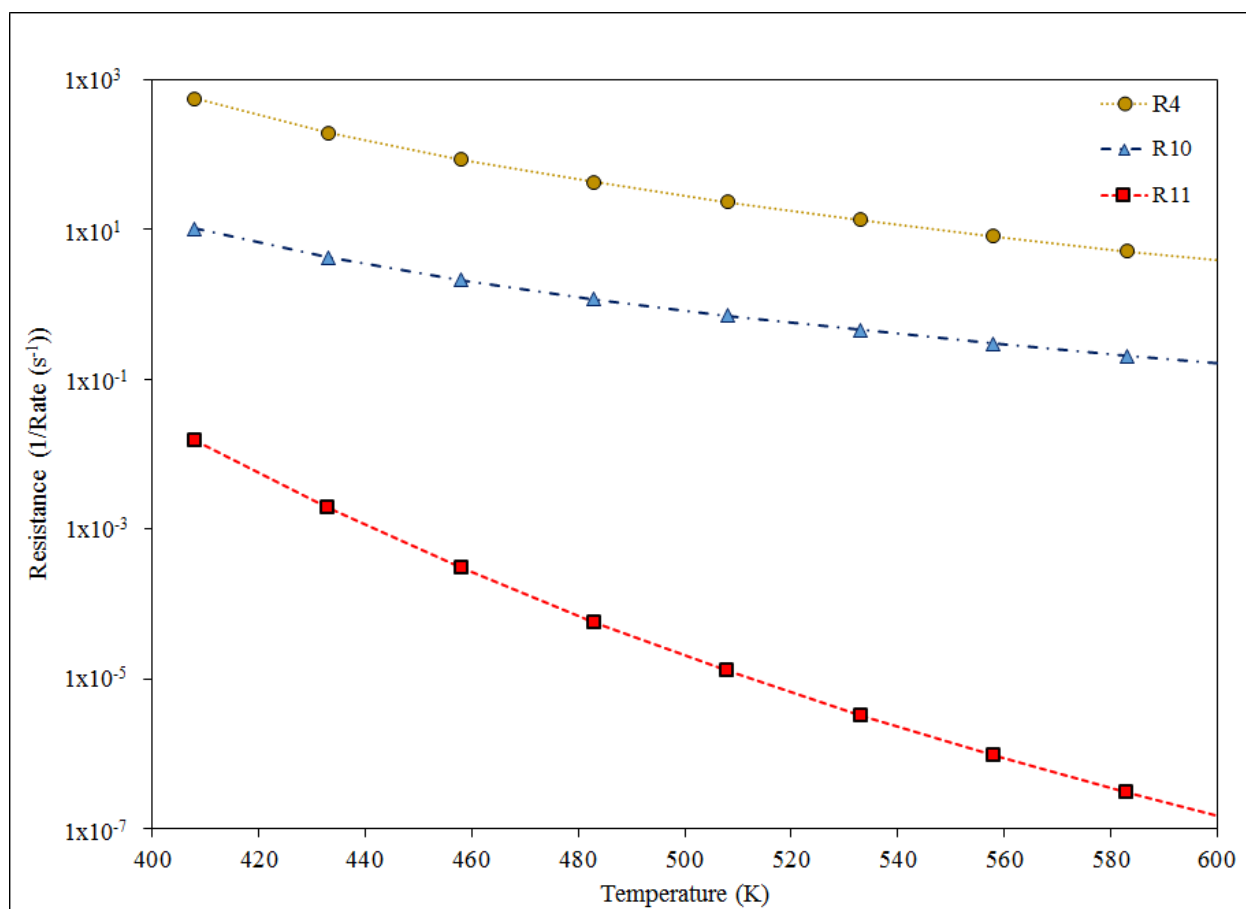
Figure 3.7: Comparison of step resistances R_i for the non-adsorption/desorption steps versus temperature for the dominant pathway of the WGS reaction on Pt-Re.

3.3.3 Explicit Rate Expression through Alternate Form of Ohm's Law

We use the Rdot approach described in section 3.2.3.5 to obtain an explicit rate expression via (Eq. 3.22) for the WGS reaction on the Pt-Re catalyst. For each step, thus, we calculate $R_\rho^\bullet$ by considering each step in turn to be the RDS, the remaining steps being at QE, and then following the conventional LHHW [26,27] approach. This allows determination of the q intermediate site fractions by identifying the appropriate QE intermediate reactions (IRs), or pathways, for the formation of intermediates. These IRs are found by a linear combination of the QE steps s_j that eliminates all the intermediate species except that of interest, I_k, formed from terminal species along with some reference intermediate, e.g., the vacant site S in case of catalytic reactions.

We start by first considering s_4 as the RDS, the remaining steps being at QE. Thus,

$$R_4^\bullet = \frac{1}{\vec{r}_4^\bullet} = \frac{1}{\vec{\omega}_4 \theta_{H_2O\cdot S,4}^\bullet \theta_{0,4}^\bullet} = \frac{1}{\vec{\omega}_4 \left(\dfrac{\theta_{H_2O\cdot S,4}^\bullet}{\theta_{0,4}^\bullet} \right) (\theta_{0,4}^\bullet)^2} \tag{3.23}$$

where the superscript dot refers to the Rdot methodology, and the subscript 4 serves as a reminder that this is for the case when s_4 as the RDS. With all other steps then at QE, appropriate IRs for the formation of the $q = 8$ independent surface intermediates, ($H_2O\cdot S$, $CO\cdot S$, $H\cdot S$, $CO_2\cdot S$, $OH\cdot S$, $O\cdot S$, $COOH\cdot S$, and $HCOO\cdot S$) are:

$IR_{H_2O\cdot S} : (+1)\, s_2$

$IR_{CO\cdot S} : (+1)\, s_3$

$IR_{OH\cdot S} : (-1)\, s_3 + (-1)\, s_5 + (-1)\, s_7 + (-1)\, s_8 + (-1/2)\, s_9$

$$IR_{\text{H·S}} : (-1/2)\, s_9$$

$$IR_{\text{O·S}} : (-1)\, s_3 + (-1)\, s_7 + (-1)\, s_8 \qquad\qquad (3.24)$$

$$IR_{\text{CO}_2\text{·S}} : (-1)\, s_8$$

$$IR_{\text{COOH·S}} : (-1)\, s_8 + (-1/2)\, s_9 + (-1)\, s_{11}$$

$$IR_{\text{HCOO·S}} : (-1)\, s_5 + (-1)\, s_8 + (-1/2)\, s_9 + (-1)\, s_{15}$$

For these steps at QE, the corresponding site fractions, thus, following the LHHW methodology, are:

$$\frac{\theta^{\bullet}_{\text{H}_2\text{O·S},4}}{\theta^{\bullet}_{0,4}} = \left(\frac{\vec{\omega}_2}{\overleftarrow{\omega}_2}\right)^{+1}$$

$$\frac{\theta^{\bullet}_{\text{CO·S},4}}{\theta^{\bullet}_{0,4}} = \left(\frac{\vec{\omega}_3}{\overleftarrow{\omega}_3}\right)^{+1}$$

$$\frac{\theta^{\bullet}_{\text{OH·S},4}}{\theta^{\bullet}_{0,4}} = \left(\frac{\vec{\omega}_3}{\overleftarrow{\omega}_3}\right)^{-1}\left(\frac{\vec{\omega}_5}{\overleftarrow{\omega}_5}\right)^{-1}\left(\frac{\vec{\omega}_7}{\overleftarrow{\omega}_7}\right)^{-1}\left(\frac{\vec{\omega}_8}{\overleftarrow{\omega}_8}\right)^{-1}\left(\frac{\vec{\omega}_9}{\overleftarrow{\omega}_9}\right)^{-1/2}$$

$$\frac{\theta^{\bullet}_{\text{O·S},4}}{\theta^{\bullet}_{0,4}} = \left(\frac{\vec{\omega}_3}{\overleftarrow{\omega}_3}\right)^{-1}\left(\frac{\vec{\omega}_7}{\overleftarrow{\omega}_7}\right)^{-1}\left(\frac{\vec{\omega}_8}{\overleftarrow{\omega}_8}\right)^{-1}$$

$$\frac{\theta^{\bullet}_{\text{H·S},4}}{\theta^{\bullet}_{0,4}} = \left(\frac{\vec{\omega}_9}{\overleftarrow{\omega}_9}\right)^{-1/2} \qquad\qquad (3.25)$$

$$\frac{\theta^{\bullet}_{CO_2\cdot S,4}}{\theta^{\bullet}_{0,4}} = \left(\frac{\vec{\omega}_8}{\bar{\omega}_8}\right)^{-1}$$

$$\frac{\theta^{\bullet}_{COOH\cdot S,4}}{\theta^{\bullet}_{0,4}} = \left(\frac{\vec{\omega}_8}{\bar{\omega}_8}\right)^{-1}\left(\frac{\vec{\omega}_9}{\bar{\omega}_9}\right)^{-\frac{1}{2}}\left(\frac{\vec{\omega}_{11}}{\bar{\omega}_{11}}\right)^{-1}$$

$$\frac{\theta^{\bullet}_{HCOO\cdot S,4}}{\theta^{\bullet}_{0,4}} = \left(\frac{\vec{\omega}_5}{\bar{\omega}_5}\right)^{-1}\left(\frac{\vec{\omega}_8}{\bar{\omega}_8}\right)^{-1}\left(\frac{\vec{\omega}_9}{\bar{\omega}_9}\right)^{-\frac{1}{2}}\left(\frac{\vec{\omega}_{15}}{\bar{\omega}_{15}}\right)^{-1}$$

and using site balance to determine the unoccupied site fraction, we finally get:

$$R^{\bullet}_4 = \left(\frac{\bar{\omega}_2}{\vec{\omega}_4\vec{\omega}_2}\right)\left(1+\frac{\bar{\omega}_2}{\vec{\omega}_2}+\frac{\bar{\omega}_3}{\vec{\omega}_3}+\frac{\bar{\omega}_3}{\vec{\omega}_3}\frac{\bar{\omega}_5}{\vec{\omega}_5}\frac{\bar{\omega}_7}{\vec{\omega}_7}\frac{\bar{\omega}_8}{\vec{\omega}_8}\sqrt{\frac{\bar{\omega}_9}{\vec{\omega}_9}}+\frac{\bar{\omega}_3}{\vec{\omega}_3}\frac{\bar{\omega}_7}{\vec{\omega}_7}\frac{\bar{\omega}_8}{\vec{\omega}_8}+\sqrt{\frac{\bar{\omega}_9}{\vec{\omega}_9}}+\frac{\bar{\omega}_8}{\vec{\omega}_8}+\frac{\bar{\omega}_8}{\vec{\omega}_8}\sqrt{\frac{\bar{\omega}_9}{\vec{\omega}_9}}\frac{\bar{\omega}_{11}}{\vec{\omega}_{11}}+\frac{\bar{\omega}_5}{\vec{\omega}_5}\frac{\bar{\omega}_8}{\vec{\omega}_8}\sqrt{\frac{\bar{\omega}_9}{\vec{\omega}_9}}\frac{\bar{\omega}_{15}}{\vec{\omega}_{15}}\right)^2$$

(3.26)

Performing a similar analysis for $R^{\bullet}_{10}$ i.e., with step s_{10} as the RDS

$$R^{\bullet}_{10} = \left(\frac{\bar{\omega}_2\bar{\omega}_3\bar{\omega}_4}{\vec{\omega}_{10}\vec{\omega}_2\vec{\omega}_3\vec{\omega}_4}\sqrt{\frac{\bar{\omega}_9}{\vec{\omega}_9}}\right)\left(1+\frac{\bar{\omega}_2}{\vec{\omega}_2}+\frac{\bar{\omega}_3}{\vec{\omega}_3}+\frac{\bar{\omega}_2}{\vec{\omega}_2}\frac{\bar{\omega}_4}{\vec{\omega}_4}\sqrt{\frac{\bar{\omega}_9}{\vec{\omega}_9}}+\frac{\bar{\omega}_3}{\vec{\omega}_3}\frac{\bar{\omega}_7}{\vec{\omega}_7}\frac{\bar{\omega}_8}{\vec{\omega}_8}+\sqrt{\frac{\bar{\omega}_9}{\vec{\omega}_9}}+\frac{\bar{\omega}_8}{\vec{\omega}_8}+\frac{\bar{\omega}_8}{\vec{\omega}_8}\sqrt{\frac{\bar{\omega}_9}{\vec{\omega}_9}}\frac{\bar{\omega}_{11}}{\vec{\omega}_{11}}+\frac{\bar{\omega}_5}{\vec{\omega}_5}\frac{\bar{\omega}_8}{\vec{\omega}_8}\sqrt{\frac{\bar{\omega}_9}{\vec{\omega}_9}}\frac{\bar{\omega}_{15}}{\vec{\omega}_{15}}\right)^2$$

(3.27)

By examining each site fraction individually, i.e., $\dfrac{\theta^{\bullet}_{k,p}}{\theta^{\bullet}_{0,p}}$, it might be possible to simplify these

further.[27] Thus, $\dfrac{\theta^{\bullet}_{H_2O\cdot S}}{\theta^{\bullet}_{0,p}} = 0.113$, $\dfrac{\theta^{\bullet}_{CO\cdot S}}{\theta^{\bullet}_{0,p}} = 0.644$, $\dfrac{\theta^{\bullet}_{OH\cdot S}}{\theta^{\bullet}_{0,p}} = 0.000131$, $\dfrac{\theta^{\bullet}_{O\cdot S}}{\theta^{\bullet}_{0,p}} = 0.000685$, $\dfrac{\theta^{\bullet}_{H\cdot S}}{\theta^{\bullet}_{0,p}} = 0.194$

, $\dfrac{\theta^{\bullet}_{CO_2\cdot S}}{\theta^{\bullet}_{0,p}} = 0.000150$, $\dfrac{\theta^{\bullet}_{COOH\cdot S}}{\theta^{\bullet}_{0,p}} = 0.0000445$, and $\dfrac{\theta^{\bullet}_{HCOO\cdot S}}{\theta^{\bullet}_{0,p}} = 0.00000315$, it is revealed that $\theta^{\bullet}_{O\cdot S}$,

$\theta^{\bullet}_{COOH\cdot S}$, $\theta^{\bullet}_{OH\cdot S}$, $\theta^{\bullet}_{CO_2\cdot S}$ and $\theta^{\bullet}_{HCOO\cdot S}$ are relatively insignificant in comparison to $\theta^{\bullet}_{CO\cdot S}$, $\theta^{\bullet}_{H_2O\cdot S}$, and $\theta^{\bullet}_{H\cdot S}$

in both $R_4^\bullet$ and $R_{10}^\bullet$, so that the smaller site fractions can be neglected when summing the site fractions to find $\theta_{0,p}^\bullet$. Thus, the above expressions simplify to

$$R_4^\bullet \approx \left(\frac{\bar{\omega}_2}{\vec{\omega}_4 \bar{\omega}_2} \right)\left(1 + \frac{\bar{\omega}_2}{\vec{\omega}_2} + \frac{\bar{\omega}_3}{\vec{\omega}_3} + \sqrt{\frac{\bar{\omega}_9}{\vec{\omega}_9}} \right)^2 \qquad (3.28)$$

and

$$R_{10}^\bullet \approx \left(\frac{\bar{\omega}_2 \bar{\omega}_3 \bar{\omega}_4}{\vec{\omega}_{10} \bar{\omega}_2 \bar{\omega}_3 \bar{\omega}_4} \sqrt{\frac{\bar{\omega}_9}{\vec{\omega}_9}} \right)\left(1 + \frac{\bar{\omega}_2}{\vec{\omega}_2} + \frac{\bar{\omega}_3}{\vec{\omega}_3} + \sqrt{\frac{\bar{\omega}_9}{\vec{\omega}_9}} \right)^2 \qquad (3.29)$$

so that the simplified expression for the overall rate from Eqs (3.22), (3.28) and (3.29):

$$r_{OR} \approx \frac{1}{\left(1 + \frac{\bar{\omega}_3 \bar{\omega}_4}{\vec{\omega}_{10} \bar{\omega}_3} \sqrt{\frac{\bar{\omega}_9}{\vec{\omega}_9}} \right) \frac{\bar{\omega}_2}{\vec{\omega}_4 \bar{\omega}_2} \left(1 + \frac{\bar{\omega}_2}{\vec{\omega}_2} + \frac{\bar{\omega}_3}{\vec{\omega}_3} + \sqrt{\frac{\bar{\omega}_9}{\vec{\omega}_9}} \right)^2} \left(1 - \frac{1}{K_{OR}} \frac{p_{CO_2} p_{H_2}}{p_{H_2O} p_{CO}} \right) \qquad (3.30)$$

Finally, substituting the rate constants and concentration of terminal species for reaction step weights ω_p (Table 3.1), we have the overall reaction rate expression in the conventional form

$$r_{OR} \approx \frac{\vec{k}_4 \vec{k}_{10} K_2 K_3 \sqrt{K_9}\, p_{H_2O} p_{CO}}{\left(\vec{k}_{10} K_3 \sqrt{K_9}\, p_{CO} + \vec{k}_4 \sqrt{p_{H_2}} \right)\left(1 + K_2 p_{H_2O} + K_3 p_{CO_2} + \sqrt{\frac{1}{K_9 p_{H_2}}} \right)^2} \left(1 - \frac{1}{K_{OR}} \frac{p_{CO_2} p_{H_2}}{p_{H_2O} p_{CO}} \right) \qquad (3.31)$$

where, $K_\rho = \vec{k}_\rho / \bar{k}_\rho$ is the equilibrium constant for step s_p, and the DFT parameters for the rate constants are provided in Table 3.1.

This equation is in good agreement with the results of the numerically calculated QSS calculation as shown in a parity plot (Figure 3.8), proving that the Rdot method and subsequent simplification are valid for the kinetic data used for the WGS reaction on Pt-Re catalyst.
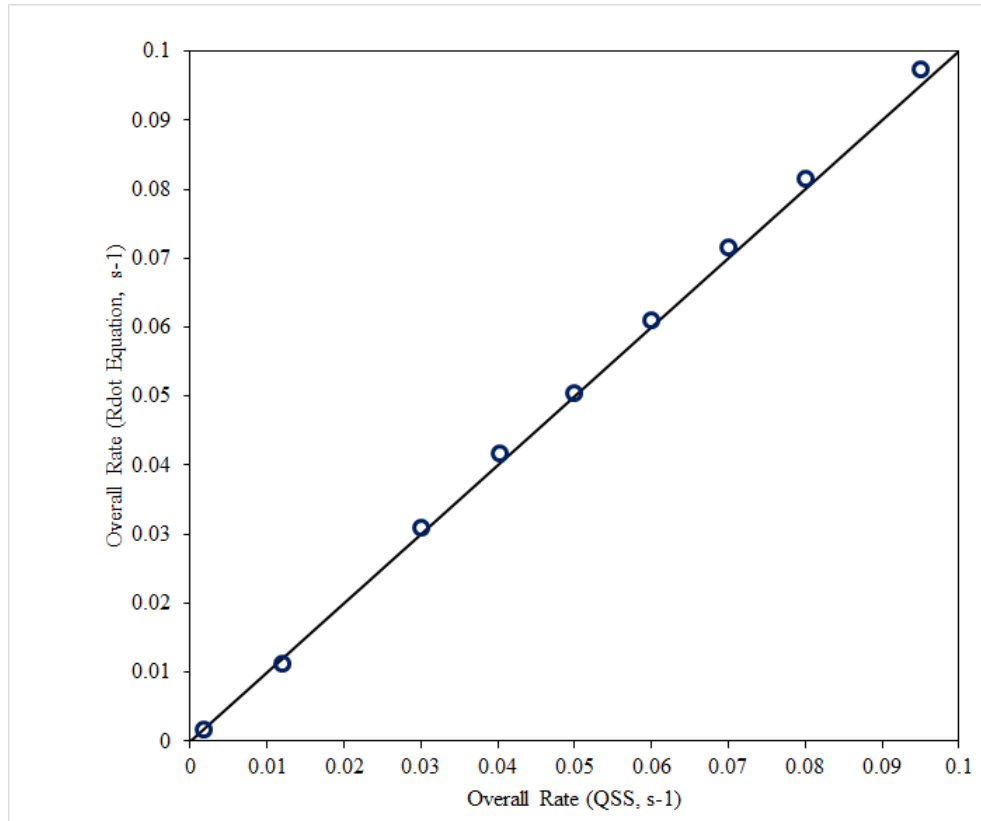
Figure 3.8: Comparison of overall QSS rate obtained from implementation of Ohm's law Eq. (3.32) and that calculated numerically for the WGS reaction on Pt-Re. Where each point is a different temperature for which the QSS rate is calculated.

3.3.4 Analysis via Campbell's Degree of Rate Control

Campbell's DRC analysis for the WGS reaction on Pt-Re catalyst was conducted from the rates for each step calculated via numerical QSS analysis for the same conditions used in the previous section, i.e., a temperature of 548K, and pressure $p = 1$ atm with a feed composition of H_2O (25%), CO (15%) and N_2 (balance), and a conversion, $X = 0.25$. To estimate $X_{DRC,\rho}$ (Eq. 3.6 or 3.9), the change in the overall rate when a rate constant changes incrementally was calculated

as follows. The forward rate constant of a chosen step was thus increased by a small amount (i.e., 1%), and since $K_\rho = \vec{k}_\rho / \overleftarrow{k}_\rho$ needs to be constant, the reverse rate constant was increased by 1% as well. The new r_{OR} was calculated using the increased $\vec{k}_\rho$ and $\overleftarrow{k}_\rho$ values, with all other rate constants remaining unchanged. Thus, the Campbell's DRC was calculated using the finite difference form of Eq (3.6)

$$X_{DRC,\rho} \approx \frac{\vec{k}_\rho}{r_{OR}} \cdot \left(\frac{\Delta r_{OR}}{\Delta \vec{k}_\rho} \right)_{\mathbf{a},k_{r \neq \rho}} \tag{3.32}$$

This process was completed for each step of the mechanism in turn and compared to the calculations for this system that are reported by Carrasquillo-Flores et al [46]. (Table 3.5). The results are similar, showing that s_{10}, the formation of the carboxyl species step, has the largest DRC and is hence the RDS, the DRC of all other steps being insignificant or zero.

A similar approach was used to estimate Campbell's Degree of Thermodynamic Control (DTC), as given in Eq. (3.11), to determine the significance of the stability of an intermediate species on OR rate. For numerical estimation, we used the finite difference form of Eq. (3.11). Since changing the GFE of formation directly changes the binding energy, to calculate Campbell's DTC for an intermediate k, the binding energy of that intermediate was reduced by 1% while all other binding energies were kept constant. The rate constants for each forward or reverse reaction step that includes that intermediate was thus changed due to the activation energy barrier being raised due to the lower energy state of the intermediate. The above described QSS numerical calculation was then performed using these new rate constants to find the change in the overall rate. This was repeated for each of the eight intermediates and the results are shown in Table 3.6.

Reaction Step	$X_{DRC,Pt\text{-}Re}$[A]	$X_{DRC,Pt\text{-}Re}$[B]
1	0	0
2	0	0
3	0	0
4	-1×10^{-4}	-3×10^{-4}
5	0	0
6	0	0
7	0	0
8	0	0
9	0	0
10	0.95	0.95
11	8×10^{-3}	9×10^{-3}
12	0	0
13	0	0
14	0	0
15	0	0
16	0	0

Table 3.5: Values for Campbell's Degree of Rate Control for Pt-Re Catalyst for [A] This Work and [B] Carrasquillo-Flores et al [46].

Reaction Intermediate	$X_{DTC,Pt\text{-}Re}$
O·S	0
OH·S	0
CO·S	-0.650
CO_2·S	-0.018
COOH·S	0
H_2O·S	0
H·S	-0.058
HCOO·S	0

Table 3.6: Values for Campbell's Degree of Thermodynamic Control for Each Reaction intermediate.

Carasquillo-Flores et al. reported coverage of CO to be approximately 2/3 ML and coverage of H atoms to range between 0.15 ML to 0.2 ML under similar conditions for their model.[46] This agrees with the results for both Campell's DoRC and the RR Graph Approach. As

seen in Table 3.6, $X_{DTC,CO}$ = -0.65 and $X_{DTC,H}$ = -0.058, which suggests that CO is the MARI for these conditions with some H atoms also occupying the surface. The site fraction comparison for the Rdot method also suggest that CO is the MARI for this reaction with H coverage having additional, although lesser, importance.

3.3.5 Comparison of Campbell's Degree of Rate Control and RR Graph Approach

For the WGS reaction on the Pt-Re catalyst, Campbell's DRC determines that the formation of the carboxyl species step (s_{10}) is the RDS of the mechanism, since its $X_{DRC,10} = 0.96$, that for the remaining steps being much smaller or zero. On the other hand, the RR approach concludes that the dissociation of water step (s_4) is the largest contributor to limiting the overall rate, with s_{10} also limiting the rate somewhat, although not to the same extent as s_4. Carrasquillo-Flores et al. [46], in fact, also eventually concluded that s_4 was the RDS despite s_{10} being indicated as the RDS from Campbell's DRC, stating: "Putting all the observations together we infer that H_2O activation, s_4, is the underlying rate-controlling step."

Carrasquillo-Flores et al. [46] further noted that based on their model and experiments, they concluded that the pathway including s_4, s_{10} and s_{11} was the only pathway with a significant amount of flux. Not only does the RR approach agree with this conclusion arrived at circuitously by the authors, it provides a quantitative estimation of how much each step contributes to the overall rate. Clearly, Campbell's DRC arrives at the wrong conclusion in this case.

Furthermore, according to Campbell's theory, the sum of the DRC of all the steps should add to unity. For the WGS reaction on Pt-Re catalyst, it is found to be 0.96, which is close to, but not precisely unity. However, there are examples that show that it is significantly different from unity. Thus, according to the results found in Ref. (25) for the WGS reaction on Cu catalyst, it

only adds up to approximately 0.83, well below unity. On the other hand, this does not seem to affect the conclusions one can make about a mechanism, as long as for one of the steps $X_{DRC,\rho}$ is much higher than that of any other step.

For the WGS reaction example under consideration, thus, there is more than one RLS and this conclusion does not much change with temperature (see Figure 3.7) or other conditions. In fact, the RR approach provides quantitative estimates of the resistance of each step and clearly identifies those that limit the rate and the pathways that contribute significantly.

3.4 Conclusions

We have shown via a detailed example of how the analysis and reduction of a reaction mechanism can be accomplished by using the electrical network analogy within our Reaction Route Graph method. Although Campbell's Degree of Rate Control is the most common technique available, currently, we show here that our RR Graph approach is superior and more insightful. The example of the WGS reaction on Pt-Re considered here, in fact, shows that Campbell's DRC can lead to erroneous conclusions that are inconsistent with experimental results [46]. Further, the contention that $\sum_{\rho=1}^{p} X_{DRC,\rho} = 1$ is not true in general. The RR Graph method is not limited to a single RDS or single pathway mechanisms in its usefulness. Further, the electrical analogy combined with the well-familiar LHHW methodology provides accurate rate expressions even for non-linear cases such as the WGS reaction example considered here, not otherwise possible. It is thus concluded that the electrical analogy and the RR Graph approach is a much more effective and revealing Ockham's razor for pruning microkinetic catalytic mechanisms than is Cambell's DRC.

A current limitation of our approach is that manually drawing the RR Graph for a system with a very large number of steps is challenging, especially for non-linear systems such as the WGS reaction. However, this does not limit the efficacy of the electrical analogy approach in pruning a large mechanism via a comparison of the reaction step resistance and affinity following a numerical analysis. Of course, we envision a tool that will eventually automate the graph drawing

3.5 References

1. Dumesic JA, Rudd DF, Aparicio LM, Rekoske JE, Treviño AA. The microkinetics of heterogeneous catalysis. American Chemical Society.1993.

2. Ertl G. Heterogeneous catalysis on the atomic scale. The Chemical Record. 2001;1(1): 33-45.

3. Cortright RD, Dumesic JA. Kinetics of heterogeneous catalytic reactions: Analysis of reaction schemes. Advances in catalysis. 2001;46:161-264.

4. Dumesic JA, Huber GW, Boudart M. Principles of heterogeneous catalysis. in Handbook of Heterogeneous Catalysis, Wiley-VCH; 2008.

5. Law CK, Sung CJ, Wang H, Lu T F. Development of comprehensive detailed and reduced reaction mechanisms for combustion modeling. AIAA journal. 2003;41(9): 1629-1646.

6. Li J, Zhao Z, Kazakov A, Dryer FL. An updated comprehensive kinetic model of hydrogen combustion. International Journal of Chemical Kinetics. 2004;36(10):566-575.

7. Kee RJ, Coltrin ME, Glarborg P. Chemically reacting flow: theory and practice. John Wiley & Sons. 2005.

8. Pandis SN, Seinfeld JH. Sensitivity analysis of a chemical mechanism for aqueous-phase atmospheric chemistry. Journal of Geophysical Research: Atmospheres (1984–2012). 1989;94(D1):1105-1126.

9. Gao D, Stockwell WR, Milford JB. First-order sensitivity and uncertainty analysis for a regional-scale gas-phase chemical mechanism. Journal of Geophysical Research: Atmospheres (1984–2012). 1995;100(D11):23153-23166.

10. Sandu A, Daescu DN, Carmichael GR, Chai T. Adjoint sensitivity analysis of regional air quality models. Journal of Computational Physics. 2005;204(1):222-252.

11. Degenring D, Froemel C, Dikta G, Takors R. Sensitivity analysis for the reduction of complex metabolism models. Journal of Process Control. 2004;14(7):729-745.

12. Smith GP, Golden DM, Frenklach M, Moriarty NW, Eiteneer B, Goldenberg M, Bowman CT, Hanson RK, Song S, Gardiner Jr WC, Lissianski VV, Qin Z. GRI-Mech – An optimized detailed chemical reaction mechanism for methane combustion. 1999. http://combustion.berkeley.edu/Combustion_Laboratory/gri-mech/

13. Mhadeshwar AB, Vlachos DG. Is the water–gas shift reaction on Pt simple?: Computer-aided microkinetic model reduction, lumped rate expression, and rate-determining step. Catalysis Today. 2005;105(1):162-172.

14. Sutton JE, Panagiotopoulou P, Verykios XE, Vlachos DG. Combined DFT, microkinetic, and experimental study of ethanol steam reforming on Pt. The Journal of Physical Chemistry. 2013;117(9):4691-4706.

15. Farberow CA, Dumesic JA, Mavrikakis M. Density functional theory calculations and analysis of reaction pathways for reduction of nitric oxide by hydrogen on Pt (111). in print, ACS Catalysis. 2014

16. Heyden A, Hansen N, Bell AT, Keil FJ. Nitrous oxide decomposition over Fe-ZSM-5 in the presence of nitric oxide: a comprehensive DFT study. The Journal of Physical Chemistry B. 2006;110(34);17096-17114.

17. Broadbelt LJ, Snurr RQ. Applications of molecular modeling in heterogeneous catalysis research. Applied Catalysis A: General. 2000;200(1):23-46.

18. Gokhale AA, Kandoi S, Greeley JP, Mavrikakis M, Dumesic JA. Molecular-level descriptions of surface chemistry in kinetic models using density functional theory. Chemical Engineering Science. 2004;59(22):4679-4691.

19. Nørskov JK, Abild-Pedersen F, Studt F, Bligaard T. Density functional theory in surface chemistry and catalysis. Proceedings of the National Academy of Sciences. 2011;108(3):937-943.

20. Shustorovich E, Sellers H. The UBI-QEP method: a practical theoretical approach to understanding chemistry on transition metal surfaces. Surface Science Reports. 1998;31(1):1-119.

21. Fishtik I, Datta R. A UBI–QEP microkinetic model for the water–gas shift reaction on Cu (111). Surface Science. 2002;512(3):229-254.

22. Waugh KC. Prediction of Global Reaction Kinetics by Solution of the Arrherius Parametrized Component Elementary Reactions: Microkinetic Analysis. Catalysis Today. 1999;53:161- 176.

23. Stoltze P. Microkinetic simulation of catalytic reactions. Progress in surface science. 2000;65(3):65-150.

24. Lynggaard H, Andreasen A, Stegelmann C, Stoltze P. Analysis of simple kinetic models in heterogeneous catalysis. Progress in surface science. 2004;77(3):71-137.

25. Madon RJ, Braden D, Kandoi S, Nagel P, Mavrikakis M, Dumesic JA. Microkinetic analysis and mechanism of the water gas shift reaction over copper catalysts. Journal of Catalysis. 2011;281(1):1-11.

26. Hougen OA, Watson KM. Solid catalysts and reaction rates—general principles. Industrial & Engineering Chemistry. 1943;35:529–541.

27. Boudart M, Djéga-Mariadassou G. Kinetics of Heterogeneous Catalytic Reactions. Princeton University Press. Princeton NJ. 1984.

28. Boudart M. From the Century of the Rate Equations to the Century of the Rate Constants: A Revolution in Catalytic Kinetics and Assisted Catalyst Design. Catal. Lett. 2000;65:1-3.

29. Broadbelt LJ, Stark SM, Klein MT. Computer generated pyrolysis modeling: on-the-fly generation of species, reactions, and rates. Industrial & Engineering Chemistry Research. 1994;33(4):790-799.

30. Hoffmann R, Minkin VI, Carpenter BK. Ockham's razor and chemistry. Bulletin de la Société chimique de France. 1996;133(2):117-130.

31. Lu T, Law CK. A criterion based on computational singular perturbation for the identification of quasi steady state species: A reduced mechanism for methane oxidation with NO chemistry. Combustion and Flame. 2008;154(4):761-774.

32. Zhang H, Linford JC, Sandu A, Sander R. Chemical mechanism solvers in air quality models.Atmosphere. 2011;2(3):510-532.

33. Nørskov JK, Bligaard T, Rossmeisl J, Christensen CH. Towards the computational design of solid catalysts. Nature chemistry. 2009;1(1):37-46.

34. Dumesic JA. Analyses of reaction schemes using De Donder relations. Journal of Catalysis. 1999;185(2):496-505.

35. Campbell CT. Future directions and industrial perspectives micro-and macro-kinetics: their relationship in heterogeneous catalysis. Topics in Catalysis. 1994;1(3-4):353-366.

36. Campbell CT. Finding the rate-determining step in a mechanism: comparing DeDonder relations with the "Degree of Rate Control". Journal of Catalysis. 2001;204(2):520-524.

37. Stegelmann C, Andreasen A, Campbell CT. Degree of rate control: How much the energies of intermediates and transition states control rates. Journal of the American Chemical Society. 2009;131(23):8077-8082.

38. Nørskov JK, Bligaard T, Kleis J. Rate control and reaction engineering. Science. 2009;24(5935):1655.

39. Dumesic JA. Reply to Finding the Rate-Determining Step in a Mechanism: Comparing DeDonder Relations with the "Degree of Rate Control". Journal of Catalysis. 2001;204:525-529.

40. Varma A, Morbidelli M, Wu H. Parametric sensitivity in chemical systems. Cambridge University Press. 2005.

41. Mhadeshwar AB, Vlachos DG. Hierarchical multiscale mechanism development for methane partial oxidation and reforming and for thermal decomposition of oxygenates on Rh. The Journal of Physical Chemistry B. 2005;109(35);16819-16835.

42. Fishtik I, Callaghan CA, Datta R. Reaction route graphs. I. Theory and algorithm. The Journal of Physical Chemistry B. 2004;108(18):5671-5682.

43. Fishtik I, Callaghan CA, Datta R. Reaction route graphs. II. Examples of enzyme-and surface-catalyzed single overall reactions. The Journal of Physical Chemistry B. 2004;108(18):5683-5697.

44. Fishtik I, Callaghan CA, Datta R. Reaction route graphs. III. Non-minimal kinetic mechanisms. The Journal of Physical Chemistry B. 2005;109(7):2710-2722.

45. Callaghan CA, Vilekar SA, Fishtik I, Datta R. Topological analysis of catalytic reaction networks: Water gas shift reaction on Cu (111). Applied Catalysis A: General. 2008;345(2):213-232.

46. Carrasquillo-Flores R, Gallo JMR, Hahn K, Dumesic JA, Mavrikakis M. Density Functional Theory and Reaction Kinetics Studies of the Water–Gas Shift Reaction on Pt–Re Catalysts. ChemCatChem. 2013;5(12):3690-3699.

47. Meskine H, Matera S, Scheffler M, Reuter K, Metiu H. Examination of the concept of degree of rate control by first-principles kinetic Monte Carlo simulations. Surface Science. 2009;603(10);1724-1730.

48. Bendtsen AB, Glarborg P, Dam-Johansen K. Visualization methods in analysis of detailed chemical kinetics modeling. Computers & chemistry. 2001;25(2):161-170.

49. Vajda S, Valko P, Turanyi T. Principal component analysis of kinetic models. International Journal of Chemical Kinetics. 1985;17(1):55-81.

50. Turanyi T, Berces T, Vajda S. Reaction rate analysis of complex kinetic systems. International Journal of Chemical Kinetics. 1989;21(2):83-99.

51. Barański A. On the usefulness of Campbell's concept of the rate-determining step. Solid State Ionics. 1999;117(1):123-128.

52. Connors KA. Chemical Kinetics: The Study of Reaction Rates in Solution, VCH. New York. Reactions, Princeton University Press. Princeton, NJ. 1990.

53. Bligaard T, Nørskov JK, Dahl S, Matthiesen J, Christensen CH, Sehested J. The Brønsted–Evans–Polanyi relation and the volcano curve in heterogeneous catalysis. Journal of Catalysis. 2004;224(1):206-217.

54. Boudart M, Tamaru K. The step that determines the rate of a single catalytic cycle. Catalysis letters. 1991;9(1-2):15-22.

55. de Donder T, Van Rysselberghe P. Thermodynamic Theory of Affinity. Stanford University Press. Stanford, CA. 1936.

56. Happel J, Sellers PH. Analysis of the Possible Reaction Mechanisms for a Chemical Reaction System. Adv. Catal. 1983;32:273−323.

57. Milner PC. J Electrochem Soc. 1964;3:228-232.

58. Chua LO, Desoer CA, Kuh ES. Linear and Nonlinear Circuits. McGraw Hill. New York. 1987.

59. Vilekar SA, Fishtik I, Datta R. The steady-state kinetics of a catalytic reaction sequence. Chemical Engineering Science. 2009;64(9):1968-1979.

60. Vilekar SA, Fishtik I, Datta R. The steady-state kinetics of parallel reaction networks. Chemical Engineering Science. 2010;65(10):2921-2933.

61. Deveau ND, Ma YH, Datta R. Beyond Sieverts' law: a comprehensive microkinetic model of hydrogen permeation in dense metal membranes. J Membr Sci. 2013; 437:298–311

62. Lund CRF. Microkinetics of Water-Gas Shift over Sulfided Mo/Al2O3 Catalysts. Ind Eng Chem Res. 1996.;35(8):2531-2538.

63. Fishtik I, Datta R. Studies in Surf Sci Catal. 2001;133:123-130.

64. Fishtik I, Datta R. De Donder relations in mechanistic and kinetic analysis of heterogeneous catalytic reactions. Ind Eng Chem Res. 2001;40:2416-2427.

Chapter 4. Kinetic and Pathway Analysis of the Oxygen Reduction Reaction

The kinetics of the oxygen reduction reaction (ORR) at the cathode of a proton exchange membrane (PEM) fuel cell is a key limitation and has a dominant impact on its performance and feasibility as an energy converter. Even with platinum catalysts, which are the most commonly used, significant overpotential occurs that greatly diminishes the power efficiency and performance of the cell. Hence the search goes on for alternatives to Pt that are cheaper but equally or more effective. An analysis of the mechanism and kinetics using our reaction route (RR) graph approach was performed to better understand the ORR on Pt and its alloys based on a DFT study recent step kinetics. The three reaction routes for this mechanism were thus analyzed on thirty-two Pt alloy onion-structured catalysts to identifying which routes are the most favored and for calculating the corresponding activity of the overall reaction. A volcano plot was developed to compare the activates of the studied catalysts. The dissociative reaction route was found to be the most active on Pt catalysts, but other reaction routes were found to be dominant in the less active catalyst. A rate equation was determined via the electrical analogy, enabling faster comparison and pruning of the mechanism. The analysis provided by our approach here is more robust than other, more common, methods as all reaction routes and elementary steps can be evaluated simultaneously without any *adhoc* simplifications.

4.1 Introduction

The slow kinetics of oxygen reduction reaction (ORR) at the cathode of a proton exchange membrane (PEM) fuel cell accounts for a large part of the inefficiency of the cell. Likewise, oxygen evolution reaction (OER) exerts the dominant effect in water electrolysis [1, 2]. Fuel cell viability is dependent on both the cost effectiveness of the cell and on its efficiency. This

technology is attractive because of its potential role in providing clean energy, but is currently not as cost effective compared to conventional energy technologies [2-4]. The slow activity of the ORR on platinum catalyst and its cost remain key deterrents towards widespread adoption. Thus, finding either a cheaper, or more active catalyst than platinum is of paramount importance to the viability of the PEM fuel cell and hydrogen economy.

Significant efforts have, thus, been made towards understanding the kinetics and mechanism of the ORR [1-21]. One promising solution to finding cheaper catalysts is to alloy Pt catalyst with nonprecious transition metals [3-13]. In particular, Adzic et al. have had success with the development of depositing a Pt monolayer on different transition metals that in fact provided higher activity than that of pure Pt [4-6]. More recent studies include onion structures that have multiple deposited layers of different transition metals on varying substrates, but all containing at least one layer of Pt [3]. Stamenkovic et al. reported that a Pt skin can be formed through annealing at 1,000K of the binary Pt_3M (M = Fe, Co, Ni, Ti, V) alloy electrocatalysts [12-15]. These alloys had higher ORR activities than Pt(111) alone, coupled with attractive stability.

The selection of alternative, superior catalysts can be aided by theoretical evaluation of the activity from the reaction mechanism and predicted step kinetics. However, the mechanisms on alternative catalysts are not adequately known. In fact, even the mechanism on Pt is debatable. Further, the assumption and simplifications for the mechanism on platinum catalyst might not be applicable to alternatives. Azdic et al. have used a Sabatier analysis in some studies [3,16]. The Sabatier principle states that in a system of catalytic reactions, there is a maximum reaction rate as a function of the adsorption energy of the key reactive intermediates [21, 22]. Thus, an activity for each pathway is calculated as a function of the forward rate constants and the activity of the pathway with the highest activity is considered to be that for the catalyst. Other researchers have

used Campbell's Degree of Rate Control (DoRC) for their analysis of other mechanisms, although this has not yet been applied to ORR [23, 24]. This method identifies the importance of reaction steps and intermediates by perturbing specific kinetic data and calculating the effect that perturbation has on the overall reaction rate. A detailed analysis and comparison of Campbell's DoRC versus our approach was recently published [25].

What many of the current studies lack and what we intend to improve upon here, is the lack of a robust analysis that encompasses the entire mechanism and quantitatively accounts for each elementary step where calculating the rate of the overall reaction. This study of the ORR mechanism aims to provide superior insights into the inner workings of the ORR pathways based on DFT kinetics [3].

Table 4.1 thus shows the 7-step mechanism for the ORR investigated by Herron et al. [3] and adopted by us for our analysis. A more detailed 14-step mechanism has been more recently published [16], but the 7-step mechanism is adequate for the scope of the conditions and catalysts in this research because the additional steps in the larger mechanism do not significantly contribute to the flux of the reaction under normal operating conditions of the cathode of a PEM fuel cell. Of course, our approach can be applied to the large mechanism as well.

The 7-step mechanism is comprised of 3 pathways, for which the stoichiometric number of each step (σ_ρ) is shown in Table 4.1 for each different pathway, namely: dissociative, peroxyl and hydrogen peroxide.

s_ρ	Elementary Reaction Step	$\sigma_{\text{Dissociative},\,\rho}$	$\sigma_{\text{Peroxyl},\,\rho}$	$\sigma_{\text{Hydrogen Peroxyde},\,\rho}$
s_1:	$O_2 + 2S \rightleftarrows 2O{\cdot}S$	+1		
s_2:	$O{\cdot}S + H^+ + e^- \rightleftarrows OH{\cdot}S$	+2	+1	
s_3:	$OH{\cdot}S + H^+ + e^- \rightleftarrows H_2O + S$	+2	+2	+2
s_4:	$O_2 + H^+ + e^- + S \rightleftarrows OOH{\cdot}S$		+1	+1
s_5:	$OOH{\cdot}S + S \rightleftarrows O{\cdot}S + OH{\cdot}S$		+1	
s_6:	$OOH{\cdot}S + H^+ + e^- \rightleftarrows HOOH{\cdot}S$			+1
s_7:	$HOOH{\cdot}S + S \rightleftarrows 2OH{\cdot}S$			+1

$$OR \equiv \sum_\rho \sigma_{g\rho} s_\rho : \quad O_2 + 4(H^+ + e^-) \rightleftarrows 2H_2O$$

Table 4.1: 7-step ORR reaction mechanism in acid electrolytes [3].

A common approach to kinetics involves reducing the mechanism, either to a single pathway, or elementary step. Here, we discuss a comprehensive approach that simultaneously considers all steps and pathways. It is based on electrical network analogy of the reaction mechanism based on the reaction route (RR) graph analysis approach [26-32] developed by us, which involves an evaluation of the reaction step "affinity," or driving force, and "resistance" under a variety of conditions. It is equally rigorous and substantially more insightful than more common methods (e.g., the DoRC), allowing transparent pruning of complex catalytic reaction networks. It allows rigorous mechanism analysis and reduction, eventually leading to a simplified but accurate rate law, as demonstrated here for the case of the ORR.

4.2 Reaction Route Graph

The RR Graph approach has been developed by us [25-32] to provide a tool for analysis of chemical reaction networks that goes beyond the current methods to elucidate the reaction pathways and identify the important kinetic steps. One can visualize a chemical network as a road map on which walks define the pathways through which the overall reaction (OR) proceeds, with the graph depicting all possible pathways to get from the reactants to the product in the OR. The RR Graph approach provides this road map and is able to assign each pathway a quantitative estimate of how difficult it is to traverse that pathway, based on an electrical resistance analogy, or alternately the flux through a given pathway.

We define a Reaction Route Graph G_R as an ordered, connected, directed, planar or nonplanar, cycle graph comprising directed edges or branches, each representing an elementary or an overall reaction $\{OR, s_1, s_2, \ldots, s_\rho\}$, and N nodes $\{n_1, n_2, \ldots, n_N\}$, that illustrate how the reaction steps are interconnected to allow for all of the direct reaction routes to be traced as walks [27, 28]. Edges are depicted on the graph as directed arrows and nodes are circles, typically blue for terminal nodes (nodes that have the OR incident to them) and red for intermediate nodes, i.e., those with only elementary steps connecting. Two or more edges are parallel if they have in common the same pair of starting and ending nodes. The direction of the edge is simply assumed, and the reaction may actually proceed in either direction by a given OR. A key distinction is that the nodes in the reaction route graphs defined above do not denote single intermediates or terminal species, which is commonly assumed in other graph-theoretical depictions [35-38], but simply the interconnection of reactions involved in reaction routes, hence the reason for labeling these "reaction route graphs." In fact, a node n_j in an RR Graph represents properties associated with the sum of products of the reactions incident to the node plus the sum of reactants of the reactions

114

incident from the node with an appropriate sign (negative for reactions incident to, and positive for reactions incident from a node).

Perhaps the most important aspect of RR Graphs is that they are analogous to electrical circuits. The laws that govern the behavior of electrical circuits, i.e., Kirchoff's laws, are very well developed [33], so that applying them to chemical reaction networks can be quite beneficial and revealing. The two network laws of most interest here are Kirchoff's Flux Law, KFL, alternatively known as Kirchoff's Node Law, and Kirchoff's Potential (KPL), alternatively called Kirchoff's Loop Law [33].

KFL states that the step rate r_p (likened to electrical current) of all edges incident at a node j sum up to zero (from QSS mass conservation). In other words, $\Delta r_j \equiv \sum_{\rho=1}^{p} m_{pj} r_\rho = 0$, where the incidence coefficient $m_{pj} = +1$, if an edge leaves the node j, and $m_{pj} = -1$, if an edge is coming into the node j [27].

KPL states that the step affinity, i.e., negative Gibbs free energy change for a reaction step, written in dimensionless form, $\mathcal{A}_p = -\Delta G_\rho / RT$ (likened to step voltage V_ρ) of all edges in a closed walk (starting and ending at the same node), or a cycle, sum up to zero, i.e., $\sum_{\rho=1}^{P} \sigma_{g\rho} \mathcal{A}_p = 0$, where the stoichiometric number $\sigma_{g\rho} = +1$, if an edge is directed in the direction of the walk around a cycle, and $\sigma_{g\rho} = -1$, if an edge is directed in the opposite direction [27]. Note that this is the equivalent of the thermodynamic Hess's law.

The affinity of a reaction step can be related to the resistance of an electrical circuit, such that the higher the resistance of a step for a given affinity, the less current that passes through,

while higher affinity of a chemical reaction leads to higher flux. Thus, the resistance of each step is defined by writing the rate of a reaction step in the form of Ohm's law [27]

$$r_\rho \equiv \frac{\mathscr{A}_\rho}{R_\rho} = \vec{r}_\rho - \bar{r}_\rho \qquad (4.1)$$

where $\mathscr{A}_\rho$ is the dimensionless step affinity akin to voltage in an electrical circuit. It is in turn related to the ratio of the rate in the forward direction $\vec{r}_\rho$ to that in the reverse direction, $\bar{r}_\rho$, via the de Donder relation [31,32]

$$\mathscr{A}_\rho = \ln\left(\frac{\vec{r}_\rho}{\bar{r}_\rho}\right) = \ln\left(\frac{1}{z_\rho}\right) \qquad (4.2)$$

which stems from the thermodynamic consistence of elementary step kinetics, so that the step resistance, by combining the last two equations, is provided in terms of step kinetics by

$$R_\rho = \frac{\ln(\vec{r}_\rho / \bar{r}_\rho)}{\vec{r}_\rho - \bar{r}_\rho} \qquad (4.3)$$

In the above, $z_\rho = \vec{r}_\rho / \bar{r}_\rho$ is the step reversibility. Clearly, unlike electrical resistance, which is substantially constant, this definition of kinetic resistance of a step strongly depends on reaction conditions – especially temperature.

Now, in view of the fact that the RR Graph follows KFL, KPL, as well as Ohm's law, it is completely consistent with a resistive electrical circuit [31]. Consequently, we can write the overall rate as the ratio of the affinity of the OR and the overall resistance of the reaction network

$$r_{OR} \equiv \frac{\mathscr{A}_{OR}}{R_{OR}} \qquad (4.4)$$

116

where the OR resistance of the network is obtained in terms of the individual step resistances, in a manner similar to resistive electrical circuits [31].

Because of these rigorous network laws applicable to RR Graphs, the construction of the RR Graph can be challenging for complex mechanisms, although the ORR case considered here it is straightforward. For the 7-step ORR mechanism [3] provided in Table 4.1, the RR Graph is readily found by first finding a linearly independent set of pathways or full routes (*FR*s), that include the OR, and cycles, or empty routes (*ER*s), the latter including only elementary steps. These reaction routes (RRs) represent a summation of the elementary steps that when combined as shown in the cycle matrix will cancel out all chemical species in the reactions. (e.g., if one were to combine steps such as: $s_4 + s_5 - s_1 - s_2$, as per ER_1, all the species will cancel out). The number of linearly independent reaction routes (μ) can be found by subtracting the number of independent intermediate species (q) from the number of mechanistic steps (p). In this case: $\mu = p - q = 7 - 4 = 3$ independent routes, which can be either full or empty routes. An example of a linearly independent set of 3 RRs for this mechanism is provided in Table 4.2. The independent set of KPL relations (Hess's law) for thermodynamic functions such as enthalpy or Gibbs free energy change is identical to these cycles.

	s_1	s_2	s_3	s_4	s_5	s_6	s_7	s_{OR}
FR_1	1	2	2	0	0	0	0	-1
ER_1	-1	-1	0	1	1	0	0	0
ER_2	0	-1	0	0	-1	1	1	0

Table 4.2: Cycle matrix for 7-step ORR mechanism.

117

Species	QSS Relation
O·S:	$(2)\, s_1 + (-1)\, s_2 + (-1)\, s_5 = 0$
OH·S:	$(1)\, s_2 + (-1)\, s_3 + (1)\, s_5 + (2)\, s_7 = 0$
OOH·S:	$(1)\, s_4 + (-1)\, s_5 + (-1)\, s_6 = 0$
HOOH·S:	$(1)\, s_6 + (-1)\, s_7 = 0$
O_2:	$(-1)\, s_1 + (-1)\, s_4 + (1)\, OR_1 = 0$
H_2O:	$(1)\, s_3 + (-1)\, OR_1 = 0$

Table 4.3: QSS Relations for each of the terminal and intermediate species.

Knowing that each of these cycles in Table 4.2 will appear in the final graph, we proceed by identifying common edges and nodes we can fuse together in these "subgraphs" and produce a graph that includes each cycle. For example, ER_1 and ER_2 share nodes that have an s_5 edge entering and leaving, so those cycle are fused to combine that step as shown in the resulting cycle graph (Figure 4.1a). Since the mechanism is nonlinear, each step, including the overall reaction step, would appear twice in the RR Graph, and the graph should be symmetric, which leads to the doubling of this fused cycle graph (Figure 4.1b). Clearly, two s_2 steps are already present in each cycle graph so they are fused together (Figure 4.1c) while retaining both s_1 steps. We then check each node to see if it conforms to KFL, which means that the rates of the steps entering the nodes equals those leaving, as provided by QSS mass balance on species as given in Table 4.3. The two nodes on the top and bottom are already balanced, which is also why the graphs were not fused using those nodes. An s_3 edge is added to both ends to balance those nodes (Fig. 4.1c). Finally, the OR is added twice to balance the terminal nodes and the complete RR Graph is found (Fig. 4.1d).
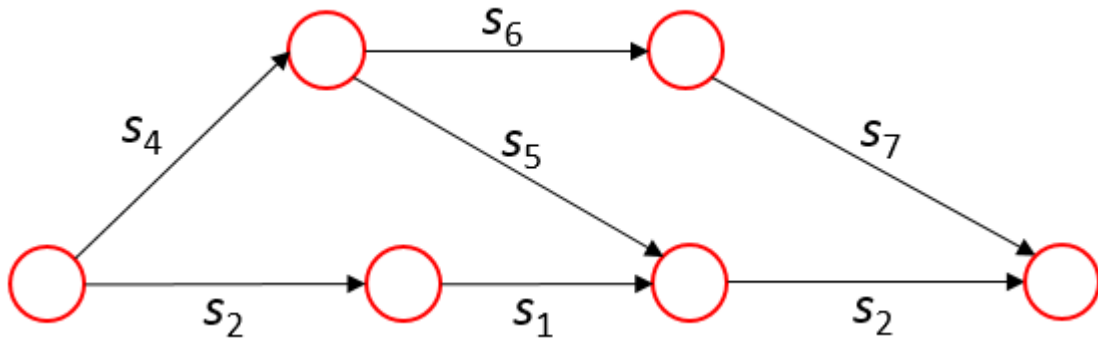
Figure 4.1a-d: Steps to construct the cycle Graph; a) Fusing Empty Routes.
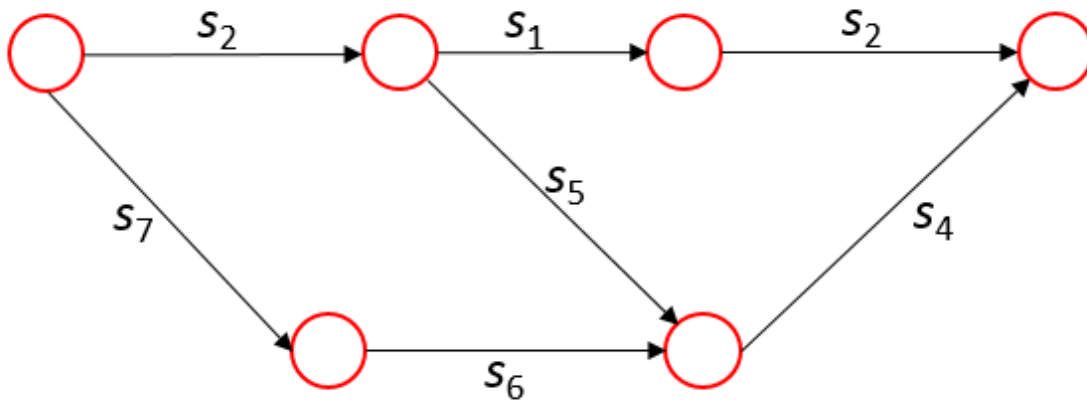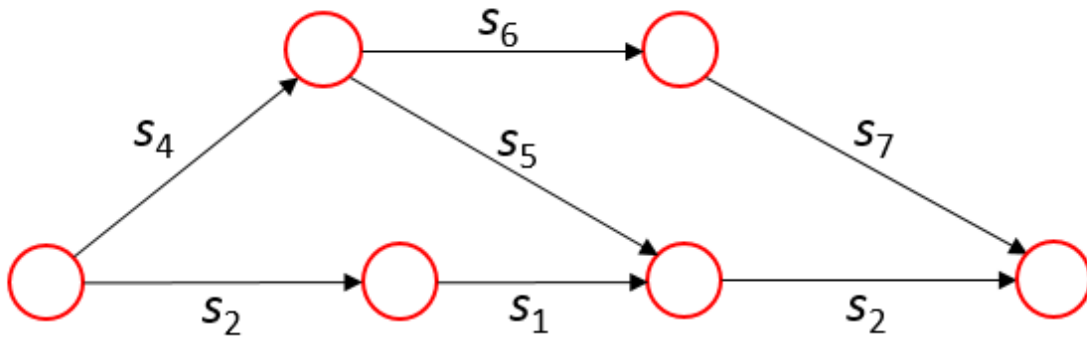
Figure 4.1b: Duplication of cycle graph.
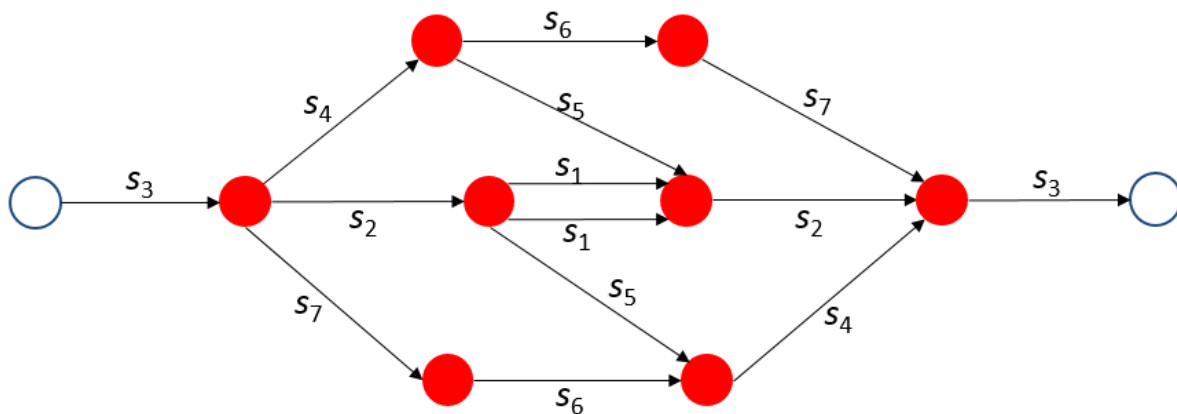
Figure 4.1c: Balancing of nodes.
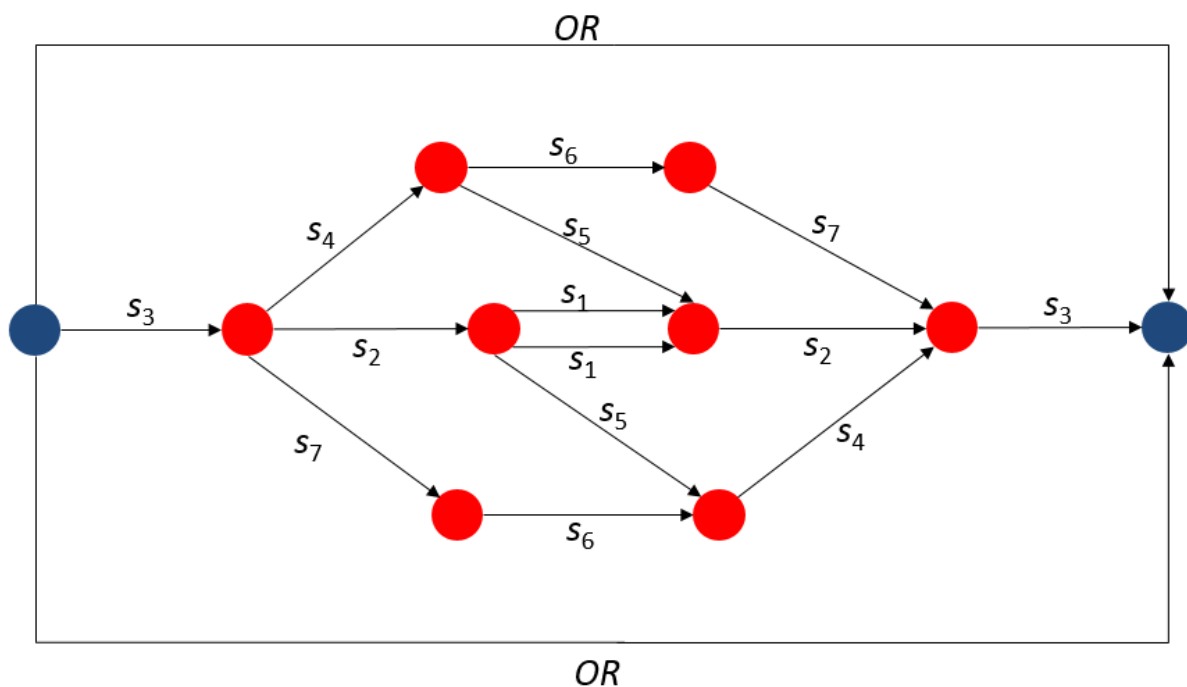
Figure 4.1d: Completed RR Graph for Oxygen Reduction Reaction.

The completed RR Graph allows the analysis of the complete reaction network by showing the inter-relationships among the elementary steps. In addition, the nodes provide us with mass balance equations that allows us to solve for the concentrations of the intermediates, based on the quasi-steady state assumption. Since kinetic data for the reaction steps is available, we can confirm

their consistence via KPL, and also calculate the overall activity for the catalyst, as described below.

4.3 Rate Analysis

Through the extensive DFT computational results of Herron et al. [3], we have access to the reaction free energy (RFE) values at electrode equilibrium potential of 1.23V for the proton exchange steps (s_2, s_3, s_4, s_6) of the reaction network and the binding energies and activation energies for oxygen bond breaking (s_1, s_5, s_7) for several alloy catalysts. From this data we can perform a quasi-steady state (QSS) balance on the system using nodes in the graph as mass balance equations. The QSS assumption allows us to determine the concentrations of intermediate species assumed as constant. Since the nodes of the RR Graph follow Kirchoff's flux law, we can derive the following independent KFL equations, which turn out to be related to QSS mass balance of indicated intermediate species (Table 4.3):

$$(+2)r_1 + (-1)r_2 + (+1)r_5 = 0 \qquad\qquad (O \cdot S) \qquad\qquad (4.5)$$

$$(+1)r_{2+} (-1)r_3 + (+1)r_5 + (+2)r_7 = 0 \qquad (OH \cdot S) \qquad\qquad (4.6)$$

$$(+1)r_4 + (-1)r_5 + (-1)r_7 = 0 \qquad\qquad (OOH \cdot S) \qquad\qquad (4.7)$$

$$(+1)r_7 + (-1)r_6 = 0 \qquad\qquad (HOOH \cdot S) \qquad\qquad (4.8)$$

The rates of each elementary reaction, $r_\rho = \vec{r}_\rho - \bar{r}_\rho$ can be written in the form

$$\vec{r}_\rho = \vec{k}_\rho \prod_{i=0}^{n} a_i^{-\vec{v}_{\rho i}} \prod_{k=0}^{q} \theta_k^{-\vec{\alpha}_{\rho k}} = \vec{\omega}_\rho \prod_{k=0}^{q} \theta_k^{-\vec{\alpha}_{\rho k}} \qquad\qquad (4.9)$$

$$\overleftarrow{r}_\rho = \bar{k}_\rho \prod_{i=0}^{n} a_i^{-\bar{v}_{\rho i}} \prod_{k=0}^{q} \theta_k^{-\bar{\alpha}_{\rho k}} = \bar{\omega}_\rho \prod_{k=0}^{q} \theta_k^{-\bar{\alpha}_{\rho k}} \qquad\qquad (4.10)$$

where $\vec{k}_\rho, \overleftarrow{k}_\rho$ are the forward and reverse rate constants for step ρ, a_i is the activity of terminal species i, θ_k is the unknown catalyst site fractions for intermediate species k and θ_0 is the unoccupied site fraction (θ_0).

The step weights (ω_ρ) for each reaction step combine the known quantities in the above rate laws, i.e., the rate constants, terminal species activity and any electrode overpotential that is being applied to the system. This leaves the step rates written explicitly in terms of the unknown surface intermediate site fractions, which may be determined either via the QSS (or KFL) relations or via the microkinetics approach [34]. The reaction rate constants are written in terms of the thermodynamic transition-state theory [28] as:

$$\overleftarrow{k}_\rho \equiv \kappa \frac{k_B T}{h} \exp\left(-\frac{\Delta \overleftarrow{G}_\rho^{\pm,o}}{RT}\right) \; ; \; \vec{k}_\rho \equiv \kappa \frac{k_B T}{h} \exp\left(-\frac{\Delta \vec{G}_\rho^{\pm,o}}{RT}\right) \tag{4.11}$$

where the Gibbs-free energy of activation includes the effect of the electrode potential:

$$\Delta \vec{G}_\rho^{\pm,o} = \Delta \vec{G}_{\rho,\Phi=0}^{\pm,o} - \beta_\rho (v_{\rho e_-} F\Phi) \tag{4.12}$$

where the first term on the right is the Gibbs free energy of activation in the absence of potential. Thus, the reaction rate constant can by expressed as

$$\vec{k}_\rho \equiv \kappa \frac{k_B T}{h} \exp\left(-\frac{\Delta \vec{G}_{\rho,\Phi=0}^{\pm,o}}{RT}\right) \exp\left(\frac{\beta_\rho v_{\rho e_-} F\Phi}{RT}\right) \tag{4.13}$$

where β_ρ, the symmetry factor, assumed to be ½, and the potential is $\Phi = \Phi_{\rho,0} + \eta_\rho$, where η_ρ is the dimensionless overpotential term defined as the difference between the potential and the

standard operating potential (1.23V for the ORR). Further, using the relation of $\Delta \vec{G}_\rho^{\pm,o} = \Delta \vec{H}_\rho^{\pm,o} - T\Delta \vec{S}_\rho^{\pm,o}$ the forward rate constant can also be expressed as

$$\vec{k}_\rho \equiv \vec{k}_{\rho,\Phi_0} \exp\left(\frac{\beta_\rho v_{\rho e^-} F\Phi}{RT}\right) = \vec{k}_{\rho,\Phi_0} e^\psi \qquad (4.15)$$

and

$$\vec{k}_{\rho,\Phi_0} = \vec{\Lambda}_\rho \exp\left(\frac{\Delta \vec{E}_{\rho,\Phi=0}^{\pm,o}}{RT}\right) \exp\left(\frac{\beta_\rho v_{\rho e^-} F\Phi_{\rho,0}}{RT}\right) \qquad (4.16)$$

where $\vec{\Lambda}_\rho = \kappa \dfrac{k_B T}{h} \exp\left(\dfrac{\Delta \vec{S}_{\rho,\Phi=0}^{\pm,o}}{R}\right)$, the preexponential factor. Utilizing these relationships, the step weights for the forward and reverse of each reaction step can be calculated from known kinetic data.

Since the ORR is an electrochemical reaction mechanism, it is comprised of reaction steps that include a proton and electron exchange. For the steps that do not include any electron exchange, $v_{\rho e^-} = 0$, there is no dependence on the electrode potential, so terms that include ψ are excluded, thus the rate constant equation is simply

$$\vec{k}_\rho \equiv \vec{\Lambda}_\rho \exp\left(-\frac{\vec{E}_{\rho,\Phi=0}}{RT}\right) \qquad (4.17)$$

Using these equations and the kinetic data obtained by Herron et al.[3] the forward and reverse rate constant for each elementary step can be calculated for a particular catalyst and reaction

conditions, e.g., for Pt (111) catalyst at 298 K the rates of the seven elementary steps of the mechanism are presented in terms of the site fractions θ_i and step weights k_ρ and e^ψ for steps that include a proton and electron exchange (Table 4.4).

s_ρ	$r_\rho = \vec{r}_\rho - \bar{r}_\rho$	$\vec{k}_{\rho,\Phi=0}$	$\bar{k}_{\rho,\Phi=0}$
s_1:	$r_1 = \vec{r}_1 - \bar{r}_1 = \vec{k}_1 a_{O_2}\theta_0^2 - \bar{k}_1\theta_{O\cdot S}^2$	4.45×10^{-7}	1.14×10^{-14}
s_2:	$r_2 = \vec{k}_2\theta_{O\cdot S}^2 e^{-\psi} - \bar{k}_2\theta_{OH\cdot S}e^{\psi}$	3.37×10^{-2}	1.36×10^{-12}
s_3:	$r_3 = \vec{k}_3\theta_{OH\cdot S}e^{-\psi} - \bar{k}_3 a_{H_2O}\theta_0 e^{\psi}$	2.43×10^{18}	2.39×10^{-3}
s_4:	$r_4 = \vec{k}_4 a_{O_2}\theta_0 e^{-\psi} - \bar{k}_4\theta_{OOH\cdot S}e^{\psi}$	2.90×10^{19}	2.76×10^{-11}
s_5:	$r_5 = \vec{k}_5\theta_{OOH\cdot S}\theta_0 - \bar{k}_5\theta_{O\cdot S}\theta_{OH\cdot S}$	5.81×10^{13}	8.18×10^{3}
s_6:	$r_6 = \vec{k}_6\theta_{OOH\cdot S}e^{-\psi} - \bar{k}_6\theta_{HOOH\cdot S}e^{\psi}$	4.08×10^{12}	1.78×10^{4}
s_7:	$r_7 = \vec{k}_7\theta_0\theta_{HOOH\cdot S} - \bar{k}_7\theta_{OH\cdot S}^2$	6.38×10^{12}	5.31×10^{1}

Table 4.4: Rate equations and rate constants for the 7-step ORR reaction mechanism on Pt (111) catalysts at 298 K [3].

We then introduce step weights (ω_ρ) as a term that lumps together the terminal species activities, rate constants and overpotential for each of the forward and reverse steps, ρ.

$$r_1 = \vec{r}_1 - \bar{r}_1 = \vec{\omega}_1\theta_0^2 - \bar{\omega}_1\theta_{O\cdot S}^2; \qquad \vec{\omega}_1 = \vec{k}_1 a_{O_2}, \ \ \bar{\omega}_1 = \bar{k}_1 \qquad (4.18)$$

$$r_2 = \vec{\omega}_2\theta_{O\cdot S}^2 - \bar{\omega}_2\theta_{OH\cdot S}; \qquad \vec{\omega}_2 = \vec{k}_2 e^{-\psi}, \ \ \bar{\omega}_2 = \bar{k}_2 e^{\psi} \qquad (4.19)$$

$$r_3 = \vec{\omega}_3\theta_{OH\cdot S} - \bar{\omega}_3\theta_0; \qquad \vec{\omega}_3 = \vec{k}_3 e^{-\psi}, \ \ \bar{\omega}_3 = \bar{k}_3 a_{H_2O}e^{\psi} \qquad (4.20)$$

124

$$r_4 = \vec{\omega}_4 \theta_0 - \bar{\omega}_4 \theta_{OOH \cdot S} ; \qquad \vec{\omega}_4 = \vec{k}_4 a_{O_2} e^{-\psi}, \quad \bar{\omega}_4 = \bar{k}_4 e^{\psi} \qquad (4.21)$$

$$r_5 = \vec{\omega}_5 \theta_{OOH \cdot S} \theta_0 - \bar{\omega}_5 \theta_{O \cdot S} \theta_{OH \cdot S} ; \qquad \vec{\omega}_5 = \vec{k}_5, \quad \bar{\omega}_5 = \bar{k}_5 \qquad (4.22)$$

$$r_6 = \vec{\omega}_6 \theta_{OOH \cdot S} - \bar{\omega}_6 \theta_{HOOH \cdot S} ; \qquad \vec{\omega}_6 = \vec{k}_6 e^{-\psi}, \quad \bar{\omega}_6 = \bar{k}_6 e^{\psi} \qquad (4.23)$$

$$r_7 = \vec{\omega}_7 \theta_0 \theta_{HOOH \cdot S} - \bar{\omega}_7 \theta_{OH \cdot S}^2 ; \qquad \vec{\omega}_7 = \vec{k}_7, \quad \bar{\omega}_7 = \bar{k}_7 \qquad (4.24)$$

For the numerical analysis, we assume the activities of the terminal species (a_i) are unity, i.e., "standard" conditions. These rate equations were then substituted into the QSS (KFL) equations for which a numerical solution for the unknown site fractions was found for a range of overpotentials across a list of several catalysts. Since calculated step rates allow us to relate them to the rate of the OR, r_{OR}, from Figure 4.1d and thus, obtain the kinetic current density, i, of the electrode for the ORR

$$i = \nu_{OR,e^-} F r_{OR} \qquad (4.25)$$

where ν_{OR,e^-} is the number of electrons produced in the overall reaction, and F is Faraday's constant.

Fig. 4.2a provides the currents density of the different steps for Pt at a temperature of 298K and a potential of Φ0.8V. The flux of the reaction entirely passes through the dissociative pathway, with only trace amounts through the other pathways. This is expected under standard conditions on Pt catalyst, however for other catalysts under other conditions this is not necessarily the case and the RR Graph can be used to easily visualize which pathways are dominant.

The RR Graph approach can provide additional insight into the mechanism through the quantification of step resistance in terms of the rate and affinity of the step. In addition to the overall activity of the catalyst, we can also then look at how much each reaction route contributes

to the overall rate of the reaction. The different pathways are compared similar to those in an electric circuit, as previously mentioned. A resistance is calculated for each step, which represents how difficult that step is to traverse along a path [29-33].

4.4 Electrical Analogy

4.4.1 Step Resistance and Rate Analysis

Since RR Graphs are constructed to be consistent with both KFL and KPL, they can be made completely analogous to an electrical circuit. This provides additional insights into the mechanism and facilitates kinetic analysis via the use of analytical techniques that are fully developed and widely known in electric circuit analysis. The steps shown in the RR Graph are, hence, replaced with a resistance as shown in Fig. 4.2b, with the caveat that, unlike in electrical circuits, these step resistances are not constant, but rather, vary with conditions such as temperature and composition, bit can be calculated using Eq. (4.3) once the site fractions have been determined for a given set of conditions. The OR is replaced with a power source with EMF

$$E_{OR} = 1 - z_{OR} \tag{4.26}$$

where the OR reversibility $z_{OR} = 1 - \exp(-\mathscr{A}_{OR})$

$i_{OR} = 7.55$ (mA/cm^2)

126
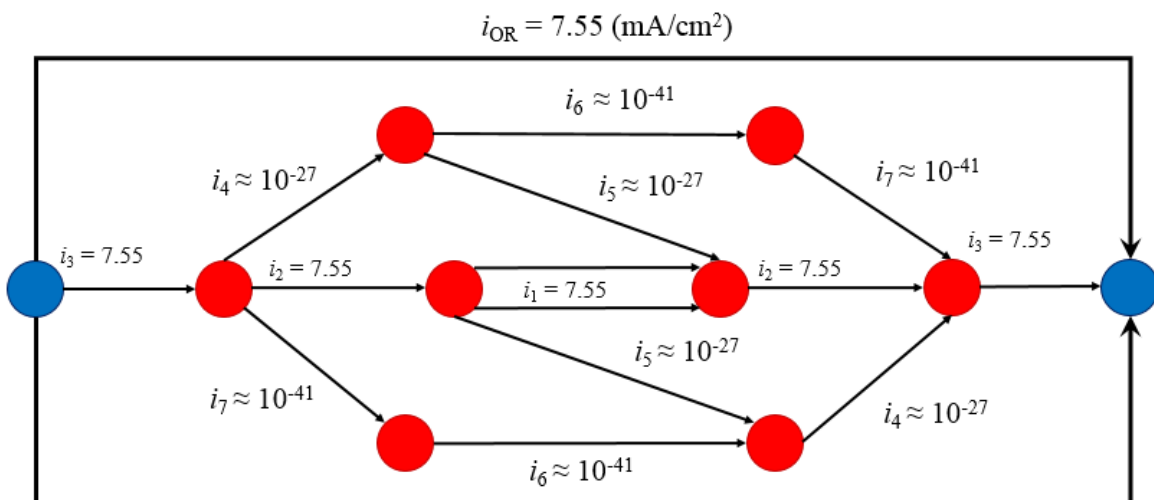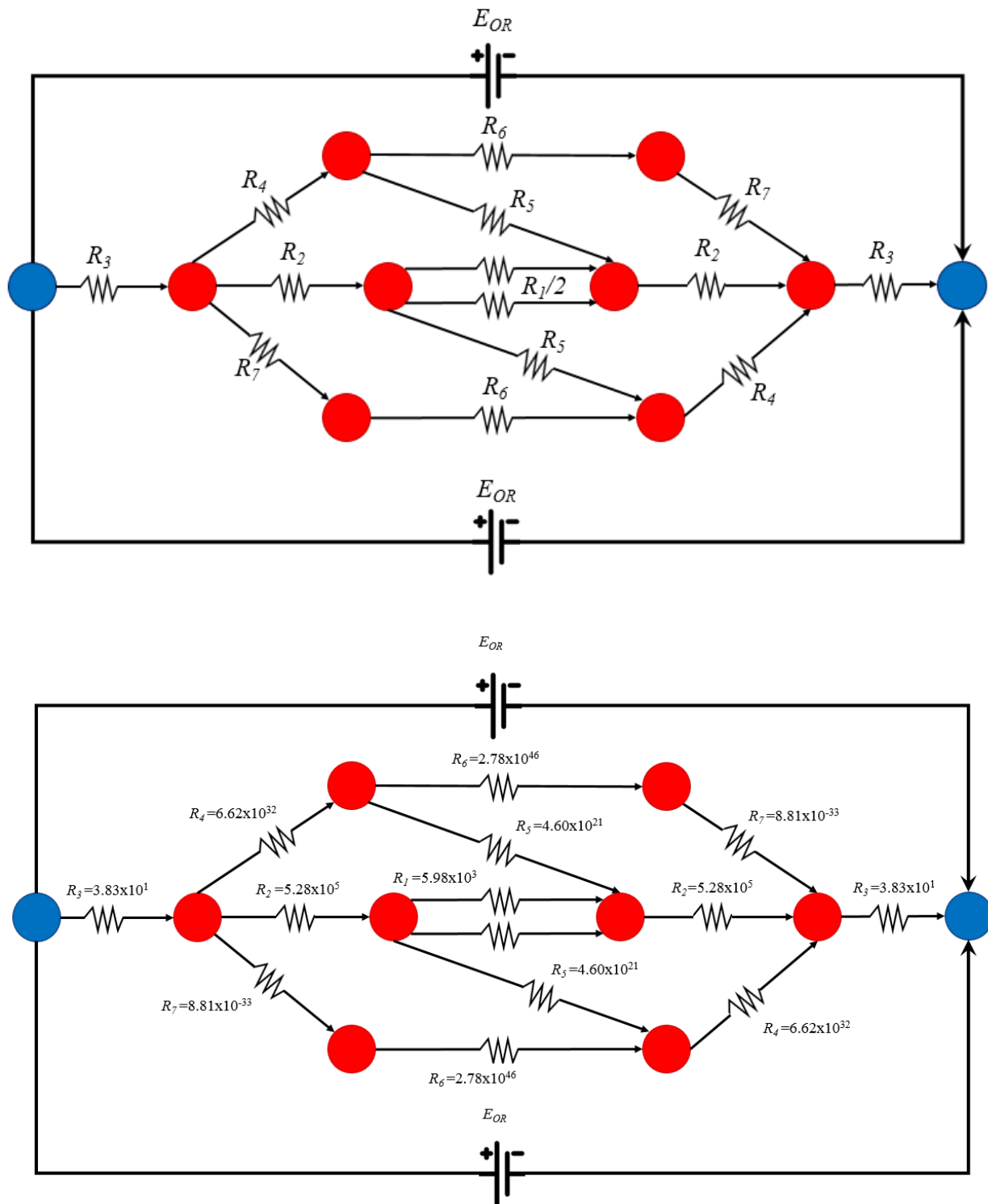
Figure 4.2: a) Electrical circuit analysis with currents for each pathway superimposed on the respective step (currents in mA/cm^2) b) Electrical circuit analysis of RR Graph for ORR wherein OR is replaced by a power source, and steps are replaced by resistors. c) Resistance values (s^{-1}) are imposed on the graph. Values evaluated on Pt catalyst at 0.8V, 298K and 1 atm.

The resistance of each step is a quantitative representation of the difficulty for the reaction to proceed through that step. The overall resistance of the electric circuit for the ORR can then be found via usual electrical circuit approaches [31] as described below, so that the overall reaction rate is written as

$$2r_{OR} \equiv \frac{\mathscr{A}_{OR}}{R_{OR}} \tag{4.27}$$

where the OR affinity is defined as: $\mathscr{A}_{OR} \equiv -\dfrac{\Delta G_{OR}}{RT}$. For example, Figure 4.2c shows the step resistances calculated for Pt catalyst at a potential of 0.8V, temperature of 298K and pressure of 1atm.

For calculating the overall resistance of the analogous electrical circuit for the RR Graph of this mechanism, three delta-Y conversions [31] must be used to properly express the summation of these resistances analytically. Figure 4.3 shows the first delta-Y conversion performed on the two symmetrical cycles of R_4, R_5, R_6 and R_7. The resistances of the new branches are:

$$R_A = \frac{R_2 R_5}{R_2 + R_5 + (R_6 + R_7)} \tag{4.28}$$

$$R_B = \frac{R_5 (R_6 + R_7)}{R_2 + R_5 + (R_6 + R_7)} \tag{4.29}$$

$$R_C = \frac{R_2 (R_6 + R_7)}{R_2 + R_5 + (R_6 + R_7)} \tag{4.30}$$
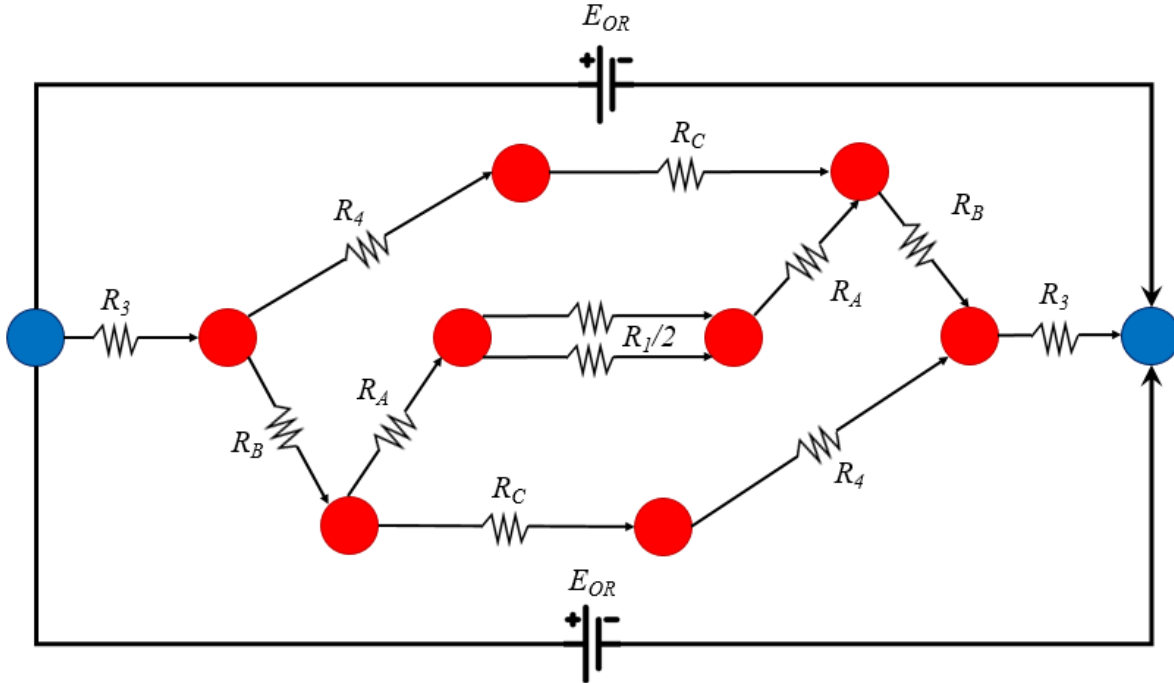
Figure 4.3: Delta-Y conversion performed on either side of the electrical graph.

A third delta-Y conversion on the left cycle of R_B, R_C, $2R_2$ and $(1/2)R_1$ results in the circuit shown in Figure 4.4. The third set of resistances are:

$$R_\alpha = \frac{R_\text{B}\left(R_4 + R_\text{C}\right)}{R_\text{B} + \left(R_4 + R_\text{C}\right) + \left(2R_\text{A} + \dfrac{R_1}{2}\right)}$$

(4.31)

$$R_\beta = \frac{\left(R_4 + R_\text{C}\right)\left(2R_\text{A} + \dfrac{R_1}{2}\right)}{R_\text{B} + \left(R_4 + R_\text{C}\right) + \left(2R_\text{A} + \dfrac{R_1}{2}\right)}$$

(4.32)

$$R_\gamma = \frac{R_\text{B}\left(2R_\text{A} + \dfrac{R_1}{2}\right)}{R_\text{B} + \left(R_4 + R_\text{C}\right) + \left(2R_\text{A} + \dfrac{R_1}{2}\right)}$$

(4.33)

129
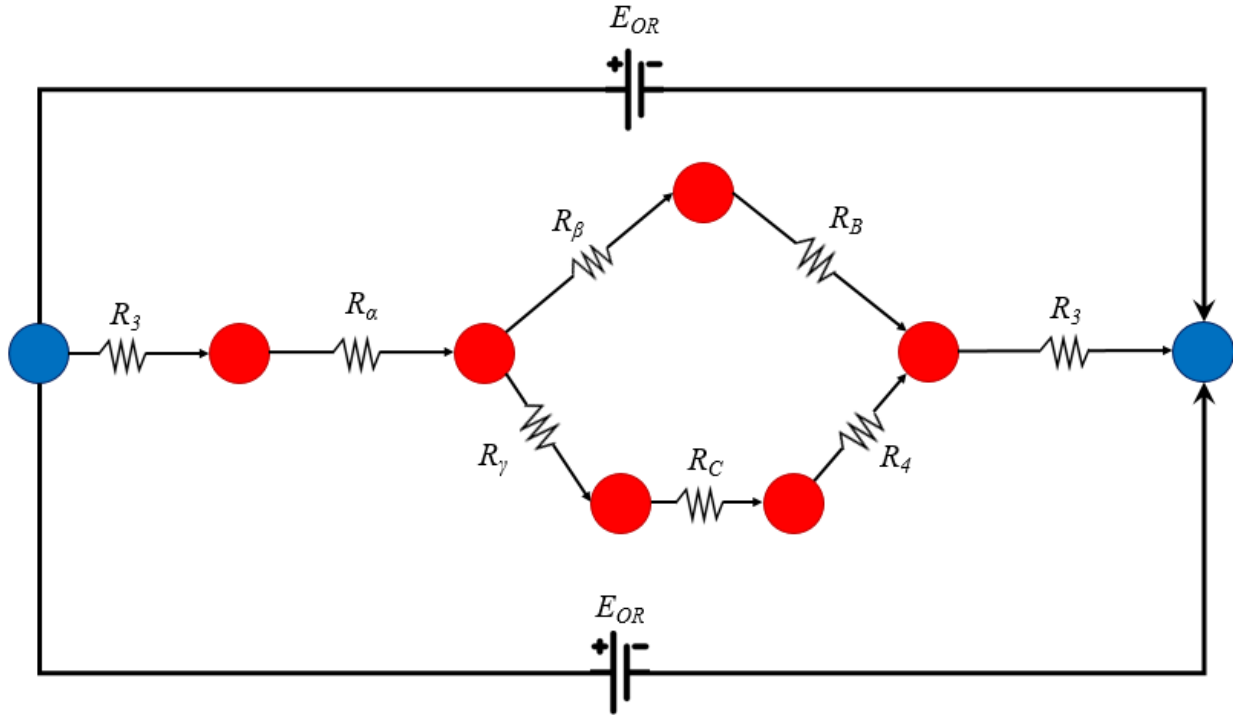
Figure 4.4: Final delta-Y transformed electrical graph.

R_{OR} can finally be expressed by adding the resistances in series and parallel

$$R_{OR} = 2R_3 + R_\alpha + \cfrac{1}{\cfrac{1}{R_\beta + R_B} + \cfrac{1}{R_\gamma + R_4 + R_C}} \tag{4.34}$$

For Pt at 298 K and $\Phi=0.8$V, the use of Eq (4.26) in Eq (4.25) with R_{OR} predicted as above, the same current density as calculated above via KFL or QSS. For catalysts which only have one dominant pathway, the overall resistance can be greatly simplified because the entire resistance is along a single pathway, or even a single reaction step. For each of the three individual reaction pathways, the pathway resistance can simply be added in series

$$R_{\text{Dissociative}} = (2)R_3 + (1/2)R_1 + (2)R_2 \tag{4.35}$$

$$R_{\text{Peroxyl}} = (2)R_3 + R_4 + R_6 + R_7 \tag{4.36}$$

$$R_{\text{Hydrogen Peroxide}} = (2)R_3 + R_2 + R_4 + R_5 \tag{4.37}$$

130

and represented as a simplified graph (Fig. 4.5a-c).

a)

b)
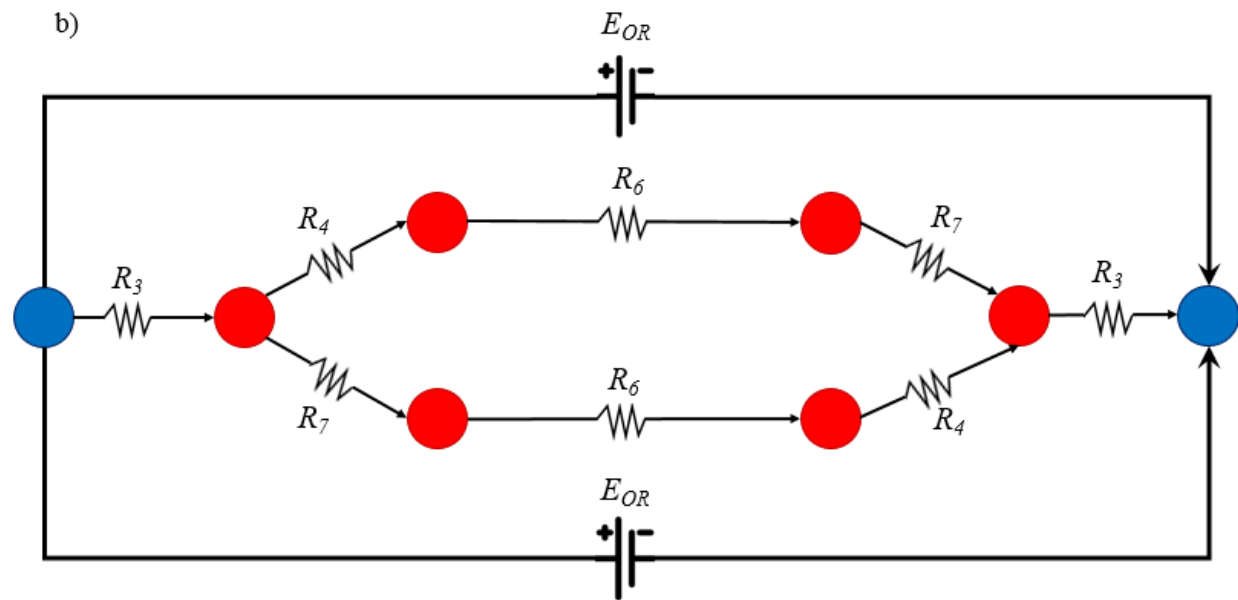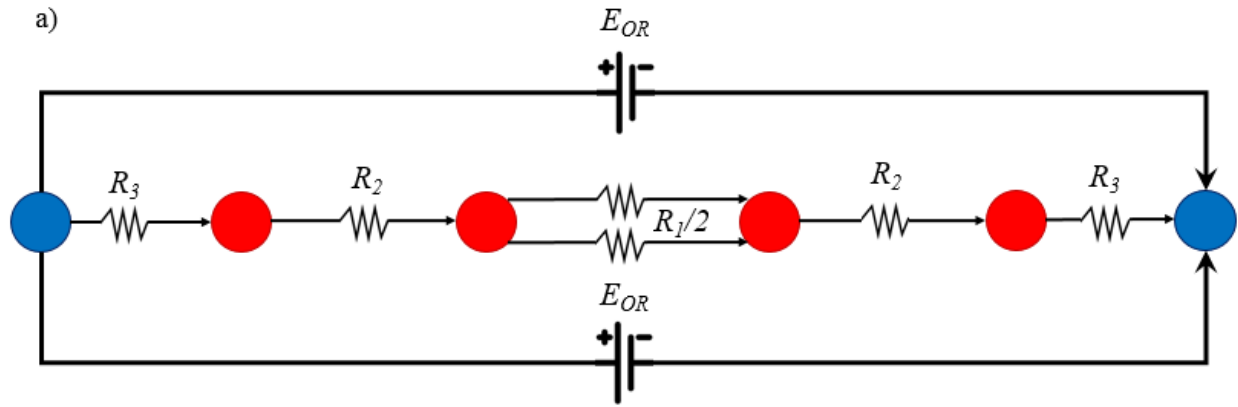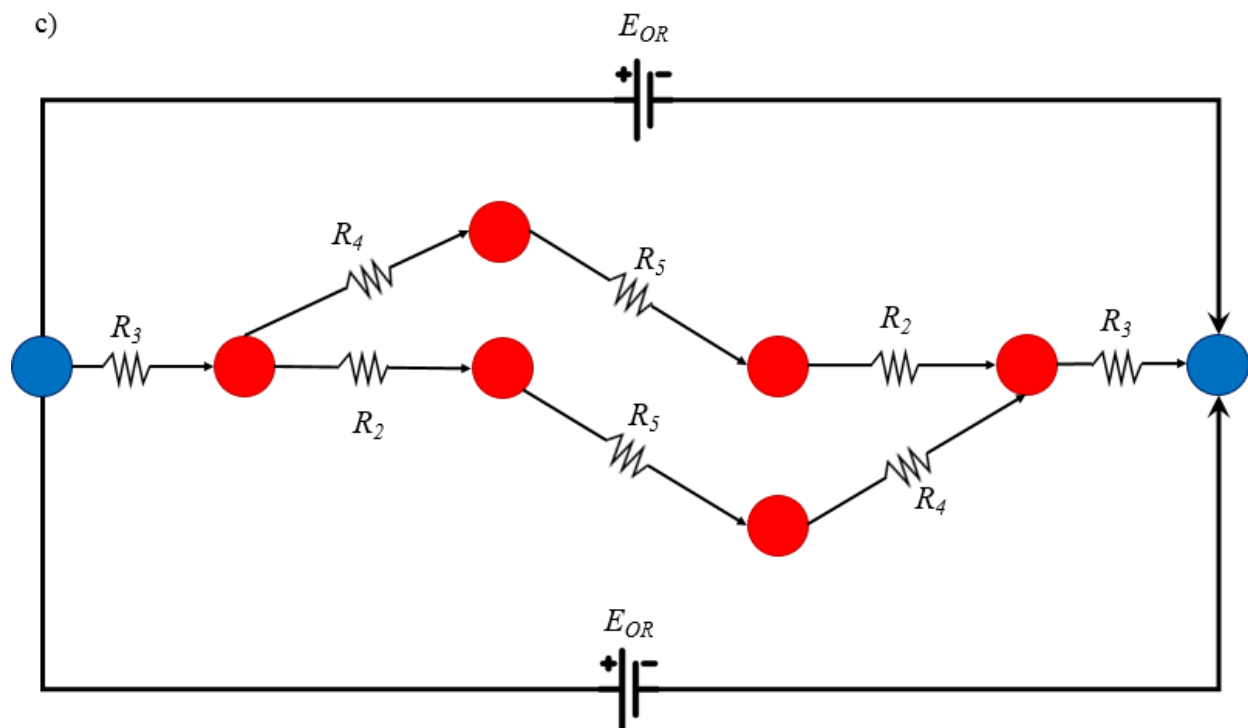
Figure 4.5: Electrical analog graphs of the three individual ORR pathways of the 7-step mechanism a) Dissociative; b) Peroxyl; c) Hydrogen Peroxide

A further discussion of the individual pathways is provided below.

4.4.2 Rdot Analysis

The Ohm's law analysis described above, while conceptually appealing, still requires numerical analysis based on the KFL relations to calculate step rates and hence resistances. Alternatively, the step resistances can be determined *a priori* using the approximate but accurate Rdot method, which further allows explicit rate laws. A simplified definition and explanation of the method follows, but the theory and process behind this method is explained in greater detail in references [27-29]. The Rdot resistance, $R_\rho^\bullet$, is defined as the resistance of the step s_ρ when it is considered as the rate-determining step (RDS), with all other steps, with the exception of those in an ER with the RDS, being at quasi-equilibrium (QE), i.e., $r_\rho^\bullet = \vec{r}_\rho^\bullet (1 - z_{OR})$, where $z_{OR} = e^{-\mathcal{A}_{OR}}$,

the OR reversibility; i.e., when the entire affinity drop of the OR occurs across the RDS step, those of the QE steps approaching zero. Further, the Rdot method provides the resistance of step ρ, R_ρ, under these conditions as: $R_\rho^\bullet = 1/\vec{r}_\rho^\bullet$, which in turn, can be determined via the Langmuir-Hinshelwood-Hougen-Watson (LHHW) formalism, as described below.

The forward rates for each step can hence be determined via the LHHW approach by assuming each of them to be the RDS in turn, the other steps being at QE. Then the site fraction for each intermediate species can be evaluated by finding an intermediate route (IR_i) and using the QE assumption for the involved steps in a manner which combine to produce the intermediate species being evaluated directly from terminal species. For example, to calculate $R_1^\bullet$, we first consider the forward step of s_1 to be RDS, then the intermediate routes for each intermediate species could be identified as

$$IR_{OS}: \text{-}s_2 - s_3 \tag{4.38}$$

$$IR_{OHS}: \text{-}s_3 \tag{4.39}$$

$$IR_{OOHS}: s_4 \tag{4.40}$$

$$IR_{HOOHS}: s_4 + s_6 \tag{4.41}$$

Care has to be exercised in choosing these pathways for formation of the intermediate species to not include steps that might not be at QE, e.g., at least one step in a parallel pathway in an ER is not at QE, otherwise KPL of that cycle will be violated. The ratio of fractional site coverage of each of the intermediate species k to the unoccupied catalyst site can now be evaluated by [28,29]

$$\frac{\theta^{\bullet}_{k,\rho}}{\theta^{\bullet}_{0,\rho}} = \left\{ \prod_{IR_k} \left(\frac{\vec{\omega}_j}{\bar{\omega}_j} \right)^{\sigma_{kj}} \right\}^{1/\gamma_k} \tag{4.42}$$

Where $\theta^{\bullet}_{k,\rho}$ is the site fraction of species k for step ρ, and ω_j is the step weight for each step j in the IR_k equation with σ_{kj} representing the stoichiometric numbers for that step in the intermediate route. The expressions for each of the intermediate species can hence be written as

$$\frac{\theta^{\bullet}_{O \cdot S, 1}}{\theta^{\bullet}_{0,1}} = \left(\frac{\vec{\omega}_2}{\bar{\omega}_2} \right)^{-1} \left(\frac{\vec{\omega}_3}{\bar{\omega}_3} \right)^{-1} \tag{4.43}$$

$$\frac{\theta^{\bullet}_{OH \cdot S, 1}}{\theta^{\bullet}_{0,1}} = \left(\frac{\vec{\omega}_3}{\bar{\omega}_3} \right)^{-1} \tag{4.44}$$

$$\frac{\theta^{\bullet}_{OOH \cdot S, 1}}{\theta^{\bullet}_{0,1}} = \left(\frac{\vec{\omega}_4}{\bar{\omega}_4} \right) \tag{4.45}$$

$$\frac{\theta^{\bullet}_{HOOH \cdot S, 1}}{\theta^{\bullet}_{0,1}} = \left(\frac{\vec{\omega}_4}{\bar{\omega}_4} \right) \left(\frac{\vec{\omega}_6}{\bar{\omega}_6} \right) \tag{4.46}$$

Where $\theta^{\bullet}_{i,k}$ is the site fraction of species i for step k and ω_k is the step weight for the forward or reverse of reaction step k. The fractions of all catalyst sites add up to unity via site balance, so the reciprocal of the unoccupied catalyst site is expressed as

$$\frac{1}{\theta^{\bullet}_{0,1}} = 1 + \frac{1}{\theta^{\bullet}_{O \cdot S, 1}} + \frac{1}{\theta^{\bullet}_{OH \cdot S, 1}} + \frac{1}{\theta^{\bullet}_{OOH \cdot S, 1}} + \frac{1}{\theta^{\bullet}_{HOOH \cdot S, 1}} \tag{4.47}$$

Finally, the Rdot resistance for step 1 is

$$R_1^\bullet = \frac{1}{\vec{r}_1^\bullet} = \frac{1}{\bar{\omega}_1 \theta_{0,1}^{\bullet\,2}} = \frac{1}{\vec{\omega}_1}\left(1 + \frac{\bar{\omega}_3}{\vec{\omega}_3} + \frac{\bar{\omega}_3}{\vec{\omega}_3}\frac{\bar{\omega}_2}{\vec{\omega}_2} + \frac{\vec{\omega}_4}{\vec{\omega}_4} + \frac{\vec{\omega}_4}{\vec{\omega}_4}\frac{\vec{\omega}_6}{\vec{\omega}_6}\right)^2 \qquad (4.48)$$

This process is applied to each step in turn to evaluate $R_{OR}^\bullet$ by an expression equivalent to Eq (4.34).

Thus assuming next s_2 to be the RDS, we obtain in terms of step weights.

$$R_2^\bullet = \frac{1}{\vec{\omega}_2}\sqrt{\frac{\bar{\omega}_1}{\vec{\omega}_1}}\left(1 + \sqrt{\frac{\bar{\omega}_1}{\vec{\omega}_1}} + \frac{\bar{\omega}_3}{\vec{\omega}_3} + \frac{\vec{\omega}_4}{\vec{\omega}_4} + \frac{\vec{\omega}_4}{\vec{\omega}_4}\frac{\vec{\omega}_6}{\vec{\omega}_6}\right) \qquad (4.49)$$

and so on. Similarly,

$$R_3^\bullet = \frac{1}{\vec{\omega}_3}\frac{\bar{\omega}_3}{\vec{\omega}_2}\left(1 + \sqrt{\frac{\bar{\omega}_1}{\vec{\omega}_1}} + \frac{\bar{\omega}_2}{\vec{\omega}_2} + \frac{\vec{\omega}_4}{\vec{\omega}_4}\sqrt{\frac{\bar{\omega}_1}{\vec{\omega}_1}} + \frac{\vec{\omega}_4}{\vec{\omega}_4}\frac{\vec{\omega}_6}{\vec{\omega}_6}\sqrt{\frac{\bar{\omega}_1}{\vec{\omega}_1}}\right) \qquad (4.50)$$

$$R_4^\bullet = \frac{1}{\vec{\omega}_4}\left(1 + \sqrt{\frac{\bar{\omega}_1}{\vec{\omega}_1}} + \frac{\bar{\omega}_3}{\vec{\omega}_3} + \frac{\bar{\omega}_7}{\vec{\omega}_7}\left(\frac{\bar{\omega}_3}{\vec{\omega}_3}\right)^2 + \frac{\bar{\omega}_1}{\vec{\omega}_1}\frac{\bar{\omega}_2}{\vec{\omega}_2}\frac{\bar{\omega}_5}{\vec{\omega}_5}\right) \qquad (4.51)$$

$$R_5^\bullet = \frac{1}{\vec{\omega}_5}\frac{\bar{\omega}_4}{\vec{\omega}_4}\left(1 + \sqrt{\frac{\bar{\omega}_1}{\vec{\omega}_1}} + \frac{\bar{\omega}_3}{\vec{\omega}_3} + \frac{\bar{\omega}_4}{\vec{\omega}_4} + \frac{\vec{\omega}_4}{\vec{\omega}_4}\frac{\vec{\omega}_6}{\vec{\omega}_6}\right)^2 \qquad (4.52)$$

$$R_6^\bullet = \frac{1}{\vec{\omega}_6}\frac{\bar{\omega}_4}{\vec{\omega}_4}\left(1 + \sqrt{\frac{\bar{\omega}_1}{\vec{\omega}_1}} + \frac{\bar{\omega}_3}{\vec{\omega}_3} + \frac{\bar{\omega}_4}{\vec{\omega}_4} + \frac{\bar{\omega}_7}{\vec{\omega}_7}\left(\frac{\bar{\omega}_3}{\vec{\omega}_3}\right)^2\right) \qquad (4.53)$$

and

$$R_7^\bullet = \frac{1}{\vec{\omega}_7}\frac{\bar{\omega}_4}{\vec{\omega}_4}\frac{\bar{\omega}_6}{\vec{\omega}_6}\left(1 + \sqrt{\frac{\bar{\omega}_1}{\vec{\omega}_1}} + \frac{\bar{\omega}_3}{\vec{\omega}_3} + \frac{\bar{\omega}_4}{\vec{\omega}_4} + \frac{\vec{\omega}_4}{\vec{\omega}_4}\frac{\vec{\omega}_6}{\vec{\omega}_6}\right)^2 \qquad (4.54)$$

so that

135

$$R_{\mathrm{OR}}^{\bullet} = 2R_3^{\bullet} + R_\alpha^{\bullet} + \cfrac{1}{\cfrac{1}{R_\beta^{\bullet} + R_{\mathrm{B}}^{\bullet}} + \cfrac{1}{R_\gamma^{\bullet} + R_4^{\bullet} + R_{\mathrm{C}}^{\bullet}}} \tag{4.55}$$

The overall rate for the ORR can then be written as

$$2\,r_{OR} = \frac{E_{OR}}{R_{OR}^{\bullet}} \tag{4.56}$$

Further, recall that the thermodynamic driving force E_{OR} is defined as

$$E_{\mathrm{OR}} \equiv 1 - z_{\mathrm{OR}} \tag{4.57}$$

where z_{OR} is the reversibility of the overall reaction [26]. The current density can finally be calculated using Eq. (4.25) with the overall reaction rate estimated according to $r_{OR} = (1 - z_{\mathrm{OR}})/2R_{\mathrm{OR}}^{\bullet}$, which provides the equation for current density as

$$i = \frac{\nu_{OR,e^-}F(1 - z_{OR})}{2R_{\mathrm{OR}}^{\bullet}} \tag{4.58}$$

Based on KPL, z_{OR} can be written in terms of step weights,

$$z_{OR} = \prod_{\rho=1}^{q+1} \left(\frac{\bar{\omega}_\rho}{\vec{\omega}_\rho} \right)^{\sigma_{g\rho}} \tag{4.59}$$

For the each of three the full routes of the 7-step ORR mechanism it can be seen that z_{OR} may be alternatively written as

$$z_{OR} = \frac{\bar{\omega}_{1,0} \; \bar{\omega}_{2,0}{}^2 \; \bar{\omega}_{3,0}{}^2}{\vec{\omega}_{1,0} \; \vec{\omega}_{2,0}{}^2 \; \vec{\omega}_{3,0}{}^2} e^{-8\psi} = \frac{\bar{\omega}_{2,0} \; \bar{\omega}_{4,0} \; \bar{\omega}_{5,0} \; \bar{\omega}_{3,0}{}^2}{\vec{\omega}_{2,0} \; \vec{\omega}_{4,0} \; \vec{\omega}_{5,0} \; \vec{\omega}_{3,0}{}^2} e^{-8\psi} = \frac{\bar{\omega}_{4,0} \; \bar{\omega}_{6,0} \; \bar{\omega}_{7,0} \; \bar{\omega}_{3,0}{}^2}{\vec{\omega}_{4,0} \; \vec{\omega}_{6,0} \; \vec{\omega}_{7,0} \; \vec{\omega}_{3,0}{}^2} e^{-8\psi} \qquad (4.60)$$

where $\bar{\omega}_{\rho,0}$ is the step weight evaluated at zero overpotential ($\psi = 0$). Further, at equilibrium, the

reversibility is unity, i.e. as ψ approaches zero, z_{OR} approaches unity. Thus, the ratio of the step

weights in the above expression also must be unity, e.g., $\bar{\omega}_{1,0}\bar{\omega}_{2,0}{}^2\bar{\omega}_{3,0}{}^2 = \vec{\omega}_{1,0}\vec{\omega}_{2,0}{}^2\vec{\omega}_{3,0}{}^2$ and

$z_{OR} = e^{-8\psi}$ simply.

This relation can be substituted into Eq. (4.45) to finally obtain

$$i = \frac{\nu_{OR,e^-} F(1 - e^{-8\psi})}{2R_{OR}^{\bullet}} \qquad (4.61)$$

Alternatively, the equation can be expressed using the exchange current density, which is defined

as the current density at zero overpotential in either direction. At zero overpotential the net current

density is zero ($i = 0$), but the rate of current in either the positive and negative direction are equal

and nonzero $\vec{i} = \bar{i} = i_0$. Thus, the exchange current density i_0 is calculated by

$$i_0 = \frac{\left| \nu_{OR,e^-} \right| F}{2R_{OR,0}^{\bullet}} \qquad (4.62)$$

with the OR resistance corresponding to equilibrium conditions. The exchange current density is

a useful value as it characterizes evaluates the intrinsic activity of the catalyst without the added

driving force of the electric overpotential.

4.4.3 Catalyst Activity Comparison

The equation for $R_{OR}^{\bullet}$ is valid, regardless of the conditions for the reaction (temperature, overpotential, catalyst, etc.). This, of course, assumes no additional chemical pathways become viable, but if ordinary fuel cell operating conditions are considered, that is a reasonable assumption. Thus, for a set of conditions and kinetic data, the $R_{OR}^{\bullet}$ and thus the kinetic current of the ORR can be approximated by Eqs (4.61 and 4.62). This facilitates the process of finding suitable catalysts and narrowing their optimal conditions by quickly comparing the resulting $R_{OR}^{\bullet}$. To ensure that the equations for $R_{OR}^{\bullet}$ are valid, the reaction rates were calculated at varying overpotentials via Rdot kinetics on Pt catalyst and compared to the values obtained through traditional QSS numerical calculations in a parity plot (Fig 4.6). The figure shows good agreement proving that the Rdot method and its simplifications are valid for the kinetic analysis or the ORR reaction.

The activity of each catalyst in terms of exchange current density was also evaluated, i.e., via Eq (4.62), to be used for comparison with the results provided by Herron et al. [3]. For a platinum catalyst at 298K and 1atm, this value was calculated to be 2.35×10^{-10} A/cm^2, which is well within the expected range for this catalyst [26, 32]. Figure 4.7 shows the kinetic current as a function of the applied overpotential for platinum catalyst. It is seen that the results agree reasonably with the experimental data of Wang et al. [17]. Exchange current densities were also calculated for the other catalysts (Table 4.5). The exchange current density for the platinum catalyst is highest among the catalysts that were analyzed, but several of the candidates have current densities that are within an order of magnitude of the platinum catalyst.
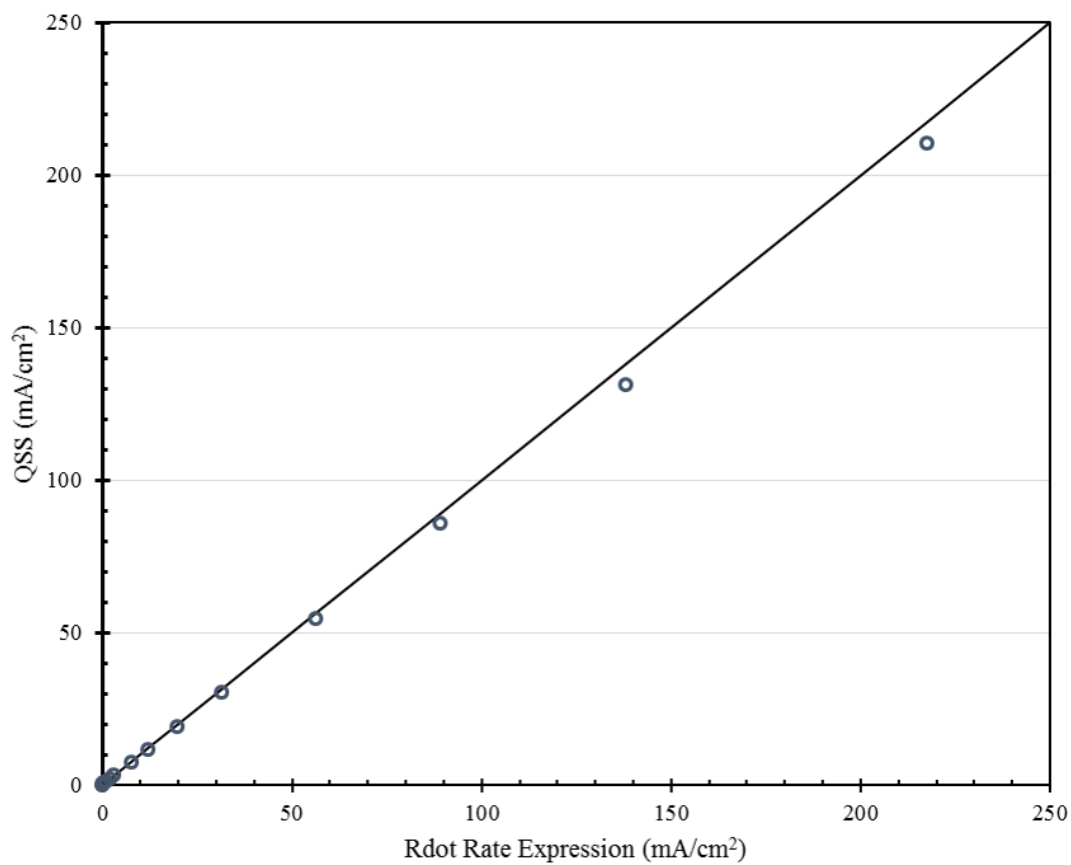
Figure 4.6: Parity plot of current density obtained from Rdot rate expression (straight line) and that calculated numerically for the ORR reaction (points). Each point is a different electric overpotential for which the current density is calculated.
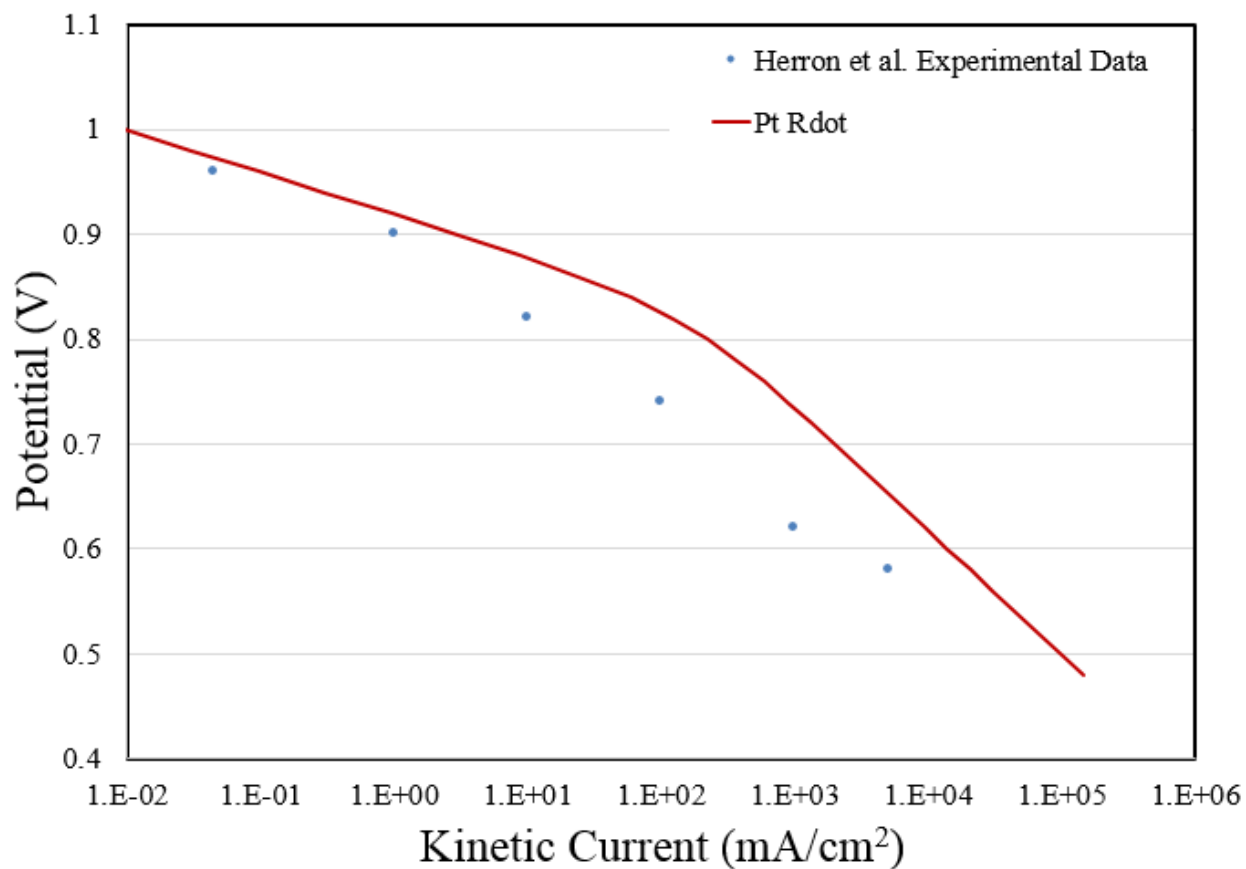
Figure 4.7: Graph of Potential (V) vs Kinetic Current (mA/cm^2) off the ORR on Pt catalyst using the Rdot method with comparison to experimental values found by Wang et al. [17]

Catalyst	Exchange Current Density (A/cm2)
Pt	2.35×10^{-10}
Pt*/Au	3.42×10^{-11}
2Pt*/Pd	2.57×10^{-11}
Pt*/Pd	9.83×10^{-12}
3Pt*/Pd	8.07×10^{-12}
Pt*/Pd/Pd$_3$Ir	3.03×10^{-12}
Pt(3.91)	1.07×10^{-12}
Pt*/Pd/Pd$_3$Cu	1.69×10^{-13}
Pt*/Pd/Pd2Ir$_2$	8.40×10^{-15}
Pt*/Pd/Pd$_3$Ni	3.30×10^{-15}
Pt(3.87)	1.45×10^{-16}
Pt/Pd$_3$Ni	8.58×10^{-18}
3Pt*/Re	1.27×10^{-18}
Pt(3.86)	9.39×10^{-20}
Pt*/Pd$_3$Ir	2.86×10^{-23}

140

Pt*/Pd/Ir	2.34×10^{-23}
Pt*/Pd$_2$Ir$_2$	9.95×10^{-25}
Pt*/2Pd/Re	2.31×10^{-26}
Pt&/2Pd/Ru	8.43×10^{-27}
Pt*/2Pd/Ir	6.51×10^{-27}
Pt*/Pd$_3$Cu	1.20×10^{-27}
Pt*/Pd$_2$Cu$_2$	5.95×10^{-28}
Pt*/Pd/Pd$_3$Fe	3.11×10^{-28}
Pt*/Pd/Pd$_2$Cu$_2$	2.49×10^{-30}
Pt*/2Pd/Rh	9.34×10^{-31}
2Pt*/Re	7.48×10^{-31}
Pt*/Ir	8.75×10^{-32}
Pt*/Pd/Re	3.22×10^{-34}
Pt*/Pd$_2$/Co$_2$	7.09×10^{-38}
Pt*/Pd$_3$Fe	2.13×10^{-38}
Pt*/Pd/Pd$_2$Co$_2$	1.75×10^{-38}
Pt*/Pd/Ru	5.45×10^{-39}

Table 4.5: Exchange current densities calculated for ORR on Pt alloy catalysts at 298 K and standard conditions (unit activities)

Pt catalyst is clearly the most active, however, knowing quantitatively the difference between different catalysts allows better insight into potential catalyst compositions that might provide improved activity or a cost benefit. Figure 4.8 shows the relative activity for each catalyst as reported by Herron et al. [3] and compared with that computed in this work. Herron et al. define the maximum activity of a catalyst as [21, 22]

$$A = k_B T \min_i \left(\log(k_i / k_0) \right) \tag{4.63}$$

where k_i is the forward rate constant for reaction step *i, k_0* normalizes the activity of non-activated proton/electron transfer steps to zero and the $\min_i$ function takes the smallest value of k_i amongst all reaction steps [3]. Since exchange current density is proportional the catalyst activity, we can relate the exchange current density found above to the activity calculated by Herron et al. [3]. The activity of Pt for Ohm's Law kinetics was thus set to that reported by Herron et al. [3] and the

activity other catalysts are reduced by the fraction equal to the ratio of the catalyst current density

to the current density of Pt. This allows a comparison of the relative activity for each catalyst in

comparison to Pt. The graph shows many similar trends, but of particular note is the great

difference in activity for catalyst that exhibit a dual pathway mechanism, as discussed below
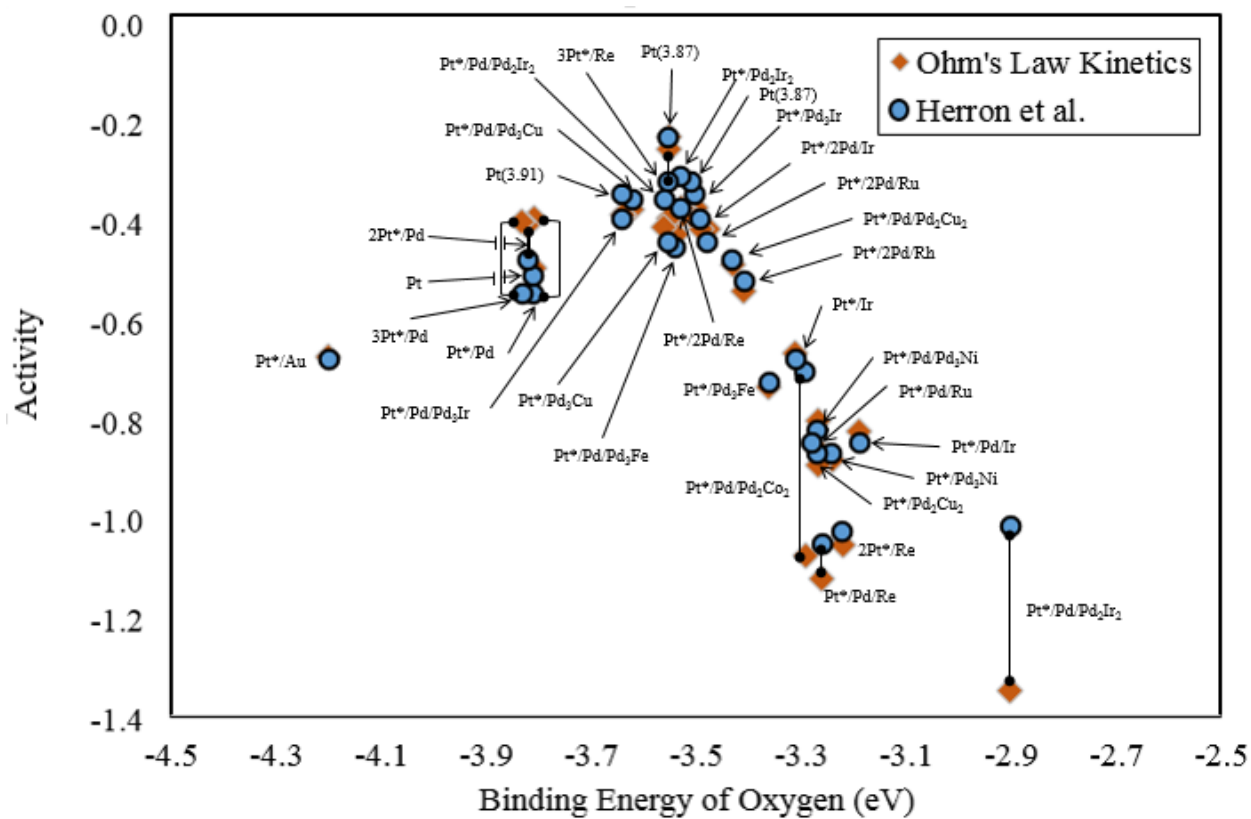
Figure 4.8: Comparison of relative catalyst activity for the ORR using Ohm's Law kinetics vs values calculated by Herron et al. [3] Large differences in values between the two methods are denoted by a connecting line. All other catalysts have overlapping or nearly overlapping points.

Of particular note are the differences in Figure 4.8 between our calculations and those of

Herron et al. [3] for the catalysts: Pt*/Pd/Pd$_2$Co$_2$ and Pt*/Pd/Pd$_2$Ir$_2$, which have multiple routes

contributing to the overall reaction rate. Since the Rdot kinetics completely evaluates the rate of

all the reaction routes, instead of estimating the activity of only the most dominant route, our results

can be considered quite robust and accurate.

For the 32 catalysts studied by Herron et al. Rdot calculations were performed over an overpotential range of 0-1.0V at 298K with terminal species activity set as unity. Figures 4.9-4.11 quantitatively compare overall resistance of each of the pathways as discussed above to determine which of the pathways are dominant for each catalyst at a range of overpotentials, with a lower resistance meaning the reaction flux is higher through that pathway.
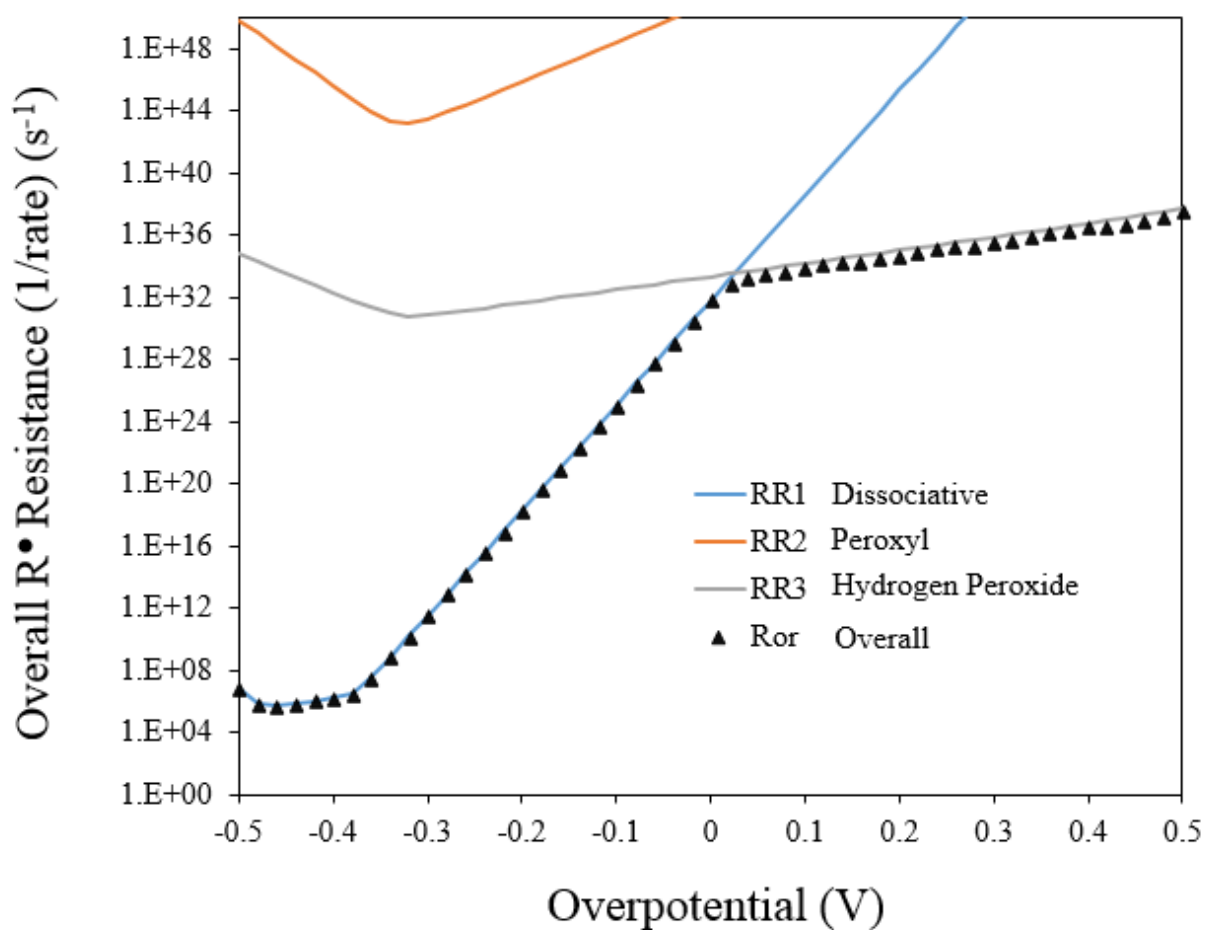
Figure 4.9: Pure Pt catalyst OR Rdot resistance graph.
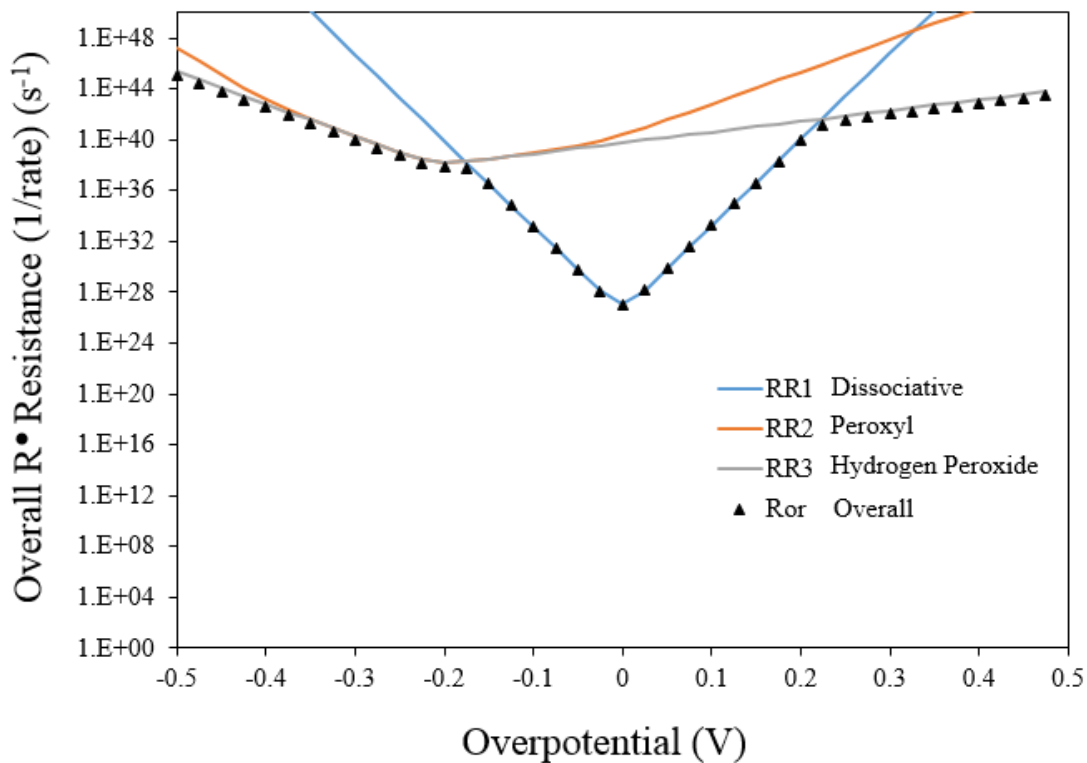
Figure 4.10: Pt*/Pd/Re catalyst OR Rdot resistance graph
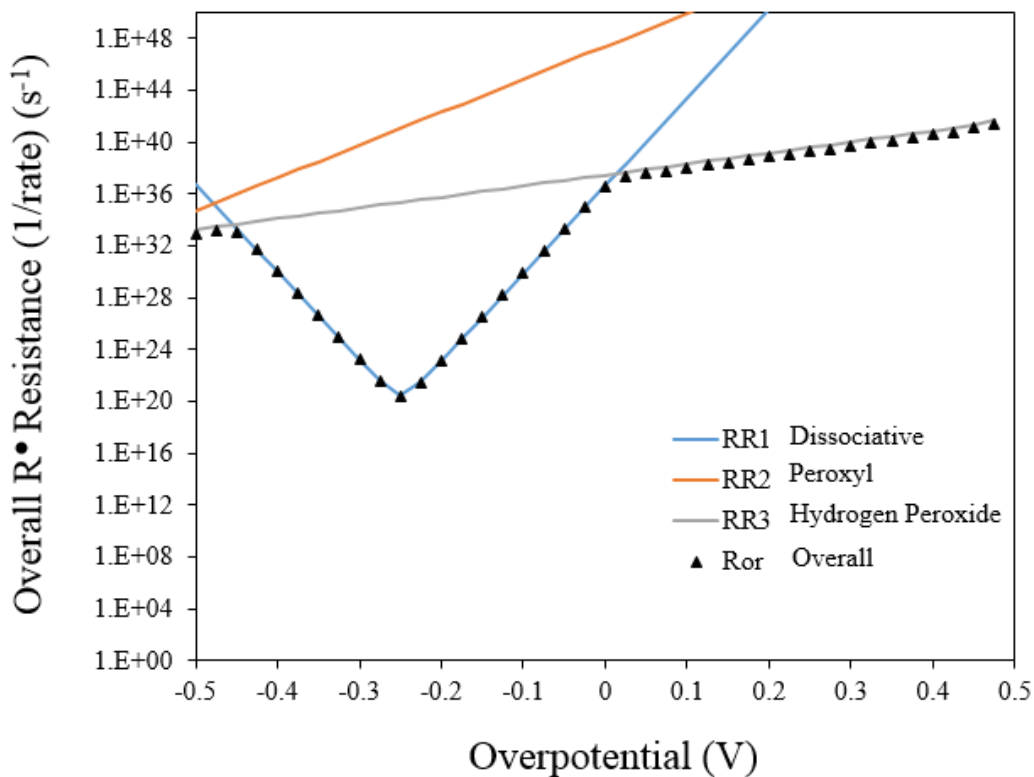
Figure 4.11: Pt*/Pd$_3$/Cu catalyst OR Rdot resistance graph

144

Figure 4.8 shows platinum catalyst as having the dissociative mechanism as the dominant pathway for any reasonable overpotential for the ORR and the peroxide pathway for the oxygen evolution reaction (OER). This is true for most of the catalysts analyzed, including all of the catalysts with higher current densities shown in Table 4.3. However, Figures 4.10 and 4.11 show examples of two catalysts that have higher flux through different RRs. In particular, at lower overpotentials the peroxyl and hydrogen peroxide mechanisms can dominate the kinetics in the catalysts.

Another valuable insight obtained from the RR approach is the identification of which exact steps are rate limiting in a given pathway. In the case for the ORR on platinum catalyst, we see that the dissociative mechanism is the dominant pathway, so looking at each individual step resistance, we can quantify the amount that step affects the overall rate. For the dissociative mechanism, thus, we compare the Rdot resistance for s_1, s_2 and s_3 in Fig. 4.12.
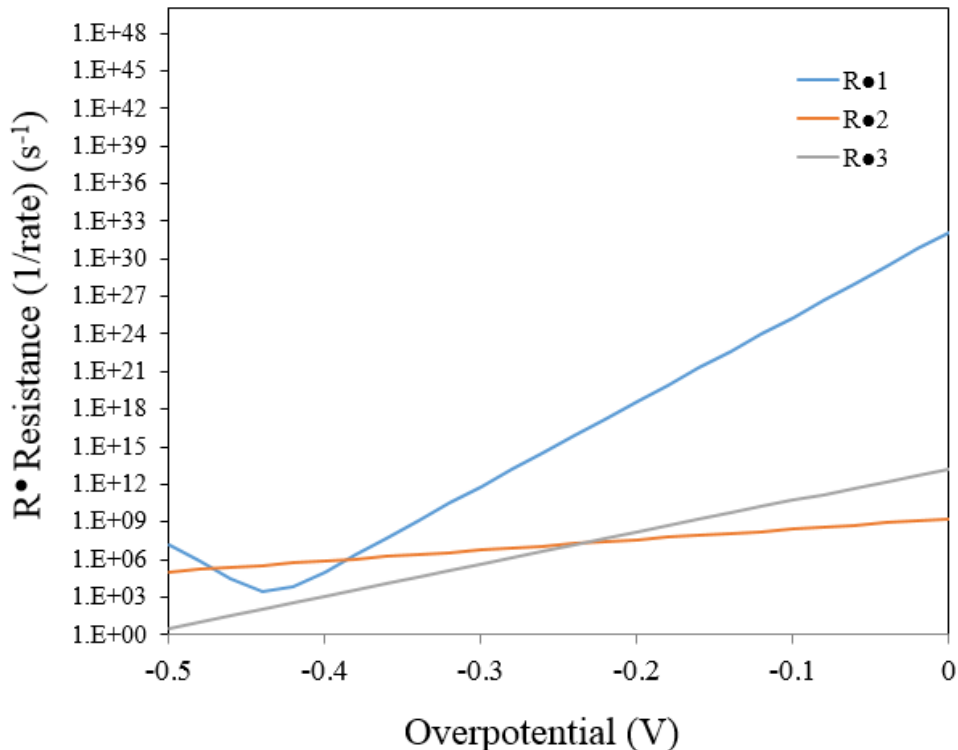
Figure 4.12: Comparison of resistance for the elementary steps in the dissociative mechanism on platinum catalyst.

It is evident that both s_1, the O-O bond breaking step and s_2, the hydrogenation of the bound O atom, are rate limiting for overpotentials of practical interest and that the overpotential greatly affects which one and to what degree. It also shows that $R_1^\bullet$ and $R_2^\bullet$ are the only significant sources of resistance for these conditions, so the overall resistance can be approximated by using Eq. (4.55) for the resistances in the dissociative pathway and Eqs. (4.48) and (4.49) for the resistances of $R_1^\bullet$ and $R_2^\bullet$.

$$R_{OR}^\bullet \approx \frac{R_1^\bullet}{2} + 2R_2^\bullet = \frac{1}{2\vec{\omega}_1}\left(1 + \frac{\vec{\omega}_3}{\vec{\omega}_3} + \frac{\vec{\omega}_3}{\vec{\omega}_3}\frac{\vec{\omega}_2}{\vec{\omega}_2} + \frac{\vec{\omega}_4}{\vec{\omega}_4} + \frac{\vec{\omega}_4}{\vec{\omega}_4}\frac{\vec{\omega}_6}{\vec{\omega}_6}\right)^2 + \frac{2}{\vec{\omega}_2}\sqrt{\frac{\vec{\omega}_1}{\vec{\omega}_1}}\left(1 + \sqrt{\frac{\vec{\omega}_1}{\vec{\omega}_1}} + \frac{\vec{\omega}_3}{\vec{\omega}_3} + \frac{\vec{\omega}_4}{\vec{\omega}_4} + \frac{\vec{\omega}_4}{\vec{\omega}_4}\frac{\vec{\omega}_6}{\vec{\omega}_6}\right)$$

(4.64)

Then, we can expand the site fraction to show an explicit equation for $R_1^\bullet$ that can be used to calculate the current density.

$$R_{OR}^\bullet = \frac{1}{2\vec{k}_1 a_{O_2}}\left(1 + \frac{\vec{k}_3}{\vec{k}_3}e^{2\psi} + \frac{\vec{k}_3 a_{H_2O}}{\vec{k}_3}\frac{\vec{k}_2}{\vec{k}_2}e^{4\psi} + \frac{\vec{k}_4 a_{O_2}}{\vec{k}_4}e^{-2\psi} + \frac{\vec{k}_4 a_{O_2}}{\vec{k}_4}\frac{\vec{k}_6}{\vec{k}_6}a_{O_2}e^{-4\psi}\right)^2 + \frac{2}{\vec{k}_2}\sqrt{\frac{\vec{k}_1}{\vec{k}_1 a_{O_2}}}\left(1 + \sqrt{\frac{\vec{k}_1}{\vec{k}_1 a_{O_2}}} + \frac{\vec{k}_3 a_{H_2O}}{\vec{k}_3}e^{2\psi} + \frac{\vec{k}_4 a_{O_2}}{\vec{k}_4}e^{2\psi} + \frac{\vec{k}_4 a_{O_2}}{\vec{k}_4}\frac{\vec{k}_6}{\vec{k}_6}e^{-4\psi}\right)$$

(4.65)

Thus, substituting Eqs. (4.65) into (4.61)

$$i = 4\vec{k}_1 a_{O_2} F\left[\left(1 + \frac{\vec{k}_3}{\vec{k}_3}e^{2\psi} + \frac{\vec{k}_3 a_{H_2O}}{\vec{k}_3}\frac{\vec{k}_2}{\vec{k}_2}e^{4\psi} + \frac{\vec{k}_4 a_{O_2}}{\vec{k}_4}e^{-2\psi} + \frac{\vec{k}_4 a_{O_2}}{\vec{k}_4}\frac{\vec{k}_6}{\vec{k}_6}a_{O_2}e^{-4\psi}\right)^2 + \frac{4}{\vec{k}_2}\sqrt{\vec{k}_1\vec{k}_1 a_{O_2}}\left(1 + \sqrt{\frac{\vec{k}_1}{\vec{k}_1 a_{O_2}}} + \frac{\vec{k}_3 a_{H_2O}}{\vec{k}_3}e^{2\psi} + \frac{\vec{k}_4 a_{O_2}}{\vec{k}_4}e^{2\psi} + \frac{\vec{k}_4 a_{O_2}}{\vec{k}_4}\frac{\vec{k}_6}{\vec{k}_6}e^{-4\psi}\right)\right]^{-1}$$ (4.66)

4.4 Conclusions:

We have demonstrated how even a relatively simple recently proposed 7-step reaction mechanism for the ORR can be quite complex when analyzing how each elementary step contributes to the rate overall reaction. The RR approach does not require the mechanism to be

simplified or reduced *a priori* and thus allows the analysis to simultaneously include each reaction pathway in the overall rate expression that was determined. Not only does it provide such a useful expression, but it is also robust enough to be used for use of new catalysts without being concerned if the dominant pathways change. However, if it is determined that any one pathway or elementary step is indeed rate determining, the resulting expressions can be simplified, as shown here.

Analysis of each catalyst confirms several of the results of Herron et al. [3], but also provides insights beyond the conditions they used as well as the effect of potential to see the effect of other conditions. The resistance graphs demonstrate how much overpotential can affect the mechanism and gives us a variable to change when searching for a suitable catalyst. The dominant pathways for the reaction can be clearly seen for each mechanism. Differences in the ORR activities for the catalysts with multiple reaction pathways demonstrated how the RR method can be a more robust method for analyzing the kinetics.   Understanding exactly which steps are limiting can prove useful when exploring new catalysts and looking for structures that could potential affect those steps. Hopefully, this approach will allow us to investigate ORR mechanism on new catalysts with increased accuracy.

4.5 References:

1. Datta, R., Martino, D. J., Dong, Y., Choi, P., (2016). Modeling of PEM Water Electrolyzer. In D. Bessarabov, H. Wang, H. Li, N. Zhao (Eds.), PEM Electrolysis for Hydrogen Production: Principles and Applications (pp. 243-247). New York, NY: CRC Press, Taylor & Francis Group, LLC

2. Katsounaros, I., Cherevko, S., Zeradjanin, A. R. and Mayrhofer, K. J. J. (2014), Oxygen Electrochemistry as a Cornerstone for Sustainable Energy Conversion. Angew. Chem. Int. Ed., 53: 102–121. doi:10.1002/anie.201306588

3. Herron, A. J., Jiao, J., Hahn, K., Peng, G., Adzic, R. R, Mavrikakis, M., "Oxygen Reduction Reaction on Platinum-Terminated 'Onion-structured' Alloy Catalysts," *Electrocatalysis* DOI 10.1007/s12678-012-0087-0 (2012)

4. J.L. Zhang, M.B. Vukmirovic, Y. Xu, M. Mavrikakis, R.R. Adzic, Controlling the catalytic activity of platinum-monolayer electrocatalysts for oxygen reduction with different substrates. Angew. Chem. Int. Ed. 44(14), 2132–2135 (2005)

5. J. Zhang, Y. Mo, M.B. Vukmirovic, R. Klie, K. Sasaki, R.R. Adzic, Platinum monolayer electrocatalysts for O2 reduction: Pt monolayer on Pd(111) and on carbon-supported Pd nanoparticles. J. Phys. Chem. B 108(30), 10955–10964 (2004)

6. Adzic RR, Zhang J, Sasaki K, Vukmirovic MB, Shao M, Wang JX, Nilekar AU, Mavrikakis M, Valerio JA, Uribe F (2007) Platinum monolayer fuel cell Electrocatalysts. Top Catal 46:249–262

7. A.U. Nilekar, Y. Xu, J.L. Zhang, M.B. Vukmirovic, K. Sasaki, R.R. Adzic, M. Mavrikakis, Bimetallic and ternary alloys for improved oxygen reduction catalysis. Top. Catal. 46(3–4), 276–284 (2007) Int. Ed. 44(14), 2132–2135 (2005)

8. Mukerjee S, Srinivasan S, Soriaga MP, McBreen J, (1995) Effect of preparation conditions of Pt alloys on their electronic, structural, J Mol Model (2015) 21: 281 Page 9 of 11 281 and electrocatalytic activities for oxygen reduction-XRD, XAS, and electrochemical studies. J Phys Chem 99:4577–4589 7.

9. Paulus UA, Wokaun A, Scherer GG, Schmidt TJ, Stamenkovic V, Radmilovic V, Marković NM, Ross PN (2002) Oxygen reduction on carbon-supported Pt−Ni and Pt−Co alloy catalysts. J Phys Chem B 106:4181–4191 8.

10. Mun BS, Watanabe M, Rossi M, Stamenkovic V, Marković NM, Ross PN (2005) A study of electronic structures of Pt3M (M=Ti, V, Cr, Fe, Co, Ni) polycrystalline alloys with valence-band photoemission spectroscopy. J Chem Phys 123:204717 9.

11. Kitchin JR, Nørskov JK, Barteau MA, Chen JG (2004) Modification of the surface electronic and chemical properties of Pt(111) by subsurface 3d transition metals. J Chem Phys 120: 10240

12. Stamenkovic VR, Fowler B, Mun BS, Wang GF, Ross PN, Lucas CA, Marković NM (2007) Improved oxygen reduction activity on Pt3Ni(111) via increased surface site availability. Science 315:493– 497

13. Stamenkovic VR, Mun BS, Mayrhofer KJJ, Ross PN, Marković NM (2006) Effect of surface composition on electronic structure, stability, and electrocatalytic properties of Pt-transition metal alloys: Pt-skin versus Pt-skeleton surfaces. J Am Chem Soc 128:8813–8819 12.

14. Stamenkovic V, Mun BS, Mayrhofer KJJ, Ross PN, Marković NM, Rossmeisl J, Greeley J, Nørskov JK (2006) Changing the activity of electrocatalysts for oxygen reduction by tuning the surface electronic structure. Angew Chem Int Ed 45:2897–2901 13.

15. Stamenkovic V, Schmidt TJ, Ross PN, Marković NM (2003) Surface segregation effects in electrocatalysis: kinetics of oxygen reduction reaction on polycrystalline Pt3Ni alloy surfaces. J Electroanal Chem 554–555:191–199 14. Shao MH, Sasaki K, Adzic RR (2006)

Pd−Fe nanoparticles as electrocatalysts for oxygen reduction. J Am Chem Soc 128:3526–3527 15.

16. D. C. Ford, A. U. Nilekar, Y. Xu, M. Mavrikakis, Partial and complete reduction of O_2 by hydrogen on transition metal surfaces, Surf. Sci. 604 (2010) 1565-1575

17. Wang, J. X., Zhang, J., and Adzic, R. R., "Double-Trap Kinetic Equation for the Oxygen Reduction Reaction on Pt(111) in Acidic Media," *J. Phys. Chem. A.*, 111, 12702-12710 (2007a).

18. Rodrigo Ferreira de Moraisa, Philippe Sautetb, David Loffredab, Alejandro A. Francoa, "A multiscale theoretical methodology for the calculation of electrochemical observables from ab initio data: Application to the oxygen reduction reaction in a Pt(111)-based polymer electrolyte membrane fuel cell" *Electrochimica Acta* 56 (2011) 10842– 10856

19. Guang-Feng Wei, Ya-Hui Fang, and Zhi-Pan Liu, "First Principles Tafel Kinetics for Resolving Key Parameters in Optimizing Oxygen Electrocatalytic Reduction Catalyst", *J. Phys. Chem*, 116, 12696−12705 (2012)

20. Matthew P. Hyman and J. Will Medlin "Mechanistic Study of the Electrochemical Oxygen Reduction Reaction on Pt(111) Using Density Functional Theory", *J. Phys. Chem. B*, *110,* 15338-15344 (2006)

21. J.K. Nørskov, J. Rossmeisl, A. Logadottir, L. Lindqvist, J.R. Kitchin, T. Bligaard, H. Jonsson, Origin of the overpotential for oxygen reduction at a fuel-cell cathode. J. Phys. Chem. B 108(46), 17886–17892 (2004)

22. T. Bligaard, J.K. Nørskov, S. Dahl, J. Matthiesen, C.H. Christensen, J. Sehested, The Bronsted–Evans–Polanyi relation and the volcano curve in heterogeneous catalysis. J. Catal. 224(1), 206–217 (2004)

23. Campbell CT. Future directions and industrial perspectives micro- and macro-kinetics: their relationship in heterogeneous catalysis. Top Catal. 1(3–4):353–366. (1994)

24. Stegelmann C, Andreasen A, Campbell CT. Degree of rate control: how much the energies of intermediates and transition states control rates. J Am Chem Soc. 131(23):8077–8082 (2009)

25. O'Malley, P. D., Datta, R. and Vilekar, S. A. (2015), Ockham's razor for paring microkinetic mechanisms: Electrical analogy vs. Campbell's degree of rate control. AIChE J., 61: 4332–4346. doi:10.1002/aic.14956

26. Vilekar, Saurabh A, Fishtik, Ilie, Datta, Ravindra, "Kinetics of the Hydrogen Electrode Reaction" *Journal of The Electrochemical Society*, 157 7 B1040-B1050 (2010)

27. Fishtik, I., Callaghan, C. A., and Datta, R., "Reaction Route Graphs. I. Theory and Algorithm," *J. Phys. Chem. B*, 108, 5671-5682 (2004a).

28. Fishtik, I., Callaghan, C. A., and Datta, R., "Reaction Route Graphs. II. Examples of Enzyme- and Surface-Catalyzed Single Overall Reactions," *J. Phys. Chem. B*, 108, 5683-5697 (2004b).

29. Fishtik, I., Callaghan, C. A., and Datta, R., "Reaction Route Graphs. III. Non-Minimal Kinetic Mechanisms," *J. Phys. Chem. A,* 109, 2710-2722 (2005).

30. S.A. Vilekar, I. Fishtik, R. Datta, Chem. Eng. Sci. 64 1968-1979 (2009)

31. I. Fishtik, R. Datta, Studies in Surf. Sci. Catal. 133 (2001) 123-130.

32. I. Fishtik, R. Datta, Ind. Eng. Chem. Res. 40 (2001) 2416-2427.

33. L.O. Chua, C.A. Desoer, E.S. Kuh, Linear and Nonlinear Circuits, Mc-Graw Hill, New York (1987)

34. Dumesic JA. Analyses of reaction schemes using De Donder relations. Journal of Catalysis. 1999;185(2):496-505.

35. K. Kinoshita, Electrochemical Oxygen Technology, Wiley, New York (1992)

36. Yung, Yuk L. DeMore, William B., Photochemistry of Planetary Atmospheres, Oxford University Press, 1998, p. 87

37. Fan, L.T., Bertok, B., Friedler, F., A graph-theoretic method to identify candidate mechanisms for deriving the rate law of a catalytic reaction, *Computer and Chemistry*, 26 (2002) 265-292

38. Fan, L.T. Shafie, S., Bertok, B., Friedler, F., Lee, D.-Y. Seo, H. Graph-theoretic approach for identifying catalytic or metabolic pathways, *Journal of the Chinese Institute of Engineers*, 28, 1021-1037

39. Fan, L. T., Zhang, T., Liu, J., Schlup, J. R., Seib, P. A., & Friedler, F. (2007). Assessment of sustainability-potential: Hierarchical approach. Industrial Engineering & Chemistry Research, 46(13), 4506–4516.

Chapter 5. Elucidation of Dry Methane Reforming Pathways and Kinetics on Ni Catalyst Using Reaction Route Graph Theory

A visualization of all the pathways for a 33-step mechanism for the Methane Dry Reforming (MDR) via reaction route (RR) graph theory is presented alongside an analysis of the flux through each pathway and identification of steps that are rate-limiting or quasi-equilibrated. The graph-theoretical visual depiction of the chemical pathways is also consistent with fundamental mass and energy balance laws and with the state-properties of thermodynamic functions, or Hess's Law, much like Kirchoff's laws of electrical circuits. Density functional theory (DFT) calculations of Fan et al. [1] for molecular steps on Ni catalyst were utilized in a microkinetic analysis of the catalyst activity under quasi-steady state (QSS) conditions. The QSS results are consistent with the networks laws and energy balance laws, and conform to Ohm's law analogy with electrical circuits. This analysis leads to an accurate quantification of the propensity of the reaction to proceed through the various possible pathways, and pinpoints which step kinetics are the most limiting in determining the flux of the reaction in these pathways. Based on these insights, the 33-step mechanism is reduced to three parallel pathways, each with a rate-limiting step (RLS), namely: i) the oxidation of C to CO by O; ii) the oxidation of C to CHO by OH; iii) and the oxidation of CH to CHO by O. Finally, explicit rate expressions are developed that accurately predict the MDR kinetics involving all these parallel pathways.

5.1 Introduction

Natural gas in the largest feedstock used in the production of hydrogen and syngas (CO + H_2). The industrial process uses steam as a source for oxygen to oxidize the carbon in the methane to CO releasing 2 molecules of hydrogen, along with a third coming from water. In addition, the

water gas shift reaction can further oxidize the CO into CO_2 with H_2O so that a third molecule of H_2 produced. An alternative process to this process methane steam reforming (MSR) is to use CO_2 as the source of oxygen in the so-called methane dry reforming ($CH_4 + CO_2 \leftrightarrows 2CO + 2H_2$) to produce syn gas. The MDR is of particular interest as it has the potential for recycling CO_2.

The study of the MDR mechanism on Ni catalyst is, thus, ever more important, due not only to its practical importance in producing syngas from two abundant greenhouse gases, CH_4 and CO_2, but also because of its significant complexity [1-17]. Some researchers have proposed mechanisms that include over 40 unique elementary steps and hundreds of possible reaction routes or pathways [2, 3]. While many of the proposed intermediate species and reaction routes are primarily theoretical and may not practically matter, it takes a great investment of time and resources to determine which. Clearly, an improved understanding the mechanism would go far in improving the MDR process and its catalysis. The reaction route (RR) graph approach developed by us [25-28] is the most rigorous and insightful tool currently available for elucidation of mechanism and kinetics [28]. We recently used it to illuminate the chemistry and kinetics of methane steam reforming (MSR) on Ni. [29] This paper extends that to the case of MDR.

Ni, Rh and Ru catalysts have been widely studied as the catalysts for MSR and MDR, and while Ru based catalysts can achieve higher activity; the Ni catalysts have comparable performance with far lower cost [2, 4]. The most significant issue with nickel catalyst performance is deactivation due to carbon formation. Much research has gone towards better understanding of how to limit carbon deposition. Despite the substantial research already devoted to this mechanism, there are still knowledge gaps concerning the discrete chemical pathways for the reaction. Understanding precisely which pathways are dominant and which steps are rate-limiting and how their kinetics can be improved could lead to improved catalysts and operation of this reaction. Fan

154

et al. [1] concluded that the dominant pathway involves direct decomposition of CO_2 forming atomic O and methane decomposing down to CH, which is then oxidized by surface atomic O into CHO or COH, which finally decomposes into CO or direct oxidation of C by O into CO. The rate-limiting steps in this study were found to be CH and C oxidation, with the reaction proceeding through CH oxidation much more so at the lower temperatures.

Wei and Iglesia [10] based their findings on kinetic and isotopic measurements, and argued that C atoms are oxidized by atomic O to form CH_xO which is the most abundant intermediate on the surface. Rostrup-Nielsen and Hansen [11] predicted that methane dissociation and atomic carbon oxidation determine the overall reaction rate and that both steam and dry reforming of methane on Ni catalyst proceed at the same rate. Bradford and Vannice [12] suggested that dry reforming of methane occurs via the reversible dissociation of CH_4 and CO_2 to produce CH_xO, and the decomposition of CH_4 as well as CH_xO is the kinetically slow step. Luo et al. [13] claimed that both the cleavage of C−H bonds and the decomposition of CH_xO ($x = 1-2$) into CO and adsorbed H species are rate-limiting steps, with the latter being the far more dominant pathway. The work by Osaki and Mori supported their conclusion, as the same pathways were identified over the K-promoted Ni catalysts [14,15]. Chang et al. proposed that the oxidization of atomic carbon by surface oxygen species is the only rate-determining step (RDS) in the reforming reaction over a K−Ni−Ca catalyst [16]. Using steady-state and transient kinetic methods, Cui et al. [17] investigated the mechanism for the MDR reaction over Ni/α-Al_2O_3 catalyst over a wide range of temperatures. They suggested that the rate limiting steps change with temperature, with CH_4 dissociation at low temperatures and the reaction between CH_x and CO_2 at high temperatures. There is much need for use of a widely accepted method for understanding chemical reaction

networks, which accurately and completely evaluates each reaction route and elementary step for the MDR reaction [18].

5.2 Mechanism and Kinetics

For our investigation, we have selected the MDR mechanism of Fan et al. [1] who provide a comprehensive list of DFT calculations for a 33-step MDR mechanism on Ni catalyst (Table 5.1). Three active sites are considered for the Ni catalyst, which Fan et al. accounts for by assuming movement of intermediate species between sites is much faster than reaction rates and their concentrations can be assumed to be at equilibrium. Thus, we take the rate constant of the step to be a sum of the fraction coverage of each site: (Ni(111) 74%, Ni(100) 15%, and Ni(211) 11%). We use this set of steps and kinetics for performing accurate analysis of the MDR mechanism. While Fan et al. provide numerical results of a mechanistic analysis, it cannot be said that the network is well understood to the point where one can identify clearly which reaction pathways and steps are dominant. Further, since the time it takes to numerically analyze microkinetics of even one facet of the reaction system (in some cases not even to the fullest extent) is prohibitively great, thus we strive to illuminate the process with RR Graph theory. Furthermore, we plan to explain which overall reactions (OR)s are needed for this mechanism, as well as establishing a method to determine a rate equation for the overall reaction.

5.2.1 Quasi-steady State Analysis

Fane et al. [1] use a microkinetic analysis of this mechanism. Another rate approach is to use the quasi-steady state (QSS) method. The QSS relations for the $q = 19$ intermediate species and the $n = 5$ terminal species in this mechanism are summarized in Table 5.2. This algebraic QSS analysis to determine intermediates calculations is an alternative to microkinetic analysis, which is a set of species mass balance differential equations applied to a packed bed reactor [1].

		Ni(111)		Ni(100)		Ni(211)	
Step	Reaction	$\vec{k}_\rho$	$\overleftarrow{k}_\rho$	$\vec{k}_\rho$	$\overleftarrow{k}_\rho$	$\vec{k}_\rho$	$\overleftarrow{k}_\rho$
1	$CH_4(g)+2S \leftrightarrows CH_3{\cdot}S +H{\cdot}S$	$1.01{\times}10^{-02}$	$1.42{\times}10^{10}$	$9.30{\times}10^{-02}$	$1.28{\times}10^{10}$	$6.35{\times}10^{-02}$	$5.66{\times}10^{8}$
2	$CH_3{\cdot}S +S \leftrightarrows CH_2{\cdot}S +H{\cdot}S$	$1.83{\times}10^{10}$	$2.16{\times}10^{10}$	$5.43{\times}10^{10}$	$1.49{\times}10^{9}$	$1.76{\times}10^{10}$	$1.60{\times}10^{11}$
3	$CH_2{\cdot}S +S \leftrightarrows CH{\cdot}S+H{\cdot}S$	$1.31{\times}10^{12}$	$2.81{\times}10^{10}$	$4.74{\times}10^{12}$	$1.41{\times}10^{9}$	$2.22{\times}10^{11}$	$8.31{\times}10^{8}$
4	$CH{\cdot}S+S \leftrightarrows C{\cdot}S +H{\cdot}S$	$3.18{\times}10^{7}$	$6.72{\times}10^{9}$	$9.93{\times}10^{10}$	$1.06{\times}10^{9}$	$9.63{\times}10^{11}$	$4.54{\times}10^{8}$
5	$CO_2(g)+S \leftrightarrows CO_2{\cdot}S$	$4.23{\times}10^{2}$	$8.39{\times}10^{12}$	$4.88{\times}10^{2}$	$1.42{\times}10^{11}$	$4.34{\times}10^{2}$	$2.39{\times}10^{11}$
6	$CO_2{\cdot}S +S \leftrightarrows CO{\cdot}S+O{\cdot}S$	$1.82{\times}10^{8}$	$5.47{\times}10^{5}$	$3.12{\times}10^{9}$	$4.98{\times}10^{5}$	$4.07{\times}10^{7}$	$1.03{\times}10^{5}$
7	$CO_2{\cdot}S +H{\cdot}S \leftrightarrows COOH{\cdot}S+S$	$7.74{\times}10^{6}$	$1.59{\times}10^{10}$	$7.60{\times}10^{4}$	$5.59{\times}10^{8}$	$5.56{\times}10^{4}$	$3.75{\times}10^{10}$
8	$CO_2{\cdot}S +H{\cdot}S \leftrightarrows HCOO{\cdot}S+S$	$3.55{\times}10^{8}$	$2.20{\times}10^{9}$	$1.60{\times}10^{8}$	$4.29{\times}10^{10}$	$3.25{\times}10^{5}$	$1.66{\times}10^{6}$
9	$HCOO{\cdot}S+S \leftrightarrows CHO{\cdot}S+O{\cdot}S$	$1.33{\times}10^{6}$	$2.89{\times}10^{9}$	$6.99{\times}10^{4}$	$3.19{\times}10^{2}$	$1.28{\times}10^{5}$	$4.37{\times}10^{7}$
10	$COOH{\cdot}S+S \leftrightarrows CO{\cdot}S+OH{\cdot}S$	$2.08{\times}10^{10}$	$2.08{\times}10^{5}$	$4.74{\times}10^{9}$	$3.89{\times}10^{3}$	$1.28{\times}10^{11}$	$1.75{\times}10^{2}$
11	$CH_3{\cdot}S +OH{\cdot}S \leftrightarrows CH_3OH{\cdot}S+S$	$5.01{\times}10^{5}$	$6.30{\times}10^{6}$	$4.72{\times}10^{1}$	$2.58{\times}10^{5}$	$1.39{\times}10^{2}$	$5.24{\times}10^{8}$
12	$CH_3OH{\cdot}S+S \leftrightarrows CH_2OH{\cdot}S+H{\cdot}S$	$2.39{\times}10^{7}$	$8.34{\times}10^{9}$	$9.70{\times}10^{8}$	$2.71{\times}10^{9}$	$5.66{\times}10^{10}$	$3.86{\times}10^{10}$
13	$CH_2{\cdot}S +OH{\cdot}S \leftrightarrows CH_2OH{\cdot}S+S$	$7.21{\times}10^{6}$	$2.67{\times}10^{10}$	$3.32{\times}10^{5}$	$1.85{\times}10^{11}$	$5.27{\times}10^{5}$	$1.49{\times}10^{11}$
14	$CH_2OH{\cdot}S+S \leftrightarrows CHOH{\cdot}S+H{\cdot}S$	$6.40{\times}10^{10}$	$1.91{\times}10^{9}$	$7.99{\times}10^{11}$	$6.39{\times}10^{9}$	$7.26{\times}10^{12}$	$3.79{\times}10^{11}$
15	$CH{\cdot}S+OH{\cdot}S \leftrightarrows CHOH{\cdot}S+S$	$1.37{\times}10^{6}$	$1.12{\times}10^{9}$	$7.42{\times}10^{3}$	$3.78{\times}10^{9}$	$6.86{\times}10^{2}$	$2.70{\times}10^{9}$
16	$CHOH{\cdot}S+S \leftrightarrows COH{\cdot}S+H{\cdot}S$	$2.41{\times}10^{13}$	$2.17{\times}10^{9}$	$1.35{\times}10^{9}$	$1.96{\times}10^{4}$	$1.14{\times}10^{13}$	$1.07{\times}10^{9}$
17	$C{\cdot}S +OH{\cdot}S \leftrightarrows COH{\cdot}S+S$	$2.23{\times}10^{6}$	$4.43{\times}10^{2}$	$3.07{\times}10^{3}$	$1.14{\times}10^{8}$	$1.54{\times}10^{4}$	$1.21{\times}10^{8}$
18	$COH{\cdot}S+S \leftrightarrows CO{\cdot}S+H{\cdot}S$	$6.67{\times}10^{8}$	$3.71{\times}10^{3}$	$1.27{\times}10^{10}$	$1.38{\times}10^{4}$	$3.49{\times}10^{11}$	$4.98{\times}10^{5}$
19	$CH_3{\cdot}S +O{\cdot}S \leftrightarrows CH_3O{\cdot}S+S$	$2.49{\times}10^{5}$	$3.58{\times}10^{6}$	$9.91{\times}10^{4}$	$2.06{\times}10^{8}$	$2.31{\times}10^{3}$	$2.31{\times}10^{6}$
20	$CH_3O{\cdot}S+S \leftrightarrows CH_2O{\cdot}S+H{\cdot}S$	$5.23{\times}10^{9}$	$6.44{\times}10^{10}$	$6.32{\times}10^{9}$	$3.07{\times}10^{8}$	$5.82{\times}10^{10}$	$7.95{\times}10^{10}$
21	$CH_2S+O{\cdot}S \leftrightarrows CH_2O{\cdot}S+S$	$2.36{\times}10^{6}$	$3.54{\times}10^{8}$	$7.40{\times}10^{3}$	$2.03{\times}10^{7}$	$1.28{\times}10^{6}$	$1.92{\times}10^{8}$
22	$CH_2O{\cdot}S+S \leftrightarrows CHO{\cdot}S+H{\cdot}S$	$1.94{\times}10^{12}$	$3.08{\times}10^{9}$	$1.93{\times}10^{12}$	$1.71{\times}10^{9}$	$1.67{\times}10^{11}$	$3.66{\times}10^{9}$
23	$CH{\cdot}S+O{\cdot}S \leftrightarrows CHO{\cdot}S+S$	$8.33{\times}10^{5}$	$9.19{\times}10^{6}$	$1.41{\times}10^{3}$	$2.10{\times}10^{7}$	$6.34{\times}10^{6}$	$5.58{\times}10^{9}$
24	$CHO{\cdot}S+S \leftrightarrows CO{\cdot}S+H{\cdot}S$	$8.63{\times}10^{10}$	$1.24{\times}10^{4}$	$1.03{\times}10^{12}$	$1.13{\times}10^{6}$	$2.64{\times}10^{13}$	$5.74{\times}10^{6}$
25	$C{\cdot}S +O{\cdot}S \leftrightarrows CO{\cdot}S+S$	$4.91{\times}10^{5}$	$3.69{\times}10^{-03}$	$2.45{\times}10^{2}$	$3.72{\times}10^{2}$	$3.03{\times}10^{4}$	$1.23{\times}10^{2}$
26	$CH_3OH{\cdot}S+S \leftrightarrows CH_3O{\cdot}S+H{\cdot}S$	$1.12{\times}10^{10}$	$1.87{\times}10^{9}$	$1.50{\times}10^{11}$	$1.12{\times}10^{9}$	$5.70{\times}10^{13}$	$4.16{\times}10^{10}$
27	$CH_2OH{\cdot}S+S \leftrightarrows CH_2O{\cdot}S+H{\cdot}S$	$2.18{\times}10^{11}$	$1.30{\times}10^{9}$	$1.31{\times}10^{11}$	$1.71{\times}10^{7}$	$4.02{\times}10^{8}$	$5.87{\times}10^{5}$
28	$CHOH{\cdot}S+S \leftrightarrows CHO{\cdot}S+H{\cdot}S$	$6.77{\times}10^{10}$	$1.35{\times}10^{8}$	$9.33{\times}10^{11}$	$1.35{\times}10^{7}$	$1.15{\times}10^{10}$	$7.06{\times}10^{6}$
29	$O{\cdot}S+H{\cdot}S \leftrightarrows OH{\cdot}S+S$	$4.36{\times}10^{7}$	$2.97{\times}10^{8}$	$1.39{\times}10^{7}$	$5.22{\times}10^{8}$	$7.14{\times}10^{6}$	$2.60{\times}10^{6}$
30	$OH{\cdot}S+H{\cdot}S \leftrightarrows H_2O{\cdot}S+S$	$1.55{\times}10^{8}$	$7.57{\times}10^{8}$	$3.26{\times}10^{5}$	$5.14{\times}10^{7}$	$1.55{\times}10^{5}$	$4.54{\times}10^{7}$
31	$H_2O{\cdot}S \leftrightarrows H_2O(g)+S$	$4.29{\times}10^{12}$	$3.52{\times}10^{2}$	$1.44{\times}10^{12}$	$5.69{\times}10^{2}$	$1.99{\times}10^{11}$	$1.78{\times}10^{2}$
32	$H{\cdot}S+H{\cdot}S \leftrightarrows H_2(g)+2S$	$7.16{\times}10^{7}$	$2.70{\times}10^{1}$	$1.52{\times}10^{8}$	$4.35{\times}10^{2}$	$4.25{\times}10^{7}$	$3.69{\times}10^{1}$
33	$CO{\cdot}S \leftrightarrows CO(g)+S$	$1.03{\times}10^{6}$	$4.89{\times}10^{0}$	$6.99{\times}10^{5}$	$3.74{\times}10^{1}$	$6.07{\times}10^{5}$	$8.11{\times}10^{0}$

Table 5.1: 33-step DMR mechanism on Ni catalyst. Rate constants calculated at 973.15 K [1]

QSS Relations for Intermediate Species:

$$Q_{\text{O·S}} = 0 = r_6 + r_9 - r_{19} - r_{21} - r_{23} - r_{25} - r_{29}$$

$$Q_{\text{H·S}} = 0 = r_1 + r_2 + r_3 + r_4 - r_7 - r_8 + r_{12} + r_{14} + r_{16} + r_{18} + r_{20} + r_{22} + r_{24} + r_{26} + r_{27} + r_{28} + r_{29} + r_{30} + 2r_{32}$$

$$Q_{\text{OH·S}} = 0 = r_{10} - r_{11} - r_{13} - r_{15} - r_{17} + r_{29}$$

$$Q_{\text{H}_2\text{O·S}} = 0 = r_{30} - r_{31}$$

$$Q_{\text{CO·S}} = 0 = r_6 + r_{10} + r_{18} + r_{24} + r_{25} - r_{33}$$

$$Q_{\text{CO}_2\text{·S}} = 0 = r_5 - r_6 - r_7 - r_8$$

$$Q_{\text{C·S}} = 0 = r_4 - r_{17} - r_{25}$$

$$Q_{\text{CH·S}} = 0 = r_3 - r_4 - r_{15} - r_{23}$$

$$Q_{\text{CH}_2\text{·S}} = 0 = r_2 - r_3 - r_{13}$$

$$Q_{\text{CH}_3\text{·S}} = 0 = r_1 - r_2 - r_{11}$$

$$Q_{\text{CHO·S}} = 0 = r_9 + r_{22} - r_{23} - r_{24} + r_{28}$$

$$Q_{\text{COH·S}} = 0 = r_{16} + r_{17} - r_{18}$$

$$Q_{\text{COOH·S}} = 0 = r_7 - r_{10}$$

$$Q_{\text{HCOO·S}} = 0 = r_8 - r_9$$

$$Q_{\text{CH}_3\text{OH·S}} = 0 = r_{11} - r_{12} - r_{26}$$

$$Q_{\text{CH}_3\text{O·S}} = 0 = r_{19} - r_{20} + r_{26}$$

$$Q_{\text{CH}_2\text{OH·S}} = 0 = r_{12} + r_{13} - r_{14}$$

$$Q_{\text{CH}_2\text{O·S}} = 0 = r_{20} + r_{21} - r_{22} + r_{27}$$

$$Q_{\text{CHOH·S}} = 0 = r_{14} + r_{15} - r_{16} - r_{28}$$

QSS Relations for Terminal Species:

$$Q_{CH_4(g)} = 0 = r_{OR_1} - r_1$$

$$Q_{CO(g)} = 0 = r_{OR_1} + r_{OR_2} - r_{33}$$

$$Q_{CO_2(g)} = 0 = r_{OR_3} - r_5$$

$$Q_{H_2O(g)} = 0 = r_{OR_1} - r_{OR_2} - r_{31}$$

$$Q_{H_2(g)} = 0 = 3r_{OR_1} - r_{OR_2} - r_{32}$$

Table 5.2: QSS relations

5.2.2 Selecting Overall Reactions

The actual chemical reactions occurring on the Ni catalyst are described in entirety by the set of elementary steps listed in Table 5.1. The overall reactions (OR)s that are used to describe conversion of the initial and final terminal species are, on the other hand, constructs in our efforts to represent the overall stoichiometry observed, which can rarely be described by a single OR. Thus, Xu & Froment made great progress in their efforts to discerning which ORs should be adopted to properly characterize the reaction system for methane steam reforming [24]. In their study of methane steam reforming (MSR), they concluded that three ORs were significant and necessary to describe the entire chemical mechanism as described below by Eqs 5.2, 5.3 and 5.5. However, their conclusion to use three ORs for the MSR system are considered as over defining the system.

What actually matters is the list of the terminal (reactants and products) species, along with the list of elementary reaction steps occurring on the catalyst surface representing the molecular mechanism in which the terminal species along with intermediate species participate. Although often lacking experimental corroboration, it is the mechanistic steps that represent the real

molecular events, not the ORs. Since ORs do not involve intermediate species, they may, in fact, be derived directly from the set of given terminal species, and their constituent elements [25]. Thus, the n terminal species are considered as made up of r "elements," or chemical building blocks, which are the radicals, or molecular fragments, that remain unchanged among the given terminal species. These are selected such that the rank of the formula matrix is equal to the number of elements, r, and are frequently, but not always, the actual chemical elements [25]. For instance, the formula matrix for the MDR case is:

$$\varepsilon = \begin{array}{c} \\ CH_4 \\ H_2O \\ CO \\ CO_2 \\ H_2 \end{array} \begin{array}{ccc} C & H & O \\ \left|\begin{array}{ccc} 1 & 4 & 0 \\ 0 & 2 & 1 \\ 1 & 0 & 1 \\ 1 & 0 & 2 \\ 0 & 2 & 0 \end{array}\right| \end{array} \qquad (5.1)$$

which has a rank, $r = \text{rank}[\varepsilon] = 3$. Thus, for this case, C, H, and O are appropriate "elements."

The number of linearly independent ORs, m, is related to the number of terminal species n and the rank of the formula matrix r via $m = n - r$ [33]. Thus, with $n = 5$ (CH_4, H_2O, CO, CO_2 and H_2), and for $r = 3$ (C, H and O), the number of independent ORs, $m = 5 - 3 = 2$. Further, the number of terminal species involved in a direct or minimal OR $= n - (m - 1) = n - (n - r) + 1 = r + 1$. For instance, for the MSR case, the maximum number of terminal species in a direct OR $= 3 + 1 = 4$.

Ultimately, any two linearly independent reactions that involve all five terminal species (CH_4, H_2O, CO, CO_2 and H_2) are suitable for defining this reaction. Knowing the rate of two of these ORs, one can determine the rate of formation of all terminal species. For MDR as well as for MSR, both of which share the same terminal species, four ORs that are commonly considered are:

$$OR_1: CH_4 + H_2O \rightleftharpoons CO + 3H_2 \qquad\qquad (5.2)$$

$$OR_2: CO_2 + H_2 \rightleftharpoons CO + H_2O \qquad\qquad (5.3)$$

$$OR_3: CH_4 + CO_2 \rightleftharpoons 2CO + 2H_2 \qquad\qquad (5.4)$$

$$OR_4: CH_4 + 2H_2O \rightleftharpoons CO_2 + 4H_2 \qquad\qquad (5.5)$$
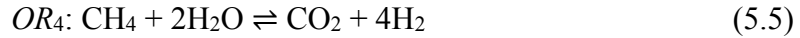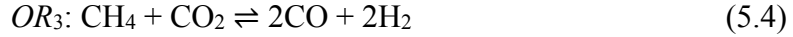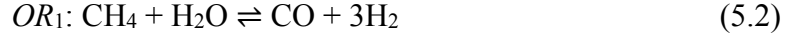
It is easily shown how by selecting any two of these reactions, the other two can be obtained through linear combinations, e.g.:

$$OR_1 + OR_2 = CH_4 + CO_2 \rightleftharpoons 2CO + 2H_2 = OR_3 \qquad\qquad (5.6)$$
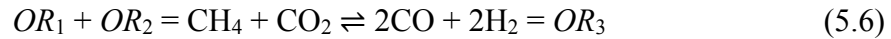
And similarly, $OR_1 - OR_2$ results in OR_4. Thus, we determine that it is of no consequence, from a mathematical standpoint, which ORs we select to represent the overall process chemistry. Regardless, it is easier to express the overall flux of the reaction in terms of these ORs, instead of a series of elementary steps, so we arbitrarily choose two ORs to form our analysis, i.e., OR_1 and OR_2. It is noteworthy that Fan et al., on the other hand, for this system picked OR_2 and OR_3.

5.3 The Reaction Route Graph

The methodology utilized in this study to analyze the MDR system is the Reaction Route (RR) Graph Theory, which was introduced by us [25, 26] and developed further in other publications [27,28]. The RR Graph of a mechanism for an OR comprising of p reaction steps s_ρ among $q + 1$ intermediate species and n terminal species (OR reactants and products), is a quantitative graph theoretical depiction of the reaction network, in which the steps as well as the OR, are represented individually as directed (arrows pointed in the assumed direction) edges, or branches, interconnected at nodes, or vertices, n_j, so that *all* reaction routes (RRs) may be traced

on it as closed walks, or cycles, and the nodal connectivity to edges is consistent with quasi steady-state (QSS) mass balance of one or a linear combination of participating species.

The RR Graph is a useful, quantitative, graph-theoretical representation of the molecular mechanism that provides: 1) consistence of nodes with species mass balance, i.e., Kirchhoff's Flux Law (KFL), alternately, Kirchhoff's First Law, i.e., the quasi-steady state (QSS) assumption of kinetics, or the Bodenstein approximation; 2) consistence of RRs with the state-property of thermodynamic functions (e.g., Gibbs free energy, G, enthalpy H, and entropy S), i.e., Kirchhoff's potential law, or KPL, also called Kirchhoff's second law, alternately known as Hess's law, according to which change in a thermodynamic state property along a cycle is zero; 3) graphical enumeration of all possible reaction routes as closed walks, normally done from stoichiometric analysis [30]; and 4) minimality, or directness [32], of both RRs as well as nodal degree, namely, the number of branches incident on a node.

It turns out that the second and third property above, i.e., consistence with KPL and enumeration of RRs, are mathematically equivalent. In other words, a RR Graph that is consistent with KPL is automatically amenable to a graph-theoretic enumeration of all RRs, and vice versa. As a result, we are concerned only with the two requirements of consistence with the two Kirchhoff's laws, along with their directness, i.e., the number of steps involved in the KPL and KFL relations are minimal.

The requirement of consistence with the two Kirchhoff's laws confers on the RR Graphs a one-to-one correspondence with electrical circuits, which is a very useful analogy [28] because of the vast and well-grounded literature on circuit analysis [34]. Thus, the electrical analog of the RR Graph is obtained by simply replacing the edges by resistors and an OR by an electromotive force

(or EMF). This analogy will be used to quantitatively evaluate all the possible pathways for the reaction.

To begin drawing the RR Graph, we first determine a suitable set of RRs to serve as a basis for construction. As per the Horiuti-Temkin theorem, an independent RR set is any set of $\mu = p - q$ RRs, which may include any full routes (FRs) that include an OR and empty routes (ERs), so long as they include among them all of the steps in the mechanism. Thus for the case of this MDR mechanism, we have $p = 33$ elementary steps and $q = 19$, the number of independent intermediate species, resulting in $\mu = 14$ independent reaction routes. In order to include all 5 terminal species, we select two linearly independent ORs to include in two linearly independent FRs, namely OR_1 and OR_2. This leaves 12 ERs to be specified to form an independent set. The RRs and those selected for our RR Graph are shown in Table 5.3. This is not a unique set and another such set may alternatively be used as the starting point. The set is obtained manually via a close inspection of the mechanism.

FR_1 : $(+1)s_1 + (+1)s_2 + (+1)s_3 + (+1)s_4 + (+1)s_{25} + (-1)s_{29} + (-1)s_{30} + (-1)s_{31} + (+3)s_{32} + (+1)s_{33} + (-1)OR_1$

FR_2 : $(+1)s_5 + (+1)s_6 + (+1)s_{29} + (+1)s_{30} + (+1)s_{31} + (-1)s_{32} + (+1)s_{33} + (-1)OR_2$

ER_1 : $(+1)s_2 + (+1)s_{11} + (-1)s_{19}$

ER_2 : $(+1)s_6 + (-1)s_8 + (-1)s_9 + (-1)s_{24}$

ER_3 : $(+1)s_{12} + (-1)s_{20} + (-1)s_{26} + (+1)s_{27}$

ER_4 : $(+1)s_2 + (-1)s_{19} + (-1)s_{20} + (+1)s_{21}$

ER_5 : $(+1)s_{13} + (-1)s_{21} + (+1)s_{27}$

ER_6 : $(+1)s_{15} + (-1)s_{23} + (+1)s_{28}$

ER_7 : $(+1)s_3 + (-1)s_{21} + (-1)s_{22} + (+1)s_{23}$

ER_8 : $(+1)s_3 + (-1)s_{13} + (-1)s_{14} + (+1)s_{15*}$

ER_9 : $(+1)s_4 + (-1)s_{23} + (-1)s_{24} + (+1)s_{25}$

163

$ER_{10} : (+1)s_4 + (-1)s_{15} + (-1)s_{16} + (+1)s_{17}$

$ER_{11} : (+1)s_{15} + (-1)s_{17} + (-1)s_{18}$

$ER_{12} : (+1)s_6 + (-1)s_7 + (-1)s_{10}$

Table 5.3: Set of independent reaction routes for the 33-step DMR

To construct the RR Graph from this set, we begin by drawing the cycle graph by overlapping the ERs in such a way that no reaction step is repeated in the graph. By identifying common edges and nodes, we can fuse two cycles into a "subgraphs", which would contain both the original two cycles, as well as a new, linearly dependent cycle. This process was repeated to produce a cycle graph that includes each ER (Fig. 5.1). All the ERs listed in Table 5.3 can be found in this graph, as well as many more that were not part of the original set. Any walk from one node through a series of edges, back to its original node is a valid ER. This means that one can identify series of reaction steps whose thermodynamic properties sum to zero because the graph is consistent with KPL.

The solid nodes of Figure 5.1 represent balanced nodes (consistence with KFL or species QSS relations given in Table 5.2, or their linear combination), and the hollow nodes represent nodes that are unbalanced and require additional incident edges. The next step in completing this graph would be to add the FRs into the graph so that KFL is satisfied for all nodes. Additionally, since some of these routes involve multiple instances of the same edge, the graph must be doubled in order for certain RRs that are known to exist to appear. Figure 5.2 is the completed graph with all possible RRs traceable as walks. We also introduce an intermediate route (IR_1: $s_{29} + s_{30} + s_{31} + (-1)s_{32}$) as a means to condense the graph. Note that there are four ORs that appear in this graph that themselves form a cycle among them, i.e., they are not all independent. As mentioned earlier, the ORs can be combined to generate the other direct ORs. Thus, if two ORs are drawn on an RR

Graph, the linear combinations of those ORs will also be able to be traced as walks. However, the additional ORs are redundant, as two ORs are satisfactory in describing the overall reaction rates of the system.

For comparison, Figure 5.3 shows the traditional reaction schematic for visualizing the mechanism and chemical pathways [34]. These reaction networks, however, can be drawn arbitrarily and are not consistent with KPL, KFL or other thermodynamic law. Because they lack these rigorous constraints, they are not suitable for the analysis of the system, unlike RR Graphs, although they serve the purpose of developing a qualitative understanding of the mechanism. The pathways represented in RR Graphs can be used to show flux analysis and compare reaction step affinities as we will demonstrate.
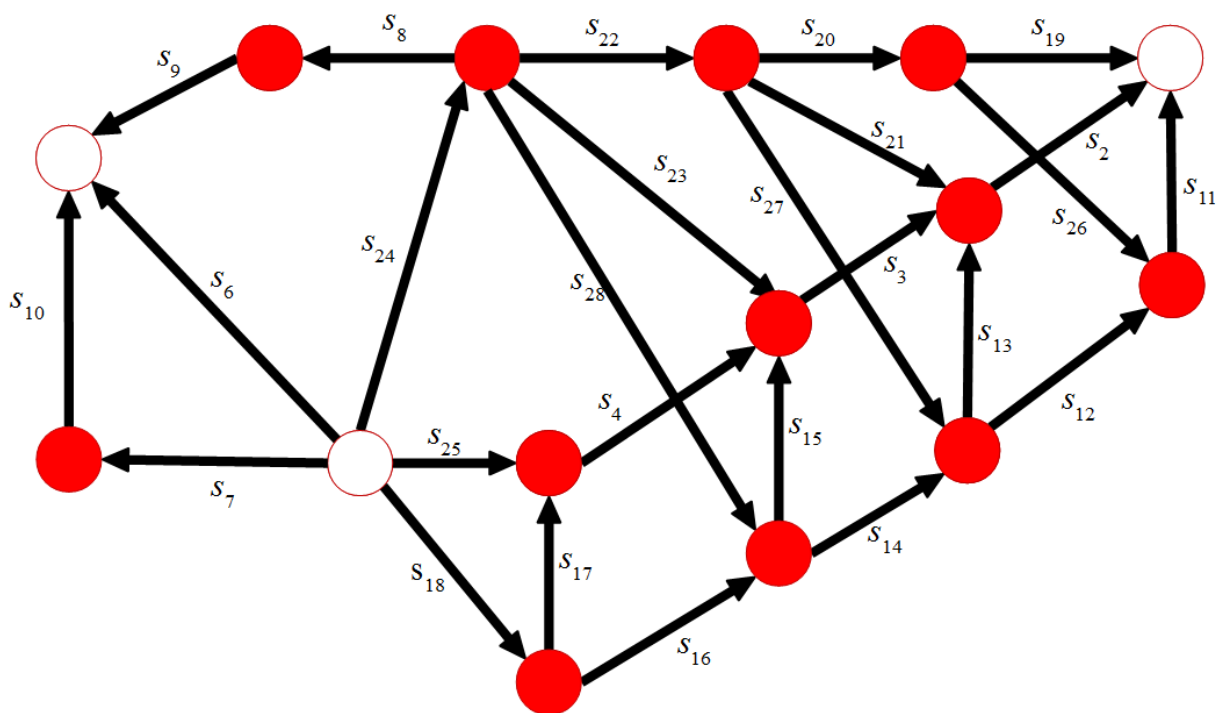
Figure 5.1: Cycle graph for the 33-step MDR mechanism on Ni catalyst

165

OR_1 : $CH_4 + H_2O \rightleftharpoons CO + 3H_2$
OR_2 : $CO + H_2O \rightleftharpoons CO_2 + H_2$
OR_3 : $CH_4 + CO_2 \rightleftharpoons 2CO + 2H_2$
OR_4 : $CO_2 + H_2 \rightleftharpoons CO + H_2O$

IR_1 : $s_{29} + s_{30} + s_{31} + (-1)s_{32}$
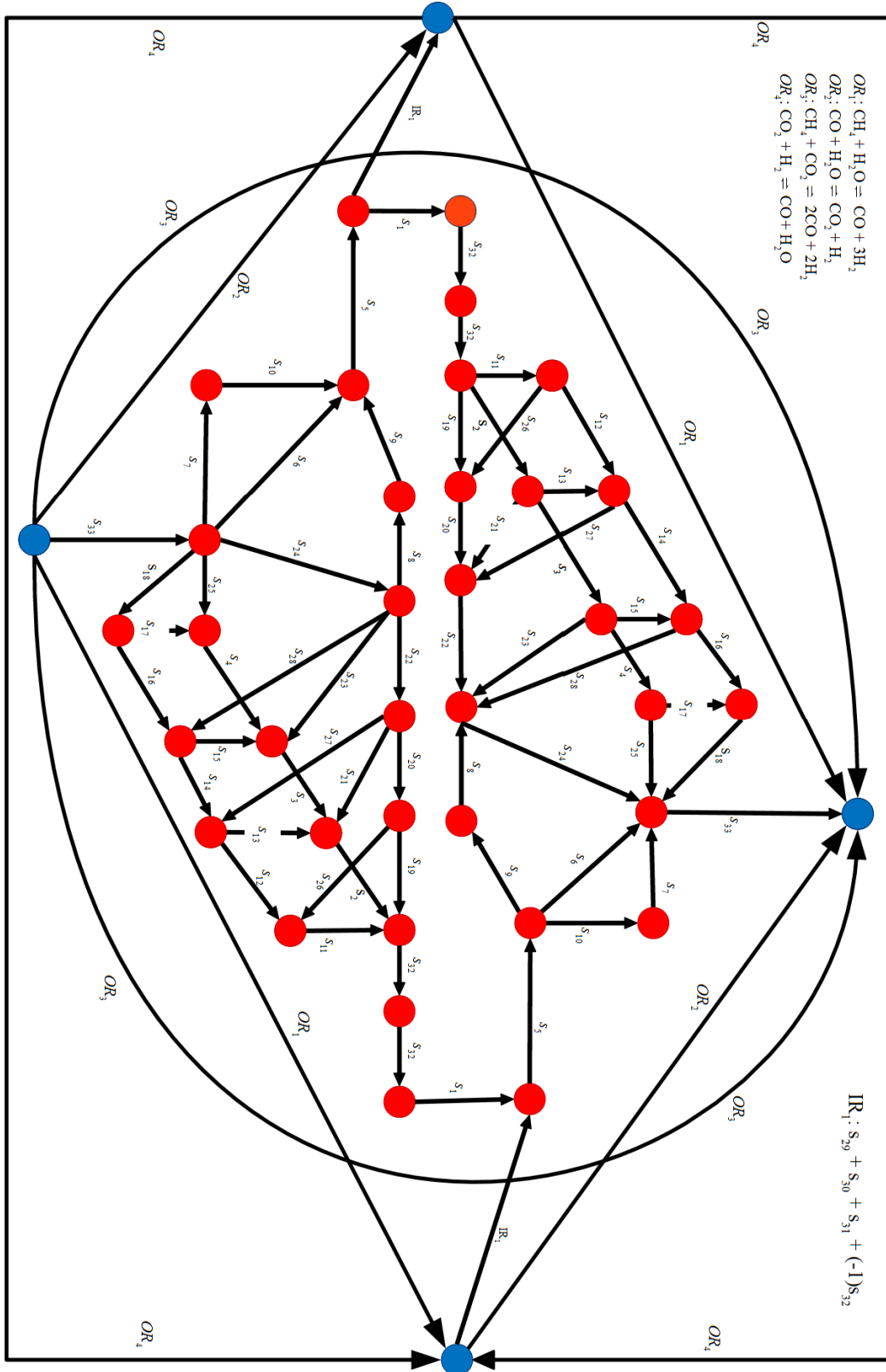
Figure 5.2: Full MDR RR Graph.
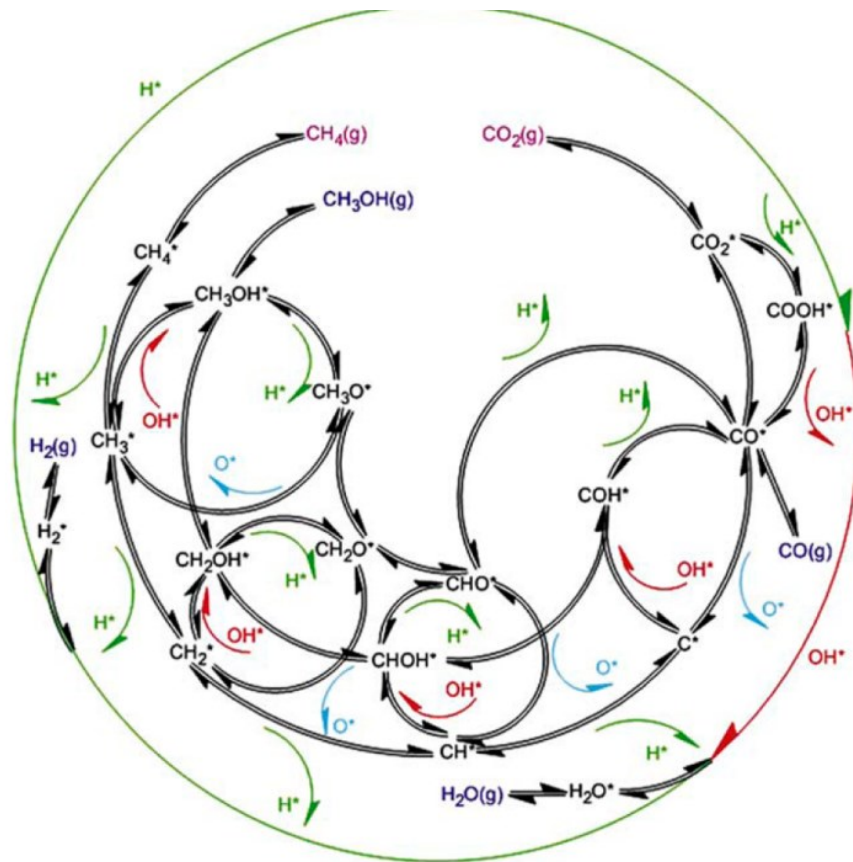
Figure 5.3: Conventionally drawn reaction network [38].
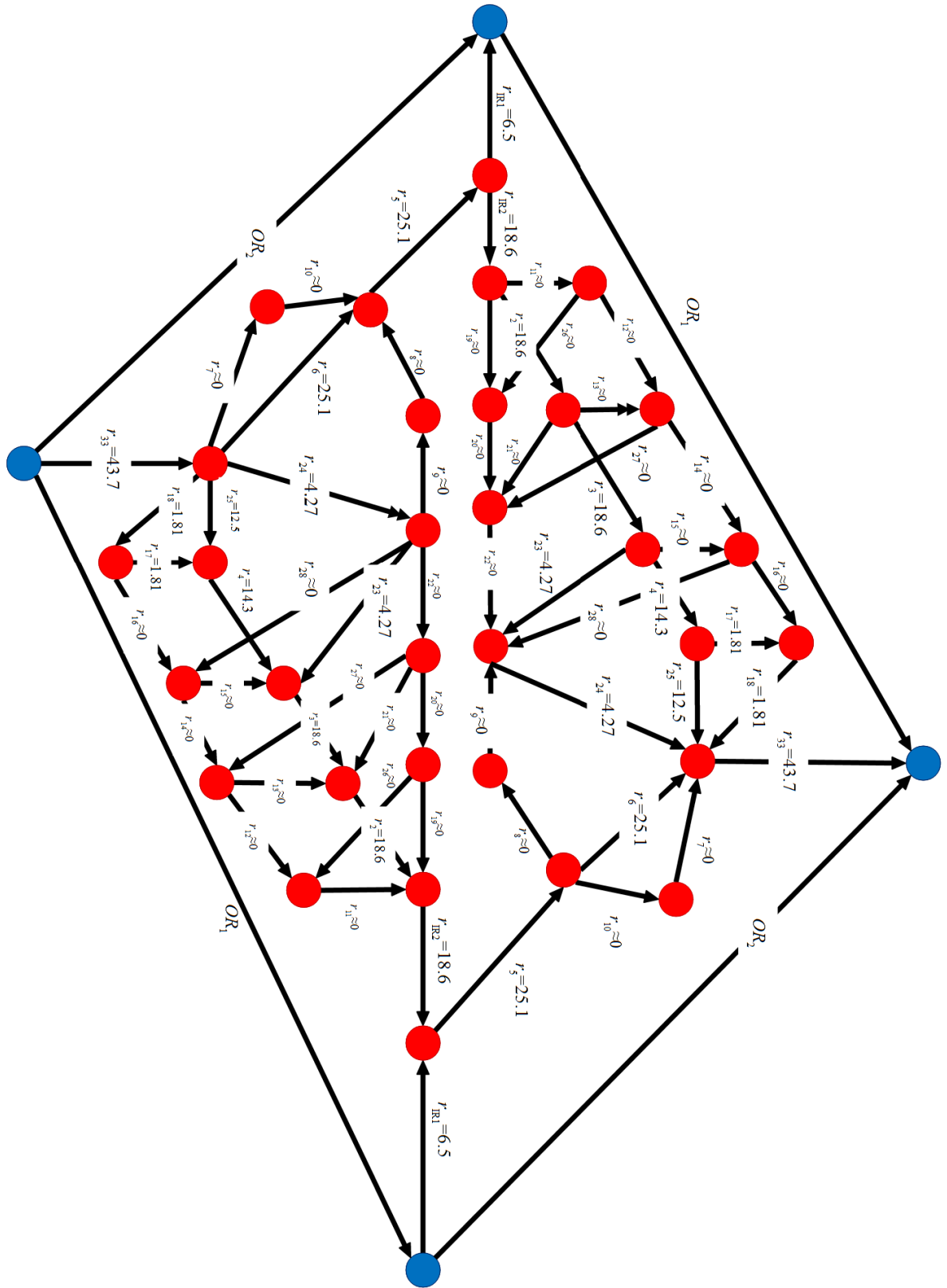
Figure 5.4: MDR rates (s⁻¹).
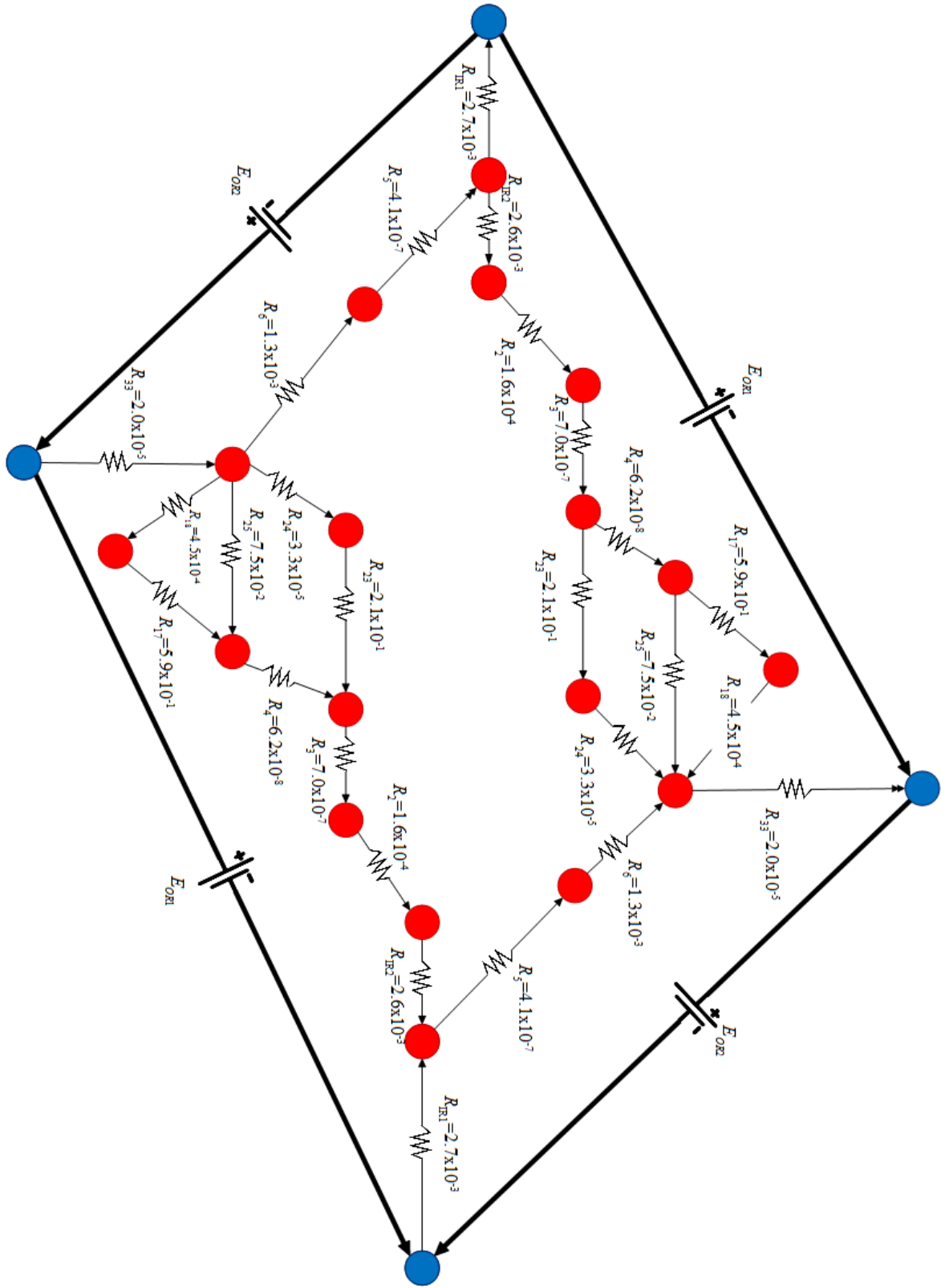
Figure 5.5: Pruned MDR graph with resistances for the steps of the dominant pathways

169

5.4 Network Analysis and Pruning

A microkinetic calculation for the MDR mechanism on Ni catalyst proposed by Fan et al. [1] was performed at temperature $T = 973.15$ K, and a pressure $p = 10$ bar. For our analysis, we chose parameters similar to those chosen by Fan 2015 et al. [1] in their calculations, with a feed composition starting at CH_4 (50%) and CO_2 (50%) and the rates evaluated at conversions of CH_4 and CO_2 of $X_{CH_4} = 15.9\%$ and $X_{CO_2} = 37.8\%$. The rates for these steps are superimposed on the RR Graph (Fig. 5.4). From this graph, we can readily discern the pathways that are most active in the network, by tracing the reaction from the terminal nodes of the reactants to the terminal nodes of the products. Superimposing the rates of each step presents a clear picture of the chemical pathways of the system, with any rate below 10^{-3} mol/g$_{cat}$•h was considered negligible and represented as approximately zero. Since these steps do not contribute appreciably to the overall kinetics they can be removed from the mechanism in this specific case. It is possible, however, that at other operating conditions, these steps might add relevant pathways and one cannot rigorously assume that they can be ignored under all conditions without evaluating other conditions, nonetheless, the graph can now be pruned to facilitate further analysis through the electrical analogy.

Figure 5.5 is a representation of the hence reduced RR graph as an analogy to an electrical circuit. The resistance of each step was evaluated using the following method. We may write the rate of a reaction step s_ρ in the form of Ohm's law [25]

$$r_\rho \equiv \frac{\mathcal{A}_\rho}{R_\rho} \tag{5.7}$$

170

where $\mathcal{A}_\rho$ is the dimensionless step affinity akin to voltage in an electrical circuit. It is in turn related to the ratio of the rate in the forward direction $\vec{r}_\rho$ to that in the reverse direction, $\overleftarrow{r}_\rho$, via the de Donder relation [36,37]

$$\mathcal{A}_\rho = \ln\left(\frac{\vec{r}_\rho}{\overleftarrow{r}_\rho}\right) = \ln\left(\frac{1}{z_\rho}\right) \tag{5.8}$$

which stems from the thermodynamic consistence of elementary step kinetics, so that the step resistance, by combining the last two equations, is

$$R_\rho = \frac{\ln(\vec{r}_\rho / \overleftarrow{r}_\rho)}{\vec{r}_\rho - \overleftarrow{r}_\rho} \tag{5.9}$$

Clearly, unlike electrical resistance, which is substantially constant, this definition of kinetic resistance of a step strongly depends on reaction conditions – especially temperature. Hence $z_\rho = \overleftarrow{r}_\rho / \vec{r}_\rho$ is the step reversibility.

Since the RR Graph follows KFL, KPL, as well as Ohm's law, it is *completely* consistent with a resistive network [34]. Consequently, we can write the overall rate as the ratio of the affinity of the OR and the overall resistance of the reaction network

$$r_{OR} \equiv \frac{\mathcal{A}_{OR}}{R_{OR}} \tag{5.10}$$

where the OR resistance R_{OR} of the reduced network is obtained in terms of the individual step resistances, in a manner similar to an electrical circuit [34].

From Figures 5.4 and 5.5, we can conclude that for OR_1, there are only three dominant pathways and only three rate-limiting steps, s_{17}, s_{23}, and s_{25}. For OR_2, we can see that s_6 is the

predominant rate-limiting step, although its resistance is smaller than those of the other steps mentioned. This implies that the WGS reaction may be considered essentially at QE under these conditions. Consequently, knowing that $OR_1 + OR_2 = OR_3$, we can reduce the graph to only show OR_3 and the steps that contribute to the overall reaction (Figure 5.6). The three major pathways shown include stepwise methane decomposition rapidly first into CH•S ($s_1 + s_2 + s_3$), which then either oxidizes into CHO•S (s_{23}), or decomposes further into elemental carbon, which can then oxidize into COH•S (s_{17}) or straight to CO (s_{25}). In this scheme, all the steps are quasi-equilibrated except for s_{17}, s_{23} and s_{25}, one in each of the three parallel branches. This is identical to the conclusions reached by Fan et al. [1] via numerical microkinetic analysis. For the MSR mechanism analysis performed by Vilekar et al. [35], we saw the same methane decomposition pathway that oxidizes elemental carbon, but neither of the other two pathways seen in the MDR were found to be significant. However another parallel pathway that oxidizes CH_3, then ultimately decomposes into CO was found. These differences are likely simply a result of a different set of elementary reactions and their energetics. While the RR Graph approach can rigorously analyze and prune a given mechanism based on the given step rates, clearly the conclusions are dependent on the input information, it evidently cannot account for any missing key steps or erroneous kinetics.

Assuming these few rate-limiting steps to be the sole contributors to the overall reaction kinetics, we can derive a QSS rate expression for any of the overall reactions. First, we identify steps that can be considered at quasi-equilibrium by computing their reversibilities as shown in Figure 5.7, which allows us to equate the forward and reverse of those equations and proceed to solve for the unknown site fractions following the LHHW approach. It is seen that all steps, including s_6 the RLS for WGS reaction, have $z_\rho \rightarrow 1$, implying they are at QE, with the exception of s_{17}, s_{23}, and s_{25}.
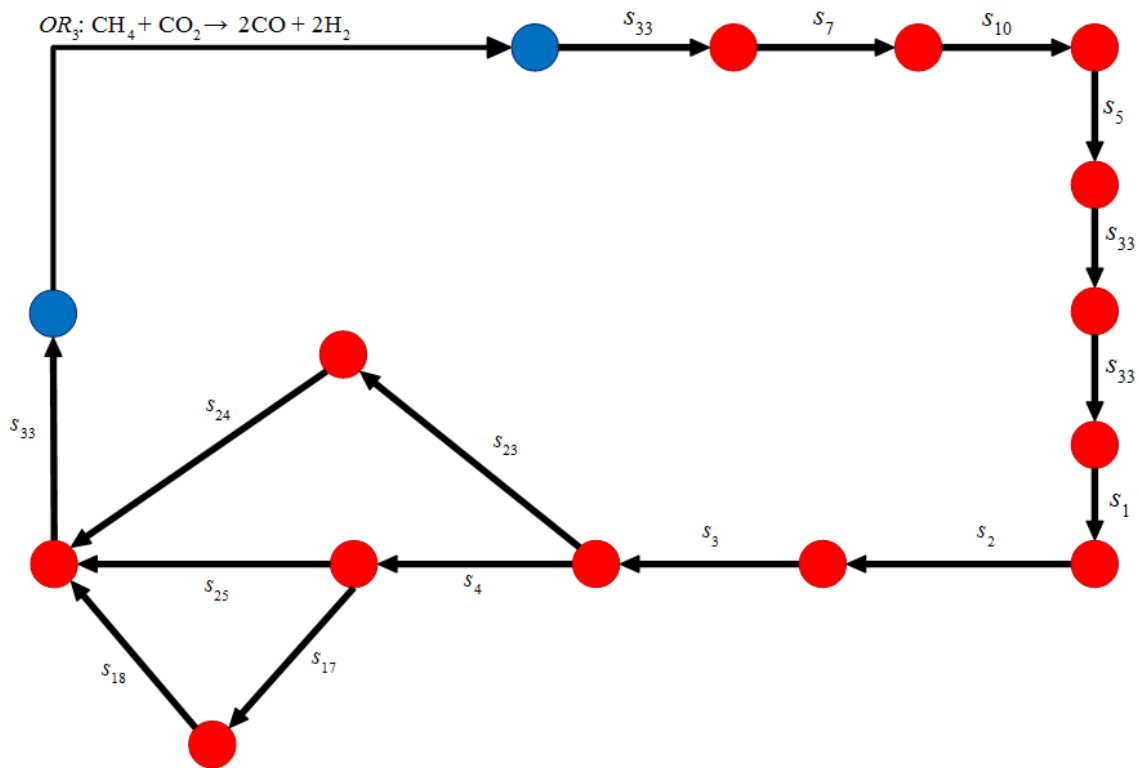
Figure 5.6: Simplified Reaction network for MDR reaction $CH_4 + CO_2 \rightleftharpoons 2CO + 2H_2$
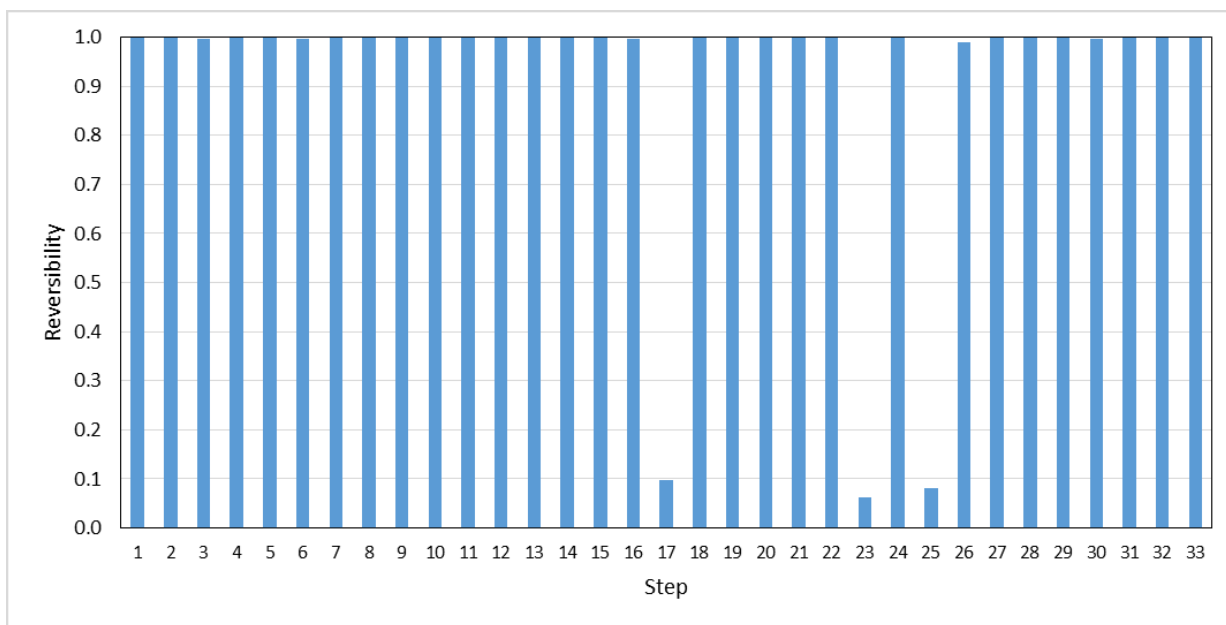
Figure 5.7: Reversibility for each step of the 33-step MDR mechanism.

The rate of the steam reforming overall reaction, OR_1, can be determined by the summation of the fluxes of the three parallel routes. Using the quasi-steady state approximation (detailed in Appendix B), the rate equations are comprised of the step rate constants ($\vec{k}_\rho$ and $\overleftarrow{k}_\rho$), equilibrium constants ($K_\rho = \vec{k}_\rho / \overleftarrow{k}_\rho$) and pressures of the terminal species:

$$r_{17} = \frac{\vec{k}_{17} K_1 K_2 K_3 K_4 K_{32}^2 P_{CH_4} P_{H_2O} \theta_0^2}{P_{H_2}^{5/2} K_{30} K_{31} \left(\overleftarrow{k}_{18} + \vec{k}_{17} \right)} \left(1 - \frac{\overleftarrow{k}_{18} K_{30} K_{31}}{K_1 K_2 K_3 K_{17} K_{32}^2 K_{33}} \frac{P_{CO} P_{H_2}^3}{P_{CH_4} P_{H_2O}} \right) \tag{5.11}$$

$$r_{23} = \frac{\vec{k}_{23} K_1 K_2 K_3 K_{32}^{3/2} P_{CH_4} P_{H_2O} \theta_0^2}{K_{29} K_{30} K_{31} P_{H_2}^{5/2} \left(\overleftarrow{k}_{24} + \vec{k}_{23} \right)} \left(1 - \frac{\overleftarrow{k}_{24} K_1 K_2 K_3 K_{32}^{3/2}}{K_{23} K_{29} K_{30} K_{31} K_{33}} \frac{P_{CO} P_{H_2}^3}{P_{CH_4} P_{H_2O}} \right) \tag{5.12}$$

$$r_{25} = \frac{\vec{k}_{25} K_1 K_2 K_3 K_4 K_{32}^2 P_{CH_4} P_{H_2}^{-2} \theta_0^2}{K_{29} K_{30} K_{31} P_{H_2}} \left(1 - \frac{\overleftarrow{k}_{24} K_1 K_2 K_3 K_4 K_{32}^{3/2}}{K_{25} K_{29} K_{30} K_{31} K_{33}} \frac{P_{CO} P_{H_2}^3}{P_{CH_4} P_{H_2O}} \right) \tag{5.13}$$

where we note that these equations are in such a form that there is combination of rate constants multiplying the pressure of terminal species raised to the power of their stoichiometric coefficients of the overall reaction. Thus, we recognize that those coefficients can be defined as the inverse of the overall reaction equilibrium ($1/K_{OR1}$). Then, combining the three rates because

$$r_{OR} = r_{17} + r_{23} + r_{25} \tag{5.14}$$

the overall reaction rate is

$$r_{OR_1} \approx \left(\frac{\vec{k}_{17} K_1 K_2 K_3 K_4 K_{32}^2 P_{CH_4} P_{H_2O}}{K_{30} K_{31} P_{H_2}^{5/2} \left(\overleftarrow{k}_{18} + \vec{k}_{17} \right)} + \frac{\vec{k}_{23} K_1 K_2 K_3 K_{32}^{3/2} P_{CH_4} P_{H_2O}}{K_{29} K_{30} K_{31} P_{H_2}^{5/2} \left(\overleftarrow{k}_{24} + \vec{k}_{23} \right)} + \frac{\vec{k}_{25} K_1 K_2 K_3 K_4 K_{32}^2 P_{CH_4}}{K_{29} K_{30} K_{31} P_{H_2}^3} \right) \theta_0^2 \left(1 - \frac{1}{K_{OR_1}} \frac{P_{CO} P_{H_2}^3}{P_{CH_4} P_{H_2O}} \right)$$

$$\tag{5.15}$$

Additionally, we estimate the free catalyst site fraction as the total minus the most abundant species on the site surface:

$$\theta_0 = 1 - \theta_{C\cdot S} - \theta_{H\cdot S} - \theta_{O\cdot S} - \theta_{CO\cdot S} - \theta_{CH\cdot S} \tag{5.16}$$

$$\theta_0 = \cfrac{1}{K_1 K_2 K_3 K_4 K_{32}^2 P_{CH_4} P_{H_2}^{-2} + \sqrt{\dfrac{P_{H_2}}{K_{32}}} + \dfrac{P_{H_2O}}{K_{29} K_{30} K_{31} P_{H_2}} + \dfrac{P_{CO}}{K_{33}} + K_1 K_2 K_3 \sqrt{K_{32}^3 P_{H_2}^{-3}} P_{CH_4}} \tag{5.17}$$

For the reverse water-gas shift reaction:

$$r_{OR_2} = r_6 = \vec{k}_6 K_5 P_{CO_2} \theta_0^2 \left(1 - \frac{1}{K_5 K_6 K_{29} K_{30} K_{31} K_{33}} \frac{P_{CO} P_{H_2O}}{P_{H_2} P_{CO_2}} \right) \tag{5.18}$$

The rate of OR_3, the dry reforming of methane can now be determined as

$$r_{OR_3} = r_{OR_1} + r_{OR_2} =$$

$$\vec{k}_6 K_5 P_{CO_2} \theta_0^2 \left(1 - \frac{1}{K_5 K_6 K_{29} K_{30} K_{31} K_{33}} \frac{P_{CO} P_{H_2O}}{P_{H_2} P_{CO_2}} \right) +$$

$$\left(\frac{\vec{k}_{17} K_1 K_2 K_3 K_4 K_{32}^2 P_{CH_4} P_{H_2O}}{K_{30} K_{31} P_{H_2}^{5/2} (\vec{k}_{18} + \vec{k}_{17})} + \frac{\vec{k}_{23} K_1 K_2 K_3 K_{32}^{3/2} P_{CH_4} P_{H_2O}}{K_{29} K_{30} K_{31} P_{H_2}^{5/2} (\vec{k}_{24} + \vec{k}_{23})} + \frac{\vec{k}_{25} K_1 K_2 K_3 K_4 K_{32}^2 P_{CH_4}}{K_{29} K_{30} K_{31} P_{H_2}^3} \right) \theta_0^2 \left(1 - \frac{1}{K_{OR_1}} \frac{P_{CO} P_{H_2}^3}{P_{CH_4} P_{H_2O}} \right)$$

$$\tag{5.19}$$

We can compare the reaction rate obtained through this equation with experimental data from Wei and Iglesia [10]. Figure 5.8 shows good agreement with predicting the reaction being first order with respect to methane.
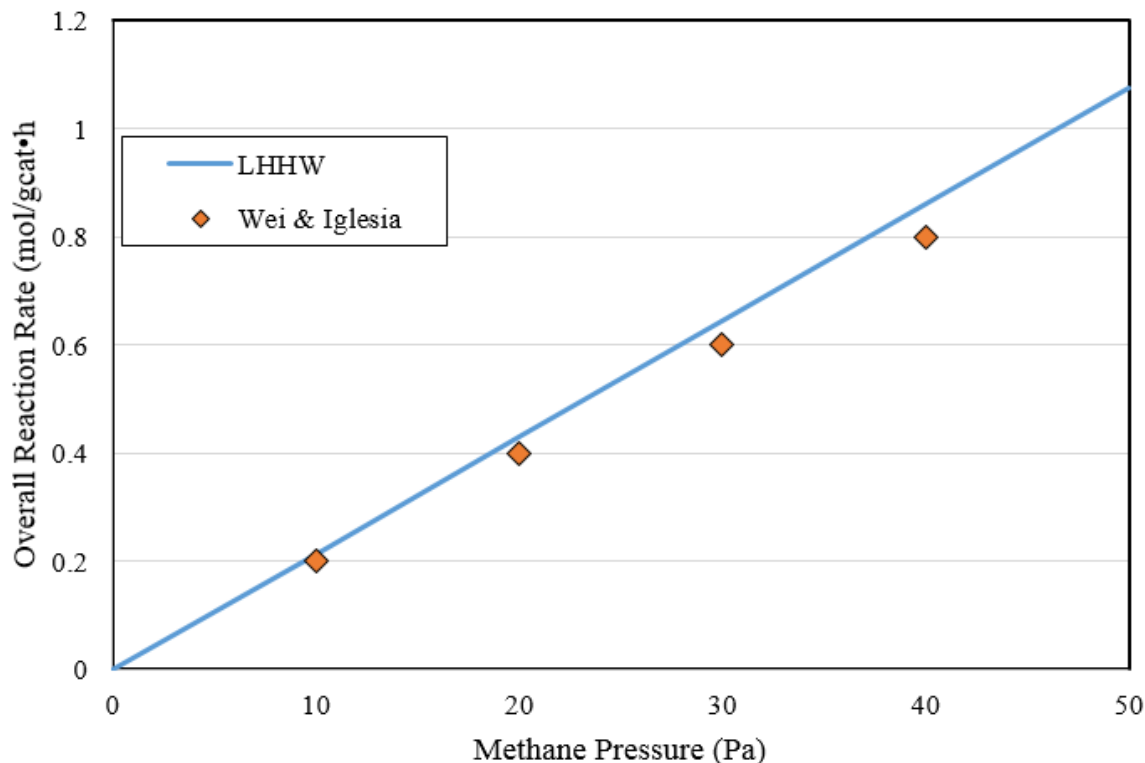
Figure 5.8: Comparison of LHHW overall reaction rate vs experimental data [10] at 973.15 K

5.5 Conclusions

We have demonstrated a method for comprehending the pathways and kinetics for the MDR system on Ni catalyst. Through RR Graph theory, all the unique pathways are enumerated and each route can be assessed for how it contributes to the overall reaction rate. This leads us to conclude that there are three parallel pathways, each having a rate limiting steps for MDR, namely, C oxidation with O, CH oxidation with O and C oxidation through OH. Furthermore, we have derived a comprehensive rate expression for the overall reaction rate through RDS and QE assumption based on resistance and reversibility calculations that is entirely productive as it is based on DFT calculations of step rates.

It is of some concern that there are some concessions made in drawing this graph. Because of the multiple ORs in this system, the rates of the formation of the terminal species cannot simply

176

be related to each other like most RR Graphs. For example: if only the WGS and no other OR had any flux through it, we can relate the rates of H_2O and H_2 as being 1:1, because of the stoichiometry. However, for the MDR mechanism with multiple ORs the ratio between each terminal species is dependent on the flux through each OR. This is relatively simple to represent in QSS equations (Table 5.2), but it is difficult to both maintain these KCL relations, while simultaneously drawing a minimal graph that contains every possible RR and adheres to KPL. In this case, we recognize that the rate for s_{32}, the hydrogen evolution step, is not correct on the graph, especially since it appears in multiple places with different rates. Based on the QSS equations, we know that the rate of s_{32} should be:

$$(+3)r_{OR_1} + (-1)r_{OR_1} = r_{33} \qquad (21)$$

Based on the rates of other terminal species we can find that:

$$r_{OR_1} = 18.6; \quad r_{OR_2} = 6.5; \quad r_{33} = 3 \times 18.6 - 6.5 = 49.3 \qquad (22)$$

Note that relationships between terminal species can be found by selecting any two of the four ORs. While this relationship could not be represented on the graph, we can still extract the exact rate of each of the relative ORs, based on other nodes that we know are balanced, and calculate the rate of hydrogen formation. Thus, despite the fact that we cannot immediately visualize the actual rate of s_{32} on the graph; we do visualize how the reactions proceeds through the steps and we can still use reaction resistances to estimate the affinities for each step.

5.5 References

1. Fan, C.; Zhu, Y., Yang, M.; Sui, Z.; Zhou, X.; Chen, D. Density Functional Theory-Assisted Microkinetic Analysis of Methane Dry Reforming on Ni Catalyst. Ind. Eng. Chem. Res. 2015, 54, 5901-5913

2. Maestri, M.; Vlachos, D.G.; Beretta, A.; Groppi, G.; Tronconi, E., J. Catal. 259. 2008, 211.

3. Maestri, M.; Vlachos, D.G.; Beretta, A.; Groppi, G.; Tronconi, E. A C1 Microkinetic Model for Methane Conversion to Syngas on Rh/Al2O3. AIChE Journal. 2009, 55-4, 993-1008

4. Munera, J.F.; Irusta, S.; Cornaglia, L.M.; Lombardo, E.A.; Cesar, D.V.; Schmal, M. J. Catal 245. 2007, 25

5. Kahle, L. C. S.; Roussiere, T.; Maier, L.; Herrera Delgado, K.; ̀Wasserschaff, G.; Schunk, S. A.; Deutschmann, O. Methane Dry Reforming at High Temperature and Elevated Pressure: Impact of Gas-Phase Reactions. Ind. Eng. Chem. Res. 2013, 52, 11920−11930.

6. Zhang, S. H.; Muratsugu, S.; Ishiguro, N.; Tada, M. Ceria-Doped Ni/SBA-16 Catalysts for Dry Reforming of Methane. ACS Catal. 2013, 3, 1855−1864. (4) Mette, K.; Kuhl, S.; Dudder, H.; Kahler, K.; Tarasov, A.; Muhler, M.; Behrens, M. Stable Performance of Ni Catalysts in the Dry Reforming of Methane at High Temperatures for the Efficient Conversion of CO2 into Syngas. ChemCatChem. 2014, 6, 100−104.

7. Serrano-Lotina, A.; Daza, L. Influence of the Operating Parameters over Dry Reforming of Methane to Syngas. Int. J. Hydrogen Energy 2014, 39, 4089−4094. (6) Munera, J.; Irusta, S.; Cornaglia, L.; Lombardo, E.; Vargascesar, D.; Schmal, M. Kinetics and Reaction Pathway of the CO2 Reforming of Methane on Rh Supported on Lanthanum-Based Solid. J. Catal. 2007, 245, 25−34.

8. Stagg-Williams, S. M.; Noronha, F. B.; Fendley, G.; Resasco, D. E. CO2 Reforming of CH4 over Pt/ZrO2 Catalysts Promoted with La and Ce Oxides. J. Catal. 2000, 194, 240−249.

9. Verykios, X. Catalytic Dry Reforming of Natural Gas for the Production of Chemicals and Hydrogen. Int. J. Hydrogen Energy 2003, 28, 1045−1063.

10. Wei, J.; Iglesia, E. Isotopic and Kinetic Assessment of the Mechanism of Reactions of CH4 with CO2 or H2O to Form Synthesis Gas and Carbon on Nickel Catalysts. J. Catal. 2004, 224, 370−383.

11. Wang, S.; Li, Y.; Lu, J.; He, M.; Jiao, H. A Detailed Mechanism of Thermal CO2 Reforming of CH4. J. Mol. Struct. 2004, 673, 181−189.

12. Bradford, M. C. J.; Vannice, M. A. CO2 Reforming of CH4. Catal. Rev. - Sci. Eng. 1999, 41, 1−42.

13. Luo, J. Z.; Yu, Z. L.; Ng, C. F.; Au, C. T. CO2/CH4 Reforming over Ni−La2O3/5A: An Investigation on Carbon Deposition and Reaction Steps. J. Catal. 2000, 194, 198−210.

14. Osaki, T.; Horiuchi, T.; Suzuki, K.; Mori, T. Kinetics, Intermediates and Mechanism for the CO2-Reforming of Methane on Supported Nickel Catalysts. J. Chem. Soc., Faraday Trans. 1996, 92, 1627.

15. Osaki, T.; Mori, T. Role of Potassium in Carbon-Free CO2 Reforming of Methane on K-Promoted Ni/Al2O3 Catalysts. J. Catal. 2001, 204, 89−97.

16. Chang, J.; Park, S.; Yoo, J.; Park, J. Catalytic Behavior of Supported KNiCa Catalyst and Mechanistic Consideration for Carbon Dioxide Reforming of Methane. J. Catal. 2000, 195, −11.

17. Cui, Y.; Zhang, H.; Xu, H.; Li, W. Kinetic Study of the Catalytic Reforming of CH4 with CO2 to Syngas over Ni/α-Al2O3 Catalyst: The Effect of Temperature on the Reforming Mechanism. Appl. Catal., A 2007, 318, 79−88.

18. Haghighi, M.; Sun, Z.; Wu, J.; Bromly, J.; Wee, H.; Ng, E.; Wang, Y.; Zhang, D. On the Reaction Mechanism of CO_2 Reforming of Methane over a Bed of Coal Char. Proc. Combust. Inst. 2007, 31, 1983−1990.

19. Nandini, A.; Pant, K. K.; Dhingra, S. C. Kinetic Study of the Catalytic Carbon Dioxide Reforming of Methane to Synthesis Gas over Ni-K/CeO2-Al2O3 Catalyst. Appl. Catal., A 2006, 308, 119−127.

20. Bradford, M. C. J.; Vannice, M. A. Catalytic Reforming of Methane with Carbon Dioxide over Nickel Catalysts II. Reaction Kinetics. Appl. Catal., A 1996, 142, 97−122.

21. Blaylock, D. W.; Ogura, T.; Green, W. H.; Beran, G. J. O. Computational Investigation of Thermochemistry and Kinetics of Steam Methane Reforming on Ni(111) under Realistic Conditions. J. Phys. Chem. C 2009, 113, 4898−4908.

22. Blaylock, D. W.; Zhu, Y.-A.; Green, W. H. Computational Investigation of the Thermochemistry and Kinetics of Steam Methane Reforming Over a Multi-faceted Nickel Catalyst. Top. Catal. 2011, 54, 828−844.

23. Chen, D.; Lødeng, R.; Svendsen, H.; Holmen, A. Hierarchical Multiscale Modeling of Methane Steam Reforming Reactions. Ind. Eng. Chem. Res. 2011, 50, 2600−2612

24. Xu, J.; Froment, G. F. Methane Steam Reforming, Methanation and Water-Gas Shift: I. Intrinsic Kinetics. AlChE J. 1989, 35, 88−96.

25. Fishtik I, Callaghan CA, Datta R. Reaction route graphs. I. Theory and algorithm. The Journal of Physical Chemistry B. 2004;108(18):5671-5682.

26. Fishtik I, Callaghan CA, Datta R. Reaction route graphs. II. Examples of enzyme-and surface-catalyzed single overall reactions. The Journal of Physical Chemistry B. 2004;108(18):5683-5697.

27. Fishtik I, Callaghan CA, Datta R. Reaction route graphs. III. Non-minimal kinetic mechanisms. The Journal of Physical Chemistry B. 2005;109(7):2710-2722.

28. O'Malley, P. D., Datta, R. and Vilekar, S. A. (2015), Ockham's razor for paring microkinetic mechanisms: Electrical analogy vs. Campbell's degree of rate control. AIChE J., 61: 4332–4346.

29. Vilekar, S. A., Fishtik, I., Liu, J. A., O'Malley, P. D., Datta, R., Kinetics and Mechanism of Methane Steam Reforming on Ni(111). A Reaction Route Graph Analysis, to be submitted.

30. de Donder T, Van Rysselberghe P. Thermodynamic Theory of Affinity. Stanford University Press. Stanford, CA. 1936.

31. Happel J, Sellers PH. Analysis of the Possible Reaction Mechanisms for a Chemical Reaction System. Adv. Catal. 1983;32:273−323.

32. Milner PC. J Electrochem Soc. 1964;3:228-232.

33. W.R. Smith, R.W. Missen, Chemical Reaction Equilibrium Analysis: Theory and Algorithms, John Wiley, New York, 1982

34. Chua L.O., Desoer C.A., Kuh E.S. Linear and Nonlinear Circuits. McGraw Hill. New York. 1987.

35. Zhu, Y. A.; Chen, D.; Zhou, X. G.; Yuan, W. K. DFT Studies of Dry Reforming of Methane on Ni Catalyst. Catal. Today 2009, 148, 260−26

36. Dumesic JA. Analyses of reaction schemes using De Donder relations. Journal of Catalysis. 1999;185(2):496-505.

37. Boudart M, Tamaru K. The step that determines the rate of a single catalytic cycle. Catalysis letters. 1991;9(1-2):15-22

38. Zhu, Y. A.; Chen, D.; Zhou, X. G.; Yuan, W. K. DFT Studies of Dry Reforming of Methane on Ni Catalyst. Catal. Today 2009, 148, 260−267

Chapter 6: Methodology of Automating RR Graph Construction

There has been some success in the automation of constructing RR Graphs through the use of a computer program written by Heineman et al. (in preparation). The current limitations have been mentioned briefly in previous chapters, but here the procedure of how the current algorithm operates is explained, as well as the goals moving forward. Hopefully, the conclusions made about the heuristics that govern RR Graph construction will be enumerated further in the future and proven through either linear algebra or graph-theory.

6.1 Algorithm for Constructing an RR Graph

The computer algorithm attempts to follow much of the linear algebra steps discussed in section 2.1, with the added benefit of automatically searching for possible solutions. Beginning with the stoichiometric matrix ($\mathbf{v}$), define r to be the rank of the stoichiometric matrix after applying a *Gauss-Jordan* transformation of $\mathbf{v^T}$ ($GJ(\mathbf{v^T})$). From $\mathbf{v}$ all possible direct ERs can be computed by performing row operations on the matrix. Since a direct ER involves no more than r +1 reaction steps, the total number of potential cycles for a mechanism with p steps is:

$$\binom{p}{r+1} = \frac{p!}{(r+1)!(p-r-1)!} \tag{6.1}$$

These ERs can be enumerated through brute force by computing the determinant of every r x r sub-matrix of $GJ(\mathbf{v^T})$. If the determinant is non-zero, then these columns are independent. Given any set of r independent columns representing steps, construct sets of steps by combining these r selected steps with one of the $(p - r)$ unselected steps. Because there can be no more than r independent columns, these $r + 1$ columns must be dependent and each set matches one of the ERs in the set of the full enumeration of ERs for the mechanism. The cycles are determined by

reading the column entries for the unselected step minus the step being added. Not all of these cycles that are enumerated are independent. The goal is to determine any one set of independent cycles, there are many such among the enumerated ERs, but the RR Graph can be constructed with any set. Although the set of independent ERs selected will not affect the resulting RR Graph when it is complete, there might be some intelligent way of selecting the optimal one so that the following graph construction steps are more effective.

Also similar to the manual method described in this work, the quasi-steady state (QSS) conditions are examined for each intermediate along with their linear combinations for determining an independent set of nodes. The algorithm checks each intermediate to identify the steps in which it is included and determines the QSS equation for each. Each node in the RR Graph represents one of these equations or their linear combination. In order to limit the number of combinations considered, the algorithm performs a similar brute force matrix search to identify combinations where the rates are summed to zero. Once a list of feasible nodes is computed, a search is performed to find a set of these nodes that is balanced by containing each reaction step twice in the whole set. Thus, we have our intermediate nodes for which we can create our RR Graph.

Taking the set of ERs found earlier, the algorithm then creates a list of possible ERs that satisfy the set that was predetermined. A specific ER will have the same steps going in the same direction, however the order in which they appear and edges that have common incidence to a node can change. The algorithm will search all possible ER combinations and for each combination, create a set of sub graphs, one for each ER and will attempt to fuse the sub graphs along common edges to create the cycle graph. The algorithm checks to makes sure that (a) no

184

cycle is lost; (b) newly formed cycles are valid; and (c) each node satisfies one of the combinations of mass-balance conditions.

Currently, the most complex network for which the algorithm can build a graph is a 13-step methanol decomposition on Pt(111) mechanism (Table 6.1) [1]. For this, the RR Graph was automatically found (Figure 6.1), with some manual intervention to enforce symmetry. An attempt to generate a graph for a 17-step WGS reaction however, failed and resulted in an estimated computational time of approximately a decade to perform an exhaustive search for the solution. Thus, the complexity for which this algorithm is suitable is around this 13 to 17 steps at this time.

	Elementary Reactions
s_1:	$CH_3OH + S \rightleftarrows CH_3OH \cdot S$
s_2:	$CH_3OH \cdot S + S \rightleftarrows CH_3O \cdot S + H \cdot S$
s_3:	$CH_3O \cdot S + 2S \rightleftarrows CH_2O \cdot S_2 + H \cdot S$
s_4:	$CH_2O \cdot S_2 \rightleftarrows CHO \cdot S + H \cdot S$
s_5:	$CHO \cdot S + S \rightleftarrows CO \cdot S + H \cdot S$
s_6:	$CH_3OH \cdot S + S \rightleftarrows CH_2OH \cdot S + H \cdot S$
s_7:	$CH_2OH \cdot S + S \rightleftarrows CHOH \cdot S + H \cdot S$
s_8:	$CHOH \cdot S + S \rightleftarrows COH \cdot S + H \cdot S$
s_9:	$COH \cdot S + S \rightleftarrows CO \cdot S + H \cdot S$
s_{10}:	$CHOH \cdot S + 2S \rightleftarrows CO \cdot S + 2H \cdot S$
s_{11}:	$CH_2OH \cdot S + 2S \rightleftarrows CH_2O \cdot S_2 + H \cdot S$
s_{12}:	$CO + S \rightleftarrows CO \cdot S$
s_{13}:	$2H \cdot S \rightleftarrows H_2 + 2S$

Table 6.1: 13-step Methanol Decomposition mechanism on Pt(111) [1]

$$IR_1: s_{OR} - s_1 + s_{12} - 2s_{13}$$
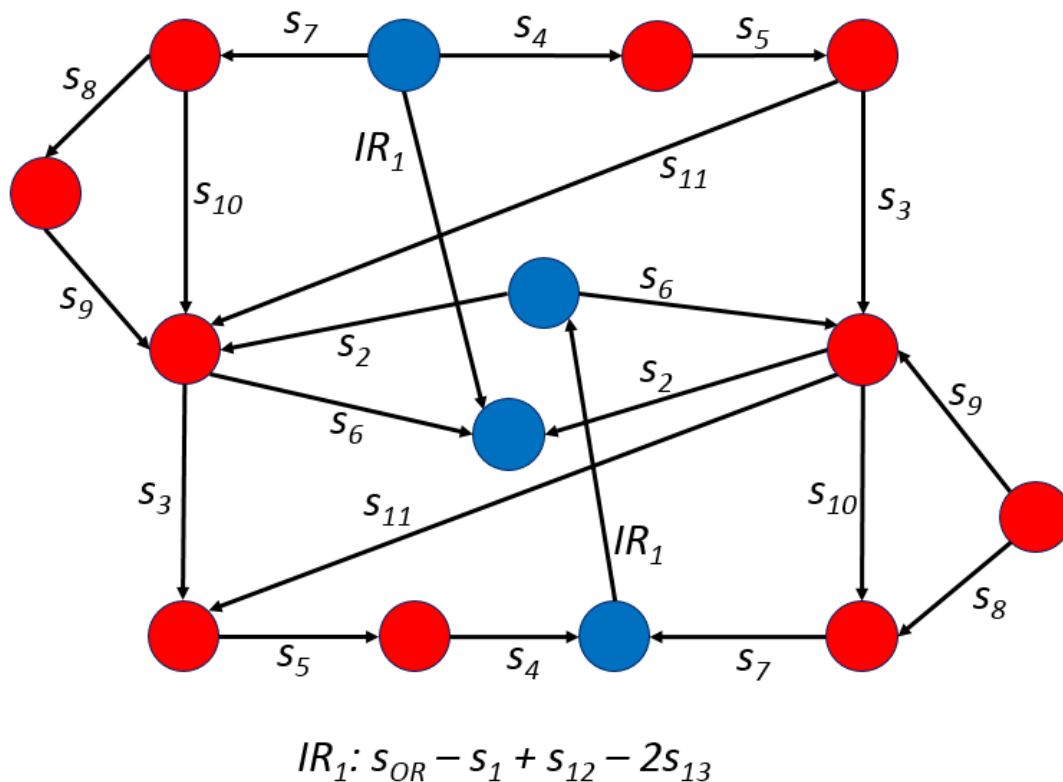
Figure 6.1: Automatically constructed RR Graph for 13-step methanol decomposition mechanism

6.2 Future Development of RR Graph Theory

The algorithm presented above certainly applies the RR Graph theory correctly and does indeed find the RR Graph under favorable conditions. However, it is a brute force approach and certainly it is not as efficient as possible. For larger systems, this brute force approach is not feasible. The program follows the heuristics that have been developed well enough, but the list of heuristics we have compiled so far is not complete.

One of the issues with the algorithm is that it arbitrarily selects a set of ERs and INs from which to create the RR Graph. While it is true that any set of ERs will eventually lead to the same RR Graph, there may be a preferred way to select this starting set. Additionally, the procedure for finding the INs should, in theory, determine a unique set for a given set of starting ERs for which

there is a minimal number of balanced nodes, but it is possible that this is not the case. If there were guidelines or heuristics for selecting the most efficient set of ERs for constructing the graph and a corresponding set of INs and for determining the placement of steps within the ERs, this would greatly facilitate their construction, both manually and automatically.

Another unresolved question posed is the best way to include overall reactions (ORs). The current algorithm treats the OR differently and tries to fit it in the end once all other steps are in place. It might be better to include the OR in the cycle matrix and treat the terminal species in the same way as intermediates. This may serve only to add to the complexity of the graph fusing, but it could also provide some flexibility in selecting the most efficient ERs to begin constructing the graph. For mechanisms with multiple ORs, this could be necessary in order to properly draw the graph. The methane dry reforming (MDR) mechanism described in Chapter 6 poses a particularly interesting problem. Since the ORs are non-linear, it makes it difficult to balance the nodes of the graph and retain consistency with KFL.

6.2.1 Guidelines for Graph Construction

Step 1: Characterize the graph in terms of complexity with regards to linearity, size and maximum stoichiometric coefficient.

Before drawing the graph, the proper method must be selected and any constraints must be recognized. The most important distinction is the linearity of the system. For a linear system, each step will occur only once, nonlinear systems are obviously much more complicated to draw and almost always require each step to be represented twice or more. In the case of mechanisms where the maximum stoichiometric coefficient is two or more, it is a requirement that the graph be symmetrical and every step be repeated. Every mechanism can be made to be symmetrical of course, if this were not necessary, then it would be simpler not to require that extra complexity.

However, symmetry is important to ensure that a step rate remains unchanged regardless of location. For linear systems, since there is only one of each step in RRs, one can use the matrix manipulation technique described in section 2.1.2 to create an incidence matrix *a priori* for the RR Graph.

Step 2: Simplification: Identify steps involved in every FR, find steps that contain unique intermediates, ignore steps that are in zero cycles, and possibly select a sub mechanism.

For larger mechanism, it is best to start by analyzing the mechanism and narrowing the steps that are most important to drawing the cycle graph. There are certain aspects of the steps that allow us to either ignore them completely, or reduce the possibilities of where it could appear in the graph. Additionally, if there is a valid subset of the mechanism, a graph of that subset must exist within the larger graph, thus we can begin graph construction starting with that subset, then building upon it.

One easy simplification is to identify steps that must be included in every FR. Since they are necessary steps, they will not be included in the cycle graph as they will not form cycles outside of the FRs. Thus, we can proceed to find the cycle graph ignoring these steps, then adding them to the completed cycle graph to fulfill the QSS conditions. These steps are often the adsorption or desorption steps. However, if there are multiple ways for the terminal species to be adsorbed or desorbed, then they must be included in the cycle matrix. The ORR mechanism in Chapter 4 is an excellent example where s_1, the primary adsorption step appears in the middle of the graph, as opposed to closer to the terminal nodes, which is more common for adsorption and desorption steps (e.g., the H_2O evolution step, s_3). Since s_4 is an alternate adsorption pathway, both s_1 and s_4 must be considered in the cycle graph. It is also common for steps that share intermediates to share a common node, again the example in Chapter 4, one might expect that s_1 and s_4, since they are

both adsorption steps, would be incident to the same node, since one or the other must be present in every FR. However, the graph shows that this assumption is not valid and the placement of the step in the physical pathway the reaction takes has little bearing on where it appears in the graph.

Several reaction steps have a species that is unique to that step, which we will refer to as deterring steps. This means that many of the steps produce something that could be considered as a dead end for the reaction, where an intermediate is formed that does not proceed to the terminal species, i.e., participate in a FR. Since these deterring steps have a unique intermediate, they cannot be a part of any cycle, unless that cycle has the same step in reverse, which would ultimately result in a trivial case where that step would be represented as a forward edge entering a node, with the same edge exiting the node in the opposite direction. Ultimately, these steps will never be part of any reaction route, including FRs, thus will not affect the OR resistance, however, their presence on the surface can affect concentrations of other intermediates and hence affect the OR rate. Thus, we can exclude them from the cycle fusing steps and add them later for the sole purpose of satisfying the QSS conditions. Also of note, these steps must be at quasi-equilibrium (QE) if the overall reaction is at QE and there will be no flux through these steps. Despite this, these deterring steps must still be considered in the kinetics analysis of the reaction because the intermediate species they produce could significantly affect the surface coverage of the catalyst. Thus, the step must be included for Rdot or microkinetic calculations when calculating site coverages. However, for the purpose of drawing the graph, they may be excluded, at least initially.

A less important, but nevertheless useful, simplification is to combine steps that must be present in a direct series in a graph. If two steps share a species and that species is unique to only those two steps, they must be adjacent to the same node and that node must have no other adjacent steps. These steps can be combined into an intermediate route (IR), or just noted as existing as an

uninterrupted series. This is especially useful if automating the search for possible cycles by significantly reducing the number of searches required by the program. Occasionally, there will be three or more steps that must be in such a series where each step produces an intermediate that only exists in exactly one other step. Expressing such a series as an immediate route frees the graph from a lot of clutter and makes managing the cycle graph construction much easier. This property was used in the MDR example in Chapter 5.

Step 3: Create the cycle matrix.

This step has been demonstrated numerous times in this thesis, see section 2.1.1 for the rationale behind the cycle matrix. For most RR Graph construction, the set of starting cycles chosen for this matrix is often arbitrary. While there are no guidelines yet, it is typically useful to select smaller cycles with common series of steps, preferably cycles with three steps. If two cycles have the same pair of steps and no other common steps, then those steps must be incident to the same node. This knowledge is very useful to constrain the amount of trial and error needed to find the RR Graph.

Step 4: Judicious fusion of cycles.

For smaller mechanisms, simple trial and error will suffice, but as the number of independent cycles grows, the complexity scales factorially. The difficultly lies in being able to identify what order the steps in a cycle are in. For example, a three step cycle could have two unique configurations (Figure 6.2a), a four-step cycle could have six (Figure 6.2b), and the number increases factorially. (In this case, unique means having the same incidence matrix, so to determine if a graph is the same or not, one must examine the nodes and note which edges and in what

direction are incident to each.) Thus, we require a smarter way of fusing cycles in order to realize

the RR Graph in a reasonable timeframe.
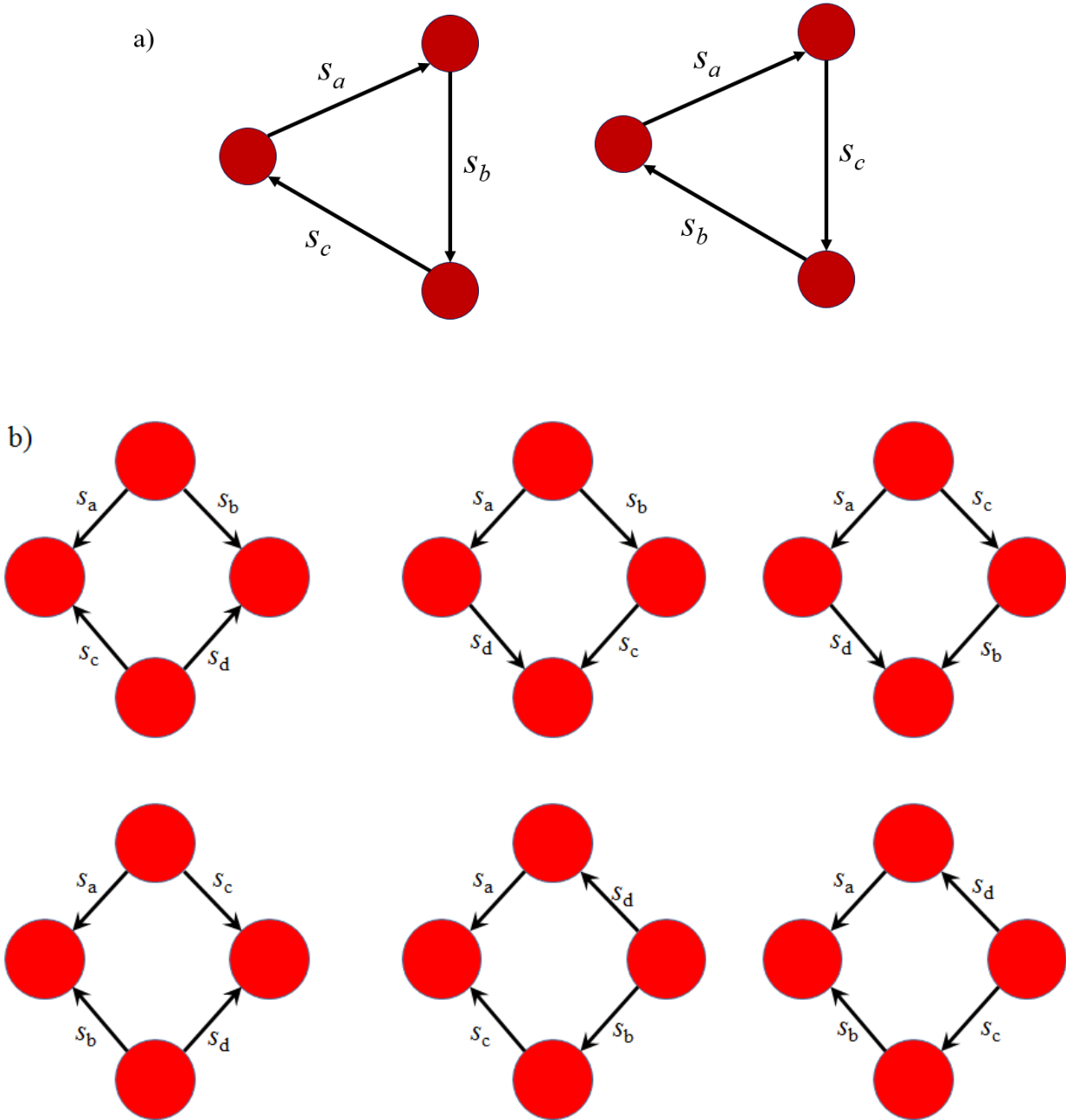
Figure 6.2: Examples of cycle multiplicity for a) 3 steps and b) 4 steps in different orders

It seems that the best way to begin constructing the cycle graph is to start with the smallest

cycles that contain steps that are present in most other RRs. Additionally, it is helpful to choose

191

steps that have intermediates that are present in the most steps, as those steps are more likely to be incident to nodes with a greater number of steps. These conditions will more commonly lead to starting with cycles that have steps that are shared with a greater number of other cycles, thus allowing the immediate realization of the constraints on how the steps are ordered. The key issue with drawing the cycles and fusing them, is that the order of the steps in the cycle is unknown until you realize that the order is incompatible with other cycles. By starting with a cycle that has several other common cycles, one can immediately recognize which orders of steps will or will not work. Also, by starting with the smallest cycles, it limits the number of configurations that cycle could have.

Step 5: Balance nodes and merge graphs to achieve symmetry.

This step is straightforward if the complete cycle graphs have been realized. Both sections 3.3.1 and 4.2 show instructive examples of this process. The important part of this step is to add the terminal nodes and fuse the graph in such a way to make the graph symmetrical. If the cycle graphs are constructed correctly, there will be few, if not a singular, ways to add or fuse edges. Rarely have we found more than two RR Graphs corresponding to a mechanism. Usually there is a unique RR Graph for a given mechanism.

Step 6: Confirm KFL and KPL.

Lastly, the validity of the graph must be confirmed. This is certainly a step that could be automated, as the cycles and QSS conditions are known, it is simply a matter of checking the graph or incidence matrix to confirm that the cycles are present and that all the QSS relations or their combinations are present in the graph. A list of all the possible combinations of QSS conditions, or INs, is useful in readily determining if such a condition exists.

6.3 Example of Complex Graph Construction

To develop the method further by utilizing the heuristics and steps mentioned previously, a complex reaction network was analyzed and particularly steps 2 and 4 were heavily utilized. This interesting mechanism proposed by Heyden et al. [2] is a NO_x decomposition mechanism comprised of 104 elementary reaction steps (Table 6.2), each of which were analyzed through DFT and values for the activation energies and the pre-exponential factors, or rate constants, were found. There is a substantial qualitative discussion and analysis of the pathways that this reaction goes through provided by Heyden et al. [2], but there could be substantially more quantitative insight that the RR approach could provide by enabling a visualization of all the pathways as well as providing a comprehensive tool for analyzing the effect of all these pathways simultaneously. The $q + 1 = 74$ intermediate species and $n = 8$ terminal species (N_2, NO, N_2O, NO_2, O_2, H_2O, *cis*-HNO_2, and *trans*-HNO_2) involved in the mechanism are summarized in Table 6.3.

Table 6.2: Mechanism for nitrous oxide decomposition on Fe-ZSM-5 zeolite catalyst [1].

s_ρ	Elementary Reaction Step		
s_1	$Z^-[FeO]^+\{M = 6\} + NO(g)$	$\rightleftarrows$	$Z^-[FeONO]^+\{M = 5\}$
s_2	$Z^-[FeONO]^+\{M = 5\}$	$\rightleftarrows$	$Z^-[Fe]^+\{M = 4\} + NO_2(g)$
s_3	$Z^-[FeO]^+\{M = 6\} + NO(g)$	$\rightleftarrows$	$Z^-[FeO_2N]^+\{M = 5\}$
s_4	$Z^-[FeO_2N]^+\{M = 5\}$	$\rightleftarrows$	$Z^-[Fe]^+\{M = 4\} + NO_2(g)$
s_5	$Z^-[FeO]^+\{M = 6\} + NO(g)$	$\rightleftarrows$	$Z^-[OFeNO]^+\{M = 5\}$
s_6	$Z^-[FeO_2]^+\{M = 6\} + NO(g)$	$\rightleftarrows$	$Z^-[FeOONO]^+\{M = 5\}$
s_7	$Z^-[FeOONO]^+\{M = 5\}$	$\rightleftarrows$	$Z^-[FeO]^+\{M = 6\} + NO_2(g)$
s_8	$Z^-[OFeO]^+\{M = 6\} + NO(g)$	$\rightleftarrows$	$Z^-[OFeONO]^+\{M = 5\}$
s_9	$Z^-[OFeONO]^+\{M = 5\}$	$\rightleftarrows$	$Z^-[FeO]^+\{M = 6\} + NO_2(g)$
s_{10}	$Z^-[OFeO]^+\{M = 6\} + NO(g)$	$\rightleftarrows$	$Z^-[OFeO_2N]^+\{M = 5\}$
s_{11}	$Z^-[OFeO_2N]^+\{M = 5\}$	$\rightleftarrows$	$Z^-[FeO]^+\{M = 6\} + NO_2(g)$
s_{12}	$Z^-[OFeO]^+\{M = 6\} + NO(g)$	$\rightleftarrows$	$Z^-[FeO_2NO]^+\{M = 5\}$
s_{13}	$Z^-[FeO_2NO]^+\{M = 5\}$	$\rightleftarrows$	$Z^-[FeO]^+\{M = 6\} + NO_2(g)$
s_{14}	$Z^-[FeONO]^+\{M = 5\} + N_2O(g)$	$\rightleftarrows$	$Z^-[FeONO]^+(N_2O)\{M = 5\}$
s_{15}	$Z^-[FeONO]^+\{M = 5\} + N_2O(g)$	$\rightleftarrows$	$Z^-[FeONO]^+(ON_2)\{M = 5\}$

s_{16}	$Z^-[FeONO]^+(ON_2)\{M = 5\}$	$\rightleftarrows$	$Z^-[OFeONO]^+\{M = 5\} + N_2(g)$
s_{17}	$Z^-[OFeONO]^+\{M = 5\} + N_2O(g)$	$\rightleftarrows$	$Z^-[OFeONO]^+(N_2O)\{M = 5\}$
s_{18}	$Z^-[OFeONO]^+\{M = 5\} + N_2O(g)$	$\rightleftarrows$	$Z^-[OFeONO]^+(ON_2)\{M = 5\}$
s_{19}	$Z^-[OFeONO]^+(ON_2)\{M = 5\}$	$\rightleftarrows$	$Z^-[O_2FeONO]^+\{M = 5\} + N_2(g)$
s_{20}	$Z^-[O_2FeONO]^+\{M = 5\}$	$\rightleftarrows$	$Z^-[O_2FeONO]^+\{M = 7\}$
s_{21}	$Z^-[O_2FeONO]^+\{M = 7\}$	$\rightleftarrows$	$Z^-[FeONO]^+\{M = 5\} + O_2(g)$
s_{22}	$Z^-[O_2FeONO]^+\{M = 7\}$	$\rightleftarrows$	$Z^-[FeO_2]^+\{M = 6\} + NO_2(g)$
s_{23}	$Z^-[OFeONO]^+\{M = 5\} + NO(g)$	$\rightleftarrows$	$Z^-[Fe(ONO)_2]^+\{M = 6\}$
s_{24}	$Z^-[Fe(ONO)_2]^+\{M = 6\}$	$\rightleftarrows$	$Z^-[FeONO]^+\{M = 5\} + NO_2(g)$
s_{25}	$Z^-[Fe(ONO)_2]^+\{M = 6\}$	$\rightleftarrows$	$Z^-[ONOFeO_2N]^+\{M = 6\}$
s_{26}	$Z^-[OFeONO]^+\{M = 5\}$	$\rightleftarrows$	$Z^-[FeO_2NO]^+\{M = 5\}$
s_{27}	$Z^-[FeONO]^+\{M = 5\}$	$\rightleftarrows$	$Z^-[FeO_2N]^+\{M = 5\}$
s_{28}	$Z^-[FeO_2N]^+\{M = 5\} + N_2O(g)$	$\rightleftarrows$	$Z^-[FeO_2N]^+(N_2O)\{M = 5\}$
s_{29}	$Z^-[FeO_2N]^+\{M = 5\} + N_2O(g)$	$\rightleftarrows$	$Z^-[FeO_2N]^+(ON_2)\{M = 5\}$
s_{30}	$Z^-[FeO_2N]^+(ON_2)\{M = 5\}$	$\rightleftarrows$	$Z^-[OFeO_2N]^+\{M = 5\} + N_2(g)$
s_{31}	$Z^-[OFeO_2N]^+\{M = 5\} + N_2O(g)$	$\rightleftarrows$	$Z^-[OFeO_2N]^+(N_2O)\{M = 5\}$
s_{32}	$Z^-[OFeO_2N]^+\{M = 5\} + N_2O(g)$	$\rightleftarrows$	$Z^-[OFeO_2N]^+(ON_2)\{M = 5\}$
s_{33}	$Z^-[OFeO_2N]^+ (ON_2)\{M = 5\}$	$\rightleftarrows$	$Z^-[O_2FeO_2N]^+\{M = 5\} + N_2(g)$
s_{34}	$Z^-[O_2FeO_2N]^+\{M = 5\}$	$\rightleftarrows$	$Z^-[O_2FeO_2N]^+\{M = 7\}$
s_{35}	$Z^-[O_2FeO_2N]^+\{M = 7\}$	$\rightleftarrows$	$Z^-[FeO_2N]^+\{M = 5\} + O_2(g)$
s_{36}	$Z^-[O_2FeO_2N]^+\{M = 7\}$	$\rightleftarrows$	$Z^-[FeO_2]^+\{M = 6\} + NO_2(g)$
s_{37}	$Z^-[OFeO_2N]^+\{M = 5\} + NO(g)$	$\rightleftarrows$	$Z^-[ONOFeO_2N]^+\{M = 6\}$
s_{38}	$Z^-[ONOFeO_2N]^+\{M = 6\}$	$\rightleftarrows$	$Z^-[FeO_2N]^+\{M = 5\} + NO_2(g)$
s_{39}	$Z^-[ONOFeO_2N]^+\{M = 6\}$	$\rightleftarrows$	$Z^-[Fe(O_2N)_2]^+\{M = 6\}$
s_{40}	$Z^-[OFeO_2N]^+\{M = 5\}$	$\rightleftarrows$	$Z^-[OFeONO]^+\{M = 5\}$
s_{41}	$Z^-[FeO_2N]^+\{M = 5\} + N_2O(g)$	$\rightleftarrows$	$Z^-[FeO_2NO]^+\{M = 5\} + N_2(g)$
s_{42}	$Z^-[FeO_2NO]^+\{M = 5\} + N_2O(g)$	$\rightleftarrows$	$Z^-[FeO_2NO]^+(N_2O)\{M = 5\}$
s_{43}	$Z^-[FeO_2NO]^+\{M = 5\} + N_2O(g)$	$\rightleftarrows$	$Z^-[FeO_2NO]^+(ON_2)\{M = 5\}$
s_{44}	$Z^-[FeO_2NO]^+(ON_2)\{M = 5\}$	$\rightleftarrows$	$Z^-[OFeO_2NO]^+\{M = 5\} + N_2(g)$
s_{45}	$Z^-[OFeO_2NO]^+\{M = 5\} + N_2O(g)$	$\rightleftarrows$	$Z^-[OFeO_2NO]^+(N_2O)\{M = 5\}$
s_{46}	$Z^-[OFeO_2NO]^+\{M = 5\} + N_2O(g)$	$\rightleftarrows$	$Z^-[OFeO_2NO]^+(ON_2)\{M = 5\}$
s_{47}	$Z^-[OFeO_2NO]^+(ON_2)\{M = 5\}$	$\rightleftarrows$	$Z^-[O_2FeO_2NO]^+\{M = 5\} + N_2(g)$
s_{48}	$Z^-[O_2FeO_2NO]^+\{M = 5\}$	$\rightleftarrows$	$Z^-[O_2FeO_2NO]^+\{M = 7\}$
s_{49}	$Z^-[O_2FeO_2NO]^+\{M = 7\}$	$\rightleftarrows$	$Z^-[FeO_2NO]^+\{M = 5\} + O_2(g)$
s_{50}	$Z^-[O_2FeO_2NO]^+\{M = 7\}$	$\rightleftarrows$	$Z^-[OFeO_2]^+\{M = 6\} + NO_2(g)$
s_{51}	$Z^-[OFeO_2NO]^+\{M = 5\}$	$\rightleftarrows$	$Z^-[OFeO]^+\{M = 6\} + NO_2(g)$

s_{52}	$Z^-[OFeO_2NO]^+\{M = 5\} + NO(g)$	$\rightleftarrows$	$Z^-[ONOFeO_2NO]^+\{M = 6\}$
s_{53}	$Z^-[ONOFeO_2NO]^+\{M = 6\}$	$\rightleftarrows$	$Z^-[FeO_2NO]^+\{M = 5\} + NO_2(g)$
s_{54}	$Z^-[ONOFeO_2NO]^+\{M = 6\}$	$\rightleftarrows$	$Z^-[NO_2FeO_2NO]^+\{M = 6\}$
s_{55}	$Z^-[Fe(OH)_2]^+\{M = 6\} + NO(g)$	$\rightleftarrows$	$Z^-[Fe(OH)_2]^+(ON)\{M = 7\}$
s_{56}	$Z^-[Fe(OH)_2]^+\{M = 6\} + NO(g)$	$\rightleftarrows$	$Z^-[Fe(OH)_2]^+(NO)\{M = 7\}$
s_{57}	$Z^-[Fe(OH)_2]^+(NO)\{M = 7\}$	$\rightleftarrows$	$Z^-[Fe(OH)_2]^+(NO)\{M = 5\}$
s_{58}	$Z^-[Fe(OH)_2]^+(NO)\{M = 5\}$	$\rightleftarrows$	$Z^-[FeOH]^+(trans\text{-}HNO_2)\{M = 5\}$
s_{59}	$Z^-[Fe(OH)_2]^+(NO)\{M = 5\}$	$\rightleftarrows$	$Z^-[FeOH]^+(cis\text{-}HNO_2)\{M = 5\}$
s_{60}	$Z^-[FeOH]^+(trans\text{-}HNO_2)\{M = 5\}$	$\rightleftarrows$	$Z^-[FeOH]^+\{M = 5\} + trans\text{-}HNO_2(g)$
s_{61}	$Z^-[FeOH]^+(cis\text{-}HNO_2)\{M = 5\}$	$\rightleftarrows$	$Z^-[FeOH]^+\{M = 5\} + cis\text{-}HNO_2(g)$
s_{62}	$Z^-[FeOH]^+\{M = 5\} + N_2O(g)$	$\rightleftarrows$	$Z^-[FeOH]^+(N_2O)\{M = 5\}$
s_{63}	$Z^-[FeOH]^+\{M = 5\} + N_2O(g)$	$\rightleftarrows$	$Z^-[FeOH]^+(ON_2)\{M = 5\}$
s_{64}	$Z^-[FeOH]^+(ON_2)\{M = 5\}$	$\rightleftarrows$	$Z^-[OFeOH]^+\{M = 5\} + N_2(g)$
s_{65}	$Z^-[OFeOH]^+\{M = 5\} + N_2O(g)$	$\rightleftarrows$	$Z^-[OFeOH]^+(N_2O)\{M = 5\}$
s_{66}	$Z^-[OFeOH]^+\{M = 5\} + N_2O(g)$	$\rightleftarrows$	$Z^-[OFeOH]^+(ON_2)\{M = 5\}$
s_{67}	$Z^-[OFeOH]^+(ON_2)\{M = 5\}$	$\rightleftarrows$	$Z^-[O_2FeOH]^+\{M = 5\} + N_2(g)$
s_{68}	$Z^-[O_2FeOH]^+\{M = 5\}$	$\rightleftarrows$	$Z^-[O_2FeOH]^+\{M = 7\}$
s_{69}	$Z^-[O_2FeOH]^+\{M = 7\}$	$\rightleftarrows$	$Z^-[FeOH]^+\{M = 5\} + O_2(g)$
s_{70}	$Z^-[OFeOH]^+\{M = 5\} + NO(g)$	$\rightleftarrows$	$Z^-[ONOFeOH]^+\{M = 6\}$
s_{71}	$Z^-[ONOFeOH]^+\{M = 6\}$	$\rightleftarrows$	$Z^-[FeOH]^+\{M = 5\} + NO_2(g)$
s_{72}	$Z^-[OFeOH]^+\{M = 5\} + NO(g)$	$\rightleftarrows$	$Z^-[FeO]^+(trans\text{-}HNO_2)\{M = 6\}$
s_{73}	$Z^-[FeO]^+(trans\text{-}HNO_2)\{M = 6\}$	$\rightleftarrows$	$Z^-[FeO]^+\{M = 6\} + trans\text{-}HNO_2(g)$
s_{74}	$Z^-[OFeOH]^+\{M = 5\} + trans\text{-}HNO_2(g)$	$\rightleftarrows$	$Z^-[OFeOH]^+(trans\text{-}HNO_2)\{M = 5\}$
s_{75}	$Z^-[OFeOH]^+(trans\text{-}HNO_2)\{M = 5\}$	$\rightleftarrows$	$Z^-[OFeOH_2]^+(NO_2)\{M = 5\}$
s_{76}	$Z^-[OFeOH_2]^+(NO_2)\{M = 5\}$	$\rightleftarrows$	$Z^-[OFeOH_2]^+(NO_2)\{M = 7\}$
s_{77}	$Z^-[OFeOH_2]^+(NO_2)\{M = 7\}$	$\rightleftarrows$	$Z^-[FeO]^+(OH_2)\{M = 6\} + NO_2(g)$
s_{78}	$Z^-[FeO]^+(OH_2)\{M = 6\}$	$\rightleftarrows$	$Z^-[FeO]^+\{M = 6\}$
s_{79}	$Z^-[FeO]^+(OH_2)\{M = 6\}$	$\rightleftarrows$	$Z^-[Fe(OH)_2]^+\{M = 6\}$
s_{80}	$Z^-[OFeO]^+\{M = 6\} + N_2O(g)$	$\rightleftarrows$	$Z^-[FeO]^+(cis\text{-}(NO)_2)\{M = 6\}$
s_{81}	$Z^-[FeO]^+(cis\text{-}(NO)_2)\{M = 6\}$	$\rightleftarrows$	$Z^-[FeO]^+(ON)\{M = 5\} + NO(g)$
s_{82}	$Z^-[FeO]^+(ON)\{M = 5\}$	$\rightleftarrows$	$Z^-[FeO]^+\{M = 6\} + NO(g)$
s_{83}	$Z^-[ONOFeO]^+\{M = 5\} + N_2O(g)$	$\rightleftarrows$	$Z^-[FeONO]^+(cis\text{-}(NO)_2)\{M = 5\}$
s_{84}	$Z^-[FeONO]^+(cis\text{-}(NO)_2)\{M = 5\}$	$\rightleftarrows$	$Z^-[FeONO]^+(ON)\{M = 4\} + NO(g)$
s_{85}	$Z^-[FeONO]^+(ON)\{M = 4\}$	$\rightleftarrows$	$Z^-[FeONO]^+\{M = 5\} + NO(g)$
s_{86}	$Z^-[OFeO_2N]^+\{M = 5\} + N_2O(g)$	$\rightleftarrows$	$Z^-[FeO_2N]^+(cis\text{-}(NO)_2)\{M = 5\}$
s_{87}	$Z^-[FeO_2N]^+(cis\text{-}(NO)_2)\{M = 5\}$	$\rightleftarrows$	$Z^-[FeO_2N]^+(ON)\{M = 4\} + NO(g)$

s_{88}	$Z^-[FeO_2N]^+(ON)\{M = 4\}$	$\rightleftarrows$	$Z^-[FeO_2N]^+\{M = 5\} + NO(g)$
s_{89}	$Z^-[OFeO_2NO]^+\{M = 5\} + N_2O(g)$	$\rightleftarrows$	$Z^-[FeO_2NO]^+(cis^-(NO)_2)\{M = 5\}$
s_{90}	$Z^-[FeO_2NO]^+(cis^-(NO)_2)\{M = 5\}$	$\rightleftarrows$	$Z^-[FeO_2NO]^+(ON)\{M = 4\} + NO(g)$
s_{91}	$Z^-[FeO_2NO]^+(ON)\{M = 4\}$	$\rightleftarrows$	$Z^-[FeO_2NO]^+\{M = 5\} + NO(g)$
s_{92}	$Z^-[OFeOH]^+\{M = 5\} + N_2O(g)$	$\rightleftarrows$	$Z^-[FeOH]^+(cis^-(NO)_2)\{M = 5\}$
s_{93}	$Z^-[FeOH]^+(cis^-(NO)_2)\{M = 5\}$	$\rightleftarrows$	$Z^-[FeOH]^+(ON)\{M = 4\} + NO(g)$
s_{94}	$Z^-[FeOH]^+(ON)\{M = 4\}$	$\rightleftarrows$	$Z^-[FeOH]^+\{M = 5\} + NO(g)$
s_{95}	$Z^-[OFeO]^+\{M = 6\} + NO_2(g)$	$\rightleftarrows$	$Z^-[OFeO]^+(NO_2)\{M = 5\}$
s_{96}	$Z^-[OFeO]^+(NO_2)\{M = 5\}$	$\rightleftarrows$	$Z^-[OFeO_2]^+\{M = 4\} + NO(g)$
s_{97}	$Z^-[OFeONO]^+\{M = 5\} + NO_2(g)$	$\rightleftarrows$	$Z^-[OFeONO]^+(NO_2)\{M = 6\}$
s_{98}	$Z^-[OFeONO]^+(NO_2)\{M = 6\}$	$\rightleftarrows$	$Z^-[O_2FeONO]^+\{M = 5\} + NO(g)$
s_{99}	$Z^-[OFeO_2N]^+\{M = 5\} + NO_2(g)$	$\rightleftarrows$	$Z^-[OFeO_2N]^+(NO_2)\{M = 6\}$
s_{100}	$Z^-[OFeO_2N]^+(NO_2)\{M = 6\}$	$\rightleftarrows$	$Z^-[O_2FeO_2N]^+\{M = 5\} + NO(g)$
s_{101}	$Z^-[OFeO_2NO]^+\{M = 5\} + NO_2(g)$	$\rightleftarrows$	$Z^-[OFeO_2NO]^+(NO_2)\{M = 6\}$
s_{102}	$Z^-[OFeO_2NO]^+(NO_2)\{M = 6\}$	$\rightleftarrows$	$Z^-[O_2FeO_2NO]^+\{M = 5\} + NO(g)$
s_{103}	$Z^-[HOFeO]^+\{M = 5\} + NO_2(g)$	$\rightleftarrows$	$Z^-[HOFeO]^+(NO_2)\{M = 6\}$
s_{104}	$Z^-[HOFeO]^+(NO_2)\{M = 6\}$	$\rightleftarrows$	$Z^-[HOFeO_2]^+\{M = 5\} + NO(g)$
OR_1	$N_2O(g) + NO(g)$	$\rightleftarrows$	$N_2(g) + NO_2(g)$
OR_2	$N_2O(g) + NO_2(g)$	$\rightleftarrows$	$N_2(g) + NO(g) + O_2(g)$
OR_3	$N_2(g) + O_2(g)$	$\rightleftarrows$	$2NO$
OR_4	$H_2O(g) + N_2O(g) + O_2(g)$	$\rightleftarrows$	$2trans\text{-}HNO_2$
OR_5	$H_2O(g) + N_2O(g) + O_2(g)$	$\rightleftarrows$	$2cis\text{-}HNO_2$

Table 6.2: Mechanism for nitrous oxide decomposition on Fe-ZSM-5 zeolite catalyst [1].

Table 6.3: Abbreviations for the intermediate species in the mechanism for nitrous oxide decomposition on Fe-ZSM-5 zeolite catalyst [1]

Intermediate Species	Abbreviation
$Z^-[FeO]^+\{M = 6\}$	I_1
$Z^-[FeO_2]^+\{M = 6\}$	I_2
$Z^-[FeO_2]^+\{M = 6\}$	I_3
$Z^-[Fe(ONO)_2]^+\{M = 6\}$	I_4
$Z^-[FeO]^+(cis^-(NO)_2)\{M = 6\}$	I_5
$Z^-[FeO_2N]^+\{M = 5\}$	I_6
$Z^-[FeO_2N]^+(cis^-(NO)_2)\{M = 5\}$	I_7
$Z^-[FeO_2N]^+(N_2O)\{M = 5\}$	I_8
$Z^-[FeO_2N]^+(ON)\{M = 4\}$	I_9
$Z^-[FeO_2N]^+(ON_2)\{M = 5\}$	I_{10}
$Z^-[FeO_2N]^+\{M = 5\}$	I_{11}

$Z^-[FeO_2NO]^+(cis^-(NO)_2)\{M = 5\}$ I_{12}

$Z^-[FeO_2NO]^+(N_2O)\{M = 5\}$ I_{13}

$Z^-[FeO_2NO]^+(ON)\{M = 4\}$ I_{14}

$Z^-[FeO_2NO]^+(ON_2)\{M = 5\}$ I_{15}

$Z^-[FeO_2NO]^+\{M = 5\}$ I_{16}

$Z^-[FeONO]^+(cis^-(NO)_2)\{M = 5\}$ I_{17}

$Z^-[FeONO]^+(N_2O)\{M = 5\}$ I_{18}

$Z^-[FeONO]^+(ON)\{M = 4\}$ I_{19}

$Z^-[FeONO]^+(ON_2)\{M = 5\}$ I_{20}

$Z^-[FeONO]^+\{M = 5\}$ I_{21}

$Z^-[FeOONO]^+\{M = 5\}$ I_{22}

$Z^-[NO_2FeO_2NO]^+\{M = 6\}$ I_{23}

$Z^-[O_2FeO_2N]^+\{M = 5\}$ I_{24}

$Z^-[O_2FeO_2N]^+\{M = 7\}$ I_{25}

$Z^-[O_2FeO_2NO]^+\{M = 5\}$ I_{26}

$Z^-[O_2FeO_2NO]^+\{M = 7\}$ I_{27}

$Z^-[O_2FeONO]^+\{M = 5\}$ I_{28}

$Z^-[O_2FeONO]^+\{M = 7\}$ I_{29}

$Z^-[OFeONO]^+\{M = 5\}$ I_{30}

$Z^-[OFeO]^+(NO_2)\{M = 5\}$ I_{31}

$Z^-[FeO]^+\{M = 6\}$ I_{32}

$Z^-[OFeO_2]^+\{M = 5\}$ I_{33}

$Z^-[OFeO_2]^+\{M = 6\}$ I_{34}

$Z^-[OFeO_2N]^+(N_2O)\{M = 5\}$ I_{35}

$Z^-[OFeO_2N]^+(NO_2)\{M = 6\}$ I_{36}

$Z^-[OFeO_2N]^+(ON_2)\{M = 5\}$ I_{37}

$Z^-[OFeO_2N]^+\{M = 5\}$ I_{38}

$Z^-[OFeO_2NO]^+(N_2O)\{M = 5\}$ I_{39}

$Z^-[OFeO_2NO]^+(NO_2)\{M = 6\}$ I_{40}

$Z^-[OFeO_2NO]^+(ON_2)\{M = 5\}$ I_{41}

$Z^-[OFeO_2NO]^+\{M = 5\}$ I_{42}

$Z^-[OFeONO]^+(N_2O)\{M = 5\}$ I_{43}

$Z^-[OFeONO]^+(NO_2)\{M = 6\}$ I_{44}

$Z^-[OFeONO]^+(ON_2)\{M = 5\}$ I_{45}

$Z^-[OFeONO]^+\{M = 5\}$ I_{46}

$Z^-[ONOFeO]^+\{M = 5\}$ I_{47}

$Z^-[ONOFeO_2N]^+\{M = 6\}$ I_{48}

$Z^-[ONOFeO_2NO]^+\{M = 6\}$ I_{49}

$Z^-[Fe(OH)_2]^+(NO)\{M = 5\}$ I_{50}

$Z^-[Fe(OH)_2]^+(NO)\{M = 7\}$ I_{51}

$Z^-[Fe(OH)_2]^+(ON)\{M = 7\}$ I_{52}

$Z^-[Fe(OH)_2]^+\{M = 6\}$ I_{53}

$Z^-[FeO(OH)_2]^+\{M = 6\}$ I_{54}

$Z^-[FeO]^+(trans\text{-}HNO_2)\{M = 6\}$	I_{55}
$Z^-[FeOH]^+(cis\text{-}(NO)_2)\{M = 5\}$	I_{56}
$Z^-[FeOH]^+(cis\text{-}HNO_2)\{M = 5\}$	I_{57}
$Z^-[FeOH]^+(N_2O)\{M = 5\}$	I_{58}
$Z^-[FeOH]^+(ON)\{M = 4\}$	I_{59}
$Z^-[FeOH]^+(ON_2)\{M = 5\}$	I_{60}
$Z^-[FeOH]^+(trans\text{-}HNO_2)\{M = 5\}$	I_{61}
$Z^-[FeOH]^+\{M = 5\}$	I_{62}
$Z^-[HOFeO]^+(NO_2)\{M = 6\}$	I_{63}
$Z^-[HOFeO]^+\{M = 5\}$	I_{64}
$Z^-[HOFeO_2]^+\{M = 5\}$	I_{65}
$Z^-[O_2FeOH]^+\{M = 5\}$	I_{66}
$Z^-[O_2FeOH]^+\{M = 7\}$	I_{67}
$Z^-[OFeOH]^+(N_2O)\{M = 5\}$	I_{68}
$Z^-[OFeOH]^+(ON_2)\{M = 5\}$	I_{69}
$Z^-[OFeOH]^+(trans^-HNO_2)\{M = 5\}$	I_{70}
$Z^-[OFeOH]^+\{M = 5\}$	I_{71}
$Z^-[OFeOH_2]^+(NO_2)\{M = 5\}$	I_{72}
$Z^-[OFeOH_2]^+(NO_2)\{M = 7\}$	I_{73}
$Z^-[ONOFeOH]^+\{M = 6\}$	I_{74}
N_2	T_1
N_2O	T_2
NO	T_3
NO_2	T_4
O_2	T_5
$trans\text{-}HNO_2$	T_6
$cis\text{-}HNO_2$	T_7
H_2O	T_8

Table 6.3: Abbreviations for the species in the mechanism for nitrous oxide decomposition on Fe-ZSM-5 zeolite catalyst [1]

Construction of an RR Graph of this magnitude has never been accomplished. This is, however, a linear mechanism, so the theory behind minimal RR Graphs should apply (Chapter 2). On the other hand, it contains multiple ORs. Theoretically, we could automate the process of creating the incidence matrix through matrix manipulation, but the amount of computational time it would take would not make it feasible. Thus, the graph was attempted to be constructed by hand as per the guidelines detailed above.

First, the mechanism was classified in order to identify the best means for drawing the graph. Although this is a very large system, it is completely linear. In theory, it would be possible to use the matrix manipulation method described in section 2.1.1, but efforts to utilize that method were unsuccessful, as it is a technique based on trial and error and there are far too many combinations to realistically sort through. However, because it is linear, we do not have to be concerned about mirroring the graph. Thus, we determined that the best approach was to simplify the mechanism into sub mechanisms and then construct the graph through fusing cycle graphs similar to the approach in Chapter 3.

Finally it was decided that, the mechanism could be simplified. The goal was to make the mechanism more manageable by identifying which steps can be ignored or combined with other steps, thus reducing the complexity. Also, since this is such a large mechanism, starting with a smaller subset of the reaction network would help to reduce some of the trial and error.

Fortunately, this mechanism has clear points where it can be simplified, most importantly it can be divided into two distinct separate mechanisms: a mechanism for the species containing hydrogen and a mechanism for species without hydrogen. It is important to note that none the hydrogenated species are involved in the steps with non-hydrogenated species so that the subgraphs with these species are independent. In other words, reactions steps with hydrogenated species only react with hydrogenated species so that the system comprises of two independent subgraphs. This means that no minimal cycle exists with steps that include hydrogenated species and those that do not. Thus, we can create a cycle matrix with only non-hydrogenated species to build the subgraph from. The mechanism is thus divided into those two parts (Table 6.4).

Hydrogenated Steps	Nonhydrogenated Steps
55-80, 92-94, 103, 104	1-54, 81-91, 95-102

Table 6.4: Division of the 104-step NO_x mechanism [2] into separate sub mechanism by hydrogenation

The case of nonhydrogenated subgraph is described next. We identify those steps that cannot possibly be included in any cycles, because of a side intermediate that does not further lead to an OR (Table 6.5). Then, steps that must be in an uninterrupted series because they uniquely share an intermediate are combined into intermediate routes and their common intermediate is ignored in further graph construction (Table 6.6). Thus, we have pruned the mechanism down to $p = 40$ steps and $q = 20$ linearly independent species, which we determine from Milner's [2] theory to have $p - q = 20$ linearly independent RRs.

Each intermediate is assigned as I_k for abbreviation, along with the terminal species (N_2, N_2O, NO, NO_2, and O_2), assigned as T_n (Table 6.3), A stoichiometric matrix can then be created for this mechanism (Table 6.7). Using this stoichiometric matrix, it would be possible to find a cut-set matrix for a linearly independent set of reaction routes. For this, a Mathematica program was written to automate this process and identify any possible RRs (Appendix 1). The program identifies routes by checking to see if a combination of steps adds up to either no intermediate

Deterring Steps	Side intermediate
s_5	I_{30}
s_{14}	I_{18}
s_{17}	I_{43}
s_{28}	I_8
s_{31}	I_{35}
s_{39}	I_3
s_{42}	I_{13}
s_{45}	I_{39}
s_{50}	I_{34}
s_{54}	I_{23}
s_{83}	I_{47}
s_{84}	I_{17}
s_{85}	I_{19}
s_{95}	I_{31}
s_{96}	I_{33}

Table 6.5: Identification of steps with side intermediates that can be ignored in the cycle graph.

Intermediate Route, IR_ρ	Steps	Common Intermediates
IR_1	s_2 & $(-1)s_4$	I_1
IR_2	s_6 & s_7	I_{22}
IR_3	s_{15} & s_{16}	I_{20}
IR_4	s_{18} & s_{19}	I_{45}
IR_5	s_{32} & s_{33}	I_{37}
IR_6	s_{43} & s_{44}	I_{15}
IR_7	s_{46}, s_{47}, s_{48} & s_{49}	I_{26}, I_{27}, I_{41}
IR_8	s_{52} & s_{53}	I_{49}
IR_9	s_{80}, s_{81} & s_{82}	I_5, I_6
IR_{10}	s_{86}, s_{87} & s_{88}	I_7, I_9
IR_{11}	s_{89}, s_{90} & s_{91}	I_{12}, I_{14}
IR_{12}	s_{97} & s_{98}	I_{44}
IR_{13}	s_{99} & s_{100}	I_{36}
IR_{14}	s_{101} & s_{102}	I_{40}

Table 6.6: Identification of intermediate routes and the intermediate species that are common.

species (ERs) or only terminal species (FRs). In the latter case, an overall reaction was added to balance the species. The most common set of terminal species were presumably involved in the following ORs, i.e., $(n - e) = 5 - 2 = 3$ ORs:

$$OR_1 : N_2O + NO \rightleftarrows N_2 + NO_2 \tag{6.1}$$

$$OR_2 : 2NO_2 \rightleftarrows \; + 2NO + O_2 \tag{6.2}$$

$$OR_3 : N_2 + O_2 \rightleftarrows 2NO \tag{6.3}$$
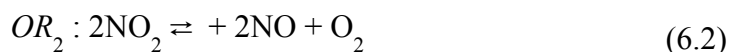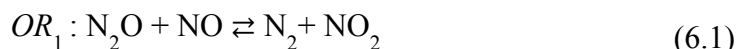
Thus, these were selected as the ORs to appear in the graph. A list RRs was selected and checked to make sure they were, in fact, linearly independent and combined into a cycle matrix (Table 6.8).

From this cycle matrix, we can now start constructing the RR Graph by combining cycles to form larger cycle graphs. This proved to be an extremely challenging endeavor, however, due to the large amount of possible cycles and combination of cycles, so some intelligent selection of which cycle to start with was required. First, we wanted to select cycles with only three steps, as

there are fewer orientations for the steps within the cycle. ER_2 and ER_3 both share s_{41}, which contains I_{11} and I_{16}, two of the most commonly occurring intermediates in the mechanism making this a good place to begin the graph construction. Unfortunately, when we fuse these two cycles, they can be oriented in one of four configurations (Figure 6.3). If the network were simple, then any configuration would be equally correct, however, as more cycles are added, some of these configurations proved to be incorrect as the cycles that needed to be added would not fit. More information was needed to determine which is correct, so we looked to other common cycles. It was noticed that s_8 and s_9 are common in ER_8, without either s_{11} or s_{10}, thus we concluded that s_9 and s_8 must be incident to the same node and either configuration 3-A or configuration 3-D have such a node and ER_8 was fused into each of those cycles producing Fig. 6.4. Unfortunately, we have the same issue, as there are still 4 viable configurations. While some of them might look similar, each one has unique nodes with different edges or direction of edges incident to it. However, we note that 4-C and 4-D are simply the negative incidence of 4-A and 4-B, thus, while they are not equivalent, they would simply produce an inverted graph with the same cycles and they do not need to be considered further.

Next, we noticed that ER_{10} contains s_{10} and s_{12}, but none of the other steps in the current cycle graph, so we determined that those steps must be incident to the same node. However, we decided to hold off from adding ER_{10} to this cycle because there are six ways to add the other three steps, resulting in six total configurations. However, we did discover that configuration 3-A is the correct configuration.

Step	S	I$_2$	I$_4$	I$_{11}$	I$_{16}$	I$_{21}$	I$_{24}$	I$_{25}$	I$_{28}$	I$_{29}$	I$_{32}$	I$_{38}$	I$_{42}$	I$_{46}$	I$_{48}$	T$_1$	T$_2$	T$_3$	T$_4$	T$_5$
s_1	-1	0	0	0	0	1	0	0	0	0	0	0	0	0	0	0	0	-1	0	0
IR_1	0	0	0	1	0	-1	0	0	0	0	0	0	0	0	0	0	0	0	0	0
s_3	-1	0	0	1	0	0	0	0	0	0	0	0	0	0	0	0	0	-1	0	0
$\underline{IR_2}$	1	-1	0	0	0	0	0	0	0	0	0	0	0	0	0	0	0	0	0	0
s_8	0	0	0	0	0	0	0	0	0	0	-1	0	0	1	0	0	0	-1	0	0
s_9	1	0	0	0	0	0	0	0	0	0	0	0	0	-1	0	0	0	0	1	0
s_{10}	0	0	0	0	0	0	0	0	0	0	-1	1	0	0	0	0	0	-1	0	0
s_{11}	1	0	0	0	0	0	0	0	0	0	0	-1	0	0	0	0	0	0	1	0
s_{12}	0	0	0	0	1	0	0	0	0	0	-1	0	0	0	0	0	0	-1	0	0
s_{13}	1	0	0	0	-1	0	0	0	0	0	0	0	0	0	0	0	0	0	1	0
IR_3	0	0	0	0	0	-1	0	0	0	0	0	0	0	1	0	1	0	0	0	0
IR_4	0	0	0	0	0	0	0	0	1	0	0	0	0	-1	0	1	0	0	0	0
s_{20}	0	0	0	0	0	0	0	0	-1	1	0	0	0	0	0	0	0	0	0	0
s_{21}	0	0	0	0	0	1	0	0	0	-1	0	0	0	0	0	0	0	0	0	1
s_{22}	0	1	0	0	0	0	0	0	0	-1	0	0	0	0	0	0	0	0	1	0
s_{23}	0	0	1	0	0	0	0	0	0	0	0	0	0	-1	0	0	0	-1	0	0
s_{24}	0	0	-1	0	0	1	0	0	0	0	0	0	0	0	0	0	0	0	1	0
s_{25}	0	0	-1	0	0	0	0	0	0	0	0	0	0	0	1	0	0	0	0	0
s_{26}	0	0	0	0	1	0	0	0	0	0	0	0	0	-1	0	0	0	0	0	0
s_{27}	0	0	0	1	0	-1	0	0	0	0	0	0	0	0	0	0	0	0	0	0
s_{29}	0	0	0	-1	0	0	0	0	0	0	0	0	0	0	0	0	-1	0	0	0
s_{30}	0	0	0	0	0	0	0	0	0	0	0	1	0	0	0	1	0	0	0	0
IR_5	0	0	0	0	0	0	1	0	0	0	0	-1	0	0	0	1	-1	0	0	0
s_{34}	0	0	0	0	0	0	-1	1	0	0	0	0	0	0	0	0	0	0	0	0
s_{35}	0	0	0	1	0	0	0	-1	0	0	0	0	0	0	0	0	0	0	0	1
s_{36}	0	1	0	0	0	0	0	-1	0	0	0	0	0	0	0	0	0	0	1	0
s_{37}	0	0	0	0	0	0	0	0	0	0	0	-1	0	0	1	0	0	-1	0	0
s_{38}	0	0	0	1	0	0	0	0	0	0	0	0	0	0	-1	0	0	0	1	0
s_{40}	0	0	0	0	0	0	0	0	0	0	0	-1	0	1	0	0	0	0	0	0
s_{41}	0	0	0	-1	1	0	0	0	0	0	0	0	0	0	0	1	-1	0	0	0
IR_6	0	0	0	0	-1	0	0	0	0	0	0	0	1	0	0	1	-1	0	0	0
IR_7	0	0	0	0	1	0	0	0	0	0	0	0	-1	0	0	1	-1	0	0	1
s_{51}	0	0	0	0	0	0	0	0	0	0	1	0	-1	0	0	0	0	0	1	0
IR_8	0	0	0	0	1	0	0	0	0	0	0	0	-1	0	0	0	0	-1	1	0
IR_9	1	0	0	0	0	0	0	0	0	0	-1	0	0	0	0	0	-1	2	0	0
IR_{10}	0	0	0	1	0	0	0	0	0	0	0	-1	0	0	0	0	-1	2	0	0
IR_{11}	0	0	0	0	1	0	0	0	0	0	0	0	-1	0	0	0	-1	2	0	0
IR_{12}	0	0	0	0	0	0	0	0	1	0	0	0	0	-1	0	0	0	1	-1	0
IR_{13}	0	0	0	0	0	0	1	0	0	0	0	-1	0	0	0	0	0	1	-1	0
IR_{14}	0	0	0	0	0	0	0	1	0	0	0	0	-1	0	0	0	0	1	-1	0

Table 6.7: Stoichiometric matrix for the reduced dehydrogenated 104-step NO$_x$ mechanism [2].

Table 6.8: Cycle matrix for the reduced nonhydrogenated NO$_x$ mechanism [3].

Cycle	OR1	OR2	OR3	s1	IR$_1$	s3	IR$_2$	s8	s9	s10	s11	s12	s13	IR$_3$	IR$_4$	s20	s21	s22	s23	s24	s25	s26	s27	s29	s30	s31	IR$_5$	s34	s35	s36	s37	s38	s40	s41	IR$_6$	IR$_7$	s51	IR$_8$	IR$_9$	IR$_{10}$	IR$_{11}$	IR$_{12}$	IR$_{13}$	IR$_{14}$
ER$_1$				1	1	-1																																							
ER$_2$								-1		1	-1																							1										
ER$_3$				1					1		1									-1	1																							
ER$_4$				1							1									-1				1							-1													
ER$_5$				1							1											1								-1													
ER$_6$				1				-1	1				1					1		-1			1																					
ER$_7$								1	1	-1	-1	-1	-1						-1																									
ER$_8$								1	1			-1	-1																															
ER$_9$								1		1		-1										1			-1	-1									1			1	-1					
ER$_{10}$										1			1		1		1	-1					1						1	1			1											
ER$_{11}$						-1	1				-1				-1					-1				-1		-1				-1			-1		1		1							
ER$_{12}$						1				-1			-1		1														-1				-1	1	1				1	-1				
ER$_{13}$													1	1														-1	1					-1						1				
ER$_{14}$						1									-1				-1								-1						-1			1					1			-1
ER$_{15}$						1							1	1													-1							1								1		
ER$_{16}$						1								1	-1			1											1					1									1	
FR$_1$	-1			1		-1	1	-1	-1	1				1	1												-1	1	1	1				-1										
FR$_2$		-1				-1		-1	-1	1																																		
FR$_3$			-1	1				-1	1	1					1			-1				-1												-1		1			1					
FR$_4$		-1						-1															-1													1	-1							-1

204

Figure 6.3: Possible configurations of the fused cycle graph of ER_2 and ER_3.
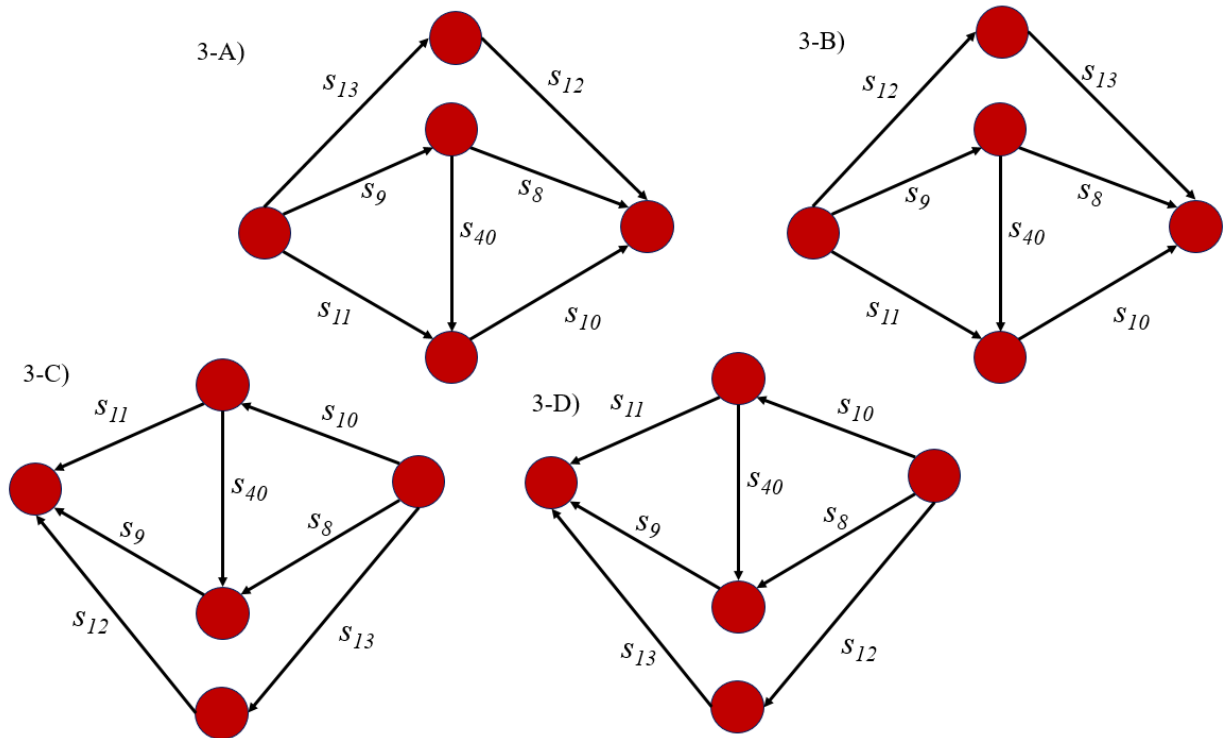
Figure 6.4: Possible configurations of the fused cycle graph of ER_2, ER_3 and ER_8.

Another approach is to look for more series of steps that are common in the RRs. ER_{15} and ER_{16} both contain s_3, s_{13} and s_{41}, thus those steps must be present in a series. To determine the order of that series, we looked at ER_1, which contains s_3 and ER_6, which contains s_{13}, and both contain s_1. In order for both of these cycles to exist and have s_3 and s_{13} be in a series, there is only one configuration that was found to be possible (Figure 6.5).
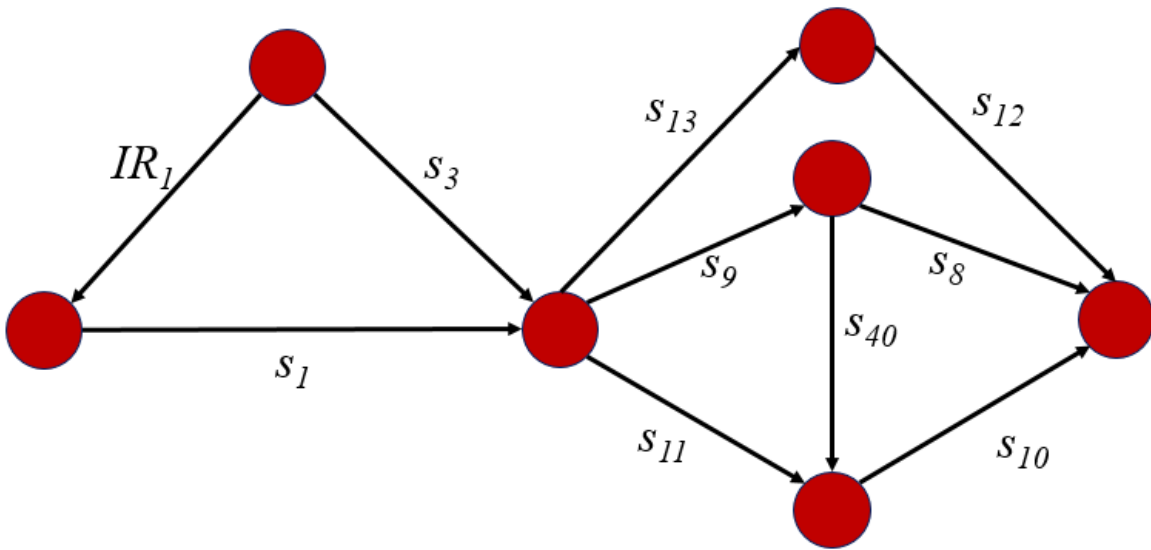
Figure 6.5: Cycle graph found by fusing cycle in Figure 6.4 and cycle ER_1.

Now, considering ER_4, ER_5 and ER_6, we note the common series of s_1, s_{11} and s_{37}, along with the common series of s_1 and s_{24}, leads us to Figure 6.6 as the partial cycle graph which has so far been realized. Note that the series of s_{38} and s_{27} might not be in the correct order.
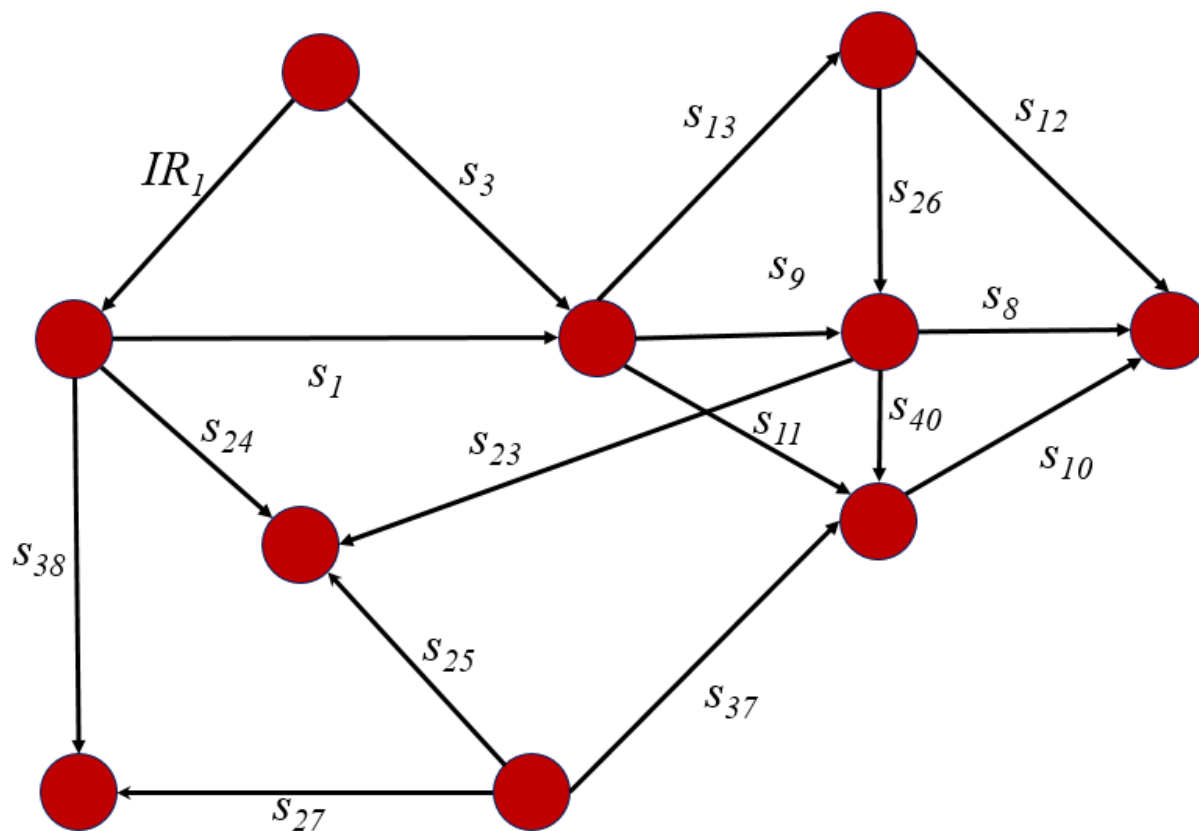
Figure 6.6: Fused cycle graph of Figure 6.5, *ER*₄, *ER*₅ and *ER*₆.

In this manner we could continue to add cycles carefully and judiciously until we realize the final RR Graph. Since this is a linear mechanism with multiple ORs included in the cycle matrix, there would be no need to mirror the graph. The ORs would finally be added to balance the nodes and then the graph much be checked for consistency with KPL and KFL. However, this is still a work in progress.

6.4 Conclusions

Much effort has been spent to make the RR Graph approach as practical as possible. It has proven to be a powerful tool, but also unwieldly at times. We recognize that making this tool more accessible is the most important step in its success. As more RR Graphs are constructed, we start to see more patterns in the steps of how they are constructed. This chapter summarizes

all the insights gained from previous examples of RR Graphs as well as the original linear algebra on which the methodology is based. Ideally, these guidelines will serve as important tools for future RR Graph analysis and, in turn, those analyses will further the understanding of the RR Graph methodology.

6.5 References

1. N. Gorban, G. S. Yablonsky, "Extended detailed balance for systems with irreversible reactions," Chem. Eng. Sci. 2011, 66, 5388–5399.

2. Heyden, A., Hansen, N., Bell, A. T., Keil, F. J., Nitrous Oxide Decomposition over Fe-ZSM-5 in the Presence of Nitric Oxide: A Comprehensive DFT Study, *J. Phys. Chem. B* 2006, *110,* 17096-17114

3. Milner, P. C., "The Possible Mechanisms of Comples Reactions Involving Consecutive Steps," J. Electrochem. Soc., 111, 228-232 (1964)

Chapter 7: Conclusions and Future Work

In summary, the significance and power of the RR Graph methodology in mechanistic and kinetic analysis along with mechanism pruning has been unequivocally demonstrated in this thesis through the analysis and examples provided. This clearly demonstrates the superiority of this approach over other methodologies. Most notably, the RR Graph was demonstrated to more completely elucidate the correct rate limiting step kinetics while Campbell's Degree of Rate Control (DoRC), which is based on sensitivity analysis, could not. Furthermore, the RR Graph properly enumerates all the potential reaction routes as walks, which other graph-theory based techniques are unable to do so rigorously.

Although there were many insights gained from a comparison of the RR Graph methodology with Campbell's DoRC, it highlights a significant knowledge gap in the understanding of why these methods provide different results. The DoRC methodology involves isolating a single step and quantifying how changing the kinetics of that step would affect the overall kinetics while holding all other step rate and equilibrium constants unchanged. This process neglects the fact that the kinetics of elementary steps are complicated and that changing the kinetics of one step could have an effect on other steps. In other words, there might be issues with maintaining thermodynamic consistence. The RR Graph methodology avoids this trap and provides the step and pathway fluxes with the given step and rate equilibrium constants so that all steps and pathways with appreciable flux can be directly identified. However, these ideas are mostly speculation and are not proven to be the reason for the discrepancy between the two methods. Researching these ideas could very well prove to be insightful for further understanding reaction kinetics in general and possibly providing a better understanding of the RR Graphs.

What is lacking for the broader application of RR Graph methodology is an efficient way to draw them. Without an RR Graph it can be difficult for many researchers to apply this technique. Hopefully, the steps detailed in Chapter 6 go a long way towards delineating drawing of these graphs and making this method more accessible. It would, of course, be desirable to automate the drawing of the RR Graph, and make it available to all researchers, but this is not yet realistic. Regardless, the quantitative aspects of the theory can be applied without the realization of an RR Graph, just as an electrical circuit can be analyzed on the basis of the Kirchoff's laws without a circuit diagram. Although the RR Graph is invaluable for flux analysis and pruning, further development of the RR Graph method needs to be continued so that it may be more broadly accessible and employed. The further development of this approach could be based on the analysis of addition examples of mechanism and kinetics for which DFT energetics are available. Some of the suggested examples are described below.

7.1 NO$_x$ Decomposition

A method for drawing the graph for a very large system was discussed in Chapter 6. However, the full RR Graph has yet to be realized for this system. The entire mechanism can be combined to include the hydrogenated steps that have not yet been introduced. Once a complete and valid RR Graph is found, the same Rdot analysis seen in section 2.1.3 could be done to prune the mechanism and establish a comprehensive mechanistic understanding along with predictive rate equations. Ultimately, the realization of the complete kinetic picture for this mechanism will likely appear as two separate RR sub-graphs that may not share ORs and any of the elementary steps. The realization of such a graph would likely provide great insight into how future RR Graphs can be constructed.

7.2 Oxygen Reduction Reaction

Further study into the oxygen reduction reaction (ORR) is warranted to better understand the mechanism so as to find catalysts that might provide actual improvement over platinum catalyst. While Chapter 4 demonstrated how powerful the RR Graph methodology can be in characterizing the activity of a catalyst, no clear activity improvement over Pt catalyst for the investigated mechanism over the many different catalysts was found. On the other hand, if cheaper catalysts can provide activity comparable to Pt, then that can lead to practical catalysts. Additional catalysts can however be analyzed and it is possible to increase the window of investigation to possibly find better alternative catalysts and determine the optimal conditions and loadings for using those catalysts.

Furthermore, it is possible that other catalysts need to consider different pathways. A larger mechanism might thus need to be considered in order to capture the full kinetics of alternative catalysts. One such larger ORR mechanisms for which the RR Graph approach can be applied to is shown in Table 7.1, which is a 14-step mechanism for the ORR on transition metal surfaces proposed by Ford et al. [1], as compared to with the 7-step mechanism analyzed in Chapter 4. An RR Graph for this mechanism is provided in Figure 7.1, but it might need to be edited to ensure proper consistence with Kirchoff's laws, and the kinetics and resistances have yet to be analyzed in detail.

	Elementary Reactions
s_1:	$O_2 + S \rightleftarrows O_2 \cdot S$
s_2:	$O_2 \cdot S + H \cdot S \rightleftarrows OOH \cdot S$
s_3:	$OOH \cdot S + H \cdot S \rightleftarrows HOOH \cdot S$
s_4:	$OOH \cdot S + H \cdot S \rightleftarrows OOHH \cdot S$
s_5:	$H \cdot S + HOOH \cdot S \rightleftarrows HOOHH \cdot S$
s_6:	$O \cdot S + H \cdot S \rightleftarrows OH \cdot S$
s_7:	$O \cdot S + OH \cdot S \rightleftarrows H_2O \cdot S$
s_8:	$2OH \cdot S \rightleftarrows H_2O \cdot S + O \cdot S$
s_9:	$O_2 \cdot S + \rightleftarrows 2O \cdot S$
s_{10}:	$OOH \cdot S \rightleftarrows OH \cdot S + O \cdot S$
s_{11}:	$HOOH \cdot S \rightleftarrows 2OH \cdot S$
s_{12}:	$OOHH \cdot S \rightleftarrows H_2O \cdot S + O \cdot S$
s_{13}:	$HOOH \cdot S \rightleftarrows HOOH$
s_{14}:	$H_2O \cdot S \rightleftarrows H_2O$
s_{OR1}:	$O_2 + 2H \rightleftarrows HOOH$
s_{OR2}:	$O_2 + 4H \rightleftarrows 2H_2O$

Table 7.1: 14-step ORR mechanism [1]
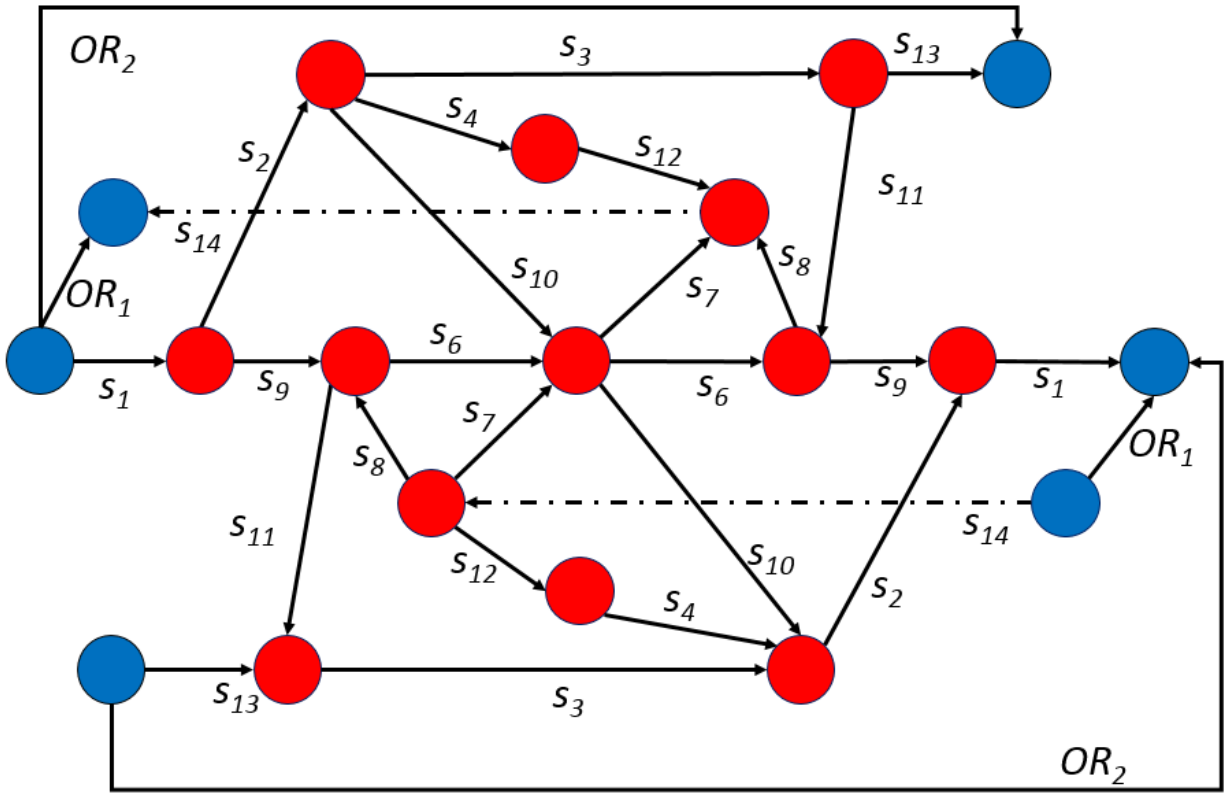
Figure 7.1: RR Graph for the 14-step ORR mechanism [1]

7.3 References

1. Ford, Denise C., Nilekar, A. U., Xub,Y., Mavrikakis, M. Partial and complete reduction of O2 by hydrogen on transition metal surfaces, *Surface Science* 604 (2010) 1565-1575

Appendix A: Mathematica Program for Enumerating Empty Routes

The code used to find the cycles of the reduced NO_x mechanism is available here. **v** is the stoichiometric matrix, **a** is an empty vector that steps are added into and is used to check for empty vectors. To change this to accommodate other mechanism, simply enter the stoichiometric matrix and adjust the empty vector to fit the number of intermediates q of the mechanism. The For loops are entered to fit the number of independent steps q. This example searches for cycles with at most 5 steps. The loops may be adjusted for any n number of steps. Where the first loop ends at q-n, the second at q-n+1 and the third at q-n+2…and the final at q.

```
v={{0,0,0,2,0,0,0,0,0,0,0,0,0,0,-1,0,0,0,0},
   {0,0,1,1,-1,0,0,0,0,0,0,0,0,0,0,0,0,0,0},
   {0,0,0,1,1,-1,0,0,0,0,0,0,0,0,0,0,0,0,0},
   {0,0,-1,0,1,-1,0,0,0,0,0,0,0,0,0,0,0,0,0},
   {0,0,0,0,0,1,0,0,0,0,0,0,0,0,0,0,-1,0,0},
   {0,0,0,0,0,0,1,0,0,0,0,0,0,0,0,0,-1,0,0},
   {0,0,0,0,0,0,0,1,0,0,0,0,0,0,0,0,0,-1,0},
   {0,0,1,0,0,0,1,-1,0,0,0,0,0,0,0,0,0,0,0},
   {-1,0,0,0,0,0,0,0,1,0,0,0,0,0,0,0,0,0,0},
   {0,-1,0,0,0,0,0,0,0,1,0,0,0,0,0,0,0,0,0},
   {0,0,0,-1,1,0,1,-1,0,0,0,0,0,0,0,0,0,0,0},
   {0,0,0,0,1,0,1,0,-1,0,0,0,0,0,0,0,0,0,0},
   {0,0,0,1,0,0,0,1,-1,0,0,0,0,0,0,0,0,0,0},
   {0,0,0,1,0,-1,-1,0,1,0,0,0,0,0,0,0,0,0,0},
   {0,0,1,0,-1,0,0,-1,1,0,0,0,0,0,0,0,0,0,0},
   {0,0,0,0,1,-1,0,-1,1,0,0,0,0,0,0,0,0,0,0},
   {0,0,0,-1,0,0,0,-1,0,1,0,0,0,0,0,0,0,0,0},
   {0,0,1,0,-1,0,0,-1,0,1,0,0,0,0,0,0,0,0,0},
   {0,0,0,0,1,-1,0,-1,0,1,0,0,0,0,0,0,0,0,0},
   {0,0,0,1,0,0,0,0,0,0,0,0,0,1,0,0,0,0,-1},
   {0,0,0,1,0,0,0,0,0,0,0,0,1,-1,0,0,0,0,0},
   {0,0,0,1,0,0,0,0,0,0,0,0,1,-1,0,0,0,0,0},
   {0,0,0,1,0,0,0,0,0,0,0,0,1,-1,0,0,0,0,0},
   {0,0,-1,0,1,0,0,0,0,0,0,0,1,-1,0,0,0,0,0},
   {0,0,1,0,-1,0,0,0,0,0,0,-1,1,0,0,0,0,0,0},
   {0,0,1,0,-1,0,0,0,0,0,-1,1,0,0,0,0,0,0,0},
   {0,0,0,0,1,-1,0,0,0,0,0,0,-1,1,0,0,0,0,0},
```

214

```
   {0,0,0,0,1,-1,0,0,0,0,0,-1,1,0,0,0,0,0,0},
   {0,0,0,0,1,-1,0,0,0,0,-1,1,0,0,0,0,0,0,0},
   {0,0,1,0,0,0,-1,0,0,0,1,0,0,0,0,0,0,0,0},
   {0,0,1,-1,0,0,-1,0,0,0,0,1,0,0,0,0,0,0,0},
   {0,0,0,-1,1,0,-1,0,0,0,1,0,0,0,0,0,0,0,0},
   {0,0,0,0,0,0,-2,1,0,0,1,0,0,0,0,0,0,0,0},
   {0,0,0,0,0,0,0,0,0,0,0,0,0,0,3,1,-1,0,-1},
   {0,0,0,0,0,0,0,0,0,0,0,0,0,0,1,-1,-1,1,0},
   {0,0,0,0,0,0,0,0,0,0,0,0,0,0,0,0,0,0,0}};
a={0,0,0,0,0,0,0,0,0,0,0,0,0,0,0,0,0,0,0}
mat={{0,0,0,0,0},{0,0,0,0,0}}
For[h = 1, h < 32, h++,
 For[i = h + 1, i <= 33, i++,
  For[j = i + 1, j <= 34, j++,
   For[k = j + 1, k <= 35, k++,
    For[l = k + 1, l <= 36, l++,
     For[c = -1, c <= 1, c = c + 2,
      For[d = -1, d <= 1, d = d + 2,
       For[e = -1, e <= 1, e = e + 2,
        For[f = -1, f <= 1, f = f + 2,
         a = {0,0,0,0,0,0,0,0,0,0,0,0,0,0,0,0,0,0,0};
         a = b*v[[h]]+c*v[[i]]+d*v[[j]]+e*v[[k]]+f*v[[l]];
         mat = {{b, c, d, e, f}, {h, i, j, k, l}};
         If[a  ==   {0,0,0,0,0,0,0,0,0,0,0,0,0,0,0,0,0,0,0},
Print["cycle,at"] Print[mat]]b=1;
        ]
       ]
      ]
     ]
    ]
   Print["step"]Print[h]
 ]
```

Appendix B

For the case of the MDR in which steps s_{17}, s_{23}, and s_{25} are considered to be reversible while all other steps are considered to be irreversible and that the three reversible steps are each in their own parallel pathway which contributes to the overall reaction rate, such that

$$r_{OR} \approx r_{17} + r_{23} + r_{25} \tag{B.1}$$

The rates constant and terminal species activities are known values, so solving for the site fractions of the intermediate species will enable the calculation of the rates. These values were calculated based on the QE approximation. The methodology is illustrated for one species, $C \cdot S$. The surface coverage of the other intermediate species can be derived following a similar procedure, unless otherwise stated in the text.

In order to obtain the QE surface coverage of $C \cdot S$, we first identify the Intermediate Reaction for the formation of $C \cdot S$ from amongst steps that can be considered to be quasi-equilibrated. Thus, for $C \cdot S$, the appropriate intermediate reaction is

$(s_1 + s_2 + s_3 + 2s_{32})$

Step	Elementary Reaction	σ_ρ
s_1	$CH_4(g) + 2S \leftrightarrows CH_3 \bullet S + H \bullet S$	+1
s_2	$CH_3 \bullet S + S \leftrightarrows CH_2 \bullet S + H \bullet S$	+1
s_3	$CH_2 \bullet S + S \leftrightarrows CH \bullet S + H \bullet S$	+1
s_4	$CH \bullet S + S \leftrightarrows CH \bullet S + H \bullet S$	+1
s_{32}	$H \bullet S + H \bullet S \leftrightarrows H_2(g) + 2S$	+2
$IR_{C \cdot S}$	$CH_4(g) + 2S \leftrightarrows CH \bullet S + H_2(g)$	

$$\theta_{C \cdot S} = K_1 K_2 K_3 K_4 K_{32}^2 P_{CH_4} P_{H_2}^{-2} \theta_0 \tag{B.2}$$

It follows for other species

$$\theta_{O \cdot S} = \left(K_1 K_2 K_3 K_4 K_{25} K_{32}^2 K_{33} P_{CH_4} P_{H_2}^2 \right)^{-1} \theta_0 \text{ or } \theta_{O \cdot S} = \left(K_{29} K_{30} K_{31} P_{H_2} \right)^{-1} P_{H_2O} \theta_0 \quad \text{(B.3)}$$

$$\theta_{CO \cdot S} = K_{33}^{-1} P_{CO} \theta_0 \quad \text{(B.4)}$$

$$\theta_{OH \cdot S} = \left(K_{30} K_{31} \sqrt{P_{H_2}} \right)^{-1} P_{H_2O} \theta_0 \quad \text{(B.5)}$$

$$\theta_{H \cdot S} = \sqrt{K_{32}^{-1} P_{H_2}} \, \theta_0 \quad \text{(B.6)}$$

$$\theta_{CO_2 \cdot S} = K_5 P_{CO_2} \theta_0 \quad \text{(B.7)}$$

$$\theta_{CH \cdot S} = K_1 K_2 K_3 \sqrt{K_{32}^3 P_{H_2}^{-3}} P_{CH_4} \theta_0 \quad \text{(B.8)}$$

For site fractions that cannot be considered at QE, we utilize the idea that certain reaction steps are equivilent and the unknown site fractions can be solved by setting certain reactions equal to each other. For s_{17}, the site fraction for COH•S is unknown, thus we set the rates for s_{17} and s_{18} equal to each other, then use substitution to develop an equation for r_{17}, which is then repeated for s_{23} and s_{25}.

$$r_{17} = \vec{k}_{17} \theta_{C \cdot S} \theta_{OH \cdot S} - \overleftarrow{k}_{17} \theta_{COH \cdot S} \theta_0 \quad \text{(B.9)}$$

$$r_{18} = \vec{k}_{18} \theta_{COH \cdot S} \theta_0 - \overleftarrow{k}_{18} \theta_{CO \cdot S} \theta_{H \cdot S} \quad \text{(B.10)}$$

$$r_{17} = r_{18} \quad \text{(B.11)}$$

$$\vec{k}_{17} \theta_{C \cdot S} \theta_{OH \cdot S} - \overleftarrow{k}_{17} \theta_{COH \cdot S} \theta_0 = \vec{k}_{18} \theta_{COH \cdot S} \theta_0 - \overleftarrow{k}_{18} \theta_{CO \cdot S} \theta_{H \cdot S} \quad \text{(B.12)}$$

$$\theta_{COH \cdot S} = \frac{\vec{k}_{17} \theta_{C \cdot S} \theta_{OH \cdot S} + \overleftarrow{k}_{18} \theta_{CO \cdot S} \theta_{H \cdot S}}{\left(\vec{k}_{18} + \overleftarrow{k}_{17} \right) \theta_0} \quad \text{(B.13)}$$

$$\theta_{\text{COH·S}} = \frac{\vec{k}_{17}K_1K_2K_3K_4K_{32}^2P_{\text{CH}_4}P_{\text{H}_2}^{-2}\theta_0\left(K_{30}K_{31}\sqrt{P_{\text{H}_2}}\right)^{-1}P_{\text{H}_2\text{O}}\theta_0 + \bar{k}_{18}K_{33}^{-1}P_{\text{CO}}\theta_0\sqrt{K_{32}^{-1}P_{\text{H}_2}}\theta_0}{\left(\bar{k}_{18} + \vec{k}_{17}\right)\theta_0} \quad \text{(B.14)}$$

$$r_{17} = \vec{k}_{17}K_1K_2K_3K_4K_{32}^2P_{\text{CH}_4}P_{\text{H}_2}^{-5/2}\left(K_{30}K_{31}\right)^{-1}P_{\text{H}_2\text{O}}\theta_0^2$$

$$- \frac{\vec{k}_{17}K_1K_2K_3K_{32}^2P_{\text{CH}_4}P_{\text{H}_2}^2\left(K_{30}K_{31}\sqrt{P_{\text{H}_2}}\right)^{-1}P_{\text{H}_2\text{O}}\theta_0^2 + \bar{k}_{18}K_{33}^{-1}P_{\text{CO}}\sqrt{K_{32}^{-1}P_{\text{H}_2}}\theta_0^2}{\left(\bar{k}_{18} + \vec{k}_{17}\right)} \quad \text{(B.16)}$$

$$r_{17} = \frac{\vec{k}_{17}K_1K_2K_3K_4K_{32}^2P_{\text{CH}_4}P_{\text{H}_2\text{O}}\theta_0^2}{P_{\text{H}_2}^{5/2}K_{30}K_{31}\left(\bar{k}_{18} + \vec{k}_{17}\right)}\left(1 - \frac{\bar{k}_{18}K_{30}K_{31}}{K_1K_2K_3K_{17}K_{32}^2K_{33}}\frac{P_{\text{CO}}P_{\text{H}_2}^3}{P_{\text{CH}_4}P_{\text{H}_2\text{O}}}\right) \quad \text{(B.17)}$$

$$r_{23} = \vec{k}_{23}\theta_{\text{CH·S}}\theta_{\text{O·S}} - \bar{k}_{23}\theta_{\text{CHO·S}}\theta_0 \quad \text{(B.18)}$$

$$r_{24} = \vec{k}_{24}\theta_{\text{CHO·S}}\theta_0 - \bar{k}_{24}\theta_{\text{CO·S}}\theta_{\text{H·S}} \quad \text{(B.19)}$$

$$r_{23} = r_{24} \quad \text{(B.20)}$$

$$\vec{k}_{23}\theta_{\text{CH·S}}\theta_{\text{O·S}} - \bar{k}_{23}\theta_{\text{CHO·S}}\theta_0 = \vec{k}_{24}\theta_{\text{CHO·S}}\theta_0 - \bar{k}_{24}\theta_{\text{CO·S}}\theta_{\text{H·S}} \quad \text{(B.21)}$$

$$\theta_{\text{COH·S}} = \frac{\vec{k}_{23}\theta_{\text{CH·S}}\theta_{\text{O·S}} + \bar{k}_{24}\theta_{\text{CO·S}}\theta_{\text{H·S}}}{\left(\vec{k}_{24} + \bar{k}_{23}\right)\theta_0} \quad \text{(B.22)}$$

$$\theta_{\text{COH·S}} = \frac{\vec{k}_{23}\theta_{\text{CH·S}}\theta_{\text{O·S}} + \bar{k}_{24}\theta_{\text{CO·S}}\theta_{\text{H·S}}}{\left(\vec{k}_{24} + \bar{k}_{23}\right)\theta_0} \quad \text{(B.23)}$$

$$r_{23} = \vec{k}_{23}K_1K_2K_3\sqrt{K_{32}^3P_{\text{H}_2}^{-3}}P_{\text{CH}_4}\theta_0\left(K_{29}K_{30}K_{31}P_{\text{H}_2}\right)^{-1}P_{\text{H}_2\text{O}}\theta_0 -$$

$$\bar{k}_{23}\frac{K_1K_2K_3\sqrt{K_{32}^3P_{\text{H}_2}^{-3}}P_{\text{CH}_4}\theta_0\left(K_{29}K_{30}K_{31}P_{\text{H}_2}\right)^{-1}P_{\text{H}_2\text{O}}\theta_0 + \bar{k}_{24}K_{33}^{-1}P_{\text{CO}}\sqrt{K_{32}^{-1}P_{\text{H}_2}}\theta_0^2}{\left(\vec{k}_{24} + \bar{k}_{23}\right)} \quad \text{(B.24)}$$

218

$$r_{23} = \frac{\vec{k}_{23}K_1K_2K_3K_{32}^{3/2}P_{\mathrm{CH_4}}P_{\mathrm{H_2O}}\theta_0^2}{K_{29}K_{30}K_{31}P_{\mathrm{H_2}}^{5/2}\left(\vec{k}_{24}+\vec{k}_{23}\right)}\left(1 - \frac{\vec{k}_{24}K_1K_2K_3K_{32}^{3/2}}{K_{23}K_{29}K_{30}K_{31}K_{33}}\frac{P_{\mathrm{CO}}P_{\mathrm{H_2}}^3}{P_{\mathrm{CH_4}}P_{\mathrm{H_2O}}}\right) \tag{B.25}$$

$$r_{25} = \vec{k}_{25}\theta_{\mathrm{C\cdot S}}\theta_{\mathrm{O\cdot S}} - \vec{k}_{23}\theta_{\mathrm{CO\cdot S}}\theta_0 \tag{B.26}$$

$$r_{25} = \vec{k}_{25}K_1K_2K_3K_{32}^2P_{\mathrm{CH_4}}P_{\mathrm{H_2}}^2\theta_0\left(K_{29}K_{30}K_{31}P_{\mathrm{H_2}}\right)^{-1}P_{\mathrm{H_2O}}\theta_0 - \vec{k}_{25}K_{33}^{-1}P_{\mathrm{CO}}\theta_0\theta_0 \tag{B.27}$$

$$r_{25} = \frac{\vec{k}_{25}K_1K_2K_3K_4K_{32}^2P_{\mathrm{CH_4}}P_{\mathrm{H_2}}^{-2}\theta_0^2}{K_{29}K_{30}K_{31}P_{\mathrm{H_2}}}\left(1 - \frac{\vec{k}_{24}K_1K_2K_3K_4K_{32}^{3/2}}{K_{25}K_{29}K_{30}K_{31}K_{33}}\frac{P_{\mathrm{CO}}P_{\mathrm{H_2}}^3}{P_{\mathrm{CH_4}}P_{\mathrm{H_2O}}}\right) \tag{B.28}$$

$$r_{OR_1} \approx \left(\frac{\vec{k}_{17}K_1K_2K_3K_4K_{32}^2P_{\mathrm{CH_4}}P_{\mathrm{H_2O}}}{K_{30}K_{31}P_{\mathrm{H_2}}^{5/2}\left(\vec{k}_{18}+\vec{k}_{17}\right)} + \frac{\vec{k}_{23}K_1K_2K_3K_4K_{32}^{3/2}P_{\mathrm{CH_4}}P_{\mathrm{H_2O}}}{K_{29}K_{30}K_{31}P_{\mathrm{H_2}}^{5/2}\left(\vec{k}_{24}+\vec{k}_{23}\right)} + \frac{\vec{k}_{25}K_1K_2K_3K_{32}^2P_{\mathrm{CH_4}}P_{\mathrm{H_2}}^2}{K_{29}K_{30}K_{31}P_{\mathrm{H_2}}}\right)\theta_0^2\left(1 - \frac{1}{K_{OR_1}}\frac{P_{\mathrm{CO}}P_{\mathrm{H_2}}^3}{P_{\mathrm{CH_4}}P_{\mathrm{H_2O}}}\right) \tag{B.29}$$

$$r_6 = \vec{k}_6\theta_{\mathrm{CO_2\cdot S}}\theta_0 - \vec{k}_6\theta_{\mathrm{CO\cdot S}}\theta_{\mathrm{O\cdot S}} \tag{B.30}$$

$$r_6 = \vec{k}_6K_5P_{\mathrm{CO_2}}\theta_0\theta_0 - \vec{k}_6K_{33}^{-1}P_{\mathrm{CO}}\theta_0\left(K_{29}K_{30}K_{31}P_{\mathrm{H_2}}\right)^{-1}P_{\mathrm{H_2O}}\theta_0 \tag{B.31}$$

$$r_{OR_2} = r_6 = \vec{k}_6K_5P_{\mathrm{CO_2}}\theta_0^2\left(1 - \frac{1}{K_5K_6K_{29}K_{30}K_{31}K_{33}}\frac{P_{\mathrm{CO}}P_{\mathrm{H_2O}}}{P_{\mathrm{H_2}}P_{\mathrm{CO_2}}}\right) \tag{B.32}$$